A mechanistic study of CO_2/Brine relative permeability

Adel R. A.Traki

Submitted for the Degree of Doctor of Philosophy

Heriot-Watt University

School of Energy, Geoscience, Infrastructure and Society

May 2016

Dedicated to

My parents, wife and son.

Abstract

CO_2 injection in geologic formations (hydrocarbon reservoirs as well as aquifers) is increasingly considered as a method for increasing oil recovery and, at the same time, storing CO_2 in these formations to reduce the CO_2 emissions, which are considered to be the main cause responsible for global warming or the greenhouse phenomenon. Among many parameters significantly impacting the flow and distribution of CO_2 in the formations is relative permeability (K_rCO_2).

The protocols being used to measure CO2 relative permeability are facing a lot of challenges and problems. In this study, an assessment package tool has been designed and applied in order to verify the protocols and data resulted from CO_2 relative permeability experiments published, with recommendations to avoid errors, all that to prospectively help in determining lab measurements which need to be defined, and thus getting reliable CO_2 relative permeability data to be used for obtaining accurate prediction of the flow properties to CO_2 through (CGS) or (EOR). Moreover, introducing some vital notices whereby the CO_2 relative permeability curves could be read and interpreted correctly was an additional work which has been done.

Another issue is that the capillary properties like wettability, IFT and viscosity are considered as the main factors controlling the shape of CO_2 relative permeability curve and subsequently its value; however, it is found that any set of rock samples, even extracted from the same formation or from different formations with the same rock type and developing the same capillary properties as well, will produce different CO_2 relative permeability curves. This phenomenon had been attributed to rock pore structure or quality, no details of the physics has been described in producing variant CO_2 relative permeability curves for the set of samples assumed. In this study, we introduced an interpretation of how the rock internal structure or quality leads to producing variant CO_2 relative permeability curves, and it was presented as an upgraded concept called 'pore and throat distributions'. This new concept has been verified using a set of pore-network models with variant pore and throat distributions. Using theoretical modelling, rather than the empirical or experimental one, was inevitable as to avoid the side effects of the interactions [1] (among the CO_2, brine and rock contents) on CO_2 relative permeability, and also to put aside the effect of other capillary properties mentioned.

[1] These interactions may leave impacts on everything, from the internal structure of the core up to all capillary properties, like wettability, IFT and viscosity ...etc , which have a considerable effect on $KrCo_2$.

Going back to Darcy's law, the CO_2 relative permeability is a decisive parameter that controls the CO_2 injection rate, but what should be mentioned here is that Darcy's law just introduces the $KrCO_2$ relative permeability as a term which affects CO_2 injection rate and never goes beyond this term to parameters or factors controlling the $KrCO_2$ value and investigates their impact on CO_2 injection rate. In this study and by using $KrCO_2$ data published and a real aquifer model we found that the normal pore and throat distributions with similar connection (a new concept introduced before) produced the best injection rates comparing with other cases of abnormal distributions.

The difference among the relative permeability of CO_2 and other gases, like methane (CH_4) and Ethane (C_2H_6), has also been studied using a theoretical model. The results illustrated that there was no difference among the relative permeabilities related to CO_2 and other gases (CH_4, C_2H_6).

Finally, the wettability distribution concept has been introduced as a factor controlling the magnitude of CO_2 endpoint relative permeability for rock samples having the same rock and capillary properties. Some differences between the systems of gas-oil and CO_2-Brine, in terms of interfacial tension, have been interpreted depending on the notion of free and adherent layers thickness.

Publications

TRAKI, A. R. & SOHRABI, M. 2014. *The impact of rock pore structure on Co2 relative permeability* [Online]. Malysia: International Petroleum Technology Conference

Available: https://www.onepetro.org/conference-paper/IPTC-18125-MS [Accessed].

ACKNOWLEDGMENTS

To

- Allah who granted me the life to live and learn.
- My extraordinary supervisor Prof. Mehran Sohrabi who without his support, this thesis would never be possible.
- IPE at heriot-watt University for granting me an amazing and motivating environment to innovate this work.
- Respected examiners who gave me priceless advices to bring out this work in best mode, and to continue in developing it in best way for the future.

ACADEMIC REGISTRY

Research Thesis Submission

Name*:*	Adel R. A. Traki		
School/PGI:	School of Energy, Geoscience, Infrastructure and Society.		
Version: *(i.e. First, Resubmission, Final)*	Final	Degree Sought (Award **and** Subject area)	PhD in Petroleum Engineering

Declaration

In accordance with the appropriate regulations I hereby submit my thesis and I declare that:

1) The thesis embodies the results of my own work and has been composed by myself
2) Where appropriate, I have made acknowledgement of the work of others and have made reference to work carried out in collaboration with other persons.
3) The thesis is the correct version of the thesis for submission and is the same version as any electronic versions submitted*.
4) my thesis for the award referred to, deposited in the Heriot-Watt University Library, should be made available for loan or photocopying and be available via the Institutional Repository, subject to such conditions as the Librarian may require
5) I understand that as a student of the University I am required to abide by the Regulations of the University and to conform to its discipline.

* *Please note that it is the responsibility of the candidate to ensure that the correct version of the thesis is submitted.*

Signature of Candidate*:*		Date:	

Submission

Submitted By *(name in capitals):*	
Signature of Individual Submitting:	
Date Submitted:	

For Completion in the Student Service Centre (SSC)

Received in the SSC by *(name in capitals):*			
Method of submission *(Handed in to SSC; posted through internal/external mail):*			
E-thesis Submitted (mandatory for final theses)			
Signature:		Date:	

Please note this form should be bound into the submitted thesis.
Updated February 2008, November 2008, February 2009, January 2011

Table of contents

List of figures

List of tables

ACRONYMS

1	EOR	Enhanced Oil Recovery
2	CC	CO_2 Capture
3	CS	CO_2 Storage
4	CCS	CO_2 Capture and Storage
5	CGS	CO_2 Geological Storage
6	CCGS	CO_2 Capture and Geological Storage

Introduction and study objectives

CO_2 injection in geologic formations (hydrocarbon reservoirs as well as aquifers) is increasingly considered as a method for increasing oil recovery and at the same time storing CO_2 in these formations to reduce the CO_2 emissions which are considered the main cause responsible for global warming or the greenhouse phenomenon.

One of the parameters that significantly affects the flow and distribution of CO_2 in the formations is the relative permeability (K_rCO_2). There are a large number of issues concerning the CO_2 relative permeability, including:

- The protocols, being used to measure CO_2 relative permeability, are facing a lot of challenges and problems; studying these problems and finding solutions became very important since the protocols are also considered as a human-made factor impacting the accuracy of CO_2 relative permeability values produced.

- The CO_2 relative permeability graph characteristics - curvature shape, endpoint and residual saturation - are significantly impacted by capillary or rock properties like rock pore structure (or quality) and wettability. The relationship wasn't interpreted and understood accurately enough; in this study, I'm trying to bridge this gap.

- Offering a deeper insight into the relation between the CO_2 relative permeability characteristics and CO_2 injection characteristics like injection rate is another objective in this research.

- Another issue is if there is any significant difference among the CO_2 relative permeability and the ones for other gases like methane (CH_4) and ethane (C_2H_6) when these variant gases are injected through the same formation and under the similar rock properties and conditions. The answer to this question will be a part of this study.

- Some differences in performance between the systems of gas-oil and CO_2-Brine, in terms of IFT, will be another aspect of the study's concerns.

Finally, the CO_2 relative permeability data to be used in this thesis are published in literatures that have been created and verified by specialists in relative permeability discipline. Selecting this way for getting the necessary CO_2 relative permeability has been due to the fact that the amount of data required is expected to be huge and such a large quantity of data will need a very long time to be generated empirically and will require enormous funding, both of which are beyond the available resources.

Chapter 1

CO_2 in CCS and EOR.

1.1. CO_2 capture and geological storage (CCGS).

1.1.1. Global warming or the greenhouse phenomenon.

The global increase of temperature (global warming) is the most serious environmental problem which is facing societies today. It is known that a small variation in earth's temperature will lead to a large impact on ecosystem (Ospina, 2007); the effects of this phenomenon are already being felt and are apparent as increases in sea levels (that increases the risks of flooding in low coastal regions) in addition to fresh water shortage and severe changes in global climate (Adesanya, 2006).

It is widely believed that the increase of global temperature is owing to the increase in greenhouse gases (GHGs) concentrations, for instance carbon dioxide (CO_2), nitrous oxide (N_2O), methane (CH_4), and chlorofluorocarbon CFxClx (Al-Abri, 2003). These gases capture the thermal waves, coming from the sun and reflected on earth toward the space, and by sending them back to the earth, result in raising the Earth temperature.

According to Figure 1.1, CO_2 emissions (now) constitute 50% of the overall greenhouse gas emissions, so we can say that carbon dioxide has the most dominant effect on global warming.

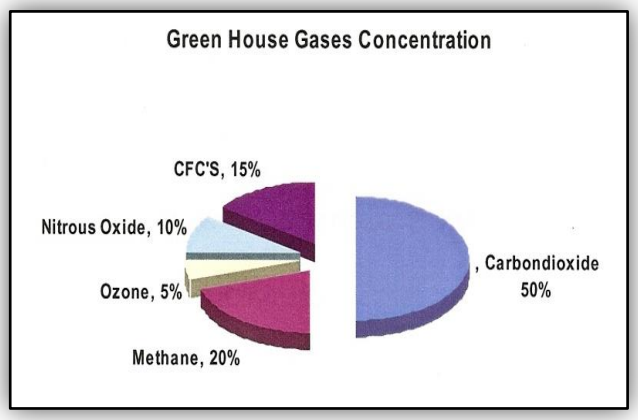

Figure 1.1: Greenhouse gas concentration in the atmosphere in 2003.
(Adesanya, 2006) Source: International Energy Agency

CO_2 emissions:

The CO_2 emissions are mainly coming from human activities like industries using fossil fuels to generate power, transportation, deforestation and production of sour reservoirs (Figure 1.2). Al-Abri (2003) pointed out that the major part of the emissions coming from the use of fossil fuels, on average from 3 – 5 tons of CO_2, is produced per one ton of oil burnt; the total amounts of CO_2 emissions coming from anthropogenic activities were 22.6 Gt/y in 1997, 21% produced from transport means (4.8 Gt/y), while 36% of total emissions (14.2 Gt/y) was emitted from power plants which increased to 54% in 2002 (Figure 1.2).

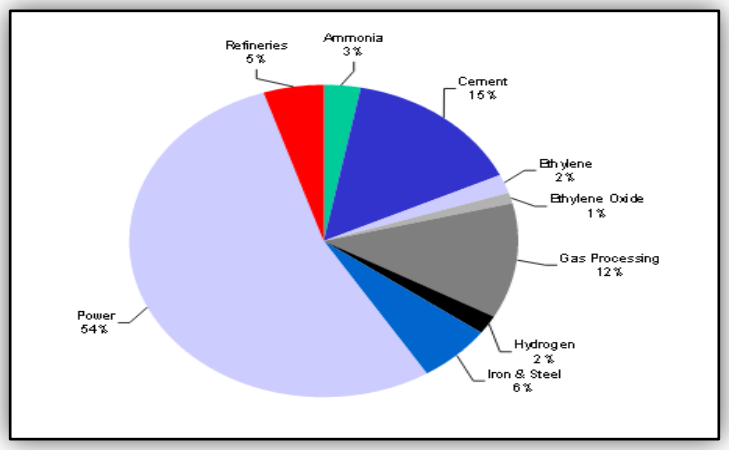

Figure 1.2: Industrial sources of CO_2 emissions (Gale, 2002)

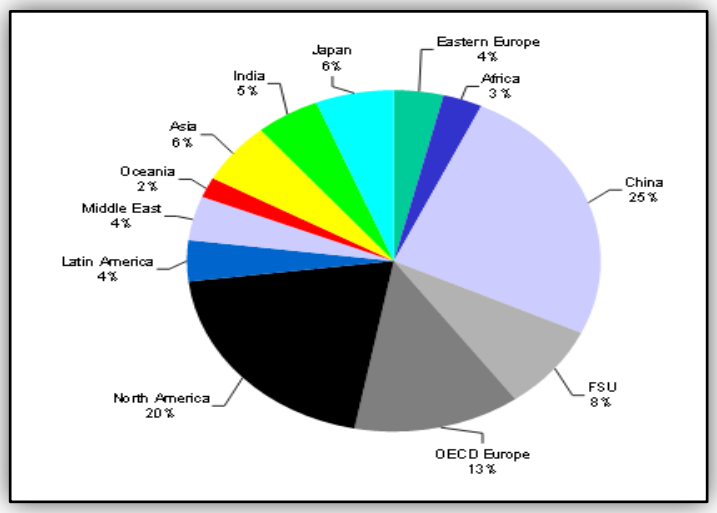

Figure 1.3: CO_2 emissions by geographical regions (Gale, 2002)

The amount of CO_2 emissions will continue to increase (owing to the increase in population and economic development, Figure 1.3) in this century; for example CO_2 projected emissions rose from pre-industrial concentration levels of 280 ppm to 384 ppm (Bielinski, 2007). Now the concentration level of CO_2 emissions is about 550 ppm (approximately double the pre-industrial age level) and will get to the peak in 2150 with concentration of about 1400 ppm (Figure 1.4, Figure 1.5) that means five times more than the concentration level in pre-industrial age. It is important that the CO_2 emissions (coming from fossil fuels) account for about 70% of the increase in CO_2 atmospheric concentrations (Adesanya, 2006); this percentage will be more since the increase in energy demand could only be met by burning of more fossil fuels. Marland et al. (2003) showed in (Figure 1.6) the total estimated amounts of CO_2 being produced from burning fossil fuel between the years 1800 – 2000.

Kiatsakulphan (2009) mentioned that about 27 billion tonnes of CO_2 are produced yearly from fossil-fuel combustion (oil, coal, natural gas).

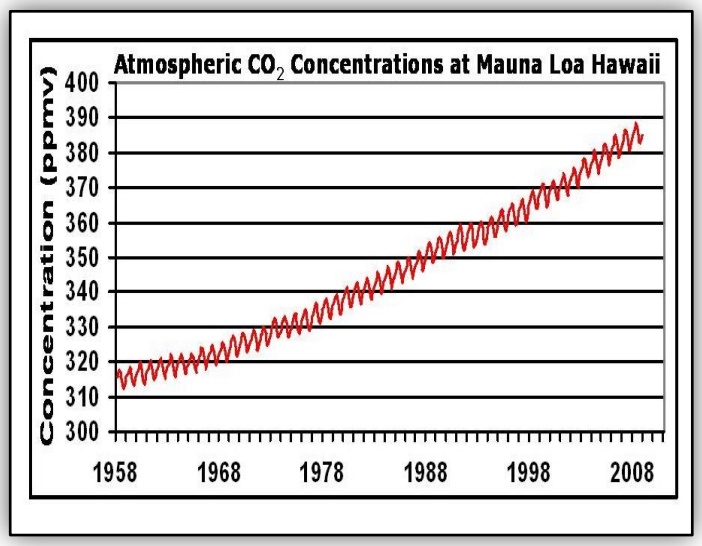

Figure 1.4: Atmospheric Carbon dioxide concentrations at Mauna Loa Hawaii (Keeling and Whorf, 2005)

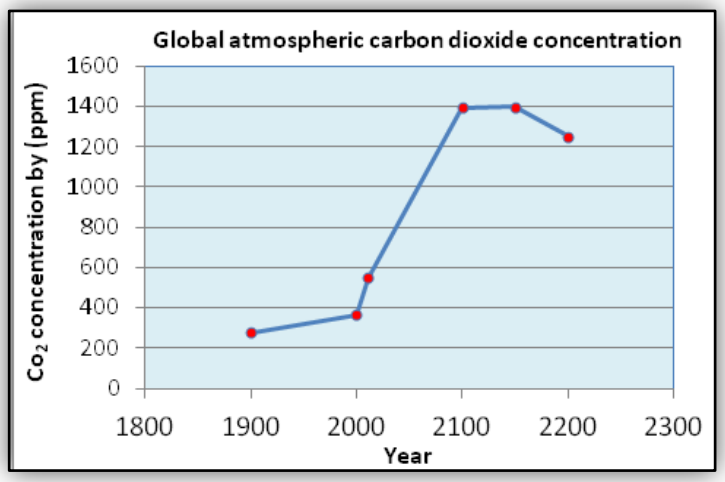

Figure 1.5: CO_2 concentration based on increase in world population and using fossil fuels and depletion of resources (Ghanbari, 2004)

Source: Intergovernmental Panel on Climate Change (IPCC)

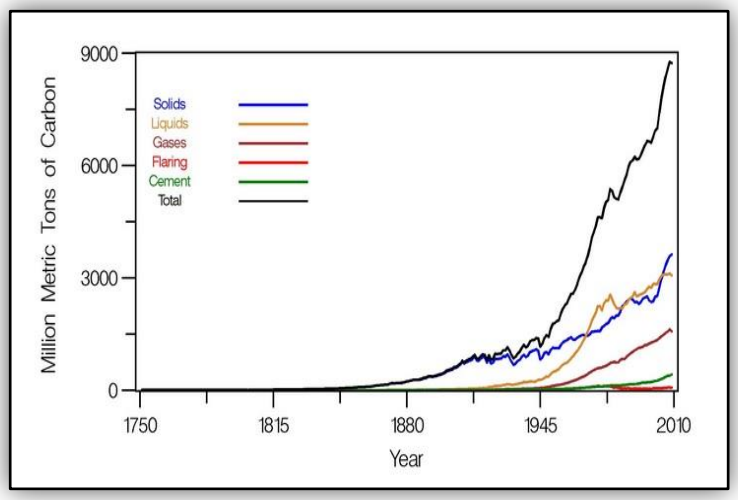

Figure 1.6: Total CO_2 emissions after fossil fuel burning (Marland et al., 2003)

The increase of CO_2 emissions (as responsible for Global warming or the greenhouse phenomenon) results in temperature rise of our planet. Predictions confirm that if human activity continues as usual, a significant climate change by the end of this century is definite, and the expected increase in global temperature will be from 1.1 to 6.3^{o}C (Bielinski, 2007, Houghton et al., 2001)

Mitigation of CO_2 emissions:

The major challenge in mitigating climate change effects is to reduce the CO_2 emissions in the atmosphere. The international agreements such as UN climate conference in Kyoto (1997), Buenos Aires (1998) and Rio (1992) committed the developed countries to reduce their CO_2 emissions by 5% compared with 1990 level (Adesanya, 2006). To keep the concentration of CO_2 emissions at the level of the year 2000 or reduce it below that level over the subsequent 100 years, a global emissions reduction of about 50–60% should be achieved by 2100 (Adesanya, 2006). This is a difficult target since fossil fuels will affect economic activity in developed and undeveloped countries through many decades.

The dependency on fossil fuel is inevitable, and to reduce or stabilize the rate of CO_2 emissions (without a negative effect on economic and social development), many ideas arose including improving energy efficiency (that result in reduction in energy demand), switching from fossil-based energy to other forms of energy, for instance nuclear (not completely accepted due to hazards and long-time contamination), solar, wind and other renewable sources, and finally the promising ideas that proposed to minimize the CO_2 emissions, which are called CCS (CO_2 Capture and Storage).

CCS (CO_2 Capture and Storage) is to play an important role in reducing CO_2 atmospheric emissions; more details for this method of CO_2 emissions reduction follows:

1.1.2. **CO2 Capture (**CC**)**

These are mechanisms used to remove CO_2 before being emitted into the atmosphere. There are many options available for this process including the following:

A) Pre–combustion capture:

In this way, coal is gasified to produce a mixture of gases which consist of Hydrogen and Carbon Monoxide (CO); the latter reacts with water to produce CO_2 which is captured and the Hydrogen is used as clean fuel in Hydrogen fuel cells (Bodipat et al., 2007).

B) Post-combustion capture or Flue gas separation

The mechanism of this method depends on absorption of CO_2 from the gas exhaust by using chemical solvents such as Amine (Adesanya, 2006). The CO_2 is bubbled and then absorbed through a liquid solvent in a packed absorber column. After that, the solution is passed through a generator unit where CO_2 is removed from the solution by steaming at 100°C - 120°C. The water is condensed and the remainder steam will have a high concentration (> 99%) of CO_2 (Bodipat et al., 2007, Figueroa et al., 2008); this high concentrated CO_2 could be captured.

C) Oxy–fuel capture

This involves burning fossil fuel in pure oxygen instead of air, which brings about a higher burning temperature and the resulted exhaust stream consists entirely of CO_2, which could be captured easily by condensing the stream (Bodipat et al., 2007, Davison and Thambimuthu, 2009, Figueroa et al., 2008). The captured CO_2 is transported in a supercritical dense phase (that saves the cost and energy of CO_2 liquefaction) and used commercially to make carbonated beverages and dry-ice as examples.

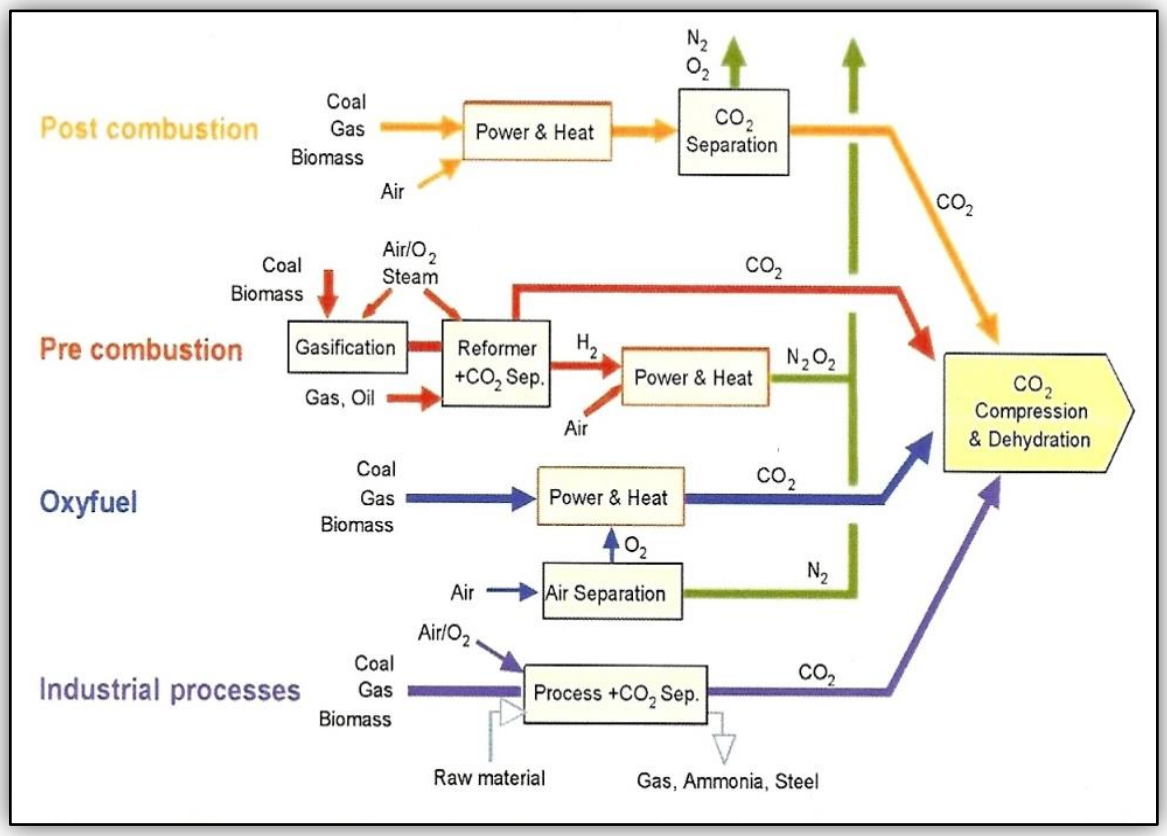

Figure 1.7: Overview of CO_2 capturing process and systems (Adesanya, 2006)

1.1.3. CO_2 storage (CS)

Bodipat et al. (2007) and Holt et al. (2000) believe this type of process includes:

A) Storage (disposal) in oceans:

According to Adesanya (2006), in this way, CO_2 is injected along the ocean floor to form a CO_2 lake but due to insufficient information on biological, chemical and physical effects that may come from the reaction between CO_2 and marine ecology, in addition to lack of data for the cost, this type of storage is considered as unattractive.

B) Geological Storage or sequestration (CGS)

The CO_2 retention time is the most important issue in this type of CO_2 storage; it should usually be thousands of years so that the CO_2 will be away from the atmosphere, and that will prevent its negative impact on the climate (Adesanya, 2006). CGS includes storage of CO_2 in the following geologic formations:

i. **In depleted oil or gas reservoirs**
ii. **In deep saline aquifers**
iii. **In un-mineable Coal beds**

As mentioned before, the characteristic of storage in these sites is the ability to keep CO_2 in for very long time, usually thousands of years; consequently, an effective impact on emissions reduction could be achieved.

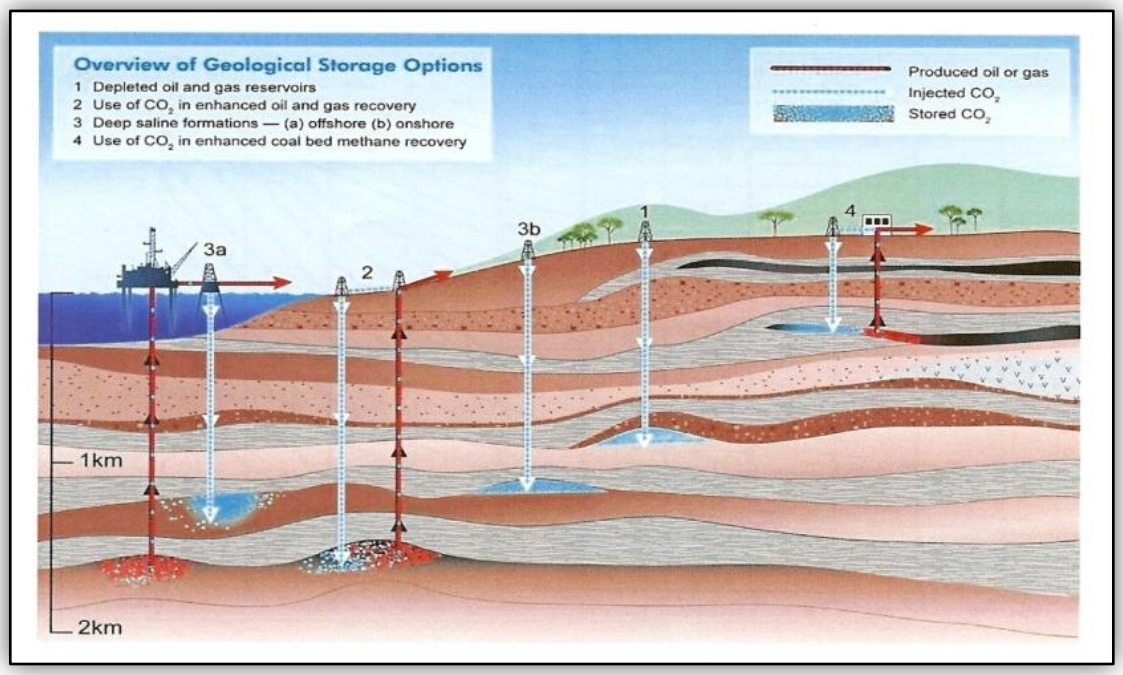

Figure 1.8: Various geological storage or sequestration options (IPCC, 2005)

Deep saline aquifers is the favourite site to store CO_2 in and since they have the biggest capacity of storage, large volumes of CO_2 could be held in this type of geological sites; therefore, a big reduction in CO_2 emissions can be reached. (Table 1.1) below gives an idea about the storage capacity of different geological sites.

Reservoir type	Lower estimate of storage capacity to CO_2 (Gt)	Upper estimate of storage capacity to CO_2 (Gt)
Oil and gas fields	615	900
Un-mineable coal seams	3 - 15	200
Deep saline aquifers	1,000	Possibly 10,000

Table 1.1: Storage capacity of different geological sites (Ukaegbu, 2007)

According to Adesanya (2006), many countries (like Norway) have applied geological storage of CO_2 in deep saline aquifers, Sleipner in the North Sea (operated by Statoil), in Salah in Algeria (operated by BP) and on Barrow island in north-western Australia (operated by Chevron). (Table 1.2) illustrates geological storage projects in some European countries.

Country	Geological Storage Sites			
	Depleted oil reservoirs (Gt)	Depleted gas reservoirs (Gt)	Deep saline aquifer (Gt)	Un-mineable Coal bed (Gt)
Denmark	0.1	0.4	0	
Netherlands	0	0.8	0	
Norway	3.1	7.2	487	
UK	2.6	4.9	248	Under research
Total	5.8	13.3	735	

Table 1.2: CO_2 geological storage projects in some European countries (Adesanya, 2006)

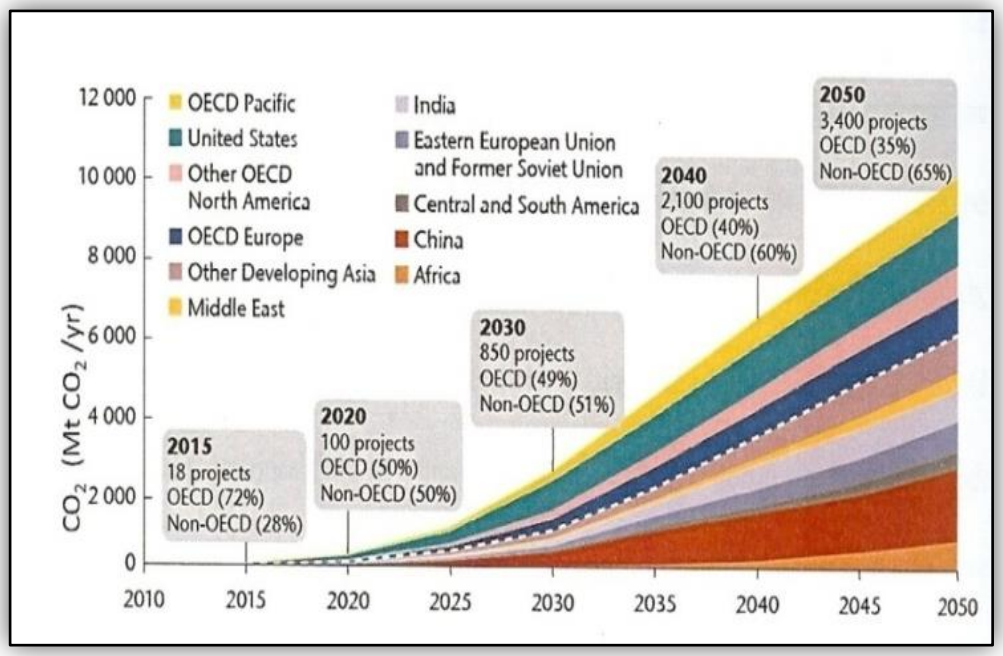

Figure 1.9: Global deployment of CCGS during the period (2010–2050), (IPCC, 2010), (Shariatipour, 2010)

Adesanya (2006) mentioned that the main challenge in deep saline aquifer storage is to reduce the cost and uncertainty of the geological information, while the advantages of using depleted oil and gas reservoirs as storage site are:

- Geology information is well understood.
- Depleted gas and oil reservoirs are proven traps with cap rock working as geological seals that keep CO_2 in the reservoir.

Generally, the suitability of any formation for CO_2 sequestration depends mainly on three factors.

a. **Capacity**. Capacity means how much carbon dioxide can be stored in the formation (Bodipat et al., 2007).

b. **Injectivity.** It means how fast CO_2 can be pumped in the formation. In order to economize the sequestration process, we certainly need to maximize injectivity per well (Bodipat et al., 2007).

c. **Containment.** This refers to how long and how effectively CO_2 can be stored in the formation (Bodipat et al., 2007).

Finally, the costs of CO_2 capture and geological storage are very high. These processes could be more effective in mitigation of CO_2 emissions if the costs could be reduced to become reasonable; this can theoretically be achieved through EOR operations (Bodipat et al., 2007).

1.2. CO_2 utilization for enhanced oil recovery

It is known that only from 30% to 40% of the original oil in place can be recovered through primary and secondary recovery stages; the rest of the oil remains in the reservoir due to its low mobility. To recover the remaining oil, enhanced oil recovery methods are applied (Bodipat et al., 2007), (Figure 1.10).

One of the most famous and efficient methods of EOR is CO_2 miscible flooding. This method uses miscible CO_2 that has a zero interfacial tension with the oil to extract the residual oil in reservoirs.

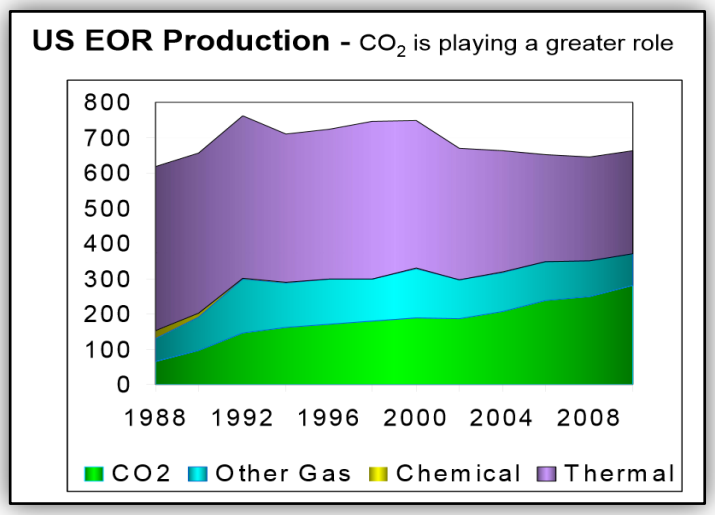

Figure 1.10: Reference: O & G J

1.3. Technical aspects relating to CO_2 in CGS process

1.3.1. Trapping mechanisms of CO_2

In geologic formations (aquifer, for instance), as injection processes continue, the saturation of CO_2 will be going up rapidly to form continuous and mobile phase, in the meantime the CO_2 displaces the other existing phase (Brine, for instance) then moves or migrates upwards, under effect of gravity (weight), to sequestrate under cap rock bed. When the injection suspends, a part of CO_2 will be displaced by Brine coming from adjacent layers, whereas the remaining CO_2 sequestrates in the pore spaces. Some of the CO_2 stays in the formation as free phase; other amounts of CO_2 dissolve in water, while the rest will react after a long time with rock minerals.

Carbon dioxide in general can be stored in deep geologic formations (aquifers, for instance) with different types of trapping. Here is a summary of each type of traps:

A) Free gas trapping

This starts after a short term of injection. In this type of trapping, the CO_2 stays in gas phase and retains its physical and chemical structure. This gas phase could be in mobile or immobile cases as follows.

A.1) **Mobile case (Hydrodynamic or structure trapping)**

When CO_2 is being injected into a deep saline aquifer, its saturation value will increase to much greater than that to the residual saturation, forming a continuous phase (Plume) around injection well. The plume moves under the effect of advection force (while more of the CO_2 is injected) and buoyancy force (CO_2 is lighter than other phases) which are greater than the opposites to flow forces (viscous, interfacial and capillary forces) (Bennion and Bachu, 2010).

Under the effect of buoyancy force, the CO_2 plume will migrate upwards until it faces a low permeability seal (caprock). After that, the CO_2 expands and migrates laterally along the cap rock, in case of horizontal cap rock, or up dip if the caprock is inclined (Ukaegbu, 2007), and as a final sequence, the CO_2 will be trapped in the structural and/or stratigraphic traps below low-permeability caprock, similar to gas and oil accumulations (Figure 1.11, Figure 1.14) (Bodipat et al., 2007). At the pore-level (pore-scale), this is equivalent to well-connected clusters of CO_2 that reside at the centres of the pores and throats (Akbarabadi and Piri, 2013).

So, in this case, to prevent CO_2 leakage from the injecting formation to the overlying strata and also into shallow freshwater aquifers or even to the surface, a cap rock (with high saturation of Brine water and very low permeability) must be present over the injected area. This type of trapping mechanism is the most important one for the early sequestration process.

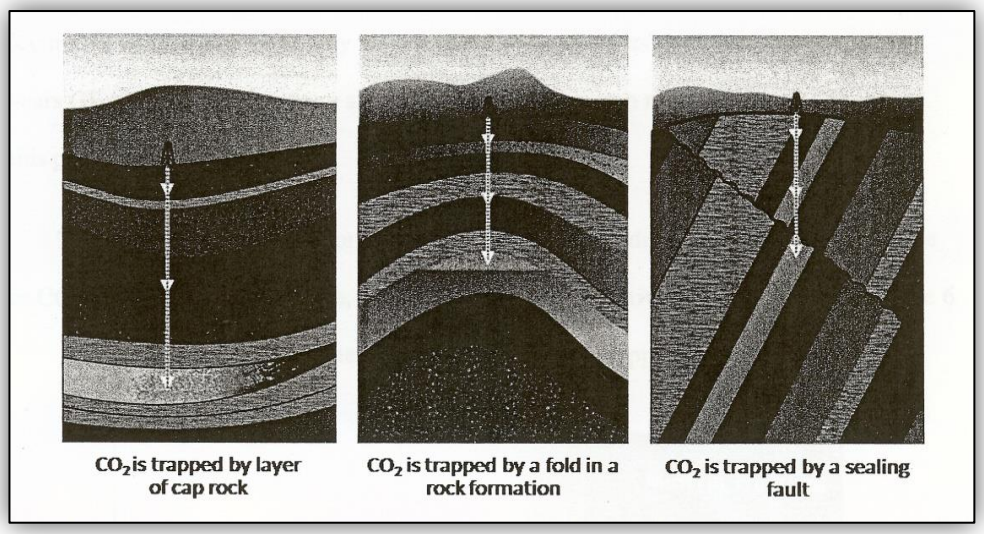

Figure 1.11: Stratigraphic or structure trapping (Kiatsakulphan, 2009)

A.2) **Immobile case (residual or capillary trapping)**

When injection stops, brine moves from adjacent layers to pores where CO_2 exists. The brine will displace the CO_2 by displacement mechanisms called snap-off and pore-body filling (Akbarabadi and Piri, 2013, Al-Dhahli, 2013). The brine influx will cut the continuous phase of CO_2, and as a result, a part of CO_2 will be displaced by imbibition action while the remaining CO_2 will stay in small pores (Bodipat et al., 2007) and its saturation decreases to residual (Figure 1.14). In this degree of saturation, CO_2 is always in a discontinuous phase and the forces which oppose flow (viscous, interfacial and capillary forces) will be greater than those activate the CO_2 flow (pressure and buoyancy); consequently, CO_2 cannot flow through the pore throats and is trapped in the pore space under the concept widely known as snap-off (Ukaegbu, 2007). At the pore-scale, the trapped CO_2 resides in randomly distributed trapped stagnant clusters (Akbarabadi and Piri, 2013). Regardless of the existence of stratigraphic and/or structural traps, the factors affecting this type of trapping are relative permeability including hysteresis and residual saturation of CO_2, which depend on rock composition of the aquifer or formation (Bielinski, 2007, Kumar et al., 2005).

B) Solubility trapping

This is also called dissolution trapping. In this type of trapping, the CO_2 dissolves in brine, and the resulted solution is heavier than pure brine and sinks to the bottom of the formation (Bodipat et al., 2007, Ukaegbu, 2007). This type of trapping is affected mainly by brine solubility, which is a function of temperature, pressure and salinity as illustrated in Figure 1.12 and Figure 1.13 (Kumar et al., 2005). In this type of trapping, CO_2 keeps its chemical structure on, but changes physically ($CO_2 - H_2O$), while dissolution of CO_2 dries out the brine and precipitates as solid salt, (Figure 1.14).

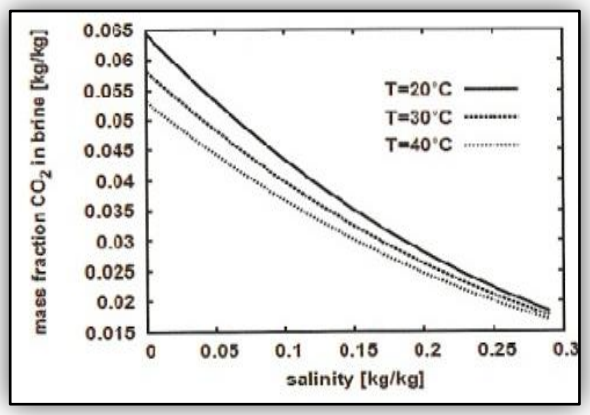

Figure 1.12: CO_2 solubility in Brine vs. Salinity at different temperatures and constant pressure (Enwongulu, 2010)

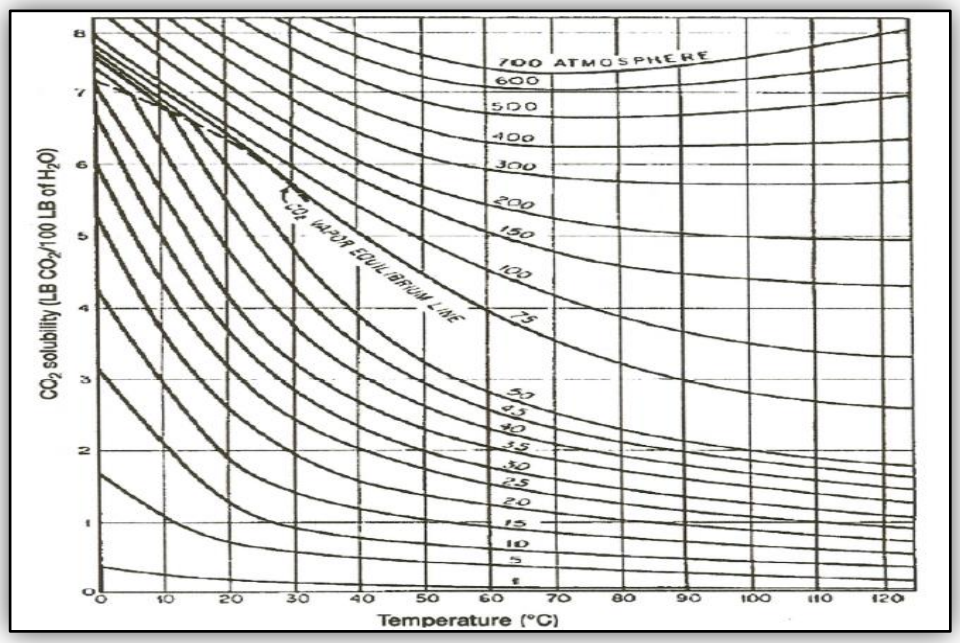

Figure 1.13: Solubility of CO2 in water (Success Donald, 2008)

C) Mineral trapping (chemical trapping)

Mineral trapping is the most permanent trapping mechanism, which can immobilize CO_2 for a very long time (thousands of years, Figure 1.15). In this type of trapping, the physical and chemical structure of CO_2 will completely change (Figure 1.14). Many publications (Bodipat et al., 2007, Xu et al., 2004, Ghanbari, 2004) explained the chemical reactions, which could be summarized as follows:

CO_2 dissolves into brine to produce a weak carbonic acid

$CO_2 + H_2O \rightarrow H_2CO_3$

Carbonic acid in the water will be ionic

$H_2CO_3 \rightarrow 2\ H^+ + CO_3^{--}$

Then, carbonate ions will react with mineral ions like (Ca^{++} , Mg^{++} , Fe^{++}) to produce precipitate carbonate salts

$(2\ H^+ + CO_3^{--}) + Ca^{++} \rightarrow Ca\ CO_3 \downarrow + H_2 \uparrow$

$(2\ H^+ + CO_3^{--}) + Mg^{++} \rightarrow Mg\ CO_3 \downarrow + H_2 \uparrow$

$(2\ H^+ + CO_3^{--}) + Fe^{++} \rightarrow Fe\ CO_3 \downarrow + H_2 \uparrow$

Mineral trapping changes porosity and permeability and consequently changes the fluid flow throughout time.

The change in porosity and permeability will not be immediate since the results of various simulation studies indicated that it takes centuries to millennia for CO_2 to dissolve in formation water and react with rock minerals.

(Table 1.3) shows probable CO_2 storage of some major rock forming minerals (Xu et al., 2004).

Mineral name	Mineral formula	Potential CO2 fixed kg/m^3 mineral
Plagioclase (anorthite)	$Ca[Al_2Si_2O_8]$	436.4
Olivine (forsterite-fayalite)	Mg_2SiO_4-Fe_2SiO_4	2014.7-1896.3
Pyroxene group-enstatite	$(Mg,Fe)_2Si_2O_6$	1404.2
Augite	$(Ca,Mg,Fe(II),Al)_2(Si,Al)_2O_6$	1306.3
Amphibole group-Anthophyllitecummingtonite	$(Mg,Fe(II),Fe(III)_{5-7}Al_{0-2}[Si_{6-8}Al_{2-0}O_{22}](OH)_2$	1169.5-1041.8
Common hornblende	$Ca_2Na_{0-1}(Mg,Fe(II))_{3-5}(Al,Fe(III))_{2-0}[Si_{6-8}Al_{2-0}O_{22}](O,OH)_2$	1000.4
Calcium amphiboles-tremolite	$Ca_2Na_{0-1}(Mg,Fe(II))_{3-5}(Al,Fe(III))_{2-0}[Si_{6-8}Al_{2-0}O_{22}](O,OH)_2$	1119.3
Mica group-glauconite	$(K,Na,Ca)_{1.2-2.0}(Fe(III),Al,Fe(II),Mg)_{4.0}[Si_{7-7.6}Al_{.-0.4}O_{20}](OH)_4nH_2O$	61.97
Mica group-phlogopite	$K_2(Mg,Fe(II))_6[Si_6Al_2O_{20}](OH)_4$	881.8
Mica group-biotite	$K_2(Mg,Fe(II))_{6-4}(Fe(III)Al)_{0-2}[Si_{6-5}Al_{2-3}O_{20}](OH)_{4-2}$	671.0
Serpentine	$Mg_6Si_4O_{10}(OH)_8$	1232.7
Chlorite group	$(Mg,Al,Fe(II))_{12}[(Si,Al)_8O_{20}](OH)_{16}$	923.4
Clay minerals-illite	$K_{1-1.5}(Fe(III),Al,Fe(II),Mg)_{4.0}[Si_{7-6.5}Al_{1-1.5}O_{20}](OH)_4$	78.42
Clay minerals-smectite	$(1/2Ca,Na)_{0.7}(Al,Mg,Fe)_4(Si,Al)_8O_{20}(OH)_4.nH_2O$	161.2

Table 1.3: Possible CO_2 storage of some major rock forming minerals

In conclusion, CO_2 could be stored in deep formations (like saline aquifers) in three main phases:

i. Gas phase, which is represented by stratigraphic-mobile and residual-immobile trapping.

ii. Aqueous phase, which is represented by solubility trapping.

iii. Solid phase, which is represented by mineral trapping.

Figure 1.16 gives an idea of which types of trapping mechanisms will be dominant based on estimated time scales in CO_2 sequestration.

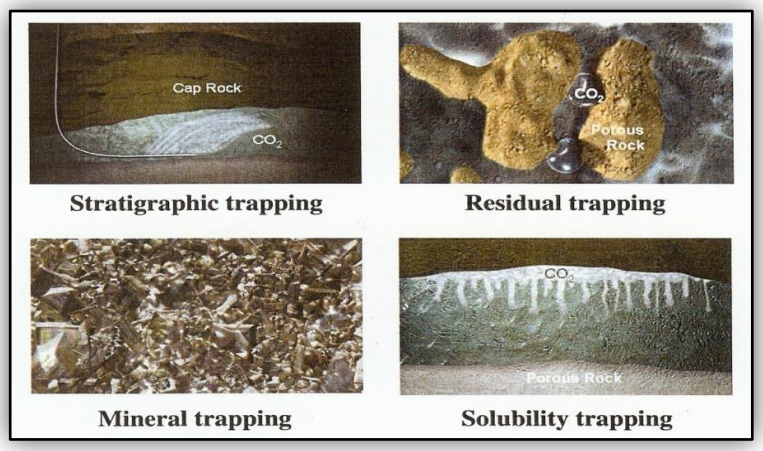

Figure 1.14: Four main CO2 trapping mechanisms (HajNasser, 2010)

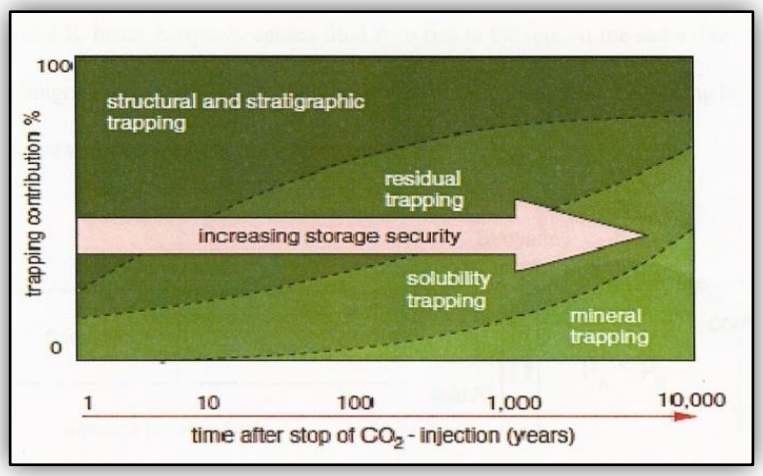

Figure 1.15: CO_2 trapping mechanisms on timescales (Class et al., 2009)

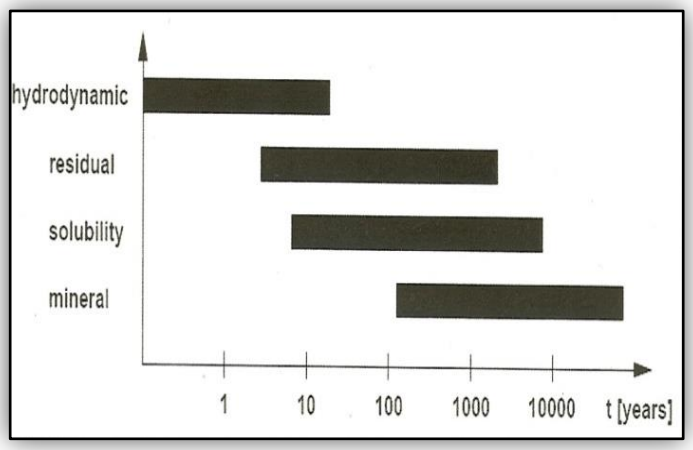

Figure 1.16: Estimated timescales for CO_2 trapping mechanisms (Bielinski, 2007)

1.3.2. **Challenges in CO_2 geological storage (**CGS**)**

The most important challenge in CO_2 sequestration is to avoid the leakage. When CO_2 is injected in deep formations and owing to buoyant forces, CO_2 tries to move up and escape out from the formation. As CO_2 is in the non-wetting phase in the formation, it has large capillary forces which help CO_2 sequestering if they are much larger than the buoyant forces, but there is the possibility of leakage if buoyant forces overcome these capillary forces (Bodipat et al., 2007).

Effective CO_2 sequestration is achieved by the overlying tight caprock having very low permeability and initially fully saturated with formation brine. The high capillary pressure resulted will prevent the penetration of CO_2 into that caprock and so to above strata. Consequently, the injection pressure must be below the capillary entry pressure and fracturing pressure of the caprock (Bennion and Bachu, 2007).

The sealing capacity of the caprock for a hydrocarbon-water system must be sufficient to prevent the leaking of CO_2 injected. Sealing capacity is a measure of the breakthrough pressure. The capillary pressure determines the breakthrough pressure of the caprock, so breakthrough pressure of the caprock should also be calculated. Furthermore, characterization of faulting and fractures must be understood in order to predict any CO_2 migration through these paths where the resistance to migration is very low.

Adesanya (2006) suggests that through the chemical trapping the carbonic acid (resulting from dissolution of CO_2 in water) may react with minerals in the caprock, causing corrosion in sealing bed and as a result, leaking of CO_2 may occur.

According to Redjao (2008), dehydration of the caprock by injecting dry CO_2 may lead to opening paths inside the caprock, through which the other amounts of CO_2 may leak out of the formations; therefore, to avoid this problem, brine-saturated CO_2 is injected instead of the dry one.

Ogamba (2010) states that the ability of the caprock to keep the CO_2 inside the formation depends on the capillary and mechanical forces; capillary failure occurs when the CO_2 pressure is higher than the pore entry pressure of the caprock, whereas the mechanical failure refers to fracturing that may occur in the caprock when the pressure of CO_2 is higher than fracturing pressure of the caprock. Tonnet et al. (2010), cited by Ogamba (2010), who mentioned that the mechanical failure may come from thermal effect that responsible of caprock expansion, by the effect of heat, which may generate fractures or reactivate the pre-existing faults.

Many methods are used to verify CO_2 leakage, for instance, observation of carbon dioxide concentrations in water and soils. PH monitoring can also provide information about CO_2 leakage since CO_2 dissolves in water to form carbonic acid. Moreover, bio-monitoring is reliable to verify CO_2 leakage since carbon dioxide is heavier than air and precipitates in soils which, leads to killing trees, bacteria and fungi.

1.4. Technical aspects relating to CO2 in the EOR process

1.4.1. The Basics of Carbon Dioxide EOR

As it is generally known, miscibility is the condition where two fluids can be mixed completely, where there is no interface between them (zero interfacial tension).

What does it mean to be miscible as a general conception? If there is some oil on a tool as an example and we want to clean that tool by removing the adherent oil, water will remove a little of the oil; water and soap will do a better job, but a solvent will remove every trace. This is because a solvent will mix with the oil, form a homogeneous mixture, and take the oil away from the tool's surface (U.S. department of energy 2010).

Similar miscible solvents could be used to clean out the oil from underground formations, but these products are refined from crude oil and therefore relatively expensive. The same goes for natural gas enriched with heavier hydrocarbons like propane; it is miscible with oil but also very expensive. Instead of these costly solvents, CO_2 could be used as a solvent to displace the oil from the rock since it is cheap and profusely available and can also easily enter all the pores in the rock due to its high mobility (U.S department of energy 2010).

Under specific conditions, when CO_2 is injected into an oil reservoir, it gets mutually soluble with the residual crude oil since the light hydrocarbons from the oil dissolve in the CO_2 and CO_2 dissolves in the oil; as a result, the interfacial tension between oil and CO_2 vanishes. This enables the CO_2 to displace the oil from the rock pores as a cleaning solvent which removes oil from tools; therefore, it is called miscible CO_2 flooding or CO_2 solvent flooding (U.S department of energy 2010).

Returning to CO_2 miscible flooding, first CO_2 is injected in the formation and moves through the pore spaces of the rock, meeting residual droplets of oil and becoming miscible with them. The oil swells and forms a concentrated oil bank which is to be swept towards the producing wells by water flooding (U.S department of energy 2010).

1.4.2. **WAG process**

The high mobility of CO_2 may cause fingering which leads to early breakthrough and, as a result, the sweep efficiency will be negatively affected. To overcome this problem, the WAG (Water Alternating Gas) is applied (Figure 1.17). In this method, water slugs and CO_2 slugs are alternately injected into the reservoir. The idea of this technique is that the water slugs will lower the mobility of the CO_2 and lead to a more piston-like displacement with higher displacement efficiencies (U.S department of energy 2010).

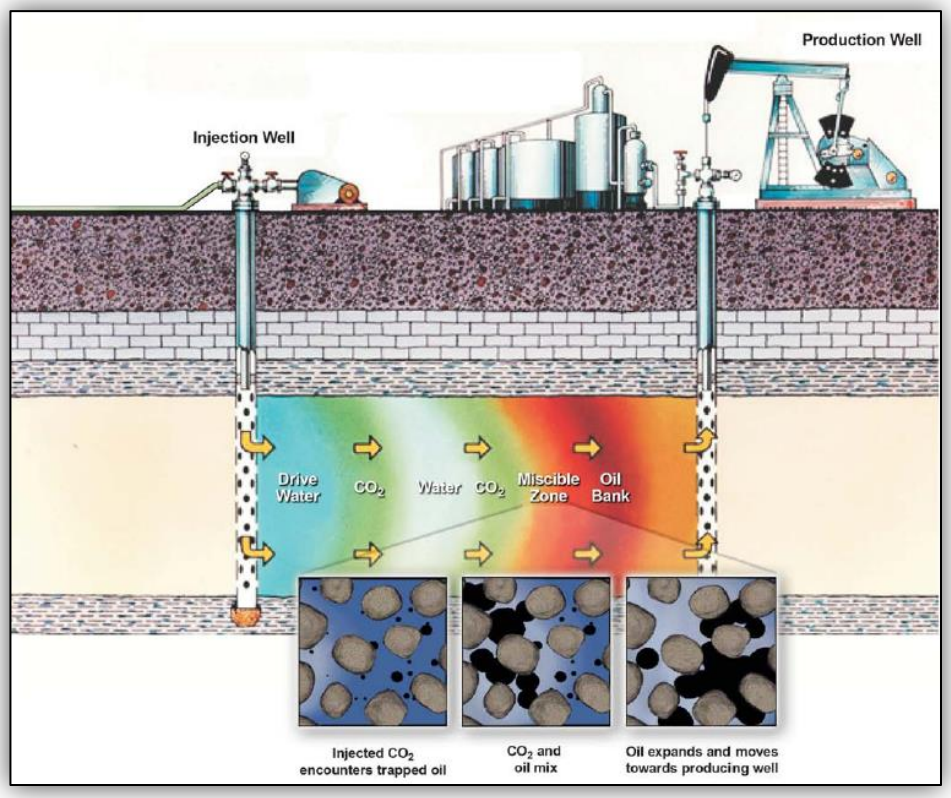

Figure 1.17: WAG Process (Bodipat et al., 2007)

1.4.3. **Additional benefits of using CO_2 in EOR**

An additional important advantage of miscible CO_2 flooding is reducing the oil viscosity, giving it higher mobility and making it easier for recovery.

Finally, using CO_2 in the enhanced oil recovery process will make the sequestration of CO_2 much more economical; consequently, more reduction of CO_2 emissions could be achievable in addition to EOR advantages.

1.5. Technical aspects relating to CO_2 in both CGS and EOR processes

1.5.1. CO_2 phase behaviour in deep formations

Marini (2006) and Ukaegbu (2007) reported that at standard conditions CO_2 is a gas, the critical pressure of CO_2 is 7.38 MPa (1070 Psi) and critical temperature of CO_2 is 30.76^{o}C (87.76^{o}F). Above these critical points, CO_2 will be in a supercritical phase (Figure 1.18), and according to Pruess et al. (2001), and Kiatsakulphan (2009), in order to keep CO_2 in a supercritical phase, the depth of formation in which CO_2 is being injected must not be less than 2600 ft. In the supercritical phase, CO_2 will be heavier like a liquid (Figure 1.19) but could penetrate the rocks and expand to fill the pores like gas. At the supercritical phase, high density of CO_2 (like liquid) means that the space required to store CO_2 will be less and the ability to penetrate the rocks (like gas) means the diffusion capability along the formation will be very high, so in order to maximize the aquifer storage capacity, the CO_2 must be injected in the supercritical phase conditions.

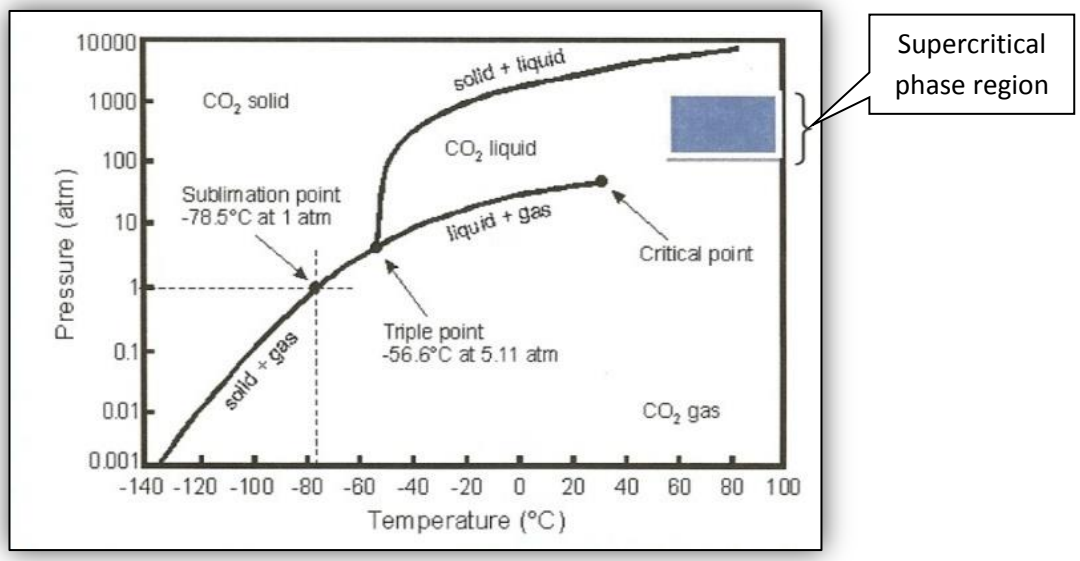

Figure 1.18: Supercritical region in phase diagram (Kiatsakulphan, 2009)

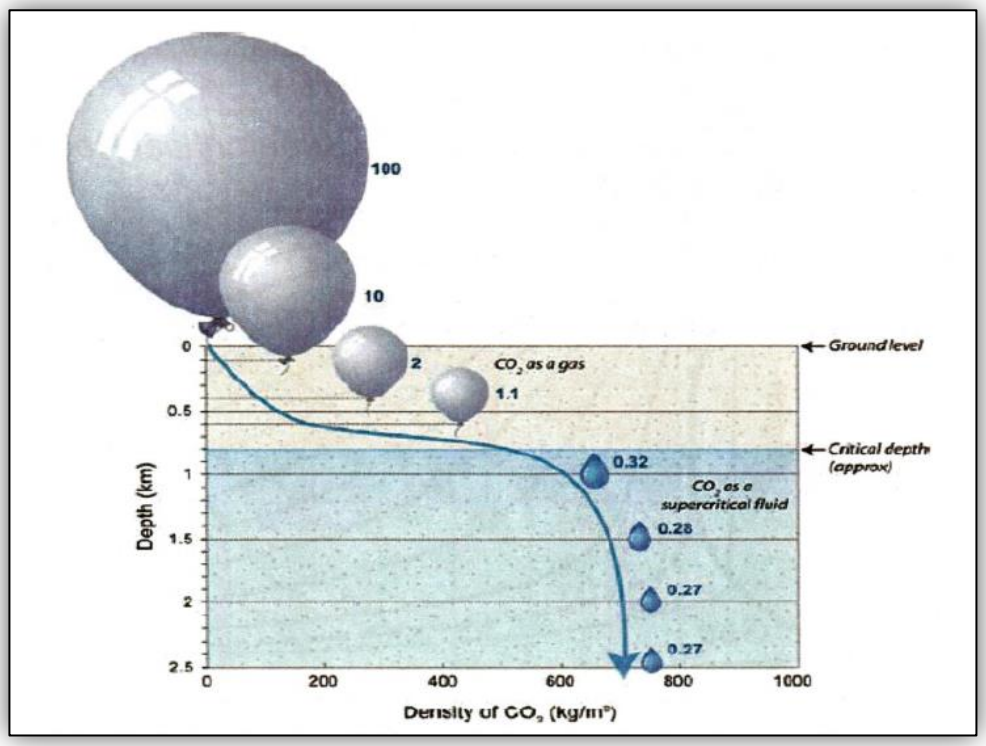

Figure 1.19: Density and unit volume of CO_2 vs. depth of injection (Success Donald, 2008)

1.5.2. CO_2 migration (flow) through geologic formations

CO_2 moves through the geologic formations (aquifer as an example) by different types of migration mechanisms such as:

A) **Advection**: CO_2 will move by the effect of pressure gradients, which means CO_2 flows away from high pressure zones towards low pressure zones. It is the same idea on which the Darcy's law was built (Ukaegbu, 2007). Through this mechanism and when the CO_2 is being injected under injection pressure, it penetrates the formation and forms plumes around the injection well; these plumes move inside the formation with velocity, called plume velocity of the CO_2, whereas plume migration is the distance the CO_2 and brine travel from injection point through the formation.

B) **Dissolution-Diffusion**: CO_2 will move by the effect of concentration or temperature gradients; CO_2 molecules will move from a higher concentration area to a lower concentration area in order to create concentration equilibrium (Ukaegbu, 2007). This movement may occur in all directions; therefore, diffusion is independent of orientation. Although diffusion is much slower in terms of movement than advection and buoyancy, it must be taken into account when talking about the long-term behaviour of CO_2 in the subsurface (Enwongulu, 2010).

During the diffusion process, and to calculate diffusion rates, it is necessary first to determine initial concentrations via CO_2 solubility. Generally, the solubility of CO_2 in water depends on temperature, pressure, and salinity (Pistone 2011). Dodds et al. (1956) did a set of experiments and the data produced were used to draw curves which represent the CO_2 solubility as a function of pressure and temperature (Figure 1.20). Since diffusion depends on CO_2 solubility, it is considered as a main factor affecting storage capacity of CO_2 in geologic formations (Ukaegbu, 2007).

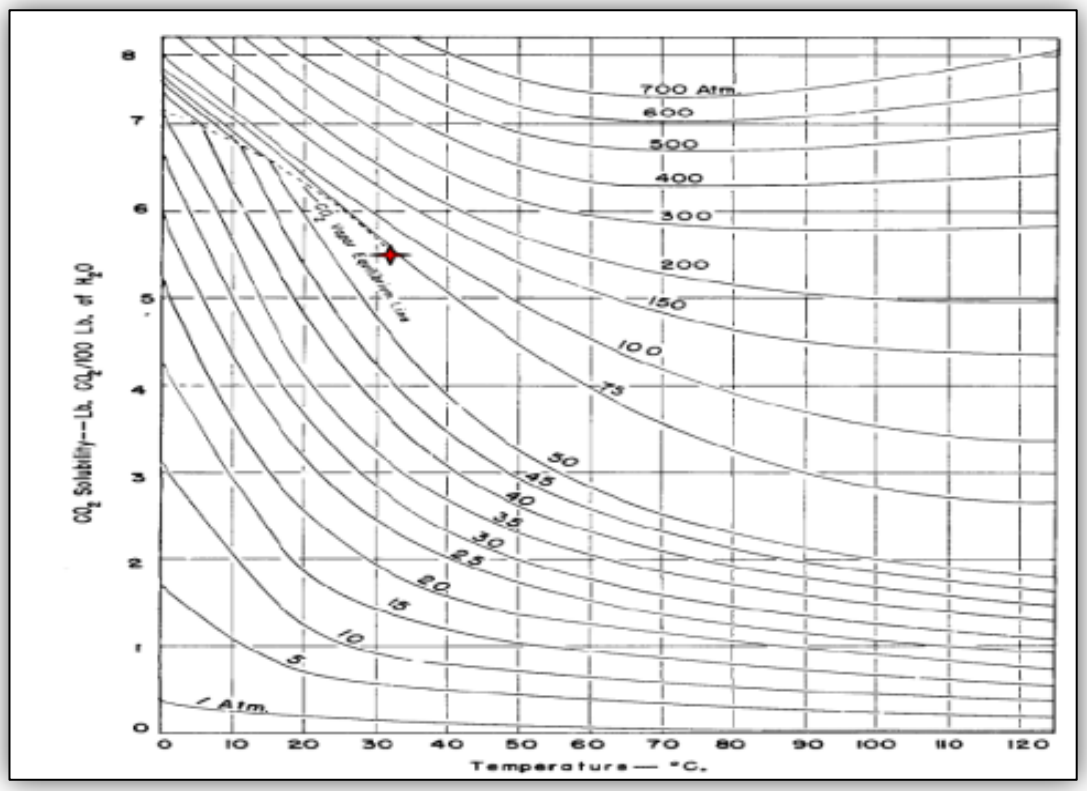

Figure 1.20: CO_2 solubility as a function of pressure and temperature (Dodds et al., 1956)

C) **Buoyancy**: CO_2 will move by the effect of density difference, since the CO_2 is lighter than other fluids so CO_2 will rise, this type of migration mechanism also depends on vertical permeability, (Ukaegbu, 2007).

D) **Active phase change (APC) phenomenon:** This concept was first presented by Chen (2005) during investigation of fundamental flow characteristics in steam-water systems. Stacey (2008) developed the concept for CO_2–water system, and depending on results obtained, this concept may serve as a fourth way of CO_2 migration, through which the CO_2 could flow in a disconnected phase in front of the main CO_2 front (Figure 1.21) (Pistone, 2011). This occurs owing to the effect of evolution, which means that the dissolved CO_2 will get free from the brine under the effect of pressure reduction, and the evolution may allow the flow to resume.

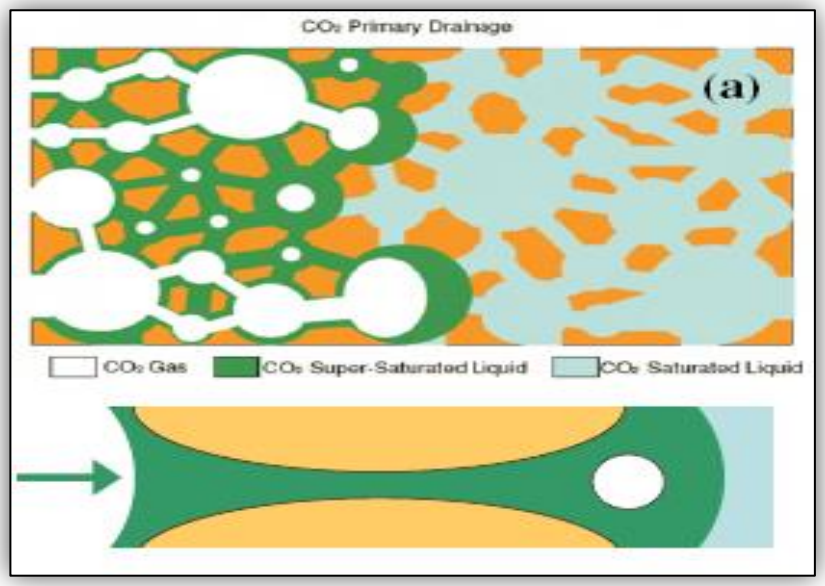

Figure 1.21: Active Phase Change phenomenon (Pistone 2011)

Generally and during the injection process, the advection transport mechanism is dominant, while the effect of buoyancy and diffusion will be clear after shut-in time point (Figure 1.22, Figure 1.23). All migration mechanisms mentioned above are classified as forces activate the flow of CO_2, while negative capillary pressure and CO_2 viscosity are considered as forces opposing the CO_2 flow and their negative effect appears mainly through advection and buoyancy migration processes. An additional important note relating to CO_2 transportation is that at high saturations CO_2 exists in continuous phase and moves freely since the forces that activate CO_2 flow are greater than forces opposing the flow, while in small saturation, like residual, CO_2 exists in discontinuous phase and cannot move easily.

Finally, both migration and trapping mechanisms mentioned above will substantially impact the capacity of CO_2 storage in geological formations.

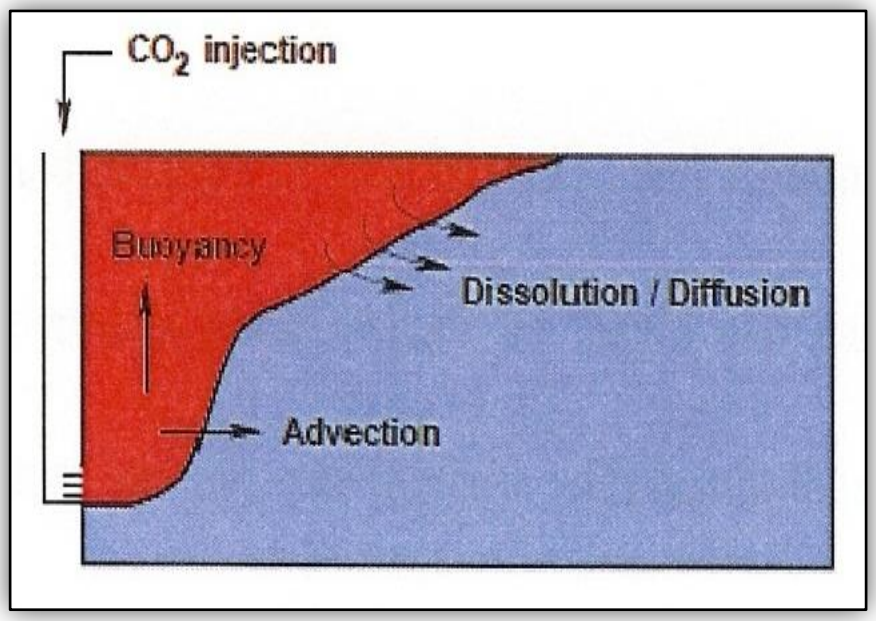

Figure 1.22: CO_2 migration mechanisms (Enwongulu, 2010)

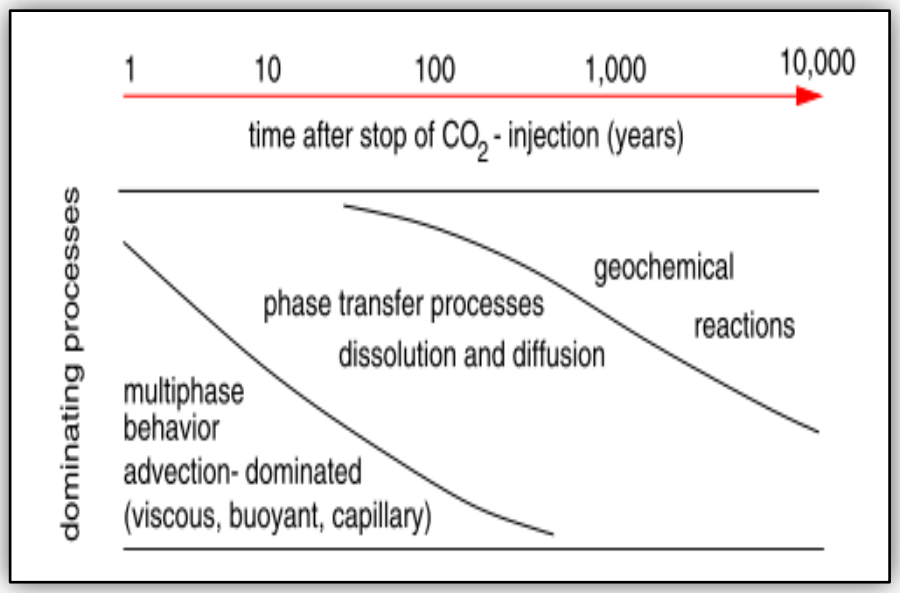

Figure 1.23: Dominant CO_2 migration mechanisms on different time scales (Class et al., 2009)

Krohn (2008), cited in Shariatipour (2010), tabulated the process and parameters of CO_2 migration in the saline aquifer as follows:

Process	Effect	Constant / Equation of state
Flow	Advection	Permeability Relative permeability – saturation relation Porosity Viscosity Density
	Capillary pressure	Capillary pressure – saturation pressure
	Phase changes	Solubility Vapour pressure
Transport	Diffusion	Diffusion coefficient Porosity tortuosity
	Dispersion	------
Heat flow	Conduction	Heat capacity Thermal conductivity Enthalpy Geothermal gradient

Table 1.4: Process and parameters of CO_2 migration in the saline aquifer

1.5.3. Factors affecting CO_2 distribution through the formations

The mentioned mechanisms of CO_2 migration and both the horizontal and vertical permeabilities are the main factors controlling the distribution of Co_2 inside the formation (Shariatipour, 2010), but in general, Obiora Ebuka (2010) argues that fluid distribution depends on pore scale factors including pore and throat distributions, viscosity ratios, wettability, interfacial tension, saturation history, density and flow velocities.

1.5.4. CO_2 and displacement process through geologic formations (field scale)

Displacement types

When CO_2 is being injected into geological formation, it displaces the fluid in the pores. The displacement process could be miscible or immiscible depending on the chemical composition of both CO_2 and other phases existing in the formation, as well as temperature and pressure (Bodipat et al., 2007).

A) Miscible displacement:

Under specific reservoir conditions (pressure and temperature), the CO_2 will be in the supercritical state. This supercritical CO_2 - with the presence of light oil compositions - could be miscible with oil phase forming a new single phase and as a result the IFT diminishes. Miscibility occurs as a result of mass transfer process, which means that the light hydrocarbons transfer from oil by vaporization mechanism to dissolve into CO_2, through which a miscible zone between oil and CO_2 is formed. The mixture produced will have a very small viscosity, which means the mobility of it will be very high, so the CO_2 may displace nearly the entire original fluid in the formation (AL-Quraini, 2006), so it could be said that CO_2 acts as a solvent to oil.

According to AL-Quraini (2006) and Nekouzad (2007), CO_2 is not completely miscible with the oil after the first contact, but as a matter of fact miscibility develops dynamically as CO_2 interacts gradually with more oil causing more mass transfer to be in between. This process is called Multiple Contact Miscibility (MCM).

In fact, the miscibility of CO_2 and oil depends mainly on pressure, and the minimum pressure required to get CO_2–oil miscibility is called a minimum miscibility pressure (MMP) (Nekouzad, 2007). The value of MMP is affected by the composition of crude oil, purity of CO_2 and reservoir temperature (Nekouzad, 2007, Sun, 2008). As the

reservoir temperature increases, the density of supercritical CO_2 decreases whereas the density of the oil increases as a result of light components' vaporization (U.S department of energy 2010).

According to Sun (2008), CO_2 has the lowest MMP compared with other gases, so it is the preferred gas in miscible flooding applications.

Since MMP is an essential parameter to miscibility of CO_2 and oil, in low-pressure reservoirs, re-pressurizing the formation by injecting water is necessary before starting CO_2 miscible process (Co_2 EOR) (U.S department of energy 2010, AL-Quraini, 2006). According to what was mentioned, the miscible CO_2 displacement is only applied when the CO_2 injection pressure is higher than that for MMP.

AL-Quraini (2006) and Nekouzad (2007) observed that the unstable flow (Viscous fingering) is the main challenge to miscible displacement and it could be explained in following words: CO_2 has a low viscosity; hence, high mobility, this disadvantage allows CO_2 to pass through oil rather than having miscibility with it. This problem is called viscous fingering. Another problem that may face the miscible displacement is the phase segregation that comes from either gravity impact (density differences between CO_2 and oil) or existence of high permeability in the reservoir. Both unstable flow and phase segregation problems may be caused by early breakthrough and as a result the sweep efficiency will be decreased.

To sum it up in a few words, when CO_2 is injected in the oil reservoirs and moves through the pore spaces of the rock, it meets residual droplets of oil and becomes miscible with the oil; the oil swells and forms a concentrated oil bank which is finally swept towards the producing wells by water flooding (U.S department of energy 2010). The oil swelling or expansion coefficient is very important in terms of the residual oil, since the greater the expansion of oil, the lower residual oil in the reservoir (Sun, 2008).

B) Immiscible displacement:

Immiscible displacement is applied when the reservoir's pressure is less than minimum miscibility pressure (MMP) or when the reservoir's oil only consists of heavy components since under such conditions the CO_2 cannot be fully miscible with oil (AL-Quraini, 2006). This is similar to solution gas drive in primary production stage and also similar to water injection in secondary oil recovery process which is used to maintain the reservoir's pressure as well as create a pushing force to drive the oil toward the

producing well (AL-Quraini, 2006). This type of displacement depends mainly on the force of CO_2 injecting pressure to increase the relative permeability of fluids, and through immiscible displacement. There are two displacement processes: the first one is displacement of water and/or oil by CO_2, and the other is displacement of CO_2 by water and/or oil during influx of fluids from adjacent aquifers or reservoirs.

Generally, in EOR the miscible CO_2 displacement is preferred as the immiscible displacement may cause fingering in which CO_2 may bypass some of reservoir fluids and leave them behind.

Another important point to notice is that it is found that through immiscible projects, a larger amount of CO_2 could be stored compared with miscible projects (Nekouzad, 2007).

The three main issues regarding the immiscible displacement are:

i. Immiscible displacement mechanisms:

There are three well-known mechanisms for immiscible displacement as follows:

- Piston like displacement
- Snap-off (Akbarabadi and Piri, 2013, Al-Dhahli, 2013).
- Pore-body filling (Akbarabadi and Piri, 2013, Al-Dhahli, 2013)

ii. The Immiscible displacement could happen under the effect of two forces:

- Injection pressure (viscous forces) is the dominant force during the injection process.
- Gravity force, which is dominant after injection suspension.

iii. Regional fronts:

The CO_2 **immiscible displacement** in deep formations (brine as an example) could be recognized with three regional fronts (Figure 1.24,Figure 1.25) including:

- Near wellbore or CO_2 / dry gas region.
- Buckley – Leverett of two–phase region.

- Brine region.

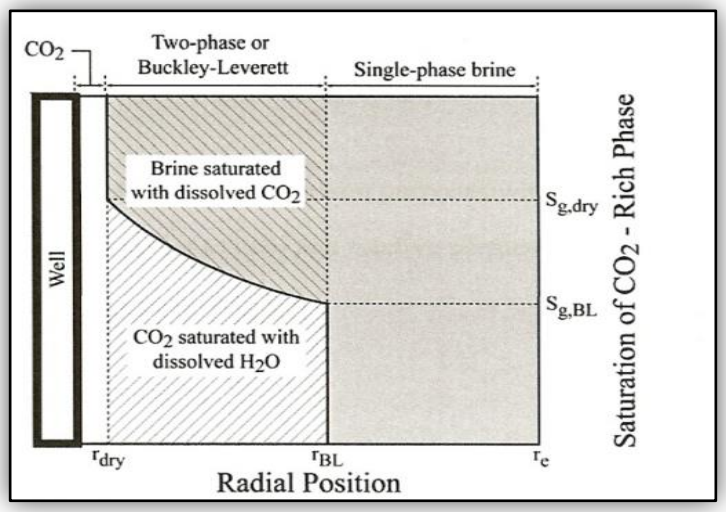

Figure 1.24: Three regional fronts of Co_2 injection

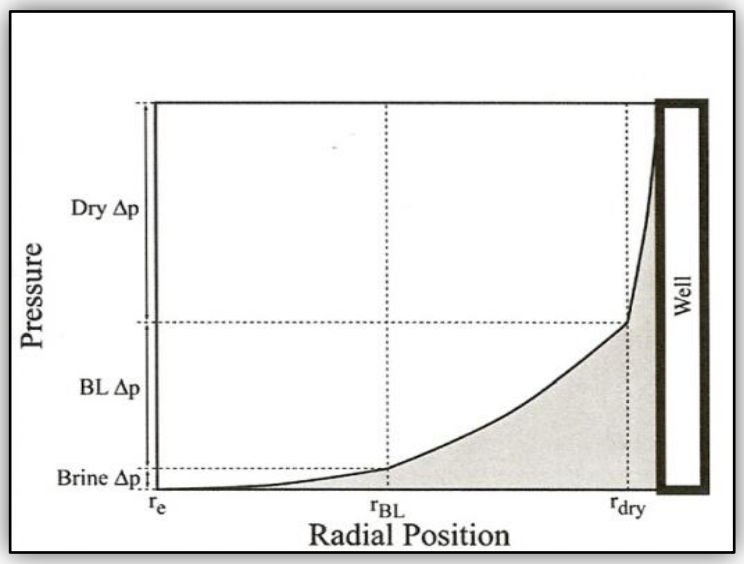

Figure 1.25: Pressure drop associated with CO_2 injection

To raise the immiscible displacement efficiency, the CO_2 should be prevented from dissolution in brine, which could be achieved by injecting brine-saturated CO_2.

C) Near miscible displacement:

This type of displacement could be obtained when the IFT's value between CO_2 and other phases is very low but not zero.

1.5.5. **Important points**

There are some important factors and parameters relating to CO_2 and other fluids through EOR or CO_2 geological storage processes, which are summarized below:

- Relative permeabilities including hysteresis, residual saturations and rock composition
- Viscosities and capillary pressures
- CO_2 Injection pressure and injection rate

The factors/parameters mentioned above have interactive relations with CO_2 migration, trapping and types of displacement (all of which are inter-active). For example, the residual trapping in immiscible displacement depends on displacement efficiency and rock composition (wettability), while the relative permeability is considered as a result of displacement that depends on capillary pressures and so on.

1.6. Monitoring CO_2 injected in geologic formations:

It is very important to monitor the CO_2 during the injection process since it gives a clear idea about how CO_2 migrates all over the formation and to confirm that the injected CO_2 is retained in the formation, Kiatsakulphan (2009) added that the monitoring of CO_2 is very important to evaluate the effectiveness of storage site and potential of leakage.

Several methods are used for monitoring the injected CO_2 (determining CO_2 concentration and aerial extension) such as Time-Lapse, seismic surveying and chemical tracing (Al-Abri, 2003).

It has been confirmed that Time-Lapse seismic gives accurate results when used to monitor CO_2 injection into saline aquifers. The tracking of CO_2 migration is done by analysing the reflective seismic waves coming from the formation (Arts et al., 2004).

Chemical tracing is executed by adding chemical Traces like fluorescent dye, perfluorocarbons, and SF6 to CO_2 over injection process and then by tracking these Tracers throughout the time the migration paths of CO_2 inside the formation could be determined (Emberley et al., 2004).

Generally, the tracers could be classified into two categories: radioactive and non-radioactive (Du and Guan, 2005).

Many advantages could be offered when using perfluorocarbon tracers (Senum et al., 1992) including the following:

- The background concentrations of perfluorocarbon tracers in the subsurface and atmosphere are negligible.
- Perfluorocarbon tracers are inflammable and non-toxic so they are safe for the environment.
- Perfluorocarbon tracers could be detected even with very low concentration like a level of pictogram/litre. Detection of perfluorocarbon Tracers could be done by using gas chromatography in conjunction with electron capture detectors.

1.7. CO_2 relative permeability effect on CO_2 injection and storage

It is assumed that the CO_2 relative permeability is a major parameter affecting the injecting and storage of CO_2 in deep formations like saline aquifers. Bennion and Bachu (2005) reported that all the processes of CO_2 injection, migration and sequestration (by residual or capillary trapping) depend on the relative permeability of CO_2 in addition to formation water systems and CO_2–brine capillary pressures.

The following two chapters will investigate the relative permeability in general first, and then focus on the relative permeability.

Refecences

ABACI, S., EDWARDS, J. S. & WHITTAKER, B. N. 1992. Relative permeability measurements for two phase flow in unconsolidated sands. *Mine Water and the Environment,* 11**,** 11-26.

ABDU, S. M. 2007. *Issues surrounding injection of Co2 in Utsira formation : Sleipner.* Msc project, Heriot - Watt umiversity.

ABDUL, O. A. 2010. *A study of termal effects on Co2 injection in saline aquifers.* Msc project, Heriot - Watt umiversity.

ADESANYA, L. 2006. *Co2 storage capacity of depleted gas fields, Esmond field case study.* Msc project, Heriot - Watt university.

AKBARABADI, M. & PIRI, M. 2013. Relative permeability hysteresis and capillary trapping characteristics of supercritical CO2/brine systems: An experimental study at reservoir conditions. *Advances in Water Resources,* 52**,** 190-206.

AL-ABRI, M. 2003. *Co2 Sequestration in saline Aquifer* Msc project, Heriot - Watt university.

AL-DHAHLI, A. 2013. *PORE TO F I E LD SCALE MODE L L ING OF THRE E PHASE FLOW PROCE SSES IN HET EROGENEOUS RES ERVOIRS WITH ARB ITRARY WE TTAB I L I TY.*, Heriot-Watt.

AL-HASHAMI, A. K. Y. 2004. *Co2 injection for enhanced gas recovery and geological storage.* Msc project, Heriot - Watt university.

AL-QURAINI, A. 2006. <*Enhanced oil recovery by water and Co2 injection in heavy oil reservoirs .pdf*>. Msc project., Heriot -Watt university.

ARTS, R., EIKEN, O., CHADWICK, A., ZWEIGEL, P., VAN DER MEER, L. & ZINSZNER, B. 2004. Monitoring of CO2 injected at Sleipner using time-lapse seismic data. *Energy,* 29**,** 1383-1392.

AULAQI, T. 2008. *Development of steam-Co2 assisted gravity drainage process in fractured reservoir.* Msc project, Heriot - Watt umiversity.

BENNION, B. & BACHU, S. 2005. Relative Permeability Characteristics for Supercritical CO2 Displacing Water in a Variety of Potential Sequestration Zones in the Western Canada Sedimentary Basin. *SPE Annual Technical Conference and Exhibition.* Dallas, Texas: Society of Petroleum Engineers.

BENNION, D. B. & BACHU, S. 2007. Permeability and Relative Permeability Measurements at Reservoir Conditions for CO2-Water Systems in Ultra Low Permeability Confining Caprocks. *EUROPEC/EAGE Conference and Exhibition.* London, U.K.: Society of Petroleum Engineers.

BENNION, D. B. & BACHU, S. 2010. Drainage and Imbibition CO2/Brine Relative Permeability Curves at Reservoir Conditions for High-Permeability Carbonate Rocks. *SPE Annual Technical Conference and Exhibition.* Florence, Italy: Society of Petroleum Engineers.

BENSON, S. M., TOMUTSA, L., SILIN, D., KNEAFSEY, T. & MILJKOVIC, L. 2005. Core scale and pore scale studies of carbon dioxide migration in saline formations.

BIELINSKI, A. 2007. Numerical simulation of CO2 sequestration in geological formations.

BLUNT, M. J. & CHRISTIE, M. A. 1994. Theory of Viscous Fingering in Two Phase, Three Component Flow. *SPE Advanced Technology Series,* 2**,** 52-60.

BODIPAT, K., DHIRAJ, D., FRYE, E., HUE, L. & MCCABE, T. 2007. Carbon capture and storge. Available: http://www.ems.psu.edu/~elsworth/courses/egee580/2010/Final%20Reports/Final_Report_CCS.pdf.

CHE, N. 2010. *The effect of the topograpgy of the top of an aquifer on Co2 stirage.* Msc project, Heriot - Watt umiversity.

CHEN, Z. 2005. *Liquid-gas relative permeabilities in fractures: effects of flow structures, phase transformation and surface roughness*, Stanford University.

CLASS, H., EBIGBO, A., HELMIG, R., DAHLE, H., NORDBOTTEN, J., CELIA, M., AUDIGANE, P., DARCIS, M., ENNIS-KING, J., FAN, Y., FLEMISCH, B., GASDA, S., JIN, M., KRUG, S., LABREGERE, D., NADERI BENI, A., PAWAR, R., SBAI, A., THOMAS, S., TRENTY, L. & WEI, L. 2009. A benchmark study on problems related to CO2 storage in geologic formations. *Computational Geosciences,* 13**,** 409-434.

CONSTABLE, K. C. 2003. *Issues regarding the modeling of WAG and SWAG process with Eclipse.* Msc project, Heriot - Watt university.

DAVISON, J. & THAMBIMUTHU, K. 2009. An overview of technologies and costs of carbon dioxide capture in power generation. *Proceedings of the Institution of Mechanical Engineers, Part A: Journal of Power and Energy,* 223**,** 201-212.

DODDS, W. S., STUTZMAN, L. F. & SOLLAMI, B. J. 1956. Carbon Dioxide Solubility in Water. *Industrial & Engineering Chemistry Chemical & Engineering Data Series,* 1**,** 92-95.

DU, Y. & GUAN, L. 2005. Interwell Tracer Tests: Lessons Learnted from Past Field Studies. *SPE Asia Pacific Oil and Gas Conference and Exhibition.* Jakarta, Indonesia: Society of Petroleum Engineers.

EKOJA, G. A. 2009. *Streamline simulation of Co2 stirage in deep saline aquifers.* Msc project, Heriot - Watt university.

EMBERLEY, S., HUTCHEON, I., SHEVALIER, M., DUROCHER, K., GUNTER, W. D. & PERKINS, E. H. 2004. Geochemical monitoring of fluid-rock interaction and CO2 storage at the Weyburn CO2-injection enhanced oil recovery site, Saskatchewan, Canada. *Energy,* 29**,** 1393-1401.

ENERGY, U. S. D. O. 2007. *Emissions of Greenhouse Gases in the United States 2006.* [Online]. U.S. Department of Energy ,Energy Information Administration. Available: http://www.eia.gov/pub/oiaf/1605/cdrom/pdf/ggrpt/057306.pdf.

ENNIS-KING, J. & PATERSON, L. 2002. Engineering Aspects of Geological Sequestration of Carbon Dioxide. *SPE Asia Pacific Oil and Gas Conference and Exhibition.* Melbourne, Australia: Copyright 2002, Society of Petroleum Engineers Inc.

ENWONGULU, M. E. 2010. *The CIPR Co2 Benchmark study.*, Heriot - Watt umiversity.

ENYINNAYA, U. C. 2009. *Numerical simulation of Co2 injection For heavy oil Recovery.* Msc project, Heriot - Watt university.

FIGUEROA, J. D., FOUT, T., PLASYNSKI, S., MCILVRIED, H. & SRIVASTAVA, R. D. 2008. Advances in CO< sub> 2</sub> capture technology—The US Department of Energy's Carbon Sequestration Program. *International Journal of Greenhouse Gas Control,* 2**,** 9-20.

GALE, J. Overview of CO2 emissions sources, potential, transport and geographical distribution of storage possibilities. Proceedings of the workshop on CO2 dioxide capture and storage, Regina, Canada, 2002. Citeseer, 15-29.

GARCIA-OLVERA, G. 2009. *Co2 EOR for an extra heavy oil in a carbonate reservoir.* Msc project, Heriot - Watt umiversity.

GHANBARI, S. 2004. <*Simulation of Co2 storage in Saline Aquifers using STARS-CMG Simulator.pdf*>. Msc project, Heriot - Watt university.

GHANBARI, S., AL-ZAABI, Y., PICKUP, G. E., MACKAY, E., GOZALPOUR, F. & TODD, A. C. 2006. Simulation of CO2 Storage In Saline Aquifers. *Chemical Engineering Research and Design,* 84**,** 764-775.

GUNTER, W. D., WIWEHAR, B. & PERKINS, E. H. 1997. Aquifer disposal of CO2-rich greenhouse gases: Extension of the time scale of experiment for CO2-sequestering reactions by geochemical modelling. *Mineralogy and Petrology,* 59**,** 121-140.

HAJNASSER, Y. 2010. *Effect od discontinuous intra-reservoir Shales on Co2 storage.*, Heriot - Watt umiversity.

HOLM, L. W. 1976. Status of CO2 and Hydrocarbon Miscible Oil Recovery Methods. *Journal of Petroleum Technology,* 28**,** 76-84.

HOLM, L. W. & JOSENDAL, V. A. 1974. Mechanisms of Oil Displacement By Carbon Dioxide. *Journal of Petroleum Technology,* 26**,** 1427-1438.

HOLT, T., LINDEBERG, E. G. B. & TABER, J. J. 2000. Technologies and Possibilities for Larger-Scale CO2 Separation and Underground Storage. *SPE Annual Technical Conference and Exhibition.* Dallas, Texas: 2000,. Society of Petroleum Engineers Inc.

HOUGHTON, J. T., DING, Y., GRIGGS, D. J., NOGUER, M., VAN DER LINDEN, P. J., DAI, X., MASKELL, K. & JOHNSON, C. 2001. *Climate change 2001: the scientific basis*, Cambridge University Press Cambridge.

HUANG, E. T. S. & TRACHT, J. H. 1974. The Displacement of Residual Oil By Carbon Dioxide. *SPE Improved Oil Recovery Symposium.* Tulsa, Oklahoma: 1974 Copyright 1974, American Institute of Mining, Metallurgical and Petroleum Engineers Inc.

ILAMAH, O. 2007. *Modelling the Effect of small-scale Heterogeneity on Co2 storage.*, Heriot - Watt university.

IMBAZI, O. 2009. *A study of termal effects of subsurface storage of Co2.* Msc project, Heriot - Watt umiversity.

IPCC 2005. IPCC Special Report on Carbon Dioxide Capture and Storage. *Prepared by Working Group III of the Intergovernmental Panel on Climate Change [Metz, B., O. Davidson, H. C. de Coninck, M. Loos, and L. A. Meyer (eds.)]. Cambridge University Press, Cambridge, United Kingdom and New York, NY, USA, 442 pp.*

JENKINS, C., AL-SHARIF, S., HARRIS, R., WEISGRAM, J. & MICHEL, D. 2004. Forty Years of Improved Oil Recovery: Lessons from Low-Permeability Turbidites of the East Wilmington Field, California. *SPE International Petroleum Conference in Mexico.* Puebla Pue., Mexico: Society of Petroleum Engineers.

JOHNSON, T. 2009. *Carbon dioxide storage in a saline aquifer using a Turbbidite model.* Msc project, Heriot - Watt umiversity.

JUANES, R., SPITERI, E. J., ORR, F. M. & BLUNT, M. J. 2006. Impact of relative permeability hysteresis on geological CO2 storage. *Water Resources Research,* 42**,** W12418.

KAMPMAN, N. 2006. *Co2 storage and monitoring in the Ketzin aquifer, Germany.* Msc project, Heriot - Watt umiversity.

KEELING, C. & WHORF, T. 2005. Atmospheric carbon dioxide record from Mauna Loa. *Trends: A Compendium of Data on Global Change. Carbon Dioxide Information Analysis Center, Oak Ridge National Laboratory, Oak Ridge, TN*.

KIATSAKULPHAN, M. 2009. *The effects of grid resolution on the simulation of Co2 storage in deep saline aquifers.* Msc project, Heriot - Watt umiversity.

KONTOURIS, I. 2008. *Sensitivity study of Co2 EGR.* Msc project, Heriot - Watt umiversity.

KRAUSKOPF, K. B. & BIRD, D. K. 1967. *Introduction to geochemistry*, McGraw-Hill New York.

KROHN, K. P. 2008. Values required for the simulation of Co2 in saline aquifers.

KUMAR, A., NOH, M. H., OZAH, R. C., POPE, G. A., BRYANT, S. L., SEPEHRNOORI, K. & LAKE, L. W. 2005. Reservoir Simulation of CO2 Storage in Deep Saline Aquifers. *SPE Journal,* 10**,** pp. 336-348.

LEVINE, J. 2011. Relative Permeability Experiments of Carbon Dioxide Displacing Brine and Their Implications for Carbon Sequestration.

MARINI, L. 2006. *Geological sequestration of carbon dioxide: thermodynamics, kinetics, and reaction path modeling,* Access Online via Elsevier.

MARLAND, G., BODEN, T. A., ANDRES, R. J., BRENKERT, A. & JOHNSTON, C. 2003. Global, regional, and national fossil fuel CO2 emissions. *Trends: A compendium of data on global change***,** 34-43.

MASSAMBA, M. 2009. *A review on EOR with reference to supercritical Co2 and Microbial methods.* Msc project, Heriot - Watt umiversity.

MUSHTAG, A. 2010. *Evironmental & Economic Impact of H2S Associated oil & gas.* . Msc project, Heriot - Watt umiversity.

NEKOUZAD, M. 2007. *Study of effects of thickneses , viscosity and depth in Co2 injection in heavy oil reservoirs.* . Heriot - Watt university.

NGHIEM, L., SAMMON, P., GRABENSTETTER, J. & OHKUMA, H. 2004. Modeling CO2 Storage in Aquifers with a Fully-Coupled Geochemical EOS Compositional Simulator. *SPE/DOE Symposium on Improved Oil Recovery*. Tulsa, Oklahoma: Society of Petroleum Engineers.

O'RIORDAN, M., JAMES, A., RAE, S. & WRIXON, A. 1983. Human Exposure to Radon Decay Products Inside Dwellings in the United Kingdom--a Memorandum of Evidence to the Royal Commission on Environmental Pollution.(NRPB-R 152). *National Radiological Protection Board, v+ 41, A 4, pounds sterling 3. 00, 1983*.

OBIORA EBUKA, E. 2010. *<Review of how relative permeability is measured expermentally for use in numerical simulation.pdf>*. Msc project., Heriot - Watt university.

OGAMBA, U. M. 2010. *Effectiveness of the Ballagan formation as Seal for Co2 storage.* Msc project, Heriot - Watt umiversity.

OSPINA, M. 2007. *Effect of geochemical process on Co2 storage in a typical North Sea reservoir.* . Msc project, Heriot - Watt umiversity.

PISTONE , S. 2011. *The significance of co2 solubility in deep subsurface environments.*, Stanford University.

PISTONE, S. 2011. *The significance of co2 solubility in deep subsurface environments.*, Stanford University.

PRUESS, K., GARCÍA, J., KOVSCEK, T., OLDENBURG, C., RUTQVIST, J., STEEFEL, C. & XU, T. 2004. Code intercomparison builds confidence in numerical simulation models for geologic disposal of CO2. *Energy,* 29**,** 1431-1444.

PRUESS, K., XU, T., APPS, J. & GARCIA, J. 2001. Numerical Modeling of Aquifer Disposal of CO2. *SPE/EPA/DOE Exploration and Production Environmental Conference.* San Antonio, Texas.

QI, R. 2009. *Simulation of geological carbon dioxide storage.* Imperial College London.

REDJAO, N. 2008. *Co2 storage in deep saline aquifers : fining up and corsening up sequences.* Msc project, Heriot - Watt umiversity.

RYAZANOV, A. 2011. *Pore-Scale Network Modelling of Residual Oil Saturation in Mixed-Wet Systems.*, Heriot - Watt university.

SAADAWI, O. 2010. *Streamline simulation of Co2 storage in saline aquifers.* Msc project, Heriot - Watt university.

SENUM, G. I., FAJER, R., DEROSE, W. E., HARRIS JR., B. R. & OTTAVIANI, W. L. 1992. Petroleum Reservoir Characterization by Perfluorocarbon Tracers. *SPE/DOE Enhanced Oil Recovery Symposium.* Tulsa, Oklahoma: Not subject to copyright. This document was prepared by government employees or with government funding that places it in the public domain.

SHARIATIPOUR, S. M. 2010. *Flow simulation of Co2 storage in saline aquifers using black oil simulator.* Msc project, Heriot - Watt university.

SHEHATA, A. M., EL-BANBI, A. H. & SAYYOUH, H. 2012. Guidelines to Optimize CO2 EOR in Heterogeneous Reservoirs. *North Africa Technical Conference and Exhibition.* Cairo, Egypt: Society of Petroleum Engineers.

SOHRABI, M., RIAZI, M., BERNSTONE, C., JAMIOLAHMADY, M. & CHRISTENSEN, N.-P. 2012. New Insights Into CO2 Injection and Storage in Saline Aquifers. *SPE Europec/EAGE Annual Conference.* Copenhagen, Denmark: Society of Petroleum Engineers.

STACEY, R. 2008. *The Impact of dynamic dissolution on Carbon dioxide sequestration in Aquifers.*, Stanford University.

SUCCESS DONALD, A. 2008. *Thermal Effects on subsurface Co2 storage.* Msc project, Heriot - Watt umiversity.

SUEKANE, T., NOBUSO, T., HIRAI, S. & KIYOTA, M. 2008. Geological storage of carbon dioxide by residual gas and solubility trapping. *International Journal of Greenhouse Gas Control,* 2**,** 58-64.

SUN, H. 2008. *Assessment of Co2 storage in C-Field of Jiangsu oilfield China.* . Msc project, Heriot - Watt umiversity.

TONNET, N., BROSETA, D. F. & MOURONVAL, G. R. 2010. Evaluation of the Petrophysical Properties of a Carbonate-rich Caprock for CO2 Geological Storage Purposes. *SPE EUROPEC/EAGE Annual Conference and Exhibition.* Barcelona, Spain: Society of Petroleum Engineers.

U.S DEPARTMENT OF ENERGY , N. 2010. *Carbon Dioxide Enhanced Oil Recovery* [Online]. Available: http://www.netl.doe.gov/technologies/oil-gas/publications/EP/CO2_EOR_Primer.pdf 2012].

UKAEGBU, C. 2007. *<Co2 Storage and Tracer monitoring in Ketzin using GEM-GHG.pdf>*. Msc project, Heriot - Watt umiversity.

VICTOR, B. T. 2008. *Simulation of Co2 EOR in heterogeneous models.* Msc project, Heriot - Watt umiversity.

XU, T., APPS, J. A. & PRUESS, K. 2004. Numerical simulation of CO2 disposal by mineral trapping in deep aquifers. *Applied Geochemistry,* 19**,** 917-936.

ZUO, L., KREVOR, S., FALTA, R. & BENSON, S. 2012. An Experimental Study of CO2 Exsolution and Relative Permeability Measurements During CO2 Saturated Water Depressurization. *Transport in Porous Media,* 91**,** 459-478.

Chapter 2

Relative permeability in general

(Fundamental aspects of relative permeability)

2.1. Relative permeability concept

As it is known, the absolute permeability concept is a capacity measure for the medium to transmit one fluid through it, but when two fluids or more exist in the medium, the transmit capacity (of the rock) for each fluid separately is called effective permeability (Figure 2.1) which is affected by the fluid's saturation and wetting characteristics of that fluid. The summation of effective permeabilities (of all fluids) is equal to absolute permeability.

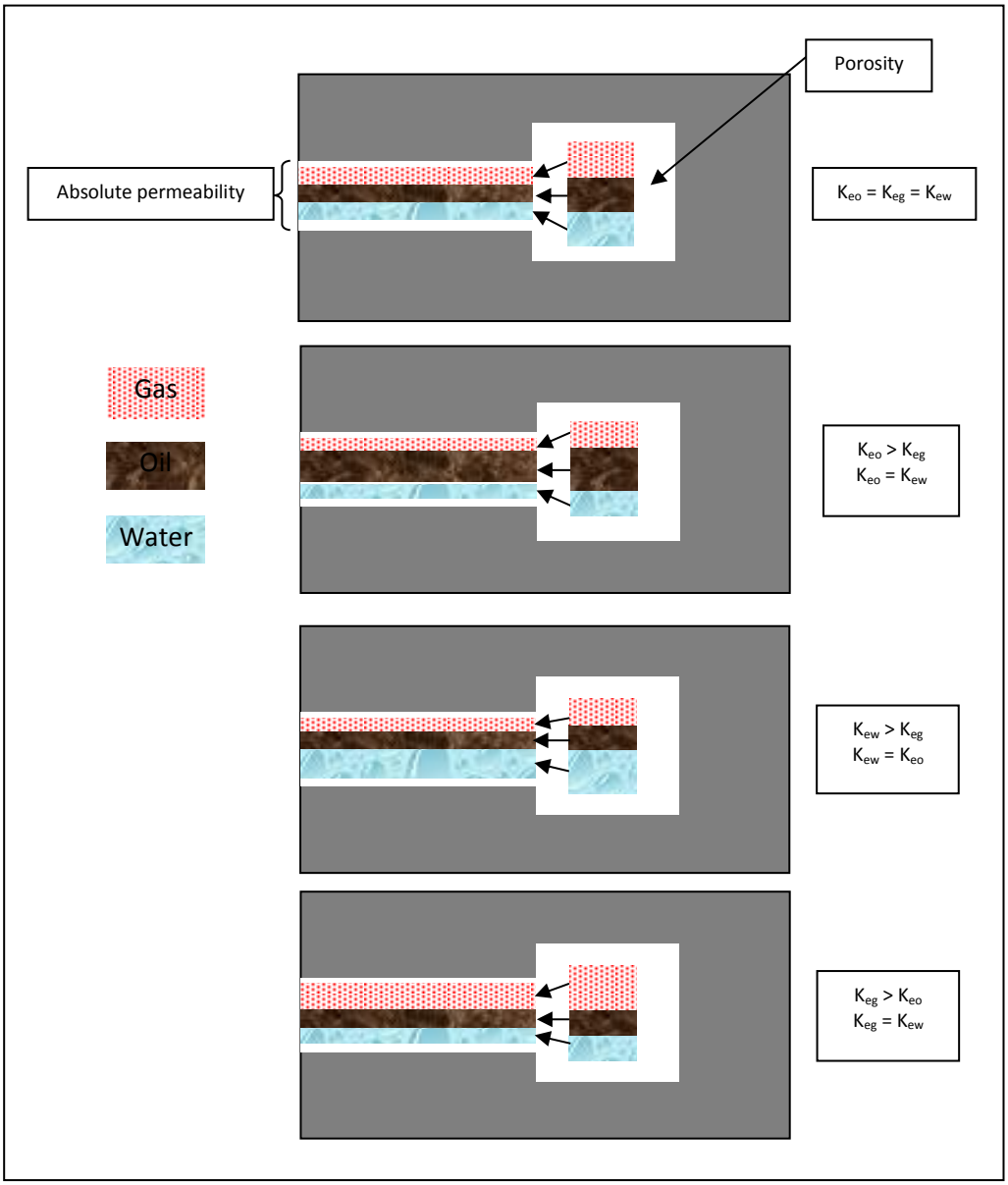

Figure 2.1: Relative permeability concept

Correlating the effective permeability

It has been found that the effective permeability for a certain fluid is affected considerably by reservoir heterogeneity (changing absolute permeability with direction), so in a heterogeneous reservoir and for a certain fluid there are a range of effective permeabilities as the absolute permeability varies with direction (Abu-Khamsin, 2004), and to beat this problem, the reservoir engineers have adopted the concept of the fluid's relative permeability, which is simply defined as the ratio of the fluid's effective permeability to base permeability:

$$k_{ri} = \frac{k_{ei}}{k_{base}} \qquad \text{Eq. 2.1}$$

Where:

k_{ri} = the relative permeability to fluid (i) at a certain saturation of fluid of the same fluid

k_{ei} = the effective permeability to fluid (i) at a certain saturation of fluid of the same fluid

K_{base} = could be absolute permeability (measured by using liquid or air) or the effective permeability of fluid (i) at irreducible saturation of other existing fluids (see paragraph 2.2)

According to Abu-Khamsin (2004), plotting all relative permeability curves set to one fluid in the reservoir (each set based on its own base permeability) will result in combining all relative permeability curves of that fluid into one curve; the curve produced represents the percentage of effective permeability for a certain fluid to base permeability in terms of the whole reservoir. Theoretically, the summation of relative permeabilities of all fluids always equal to unity. As known, each porous rock system has unique relative permeability characteristics. Honarpour et al. (1986) mentioned that Muskat and Meres are the first who introduced the concept of relative permeability; they extended Darcy's law to the two-phase system. For oil reservoirs, the relevant two-phase fluid combinations are liquid-gas (usually thought of as oil-gas) and water-oil. The relative permeability curves of Gas-water system are used to describe the performance of gas reservoirs and gas-liquid curves are used for condensate reservoir.

2.2. Base permeability and relative permeability

The absolute permeability concept is a permeability of the rock when saturated 100% with one fluid that doesn't react with rock components; the fluid could be liquid or gas, and in many cases the absolute permeability is measured by using the dry air at atmospheric pressure and then called dry air permeability K_{air}.

The relative permeability is effective permeability divided by base permeability. The base permeability could be absolute permeability (measured by using liquid or air) or the effective permeability of the hydrocarbon phases at irreducible water saturation S_{wi}. The three types of base permeabilities are different from each other in value, so that the relative permeability value is depending on which type of base permeability has been used.

Something which cannot be overlooked is that when dealing with relative permeability ratios ($\frac{k_{rg}}{k_{ro}}$, $\frac{k_{rw}}{k_{ro}}$), both of the relative permeabilities should be calculated depending on the same base permeability.

2.3. Effective or normalized saturation

As Standing (1975) states, since the relative permeability of any phase, including that for wetting phase, is mainly depending on mobile amount of that phase, the irreducible amount of wetting phase (which is immobile) and smallest pores (where that irreducible saturation exists) may be excluded from the saturations calculation. This procedure produces the effective or normalized saturation which is defined as a fluid saturation as a fraction of mobile fluids only.

Effective or normalized saturations are indicated by using superscript asterisk or subscript (e), such as, (S_w^* / S_{we}), (S_o^* / S_{oe}) , (S_g^* / S_{ge}) for water and oil and gas respectively.

If the rock is water wet, then:

$$S_w^* = \frac{(S_w - S_{wi})}{(1 - S_{wi})} \qquad \text{Eq. 2.2}$$

$$S_o^* = \frac{S_o}{(1 - S_{wi})} \qquad \text{Eq. 2.3}$$

$$S_g^* = \frac{S_g}{(1-S_{wi})}$$ Eq. 2.4

Pore saturations and their corresponding effective or normalized saturation are showed in the Figure 2.2 below:

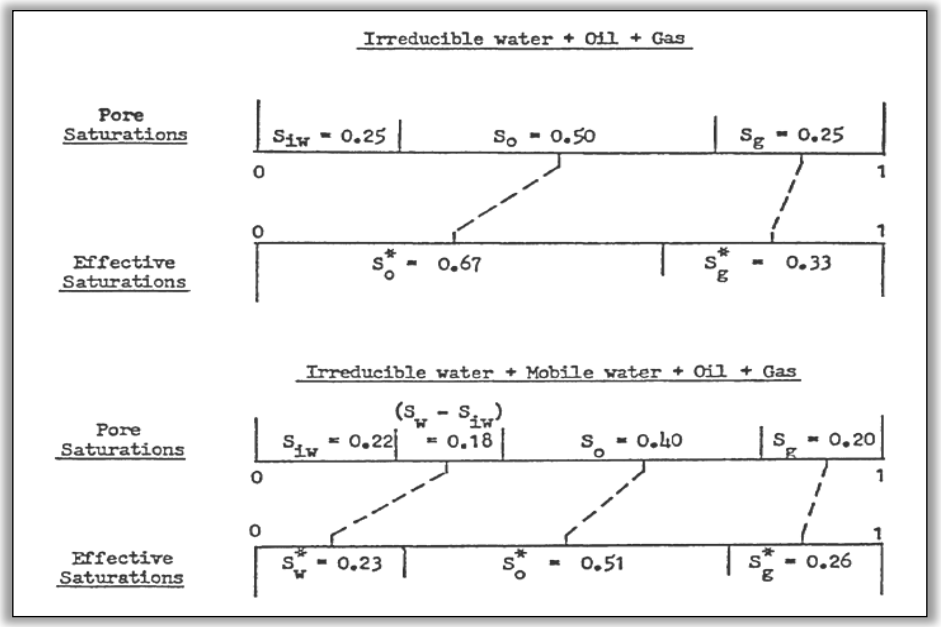

Figure 2.2: Pore saturations and their corresponding effective or normalized saturation (Standing, 1975).

According to Standing (1975), sometimes the rock is oil wet so the effective saturations will be:

$$S_o^* = \frac{(S_o-S_{oi})}{(1-S_{oi})}$$ Eq. 2.5

$$S_w^* = \frac{S_w}{(1-S_{oi})}$$ Eq. 2.6

$$S_g^* = \frac{S_g}{(1-S_{oi})}$$ Eq. 2.7

2.4. Normalized relative permeability

As Standing (1975) states, normalized relative permeability of non-wetting phase is a term applied when the base permeability is considered as the maximum effective permeability of the non-wetting phase at irreducible saturation of the wetting phase during drainage process, or when capillary pressure and normalized saturation data are applied to calculate the relative permeability, as an example, the normalized relative permeability of oil during drainage for water wet sample is:

$$k_{ro\ Normalized} = \frac{k_{eo}}{k_{eo\ (at\ S_{wi}\ or\ at\ S_w^*=0)}} = (1 - S_w^*)^2 \quad \frac{\int_{S_w^*}^{1} \left(1/P_C\right)^2 dS_w^*}{\int_{0}^{1} \left(1/P_C\right)^2 dS_w^*} \qquad \text{Eq. 2.8}$$

Normalized value of oil relative permeability might be converted to standard values by:

$$k_{ro\ standared} = \frac{k_{eo}}{k_{absolute}} = \frac{k_{ro\ Normalized} * k_{eo\ (at\ S_{wi}\ or\ at\ S_w^*=0)}}{k_{absolute}} \qquad \text{Eq. 2.9}$$

Where k_{eo} = effective oil relative permeability.

2.5. Some very important aspects related to relative permeability curves

2.5.1. Relative permeability curve shape

Generally, the curve-shape of wetting phase relative permeability is concave upward, whereas for the non-wetting phase, relative permeability is an "S" shape. If there is no interfacial tension (IFT) between the phases, the relative permeability curves will be straight lines (Yuqi1 et al., 2004, Ahmed, 2011), (Figure 2.3). It is known that the fluid which has the highest relative permeability at the residual saturation of another one is considered as a non-wetting phase fluid (Asar and Handy, 1988).

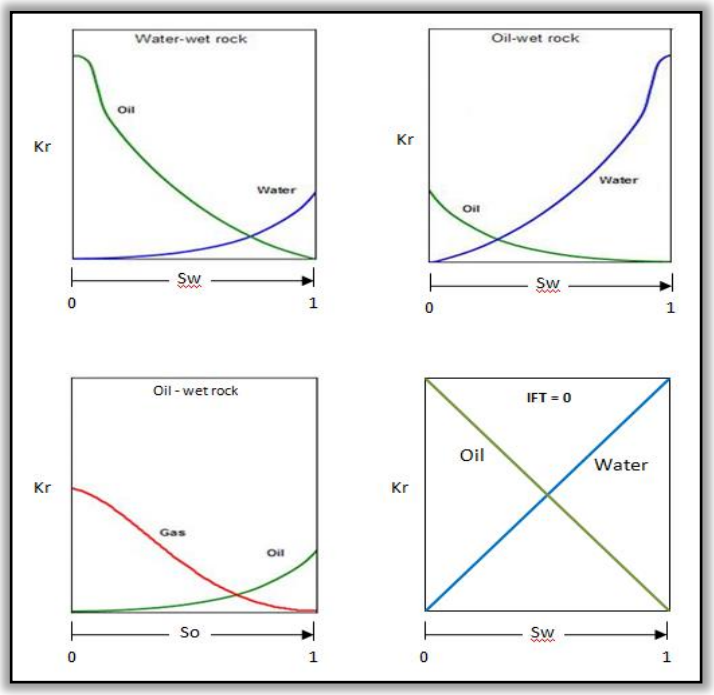

Figure 2.3: Relative permeability curve shape

2.5.2. Saturation increase direction

The saturation increase direction of wetting phase (on X axis) is usually from left to right and it is the converse of non-wetting phase.

2.5.3. General definition of drainage and Imbibition process

- **Drainage**: It is a fluid flow operation in which the saturation of the non-wetting phase increases. Mobility of non-wetting fluid phase increases as non-wetting phase saturation increases e.g., water flood in an oil-wet reservoir, gas injection in an oil- or water wet reservoir.

- **Imbibition:** It is a fluid flow operation in which the saturation of the wetting phase increases and the non-wetting phase saturation decreases (e.g., water flood in water-wetted reservoir). Mobility of wetting phase increases as wetting phase saturation increases. If a water-wet rock saturates with oil placed in water, it will imbibe water into the smallest pores, displacing oil. If an oil-wet rock saturates with water placed in oil, it will imbibe oil into the smallest pores, displacing water.

In water wet oil reservoirs, the imbibition values are used in water flood and influx calculations where the wetting phase (water) displaces non-wetting phase (oil) (Ahmed, 2011).

Imbibition is usually categorized into:

A) Forced Imbibition

It is defined as driving the wetting phase by external pressure or force to overcome capillary forces, thus displacing the non-wetting phase.

B) Spontaneous Imbibition

According to Abe (2005), this type of imbibition is described as the process of absorbing the wetting phase into rock pores. In this type of imbibition, the wetting phase is invading a porous medium in the absence of any external driving force applied. The invading action could be done just by the suction effect being created by the capillary forces. More obviously, the capillary forces in pores creates a surface energy that results in absorption of the wetting phase which is to be in contact with the rock surface.

In water-wet formation and at irreducible water saturation (S_{wr}), the water may be spontaneously sucked and displace the oil (Sorbie et al., 2005), (Figure 2.4).

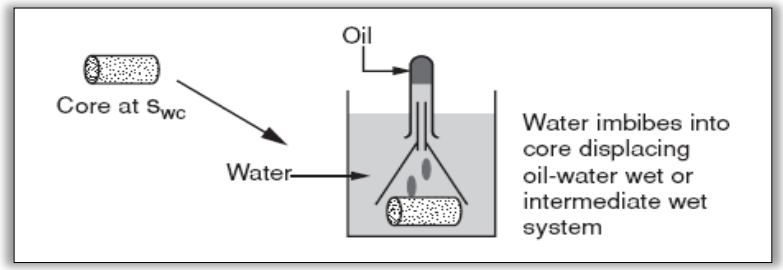

Figure 2.4: Spontaneous Imbibition (Sorbie et al., 2005)

It is observed that in an Intermediate Wettability, the both phases could be spontaneously sucked under certain conditions (Sorbie et al., 2005), (Figure 2.5).

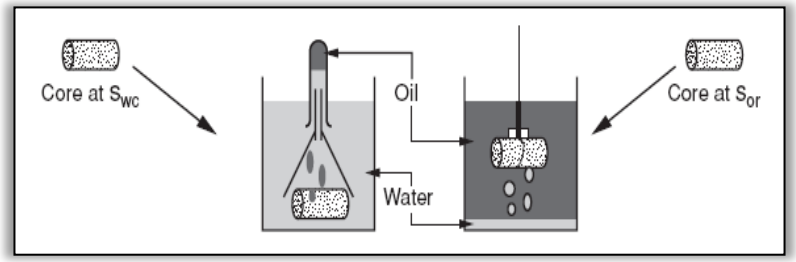

Figure 2.5: Spontaneous imbibition in an Intermediate Wettability (Sorbie et al., 2005)

Generally, in naturally-fractured reservoirs, oil recovery usually takes place by the effect of spontaneous imbibition process.

Co-current and Counter-current imbibition are other classifications that could be found in petroleum literatures; the Co-current imbibition happens when both the inlet and outlet are open to an invading fluid, whereas the Counter-current imbibition term is used when only one of the ends (Inlet) is open (Abe, 2005).

2.5.4. **Connate, irreducible and residual saturations**

When just one immiscible fluid displaces another, it is impossible to reduce the displaced-fluid saturation to zero. In water-wet rocks (as an example), as the oil displaces the water during the primary drainage process, the saturation of water will be decreasing to minimum saturation which is called connate or irreducible water saturation, and the relative permeability of water at this point is zero. According to Honarpour et al. (1986), at irreducible water saturation only oil can flow. On the other

hand, and during imbibition (throughout the same water-wet rock) the water will displace the oil and oil saturation will drop to minimum level, which is called residual oil saturation, where the relative permeability to oil is zero and the relative permeability to water is maximum.

The residual oil saturation concept is a very significant concept as it determines the maximum recoverable oil from the reservoir (Ahmed, 2011).

In water-wet rocks, for instance, during drainage process, why can some water not be displaced by the oil and remains in the reservoir as irreducible saturation? The same question is for the imbibition process since some oil remains in the reservoir as residual saturation.

The answer is that during drainage process, through water-wet rocks, the oil is entering the reservoir (filled by water) and cuts the continuous phase of water, and as a result, a part of water (existing in large pores) will be displaced by drainage action while the remaining water will be kept in small pores and its saturation decreases to irreducible. At this saturation, water is always in a discontinuous phase, and inside the small pores the forces which oppose flow will be greater than those which activate the water flow; consequently, water cannot flow and is trapped in the small pore space. It is the same as to residual oil saturation during Imbibition process.

2.5.5. **Total irreducible and residual saturations**

It is important to remember that, in water-wet rocks, some water is adherent on the rock as wetting phase, and it cannot be displaced by oil, so the total water, remaining after drainage process in water-wet rocks and known as total irreducible water, consists of water kept in the small pores (as mentioned) in addition to that adherent on the rock as wetting phase; therefore, in water-wet rocks, the total irreducible water after drainage is always greater than residual oil after Imbibition process. In petroleum literature, the total irreducible water is known just as irreducible water.

As well as, in water-wet rocks, and by the effect of attraction forces between water molecules, the irreducible water in the small pores is connected with the other water adherent on the pore walls and forming the almost free wet-phase layers, whereas the residual oil is mostly kept in the middle of small pores and does not touch the walls. The two ideas are the same but inverse for residual oil saturation in oil-wet rocks.

2.5.6. **Endpoint relative permeability and irreducible, residual saturations**

Abu-Khamsin (2004) argues that in water-wet rocks, the maximum water relative permeability (K_{rw} endpoint) at the end of imbibition is always smaller than the maximum value of oil relative permeability (K_{ro} endpoint) at the end of drainage; this is because at the end of imbibition process the residual oil (S_{or}) stays in the centre of small pores and considerably impedes the flow of water, while at the end of drainage the irreducible water (S_{wi}) is kept on the walls of small pores, so it cannot impede the flow of oil as efficiently as the residual oil (S_{or}) doing against water flow at the end of drainage process (Figure 2.6). The idea is the same but reversed in oil-wet rocks.

Müller (2011) mentioned that as the drainage and imbibition cycles repeat, the residual and irreducible saturations of wetting and non-wetting phase increase respectively. All that will reduce the endpoint relative permeability of both phases.

Honarpour et al. (1986) argue that the immobile phase (irreducible, residual) impedes the flow of the other phase existing in the same pores. This impedance will negatively affect the other phase and result in reducing the other phase's relative permeability.

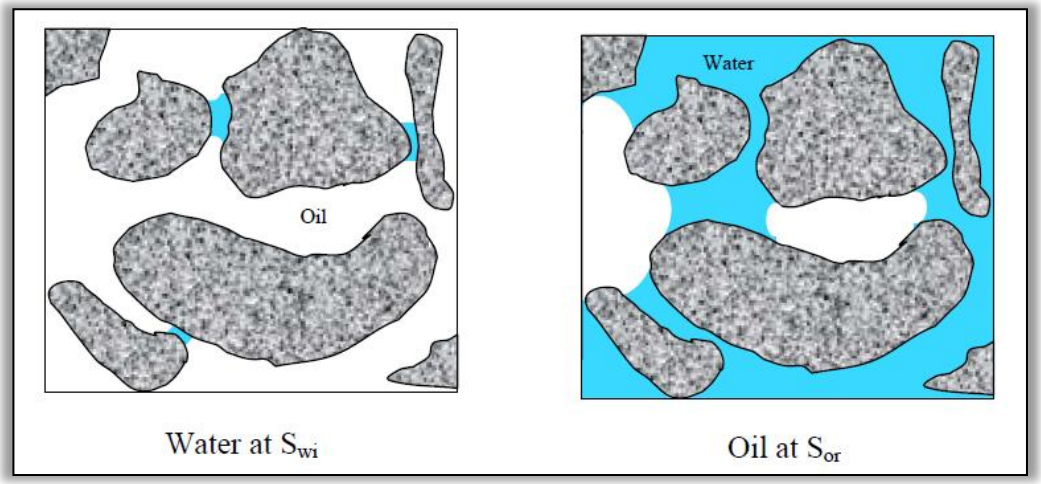

Figure 2.6: S_{wi} at end of drainage, S_{or} at end of imbibition (Abu-Khamsin, 2004).

2.5.7. **Critical saturation**

This is the minimum fluid saturation required to form a continuous phase which enables fluid to move and flow; therefore, any phase will be immobile at saturation less than the critical value, for instance, at the irreducible and residual saturations. The most known critical saturations are the critical saturation of oil in drainage process and critical water or gas saturations in imbibition operation for water-wet rocks, as an instance.

2.5.8. **Critical saturation and irreducible, residual saturations**

The- connate, irreducible, residual and critical saturations are very small and sometimes approximately with the same value but it is very important that this (connate, irreducible, residual) is always measured in the direction of reducing saturation, while critical saturation is always measured in the direction of increasing saturation (Ahmed, 2011); therefore, the saturation history is different in both of these measurements.

In water-wet rocks, for example, the wetting phase critical saturation is usually higher than the wetting phase irreducible saturation. This is owing to the fact that the irreducible wetting phase is usually connected with wetting phase adherent layer which represents the wettability; therefore, additional amount of wetting phase should be added to irreducible saturation to get over the effect of connection with the adherent layer, whereas the non-wetting phase (at residual saturation) exists in the middle of pores where the capillary pressure is very low, so there is no need to add more amount to residual saturation to get to the critical saturation. Consequently, the residual saturation of non-wetting phase is almost the same as that of critical saturation.

Generally, the critical saturation of wetting phase is much higher than that of the non-wetting phase and it is due to the same reason mentioned about adding additional amount of wetting phase.

In predicting hydrocarbon reservoir performance, all water saturations less than critical (like irreducible) are not accounted in the calculations as there are no water relative permeability data of these very low saturations (Honarpour et al., 1986).

2.5.9. **Saturation history**

This term refers to the saturation direction of a certain fluid, indicating whether the saturation of that fluid increases or decreases. As an example, during the drainage process the saturation of the non-wetting phase always increases, while in imbibition the saturation of that non-wetting phase must be decreasing.

2.5.10. **Hysteresis**

For a certain fluid, it has been reported that when saturations are changing in opposite directions (changing saturation history) and at the same point of saturation the relative permeability values obtained (at that same point) will be different, namely the relative permeability is to be higher when fluid saturation rises than when fluid saturation declines, (Figure 2.7).

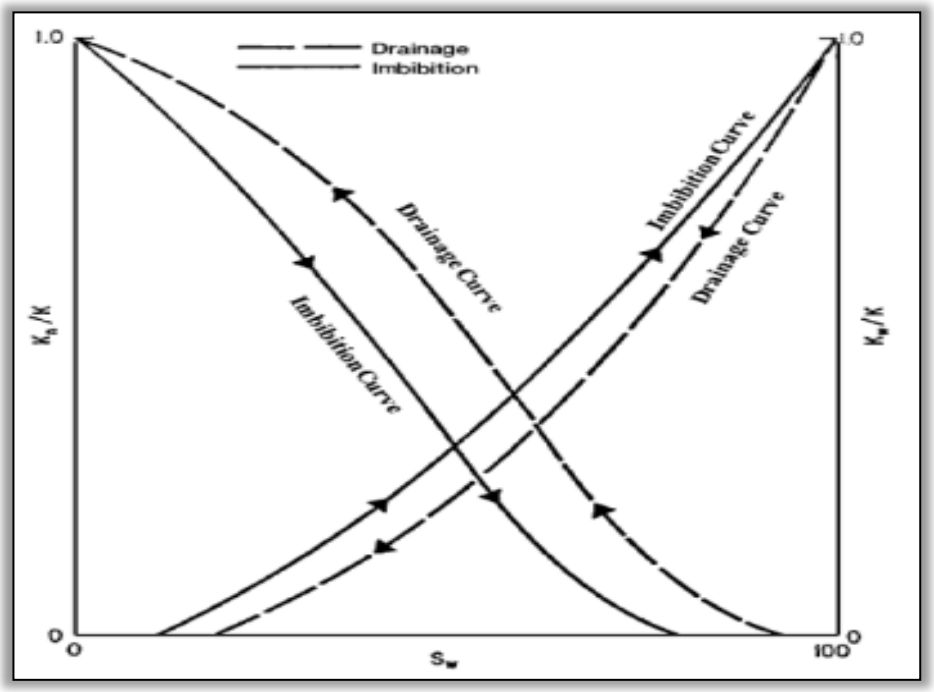

Figure 2.7: Hysteresis in relative permeability curves (Ahmed, 2011)

2.5.11. **Additional notes about relative permeability curves in different systems**

A) Relative permeability of a two phase system (Oil – water)

Ahmed (2011) establishes that in a two-phase system (like oil-water where water is considered as wetting phase) the wetting and non-wetting phases flow separately and in different paths. The distribution of both phases according to their wetting features results in each phase having a different relative permeability value.

The wetting phase relative permeability curve declines sharply for small increases in non-wetting phase saturation, whereas the relative permeability of non-wetting phase declines less sharply as the wetting phase saturation increases. This is because the non-wetting phase flows in the centre of the pore space, as a tubular flowing, without touching the walls and as a result the oil would disrupt the movement (reduced velocity) of water forward by pushing the water towards the walls. All that would highly adversely affect wetting phase relative permeability, and as a result a considerable reduction in wetting phase relative permeability would take place. In contrast, the wetting phase usually covers the walls of the pores and flows along the walls through a more-or-less thin liquid "sheet", which means the wetting phase will flow with some difficulty and does not affect the movement of the non-wetting phase very negatively, meaning that it would affect the non-wetting phase relative permeability less negatively, and as a result just a smaller reduction in the non-wetting phase relative permeability will appear (Ahmed, 2011).

B) Relative permeability of two phase system (oil – gas)

The above discussion might also be applied to oil-gas system. In this system, the reservoir water is considered but not exceeds the connate water saturation, which means that the water is not mobile; however, it exists in the pore space and reduces the available pores that the oil and gas could occupy.

Since there is connate water as a part of the total existing liquid (oil + water), liquid saturation in X axis is usually applied rather than saturation history of one fluid (Figure 2.8). The oil is considered as wetting phase and the curve shape of oil relative permeability in this system is completely different from that in water-wetted oil system. In the later system (where the water is the wetting phase) the oil relative permeability takes the S shape, whereas in oil-wetted gas system (where the oil represents the wetting phase) it takes concave upward.

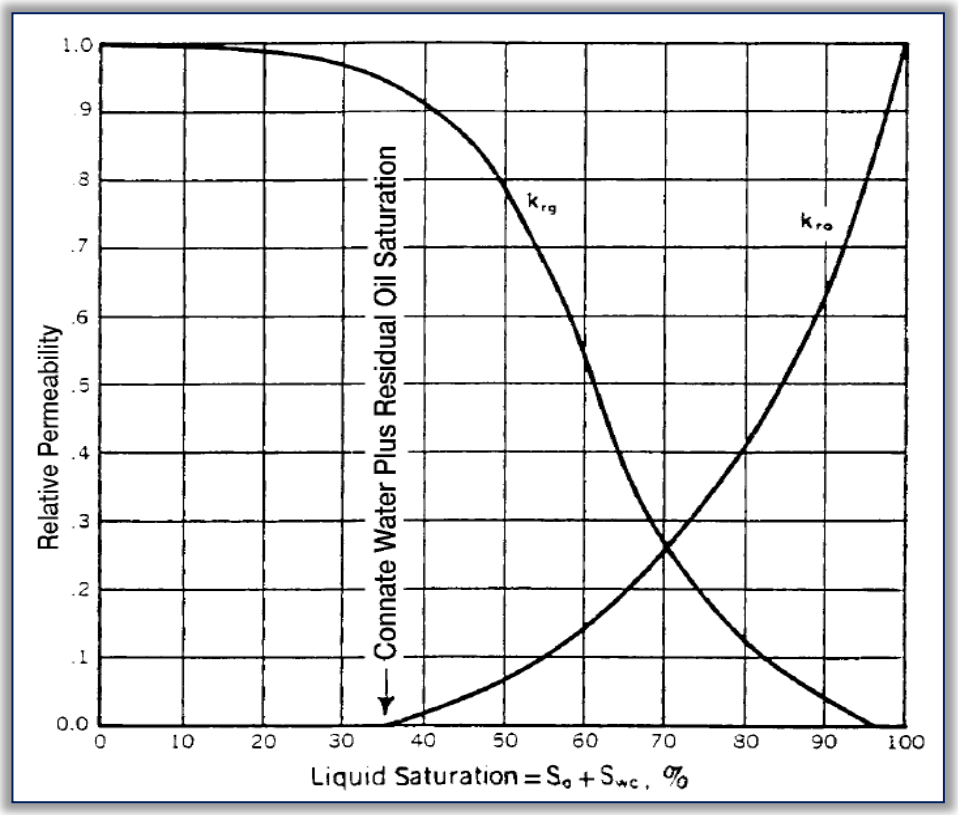

Figure 2.8: Relative permeability curves for oil-gas system (Ahmed, 2011)

2.6. Fluid behavior, rock properties, and fluid properties as factors impacting relative permeabilities

The impact of rock and fluid properties and behaviour on immiscible displacement (wetting and non-wetting relative permeabilities) could be summarized as follows:

A) Capillary forces balance

This controls the displacement of the wetting phase by the effect of non-wetting phase through the pore-throat system and thus the relative permeabilities of both phases. These capillary forces could be divided into two groups as follows:

A.1) Wetting phase capillary forces which include:

A.1.1) Wetting phase pressure: this pressure increases as wetting phase saturation goes up (head → density) and also increases as diameter of both pores and throats reduces.

A.1.2) Wetting phase wettability

A.1.3) Wetting phase viscosity

A.2) Non-wetting phase capillary forces which include:

A.2.1) Non-wetting phase pressure: this pressure increases as non-wetting phase saturation goes up (weight pressure), and also increases as injection pressure increases.

A.2.2) Non-wetting phase wettability

A.2.3) Non-wetting phase viscosity

A.3) Buoyancy force (in vertical direction)

B) Repulsion forces between different molecules at the interface between wetting and non-wetting phase

Industrially or in a core scale, the rock and fluid properties and behaviour mentioned above are dealt with through the following concepts:

Interfacial Tension (IFT) concept including (Wetting phase pressure + Non-wetting phase pressure + Buoyancy force + Repulsion forces between different molecules)

Viscosity ratio concept includes (Wetting phase viscosity + Non-wetting phase viscosity).

Throat distribution concept represents throat size (diameter).

Pore distribution concept represents pore size (diameter).

Wettability concept including (wettability of wetting and Non-wetting phases)

The above applied concepts, in addition to some other concepts like Hysteresis effect, Interference effect, Heterogeneity and rock type, will be introduced in detail later.

2.6.1. **Wettability and relative permeability**

According to Honarpour et al. (1986), the microscopic distribution of fluids in a porous medium is greatly affected by the degree of rock preferential wettability. Wettability is also considered as the main factor that controls locating the flow (Gawish and Al-Homadhi, 2008). The microscopic distribution and flow location are the major factors which control the relative permeability.

It can be seen in Figure 2.9 that the wettability of a rock has a dramatic influence on relative permeability curves, since as the rock becomes more water-wet, it means the rock has more tendency to absorb water and the water would prefer to stay or flow more on pore's wall (grain surface) rather than in the centre of the pores (Pirson, 1977). Consequently, the capability of the water to obstruct the flow of oil declines, and as a result, the relative permeability to oil increases, but it is conversely whenever the rock becomes more oil-wet as the rock will have more tendency to absorb oil and more water will be kept in the centre of pores as discontinuous droplets increasingly resist the procession of oil, with the result that the relative permeability to oil will be decreasing. This result is unfavourable in the recovery efficiency.

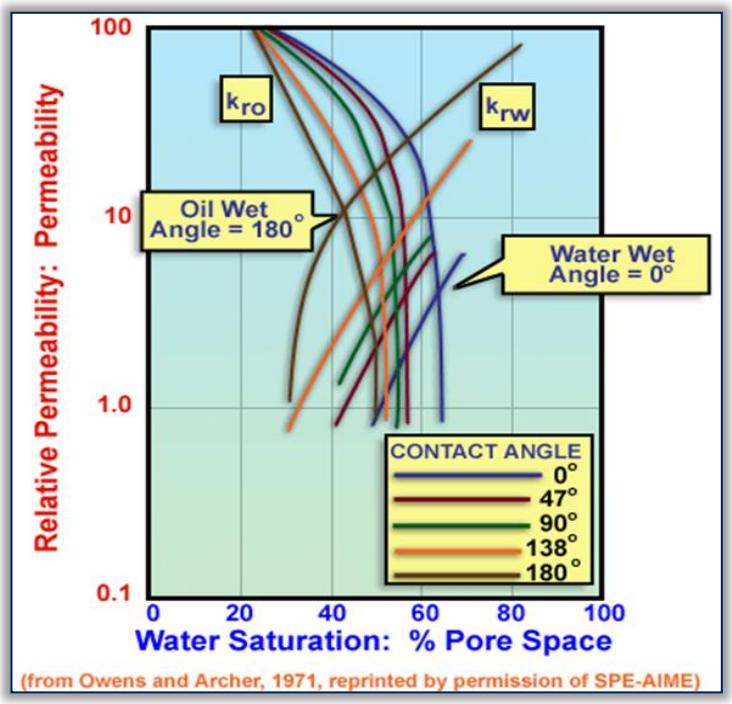

Figure 2.9: Impact of wettability on relative permeability curves

Figure 2.10 illustrates that the endpoint of water relative permeability in oil-wet oil-saturated samples is much higher than that in the water-wet oil-saturated one. This is because in water-wet oil-saturated rock the oil flows in the centre of the pore space and considerably impedes the flow of water, which would affect the water relative permeability highly negatively and make it very low (0.1 – 0.2), whereas in oil-wet oil-saturated sample the oil covers the walls of the pores and flows along the walls through a more-or-less thin liquid "sheet" so it cannot impede the flow of the water as it does in water-wet rocks, and as a result, the oil would affect the water relative permeability values less negatively which will be in the range of (0.7 -1).

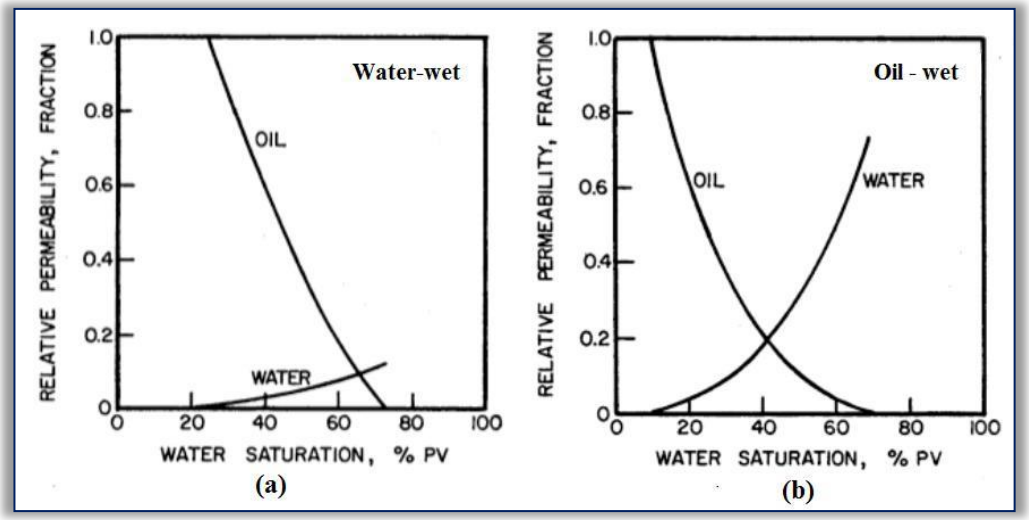

Figure 2.10: Relative permeability of brine invading different-wet samples filled with oil (Levine, 2011)

2.6.2. **Hysteresis effect**

This appears graphically as two different relative permeability curves are obtained when saturations are changing in opposite directions (changing saturation history direction), (Figure 2.11). Generally, hysteresis causes the relative permeability to be higher when saturation arises than when saturation decreases at the same point of saturation. This effect was attributed to the fact that during imbibition, as an example, the wetting phase cuts the continuous phase of the non-wetting phase, and consequently, the non-wetting phase will lose a part of its ability to move (mobility), which leads to depression in the relative permeability of non-wetting phase. This phenomenon is repeated through drainage process, and it is considered as one of the factors responsible for formation of irreducible and residual saturations (Paragraph:2.5.4).

As the drainage and Imbibition cycles repeat, the irreducible and residual saturations of wetting and non-wetting phases increase respectively. All that will reduce the endpoint relative permeability of all the phases and the hysteretic effect also increases (Müller, 2011).

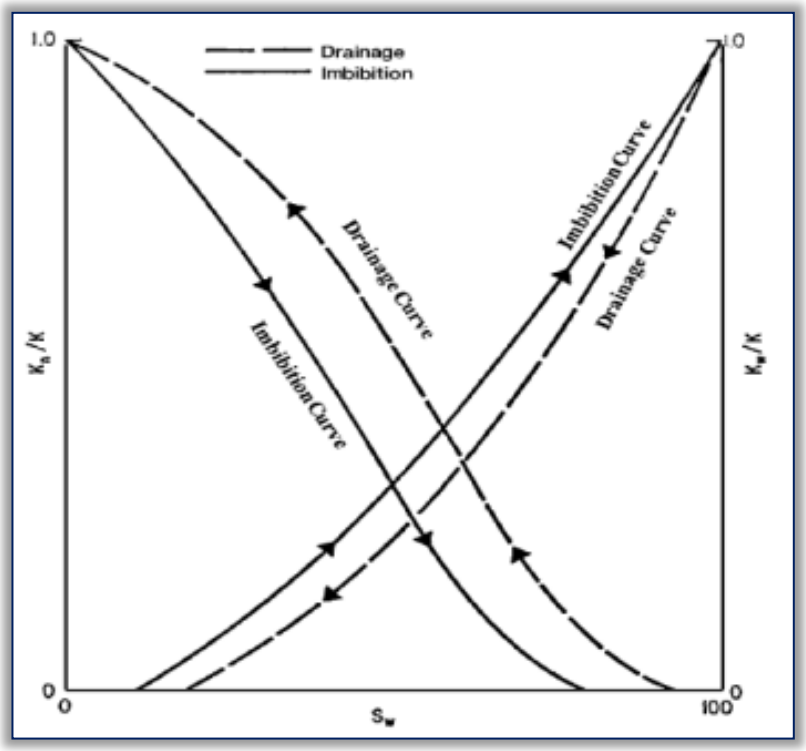

Figure 2.11: Hysteresis in relative permeability curves (Ahmed, 2011)

2.6.3. **Interfacial tension (IFT) and relative permeability**

Since the IFT is a phenomenon resulting from the repulsion forces between different molecules at the interface, it produces resistance to displacing the wetting phase by the non-wetting phase. All that will negatively impact non-wetting phase relative permeability by reducing the number of invaded throats (capillary channels), which generates the non-wetting phase relative permeability value.

Furthermore, as already established, when the pressure of non-wetting phase (displacing force) increases the relative permeability improves, but the increase of pressure will result in reduction in IFT as the latter has an inverse function with pressure. So inverse function controls the relationship between the relative permeability and IFT but this function is not direct but subject to the impact of pressure. Other factors, such as temperature and salinity, which have a negative-decisive effect on IFT and thus on relative permeability, must always be considered. The relationship between IFT and

temperature is directly proportional, so when temperature increases, the IFT also goes up (Figure 2.12a). It should be noted that this effect is not as strong as the decrease in IFT with increasing pressure. Salinity also affects IFT; this effect is weaker than that coming from temperature or pressure, but generally increasing salinity leads to increase in IFT (Figure 2.12b). Some authors prefer to add the solubility to the factors impacting the IFT, and as mentioned in the previous chapter, the solubility has a direct function with the pressure and an inverse function with temperature and salinity, so logically the IFT will have an inverse function with the solubility.

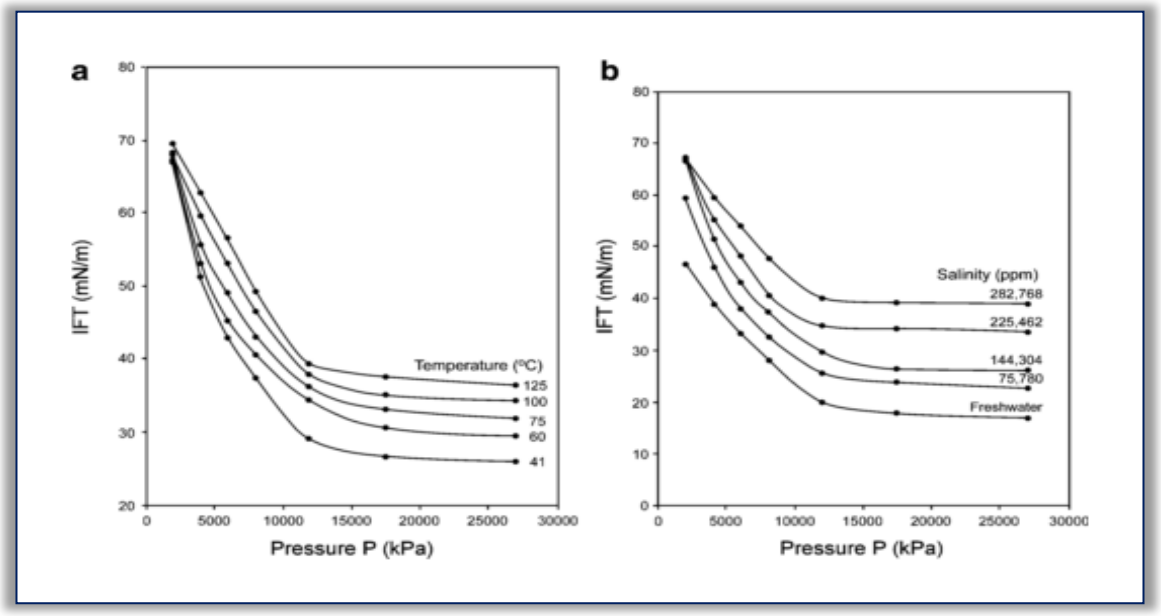

Figure 2.12: a) Constant-salinity IFT variation with (P & T), b) Constant-temperature variation of IFT with (P & salinity) (Bachu and Bennion, 2008)

The impact of IFT on relative permeability characteristics

a) Effect of IFT on relative permeability curve shape

High IFT leads the relationship between relative permeability and fluid saturation to be non-linear (Bennion and Bachu, 2008a), and at IFT equal to zero the relative permeability curves are commonly assumed to be straight-line diagonals passing through the zero saturation and zero relative permeability at one end and through 100% saturation and 100% relative permeability at the other end for each phase, (Figure 2.13).

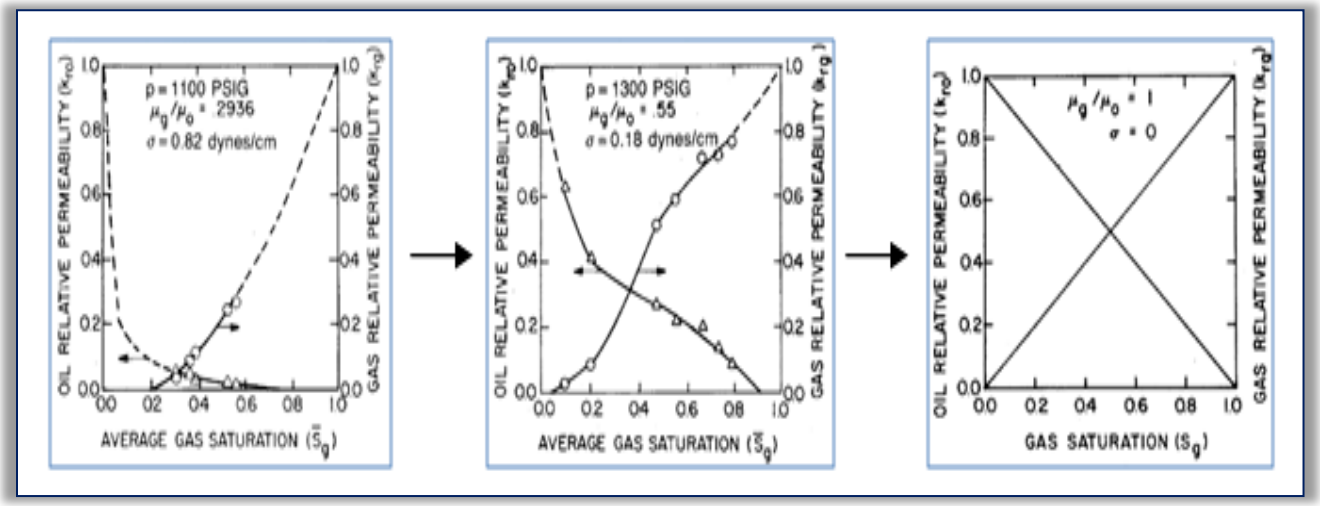

Figure 2.13: IFT and relative permeability curves (H. and Handy, 1988)

b) Effect of IFT on endpoint relative permeability, maximum and residual saturations

As the value of interfacial tension decreases, the resistance to flow will be weaker which gives potential to invade more pore-throats and displacing out more amounts of defending fluid. All that will be resulting in raising the endpoint of relative permeability and maximum saturation values of displacing fluid, and at the same time causing more reduction in the displaced-fluid residual saturation that approaches to zero at very low IFT values.

c) Effect of IFT on hysteresis

Depending on the concept of IFT, it is logical to say that as the IFT increases, the hysteresis will be more and more significant.

2.6.4. The viscosities ratio $\frac{\mu_1}{\mu_2}$

The existence of high viscous oil may cause a fingering phenomenon (Blunt and Christie, 1994), in which the injected fluid does not contact the entire reservoir and bypasses some sections (macroscopic channelling) of the reservoir fluids in a finger-like way. Fingering phenomenon is not desirable, because portions of the reservoir are not contacted by the injection fluid and as a result the assumption of uniform saturation in dynamic displacement is cancelled. It also leads to rapid injected fluid breakthrough at the outlet point, and makes the displacement to be inefficient, which in turn results in

the irreducible and residual saturations to be higher than expected. All mentioned above will result in the false data of relative permeability being produced.

2.6.5. **Interference effect**

In general, the interference affects relative permeability negatively. The cause of interference is the fact that in the ideal case the different fluids flow separately, but in actual cases they mostly interfere with each other. Honarpour et al. (1986) summarized the reasons that activate sharing flow which are as follows:

- By other fluids present; a part of the capillary channels available for flow might be reduced in size.
- Some constrictions in a pore channel where another fluid will flow may be completely plugged by immobilized droplets of a fluid.
- Some pore channels may become effectively plugged by adverse capillary forces if the pressure gradient is too low to push an interface through a constriction.

Interference appears graphically in the curve shape; the more concave shape means the more interference. The interference makes the summation of the relative permeabilities always less than one (unity) (Yuqi1 et al., 2004). The Interference was found to be affected by the median pore size (pore characteristics), as the bigger median pore size leads the relative permeability curves generally to be less-concaved, which indicates a reduction in multiphase interference effects (Bennion and Bachu, 2008a). The bigger median pore size leads as well to higher porosity and permeability (Bennion and Bachu, 2010).

2.6.6. **Heterogeneity of absolute permeability**

It has been found that severe heterogeneity causes incomplete fluid saturation (Müller, 2011) as a result of channelling and bypassing the low-permeability parts of the pore system and the flow goes throughout the higher permeable channels (Bennion and Bachu, 2010), so the fluid does not flow the entire sample, and consequently, false data of relative permeability will be obtained. Sigmund and McCaffery (1979) added that the existence of large-scale heterogeneities (for instance, vugs, fractures and stratification) could cause the derived relative-permeability relations to be impacted by displacement rate and viscosity ratio.

Rock homogeneity and uniform or complete fluid saturation could be verified by performing imaging for the core sample using techniques of imaging the core such as:

- Computerized tomography (CT) Scan; it uses x-rays and tomographic techniques to produce full 3D high resolution image of the fluid saturations in the core during an experiment. The idea of this method depends on the contrast in absorption of X-rays by different fluids.

- Nuclear magnetic scattering (NMR); it is a very new application and similar to the CT scanning with increased resolution, but it is very expensive.

2.6.7. **The effect of rock type**

It is admissible that each type of rock has a distinguished shape of relative permeability curves and always different from curves that are related to other types of rock; therefore, the relative permeability curves are not identical for all reservoir rocks, and what is more important is that the relative permeability was found to vary a lot from one portion to another through a heterogeneous formation (Honarpour et al., 1986).

2.6.8. **Temperature**

The temperature has an indirect relationship with relative permeability; it impacts relative permeability through the interfacial tension (IFT).

2.7. Importance and sources of relative permeability data

Relative permeability concept is one of the most important parameters as being used in numerical simulation; it is classified as one of the most common parameters that lead to uncertainty in the simulation results, such as oil recovery and water-flooding efficiency. Therefore, there is always need to use accurate methods for getting correct relative permeability data. Practically, there are five ways used to get the relative permeability data which are:

A) Laboratory

B) Field

C) Correlations

D) Theoretical modelling (history matching model, pore-network model)

E) Analogy

Methods (A) and (B) are considered as ways to measure the relative permeability, and they are (in addition to analogy method) sources of real values to relative permeability, while the correlations and theoretical modelling produce estimated data to relative permeability. All these methods are explained in detail below:

2.7.1. **Laboratory measuring of relative permeability (Real data)**

As a matter of fact, relative permeability data cannot be measured directly. It is usually done indirectly by using production and pressure drop data along the core sample. This could be summarized in the following:

Laboratory techniques used to measure relative permeability (Real data)

In General, two techniques are applied in laboratory to gauge the relative permeability, which are steady state test and unsteady state test (Dake, 1983).

Steady state technique is the most accurate one, but it requires a long time and is too expensive since it includes injecting water and oil at the same time until output rates become equal to input rates. The unsteady state method is faster with less accuracy as it includes saturating the sample with oil and flooding it with water. Thus, the results from the two methods are commonly very different.

The main assumption, on which these techniques have been established, is that for each phase the fluid flow remains continuous and in the same direction (Obiora Ebuka, 2010).

Additional methods like centrifuge technique and capillary pressure are also applied. In the capillary pressure method, the relative permeability is calculated from capillary pressure data and it is developed for drainage process, whereas in centrifuge method, a fluid is expelled from the sample by centrifugal forces and collected in a graded flask.

The unsteady state method is generally considered to be the most realistic in matching water-oil displacement in the reservoir since it is based on the Buckly and Leverett concept for displacement.

A summary of the laboratory techniques mentioned is provided below:

A) Steady state technique

Al-Yaseri (2010) mentioned that the first study on measuring relative permeability using steady state technique was conducted by Wyckoff and Botest, and Leverett and Lewis (1941), cited in Al-Yaseri (2010), extended the study by Wyckoff and Botest to handle the three phase systems (oil, water, and gas). The fundamental issues relating to this technique are as follows:

A.1) **General concept**

The main assumption of steady state technique is built on the following: under steady state conditions (pressure equilibrium) the pressure gradient across the core is constant and directly proportionate with fluid velocity. The relative permeability could be calculated using Darcy's law formula.

$$k_{ri} = \frac{q_i \, \mu_i \, L}{k_a \, A \, \Delta P} \qquad \text{Eq. 2.10}$$

Where:

K_{ri} = relative permeability of phase (i)

q_i = flow rate of phase (i).

μ_i = viscosity of phase (i).

A = cross sectional area of the core sample.

ΔP = Pressure drop.

K_a = absolute permeability.

According to Abu-Khamsin (2004), Abaci et al., (1992), Dullien (1991) and Müller (2011), in this technique, fixed ratios (fractional flows) of the different phases are injected concurrently at constant rate into the rock sample for extended duration until constant pressure drop (pressure equilibrium) and constant saturations (saturation equilibrium or uniform saturation) are reached (both of which are called capillary equilibrium) and the produced ratio equals the injected ratio. Pressure and fluids saturation at this condition are measured, and the relative permeability is calculated. Consequently, a point of relative permeability values versus saturations is obtained.

To obtain complete relative permeability curves of oil and water, the injection ratio of oil to water is continuously changed between 100% oil and 100% water (Figure 2.14). For each ratio the fluids will be allowed to flow (until the system being in steady state case) to calculate additional point of permeability values and saturations (Dullien, 1991). The saturation change in this case is one dimensional to avoid hysteresis.

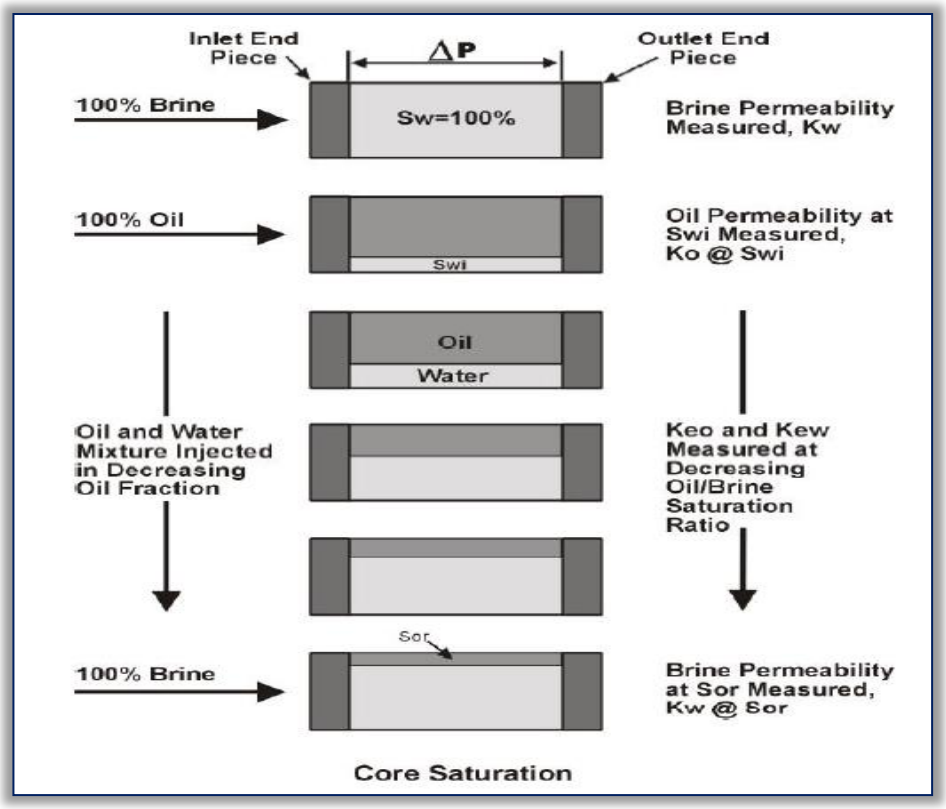

Figure 2.14: steady-state water flood procedures (Glover, 2011)

Figure 2.15 illustrates a schematic of the laboratory used in steady state technique; it consists of constant-rate pumps, one for each fluid, discharging a fixed-ratio mixture into the core sample. The flowing fluid mixture will be identical in composition to that being received by pumps upstream, so the effective permeability could be calculated since the pumps' rates for both fluids will be known.

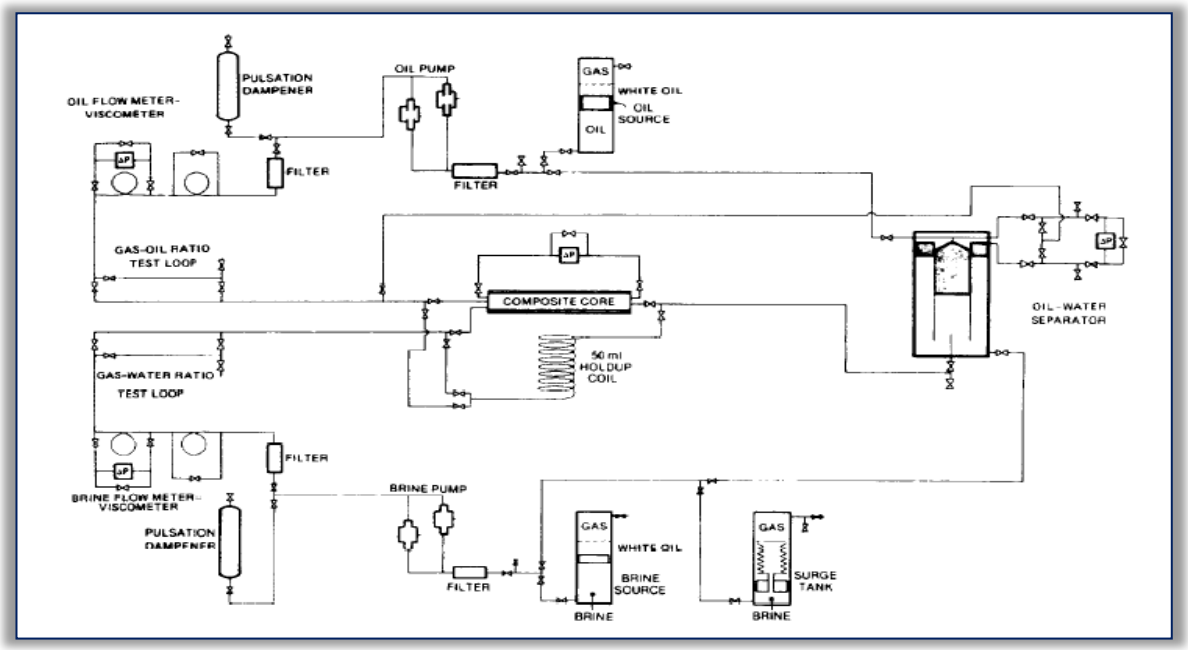

Figure 2.15: steady- state relative permeability lab instruments (Rose, 1987)

Saturation equilibrium, as mentioned before, is a regular saturation along the core sample and must be verified, but there is a problem called capillary end effects that may prevent the condition of saturation equilibrium. This problem could be explained as follows:

Capillary end effects

Capillary end effect is defined as a phenomenon making the wetting phase saturation to be higher at / near to the outlet of the sample (wetting phase collecting at the outlet of a porous medium). This phenomenon occurs due to the great tendency of the wetting phase to stay inside the rock's pore-capillaries rather than exiting to non-capillary space (Honarpour and Mahmood (1998), cited in Obiora Ebuka, 2010), and as a result of the capillary discontinuity at the outlet, the wetting phase tends to mobilize through the region near outflow boundary to remain in capillary-contacted case. If this negative side effect is not well managed, it will nullify the assumption of uniform saturation along the core sample (saturation equilibrium) thus causes an undue delay in the time of water breakthrough, all that results in creating an error in relative permeability measurement (Obiora Ebuka, 2010).

A.2) **Steady state methods**

Many researchers have studied different methods of getting both saturation and pressure equilibrium (**capillary equilibrium)** under steady state method.

Honarpour and Mahmood (1988) cited in Obiora Ebuka (2010) mentioned that the main differences among these methods could be summarized in the way by which the capillary equilibrium between fluids is established, and the way of reducing or getting over capillary end effects. The methods could be summarized as:

A.2.1) Penn state or multi-core method, (Honarpour et al., 1986).

A.2.2) Hassler or uniform-capillary-pressure method, (Hassler, 1944).

A.2.3) Single sample or high rate method, (Honarpour et al., 1986).

A.2.4) Stationary fluid method, Obiora Ebuka (2010).

A.2.5) Hafford method, (Honarpour et al., 1986, Obiora Ebuka, 2010).

A.3) Challenges facing steady state technique

There are two challenges in the steady state techniques: saturation determination and capillary end effects. The capillary end effect puts up the wetting phase saturation in the region of the outlet flow border throughout immiscible flow in core sample, and this is a result of the capillary discontinuity at the outflow end. Consequently, the wetting phase tends to mobilize through the region near outflow boundary to remain in capillary-contacted case and causes an undue delay in time for the breakthrough (Obiora Ebuka, 2010).

- Capillary end effects

To control the capillary end effect, many techniques are applied and summarized in the table below from Donaldson et al. cited in Obiora Ebuka (2010):

Steady-state method	Capillary end effect control
Penn state	Using three cores where the end piece absorbs the boundary effect
Hassler	Using semi-permeable membranes to control capillary pressure at both inlet & outlet. The main advantage of this method is the ability to eliminate the end effect almost completely.
Single-sample Dynamic	End effect could be controlled by applying high flow rates that result in the end effect being negligible.
Hafford method	The non-wetting phase is injected directly into the core sample while the wetting phase is injected across a semi-permeable disc which allows only the wetting phase to move.
Stationary fluid	Controls end effect by allowing the non-wetting phase to flow

Table 2.1: Techniques applied in steady state to get over capillary end effect problem

Some modifications, like using a longer core sample than standard, enable to remove capillary end effect; through these longer cores, the pressure and saturation measurements could be conducted only through a region that is away from ends where end effect exists (Osoba et al., cited in Obiora Ebuka, 2010).

Even after applying techniques that prevent the capillary end effect, there are some methods helping to verify the saturation equilibrium (uniform saturation) by performing imaging for saturation distribution inside the core sample (Busch and Müller, 2011 and Müller, 2011). These means were described in paragraph 2.6.6.

B) Unsteady state technique

B.1) General concept

According to Honarpour et al., (1986), and Obiora Ebuka (2010), unsteady state technique includes pushing out in–situ phases by injecting the displacing fluid continuously at constant rate or constant pressure (flow and pressure stabilization are not required). It is considered as the most realistic way in matching water-oil displacement. For each phase, the saturation distributions will be changing with the time and so the relative permeability, pressure and velocity. Displacing and displaced phases flow rates and pressure are measured at the outlet end as a function of time or as a function of pore volume injected, (Figure 2.16). These measurements are used to calculate relative permeability values for both phases based on Buckley and Leverett (1942) theory. The disadvantage of an unsteady-state method lies in calculations, as being very complex and not easy to apply.

Müller (2011) observed that the ratio of displacing phase versus defending phase is derived from the cumulative displacing phase injected and cumulative displaced phase produced throughout time, and the saturation and pressure are usually analyzed by numerical modelling to calculate the relative permeability. If capillary pressure (Pc) could be neglected, then the Buckley–Leverett displacement method could be applied by using the analytical-solution way, but as a matter of fact, capillary pressure cannot be neglected, so correcting the interpretation by using the simulations is needed.

As the saturation equilibrium is not required in this method, the relative permeability values could be obtained in very short time (Abaci et al., 1992, Dullien, 1991), in a few hours, for example. This method is also used to predict saturation, water breakthrough time and water-cut versus time (Obiora Ebuka, 2010).

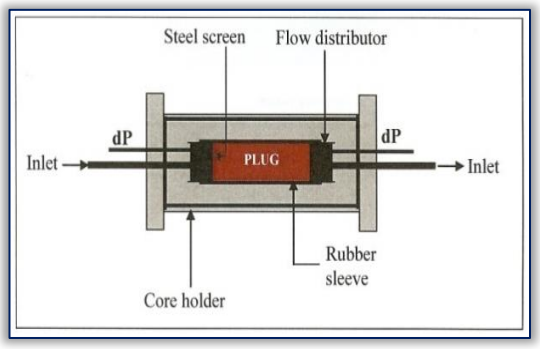

Figure 2.16: Schematic diagram of water flood apparatus (Obiora Ebuka, 2010)

B.2) Methods applied under the unsteady state technique

There are two methods commonly followed:

- **High-rate method**

In this method the injection rate should be sufficiently high so that the capillary end effects can be eliminated (PetroWiki).

- **Low- rate method**

Most researchers prefer this method to high-rate one when samples have fine parts which may become mobile at high rates. Although the equipment is identical to that being used for high-rate methods, calculations applied for interpreting the data of the production and pressure-drop are different (PetroWiki).

B.3) Buckley – Leverett displacement theory

Buckley and Leverett (1942) developed the first displacement theory known as frontal advance theory (Figure 2.17), and as mentioned before, all unsteady state techniques for measuring relative permeability are based on Buckley-Leverett theory (Johnson et al., 1959). According to Pistone (2011), this theory includes some assumptions such as:

- Fluids are immiscible and uncompressible.
- Fluid viscosity values are constant (independent to pressure).
- Rock is homogeneous.
- Porosity is constant.
- Flow in one direction, and perfectly dispersed flow.
- No capillary pressure or capillary end effects.
- No gravitational effects.
- Calculation is only applicable after gas breakthrough in a drainage experiment.

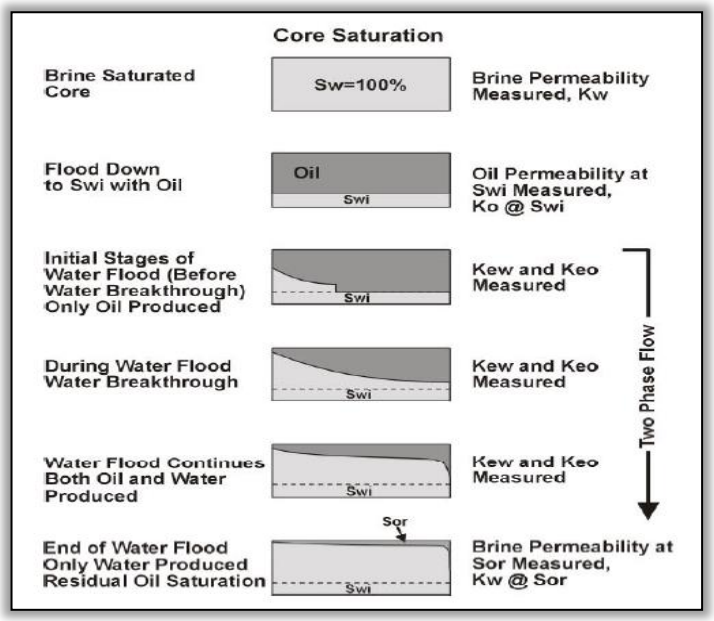

Figure 2.17: Unsteady- state water flood procedures (Glover, 2011)

B.4) Challenges to unsteady state technique

- Regarding the calculations

Buckley-Leverett assume ideal Darcy flow behavior including:

i. Fluids are immiscible and uncompressible.

ii. Fluid viscosities are constant.

iii. Homogenous rock.

iv. Porosity is constant.

v. Flow in one direction (linear).

vi. No capillary pressure, negligible.

vii. No gravitational effects.

Since the Johnson-Bossler-Naumann (JBN) method derived from Buckley-Leverett flow theory, JBN method inherited all the above assumptions, and as a consequence the effects of capillary pressure and wettability were not included in the measurement of relative permeability. Furthermore, the calculations should be done only after water breakthrough.

As for capillary pressure, if it could be neglected by using high injection rate, Buckley-Leverett is supposed and the interpretation could be done by analytical solution, but in fact, the Pc cannot be ignored and the interpretation must be corrected by using the simulation (correlations) since gravity and capillary pressure effects can be incorporated into the simulation.

- Capillary end effects

To control the capillary end effect, Hassler core sample may be used to eliminate the end effect almost completely.

Table 2.2 below presents a comparison between steady state and unsteady state techniques (Obiora Ebuka, 2010).

	Steady state technique	Unsteady state technique
1	Capillary equilibrium is a fundamental issue thereby keeping the capillary properties of the reservoir rock, so this technique is more representative to reservoir conditions.	• Puts aside the effect of capillary pressure with the core by applying high injection rate; therefore, the effects of capillary pressure and wettability have not been accounted for in relative permeability measurement. • But it is considered to be the most realistic in matching water–oil displacement.
2	Mostly applicable when the rock is strongly wet by one phase. As for intermediate and mixed wettability, this technique gives inaccurate results. It is a favourite technique for sandstone and carbonates.	Could be applied to strong and intermediate wettability and the results are mostly reliable.
3	No viscous fingering, so it could be applied for viscous and non-viscous oil.	Viscous fingering is a major problem with high viscous oil that will cancel out the uniform saturation assumption in dynamic displacement; therefore, measurement of relative permeability becomes not easy to understand.
4	To measure the core saturation, the sample should be stripped from the apparatus then weighted. Dismantling the sample causes to expose it to atmospheric pressure that results in gas expansion and fluid loss; therefore, an error in fluid saturation measurements will be introduced.	Measuring the saturations indirectly from production data so it gives more flexibility with less error.
5	Covers a broader range of saturation	Covers a small range of saturation.
6	Mathematical process needed to calculate the relative permeability is very simple since it includes application of Darcy's law equation.	• Many simplifying assumptions (the seven) that weakens the accuracy of results. • As for capillary pressure, If it could be neglected by using high injection rate, then Buckley-Leverett is supposed and the interpretation could be got by analytical solution but in fact the Pc cannot be ignored and the interpretation must be corrected by using the simulation (correlations) since gravity and capillary pressure effects can be incorporated in correlation, and it should be rememberd that no correlation is with 100% accuracy. • Relative permeability calculations should be done only after water breakthrough.
7	Very long time needed to get to steady state (equilibrium) case, so this technique is not practical to low permeability rocks.	No steady state (equilibrium) case required; therefore, the time needed for one run is much shorter. It is considered a fastest way for both high and low permeability rock.
8	Uses a lot of instruments.	Uses a fewer number of instruments since it allows loading up multiple core samples on a one water flood rig where data could be obtained at the same time for relative permeability.
9	Based on 7 and 8, The cost of this technique is quite high.	Based on 7 and 8, this technique is much cheaper; therefore, this technique has been applied in the industry to predict saturation, water breakthrough time and water cut as a function of time.

Table 2.2: Comparison between steady-state and Unsteady-state techniques

Since the steady state technique produces more reliable relative permeability data than those got from unsteady state, the first one is used in appraisal and development stages where the reliability is essential for history–-matching. The relative permeability coming from unsteady state is usually used in exploration stages like Oil-In-Place calculations where the high degree of accuracy is not very important (Obiora Ebuka, 2010).

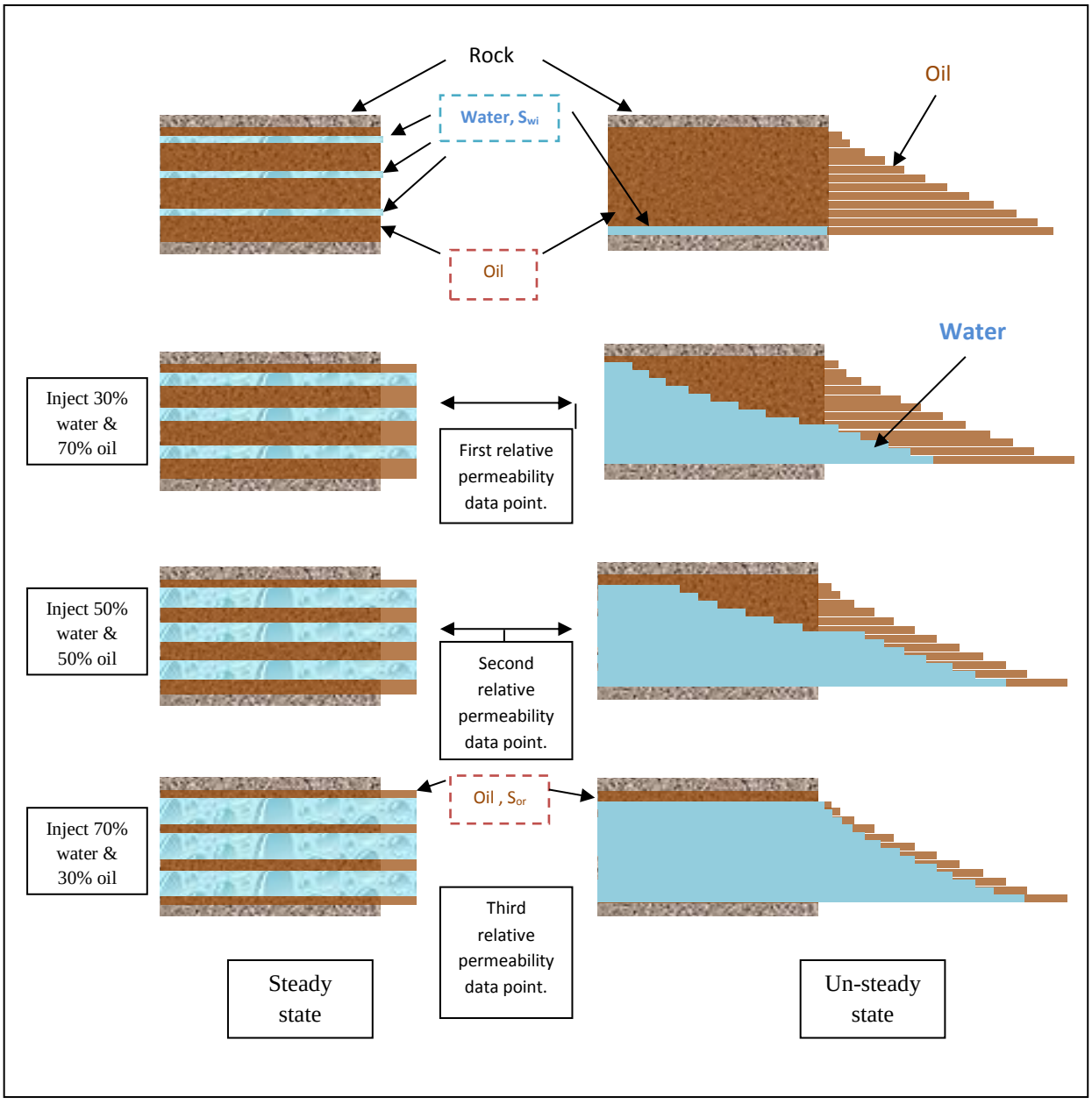

Figure 2.18: Difference between steady state and unsteady state techniques.

C) Capillary pressure technique

Honarpour et al. (1986) mentioned that this method is applied for calculating relative permeability from capillary pressure data, and it was developed for drainage process, where a non-wetting phase (gas) displaces a wetting phase (water or oil), so the technique is generally exclusive to gas-water or gas-oil systems, where the reservoir is being produced by a drainage process. Although this technique is not usually favoured, it is practical for obtaining gas-oil or gas-water relative permeabilities when rock samples are too small for flow tests but large enough for mercury injection. The technique is also useful in a rock which has so low permeability that flow tests are impractical and, for example, where capillary pressure could be measured but the rock sample is not appropriate for measuring relative permeability. Another benefit, as known, is that the unsteady-state method is not designed for very low oil saturations; therefore, the capillary pressure technique could be employed instead.

The steps of this method could be summarized as the following:

The core is evacuated and mercury (the non-wetting phase) is injected in measured increments at increasing pressures. About 20 data points are enough for drawing a complete capillary pressure curve. These points are used in order to calculate relative permeability by the methods described below.

Generally, there are different approaches being used to calculate relative permeability from capillary pressure data as follows:

C.1) **Purcell equations.**

It is used to calculate relative permeability for two phases, noting that the tortuosity factor is not considered. According to Purcell (1949), cited in Li and Horne (2006) and Castaneda G. (2008), the equations used are:

$$k_{rwt} = \frac{\int_0^{S_w} \frac{dS_w}{(P_c)^2}}{\int_0^1 \frac{dS_w}{(P_c)^2}} \qquad \text{Eq. 2.11}$$

The area under $1/P_c^2$ curve from 0 to S_w on plot of $1/P_c^2$ .vs. S_w.

$$k_{rnwt} = \frac{\int_{S_w}^1 \frac{dS_w}{(P_c)^2}}{\int_0^1 \frac{dS_w}{(P_c)^2}} \qquad \text{Eq. 2.12}$$

The area under $1/P_c^2$ curve from S_w to 1 on plot of $1/P_c^2$ .vs. S_w.

Where:

K_{rwt} = Relative permeability of wetting phase

K_{rnwt} = Relative permeability of non-wetting phase

P_c = capillary pressure as a function of S_w

C.2) **Burdine**

Burdine (1953), cited in Li and Horne (2006), introduced a tortuosity factor as a function of wetting phase saturation. The relative permeabilities of wetting and non-wetting phases can be calculated as follows:

- For the wetting phase:

$$k_{rwt} = (\lambda_{rwt})^2 \frac{\int_0^{S_w} \frac{dS_w}{(P_c)^2}}{\int_0^1 \frac{dS_w}{(P_c)^2}} \qquad \text{Eq. 2.13}$$

λ_{rwt} = tortuosity ratio of wetting phase , which could be calculated as follows:

$$\lambda_{rwt} = \frac{\tau_w(1.0)}{\tau_w(S_w)} = \frac{S_w - S_m}{1 - S_m} \qquad \text{Eq. 2.14}$$

S_m is the minimum wetting phase saturation from capillary pressure curve.

τ_w (1.0) and $\tau_w(S_w)$ are the tortuosities of the wetting phase when the wetting phase saturation is equal to 100% and S_w respectively.

- For non-wetting phase

$$k_{rnwt} = (\lambda_{rnwt})^2 \frac{\int_{S_w}^0 \frac{dS_w}{(P_c)^2}}{\int_0^1 \frac{dS_w}{(P_c)^2}} \qquad \text{Eq. 2.15}$$

λ_{rnwt} = tortuosity ratio of non-wetting phase, which could be calculated as follows:

$$\lambda_{rnwt} = \frac{\tau_{nw}(1.0)}{\tau_{nw}(S_w)} = \frac{S_w - S_m - S_e}{1 - S_m - S_e} \qquad \text{Eq. 2.16}$$

S_e is the equilibrium saturation of the non-wetting phase.

τ_{nw} is the tortuosity of the non-wetting phase.

D) Centrifuge technique

In this technique, a fluid is expelled from the sample (that was initially saturated uniformly with one or two phases) by centrifugal forces and collected in a graded flask (Figure 2.19). The produced fluid could be controlled by a stroboscope system. This technique is not common, but has the advantage of not subjecting to the viscous fingering problems which are common in unsteady-state measurements, whereas the disadvantage of this technique is that it does not provide a means for determining relative permeability to the invading or non-wetting phase (Honarpour et al., 1986).

Generally, in the centrifuge technique, there are two types of experiments which are conducted; a multi-speed run to measure capillary pressure and a single high-speed run to measure relative permeability.

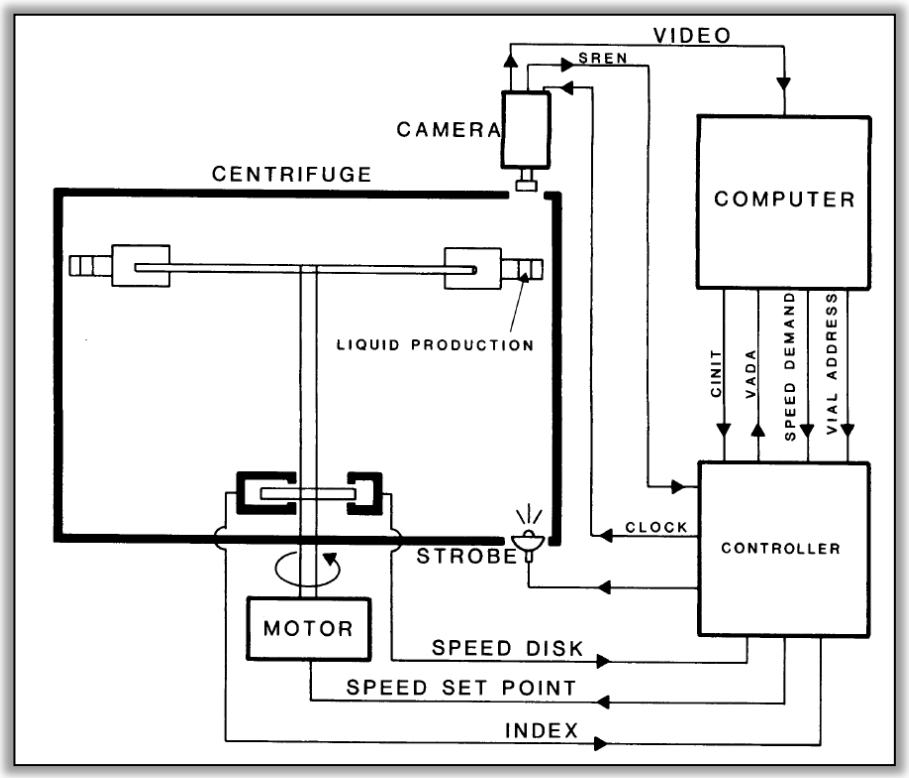

Figure 2.19: Centrifuge system (Honarpour et al., 1986)

2.7.2. **Field measurement of relative permeability (real data)**

A) Production data method.

A.1) First technique

According to Honarpour et al. (1986), it is possible to calculate relative permeability ratios directly from field production data. It is important to know that part of the gas produced on surface is dissolved in the liquid phase in the reservoir, so:

(Produced gas) = (free gas) + (solution gas)

The relative permeability ratio is given by:

$$\frac{k_g}{k_o} = \frac{(R_P - R_S)}{5.615} \frac{B_g}{B_o} \frac{\mu_g}{\mu_o} \qquad \text{Eq. 2.17}$$

Where:

R_P = Cumulative gas/oil ratio, R_S = solution gas oil ratio.

The total liquid saturation inside the reservoir is expressed as:

$$S_L = S_w + (1 - S_w)\left(\frac{N - N_P}{N_P}\right)\left(\frac{B_o}{B_{oi}}\right) \qquad \text{Eq. 2.18}$$

Where:

N = initial stock tank barrels of oil in place.

N_P = the number of stock tank barrels of oil produced.

B_{oi} = the ratio of the oil volume at initial reservoir conditions to oil volume at standard conditions.

The relative permeability curve is obtained by plotting $\frac{k_g}{k_o}$ as function of S_L on semi log paper, with $\frac{k_g}{k_o}$ on the logarithmic scale.

This technique is practical even if only a few high liquid-saturation data points can be plotted.

The ratio of $\frac{k_g}{k_o}$ could be used to verify relative permeability accuracy, whether measured in lab or by using other techniques or estimated by correlations.

The difference between the relative permeability data coming from field production measurements and that produced in the lab measurements may be due to one or more of following reasons:

i. The core on which relative permeability is measured may not be representative of the reservoir in regard to some factors such as fluid distributions, secondary porosity, etc.

ii. The technique (customarily used to compute relative permeability from field production data) does not allow for the pressure and saturation gradients which are present in the reservoir, nor does it allow for the fact that the production might be coming from multi-strata wells that are at various stages of depletion.

iii. The usual technique for calculating relative permeability from field production data assumes that R_P at any pressure is constant throughout the oil zone. This assumption can lead to computational errors if gravitational effects within the reservoir exist.

A.2) Second technique

Abu-Khamsin (2004) noted that effective permeabilities (thus relative permeability) could also be obtained from field production data. The well will produce oil and water if the saturations of oil and water through the well's drainage area are greater than critical values. For each fluid, the production rate and then the ratio of effective permeabilities would be calculated through Equations 2.19 – 2.20. The effective permeabilities are to correspond to the average water saturation inside the well's drainage area, which is estimated from well logs. Other producing wells within the same reservoir could provide additional data points to draw the curves completely.

For several reasons, including the ones below, this technique is not entirely reliable.

- The engineer would be forced to resort to average rates since the daily production rate fluctuations result in inaccuracy in the findings.
- There is not a uniform distribution for both fluids around the well, which makes the parameter of average water saturation very difficult to assess.

- Effective-permeability ratio corresponding to the average water saturation is not technically correct.

$$q_i = -\frac{k_i A}{\mu_i}\frac{\partial \Phi}{\partial S} \quad \text{Eq. 2.19}$$

$$\frac{k_o}{k_w} = \frac{q_o}{q_w}\frac{\mu_w}{\mu_o} \quad \text{Eq. 2.20}$$

B) Resistivity data method

Measuring relative permeability is sometimes very difficult owing to some problems like very small permeability, and some fluid systems in which the mass transfer is to be between the two phases whenever the pressure changes (Li, 2008); therefore, getting relative permeability using resistivity data is very helpful as the latter are very easy to measure and widely available from well-logging. Pirson and Boatman, cited in Li (2008), designed an imperial model to generate relative permeability from resistivity information. Li (2008) derived a theoretical model to deduce relative permeability using resistivity data. The relative permeability values obtained from the theoretical model were found to have been near to those calculated by using the capillary pressure data for the same rock. The method consisted of two steps of calculations:

i. Calculation of the Wetting-Phase Relative Permeability (k_{rw})

$$K_{rw} = S_w^* \frac{1}{I} \quad \text{Eq. 2.21}$$

$$I = \frac{R_t}{R_o} = (S_w)^{-n} \quad \text{Eq. 2.22}$$

$$S_w^* = \frac{S_w - S_{wr}}{1 - S_{wr}} \quad \text{Eq. 2.23}$$

Where:

R_o = the resistivity at a water saturation of 100%.

R_t = the resistivity.

I = the resistivity index.

n = the Archie's saturation exponent.

S_w^* = wetting phase normalized saturation.

S_{wr} = wetting phase residual saturation.

ii. Calculation of the non-Wetting-Phase Relative Permeability (krnw)

From the resistivity data, the relative permeability of non-wetting phase cannot be obtained directly, but by using the wetting phase relative permeability from the resistivity is as follows:

Purcell (1949), cited in Li (2008), presented the Eq. 2.24 to calculate the relative permeability of wetting (k_{rw}) phase from capillary-pressure data, and by applying k_{rw} obtained from resistivity data in Eq. 2.24 the λ (pore-size distribution index) could be calculated .

$$K_{rw} = (S_w^*)^{\frac{2+\lambda}{\lambda}} \qquad \text{Eq. 2.24}$$

Once the λ is available, the non-wetting phase relative permeability could be obtained from Eq. 2.25 presented by Brooks and Corey (1966) cited in Li (2008).

$$K_{rnw} = (1 - S_w^*)^2 \left[1 - (S_w^*)^{\frac{2+\lambda}{\lambda}}\right] \qquad \text{Eq. 2.25}$$

C) Well testing data method

This technique has been developed for the first time by Al-Khalifah (1988), and it needs a short drawdown test which consists of a number of steps with increasing flow rate. The relative permeabilities estimated by this technique reflect the flow behaviour to the well's entire drainage area rather than flow performance of a small laboratorial sample. This technique estimates the relative permeabilities at sand face saturations, which cover a wide range of reservoir conditions that will take place in the future.

2.7.3. **Using imperial Correlations method to calculate relative permeability (Estimated data)**

This technique depends on using easy obtainable laboratory data and correlations to get relative permeability data, and it is considered quick and quite cheap. We can classify the techniques as follows:

Two–phase system correlations

Some issues should be remarked before listing the two-phase system correlations, which include:

- Different parameters are used to estimate the relative permeability through these correlations or relationships, including:
- Capillary pressure data
- Initial and residual saturations.

Furthermore, the effective phase saturation is used in most of the correlations and calculated by using the following equations (Ahmed, 2011):

$$S_o^* = \frac{S_o}{1-S_{wc}} \qquad \text{Eq. 2.26}$$

$$S_w^* = \frac{S_w-S_{wc}}{1-S_{wc}} \qquad \text{Eq. 2.27}$$

$$S_g^* = \frac{S_g}{1-S_{wc}} \qquad \text{Eq. 2.28}$$

Where:

S_o^* , S_w^* , S_g^* = effective oil, water and gas saturations.

S_{wc} = S_{wi} = Connate or initial water saturation.

The following Two–phase system correlations (as example) are being applied for any wetting and non-wetting phases:

A.1) Wyllie and Gardner, cited in Honarpour et al. (1986), introduced general expressions for any wetting and non-wetting relative permeability and may be written as:

$$k_{rwt} = \left(\frac{S_L - S_{wi}}{1 - S_{wi}}\right)^2 \frac{\int_{S_{wi}}^{S_L} dS_w / P_c^2}{\int_{S_{wi}}^{1} dS_w / P_c^2} \qquad \text{Eq. 2.29}$$

$$k_{rnwt} = \left(\frac{1 - S_L}{1 - S_{wi}}\right)^2 \frac{\int_{S_L}^{1} dS_w / P_c^2}{\int_{S_{wi}}^{1} dS_w / P_c^2} \qquad \text{Eq. 2.30}$$

k_{rwt} = wetting phase relative permeability (k_{rw} and k_{ro}).

k_{rnwt} = Non-wetting phase relative permeability (k_{rg}).

S_{wi} = Irreducible water saturation.

S_L= Total liquid saturation = (l - S_g).

A.2) Corey and Brooks

Standing (1975) cited that Brooks and Corey (1966) introduced the following equations to predict drainage relative permeability using pore size distribution and capillary pressure data.

$$k_{rwt} = (S_w^*)^{\frac{2+3\lambda}{\lambda}} \qquad \text{Eq. 2.31}$$

$$k_{rnwt} = (1 - S_w^*)^2 \left[1 - (S_w^*)^{\frac{2+\lambda}{\lambda}}\right] \qquad \text{Eq. 2.32}$$

Where λ is pore size distribution index and is calculated from the following equation:

$$\log P_c = \log P_b - \frac{1}{\lambda} S_w^* \qquad \text{Eq. 2.33}$$

The values of λ and Pb are obtained by plotting S_w^* vs. capillary pressure on a log-log scale; λ is slope inverse and Pb is the intercept at $S_w^* = 1$.

Pore size distribution index of 2 yields the so–called Corey equations that are used extensively in reservoir engineering.

A.3) Relative permeability from Analytical equations

Ahmed (2011) stated that this method is commonly applied in numerical simulation and consists of many equations as follows:

- For Oil water system

$$k_{ro} = (k_{ro})_{Swc} \left[\frac{1-S_w-S_{orw}}{1-S_{wc}-S_{orw}}\right]^{n_o} \quad \text{Eq. 2.34}$$

$$k_{rw} = (k_{rw})_{Sorw} \left[\frac{S_w-S_{wc}}{1-S_{wc}-S_{orw}}\right]^{n_w} \quad \text{Eq. 2.35}$$

$$P_{cwo} = (P_c)_{Swc} \left[\frac{1-S_w-S_{orw}}{1-S_{wc}-S_{orw}}\right]^{n_p} \quad \text{Eq. 2.36}$$

- For Gas - Oil system

$$k_{ro} = (k_{ro})_{Sgc} \left[\frac{1-S_g-S_{lc}}{1-S_{gc}-S_{lc}}\right]^{n_{go}} \quad \text{Eq. 2.37}$$

$$k_{rg} = (k_{rg})_{Swc} \left[\frac{S_g-S_{gc}}{1-S_{lc}-S_{gc}}\right]^{n_g} \quad \text{Eq. 2.38}$$

$$P_{cgo} = (P_c)_{Slc} \left[\frac{S_g-S_{gc}}{1-S_{lc}-S_{gc}}\right]^{n_{pg}} \quad \text{Eq. 2.39}$$

Where:

S_{lc} = Total critical liquid saturation = S_{wc} + S_{org}.

$(k_{ro})_{Swc}$ = oil relative permeability at connate water saturation.

$(k_{ro})_{Sgc}$ = oil relative permeability at critical gas saturation.

S_{orw} = Residual oil saturation in the water–oil system.

S_{org} = oil residual saturation in the gas–oil system.

S_{gc} = gas critical saturation.

$(k_{rw})_{Sorw}$ = relative permeability of the water at residual oil saturation.

n_o , n_w , n_g , n_{go} = exponents on relative permeability curves.

P_{cwo} = Capillary pressure of water-oil system.

$(P_c)_{Swc}$ = Capillary pressure at connate water saturation.

n_p = Exponent of capillary pressure curve for the oil–water system.

P_{cgo} = Capillary pressure of gas–oil system.

n_{pg} = Exponent of capillary pressure curve in gas–oil system.

$(P_c)_{Slc}$ = Capillary pressure at critical liquid saturation.

Determination of coefficients and exponents in equations 2.34 - 2.38 is done using least-squares method so as to match the experimental capillary pressure and relative permeability data.

Figures hereafter show the corresponding relative permeability and critical saturation values which are used in correlations 2.34 - 2.39.

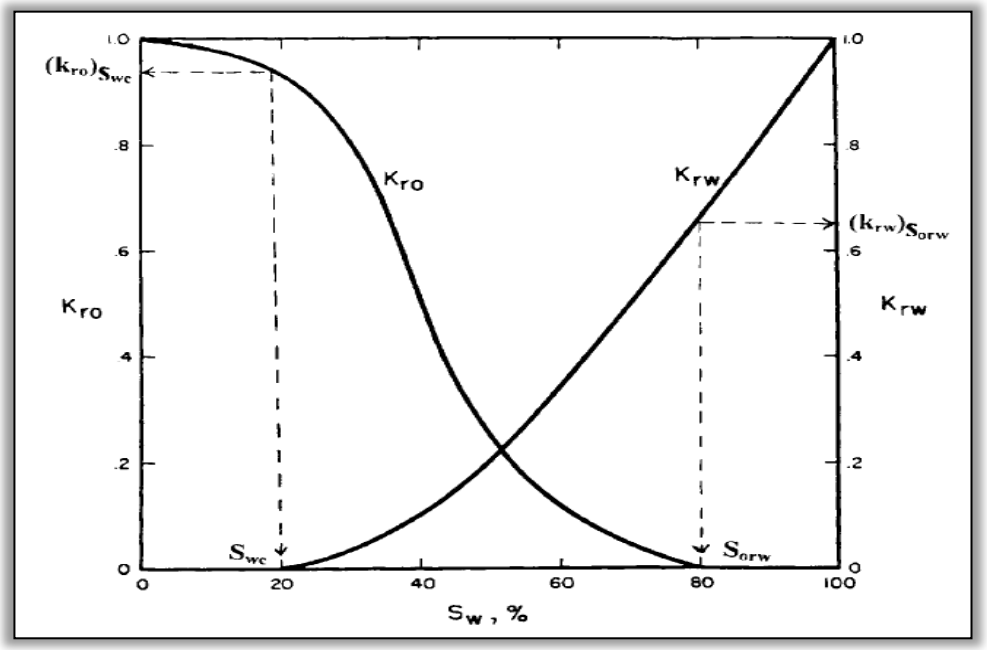

Figure 2.20: Water – oil relative permeability (Ahmed, 2011)

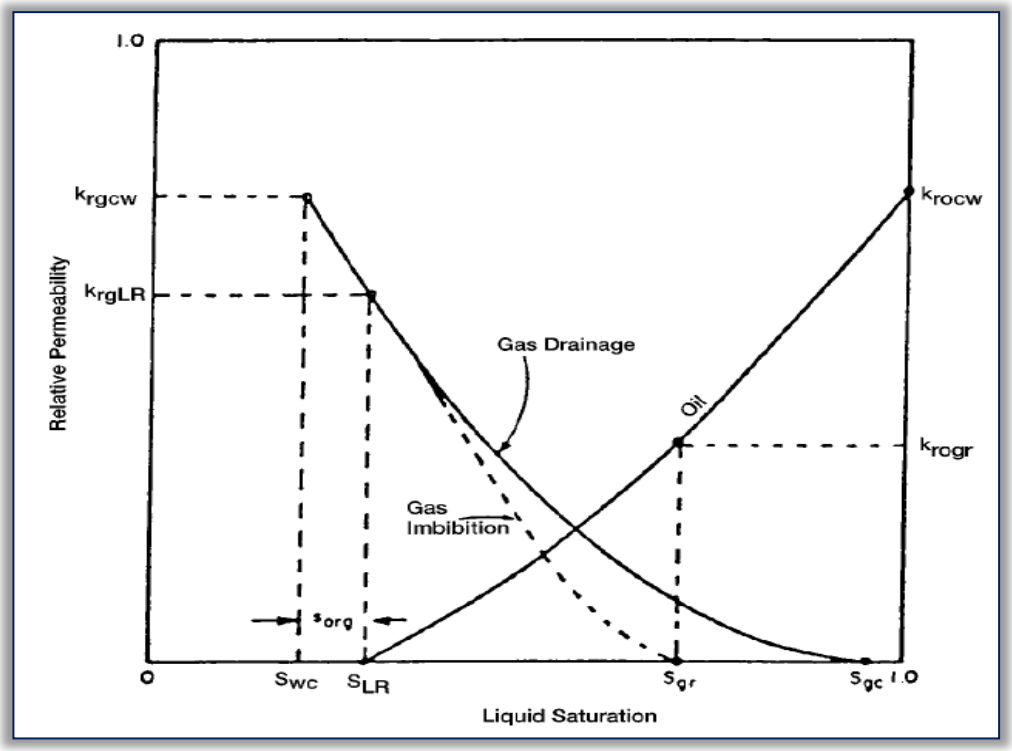

Figure 2.21: Gas-oil relative permeability (Ahmed, 2011)

2.7.4. **History matching method to predict relative permeability (Estimated data)**

According to Berg et al. (2013), and Sigmund and McCaffery (1979), this method uses real core empirical model (unsteady state experiment) in addition to theoretical core simulation model (mathematical model). In this way, the relative permeability values applied in simulator are adjusted until the pressure and production data produced from both empirical and mathematical models will match well. Then, the relative permeability data used in simulation core model is considered as the most representative to the targeted formation. Compared with unsteady state method, this approach is preferred since the gravity and capillary pressure effects can be incorporated into the simulation (Bennion and Thomas, 1991 cited in Pistone, 2011).

2.7.5. **Using pore-network modelling to calculate relative permeability (Estimated data)**

According to Al-Dhahli (2013), pore-network modelling (a physically-based simulation) has been introduced in the last two decades as an alternative way to estimate relative permeability and capillary pressure data (Figure 2.22). This method uses CT imaging or

2D thin sections to obtain a 3D digital rock. Then the 3D digital rock is either employed directly to simulate fluid flow and calculate the relative permeabilities or used to extract a pore-network (a network of pore bodies that are connected by pore throats). The pore-network obtained could be used to simulate the flooding sequence that occurs in the real reservoir which in turn produces the relative permeability data.

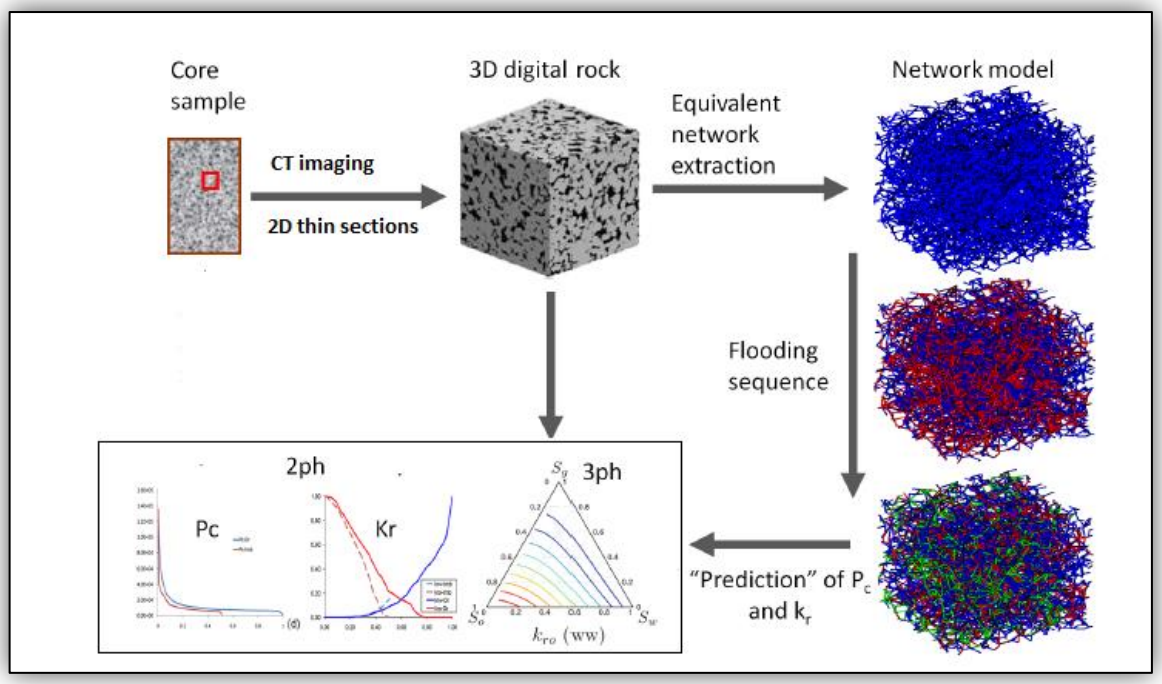

Figure 2.22: Simulations method to calculate relative permeabilities (Al-Dhahli, 2013)

2.7.6. **Analogy method**

Yuqi1 et al. (2004) mentioned that when there is no possibility to get relative permeability data either through measuring or by estimation, the analogy method presents a substitute way. It is based on getting relative permeability data from another reservoir with the same formation type.

Relative permeability data treatment

It is known that using a single method to get relative permeability data is always not sufficient to fully describe a system; therefore, applying more than one way is essential for obtaining a good representative data for the core sample. For example, Bennion and Thomas (1991) used Johnson-Bossler-Naumann (JBN) method (unsteady state based on Buckley-Leverett theory) to get real data, and then did simulation (based on correlations) to generate estimated data. After that a history matching was applied to verify the experimental data. The history matching method assumes a functional form of the system that is fit to the data using an iterative, minimum least-square solution scheme.

As it is known, the relative permeability data got from laboratory describe only the flow performance through the core sample. These data should be modified before being used in modelling of a well or reservoir performance. The data modification includes correlations of overall curve shape, cross-over points, recovery at a given produced volume, permeability at residual saturation etc., and all these procedures must be made with reference to permeability, initial fluid saturations and lithology.

Good relative permeability reports should show any experimental difficulties which may emerge, and unfortunately it is not always possible to assess service company data since flow rates are rarely constant and $\Delta p/\Delta p_i$ versus Q_i curves are not reported, so it is highly recommended that such information be a part of the contract.

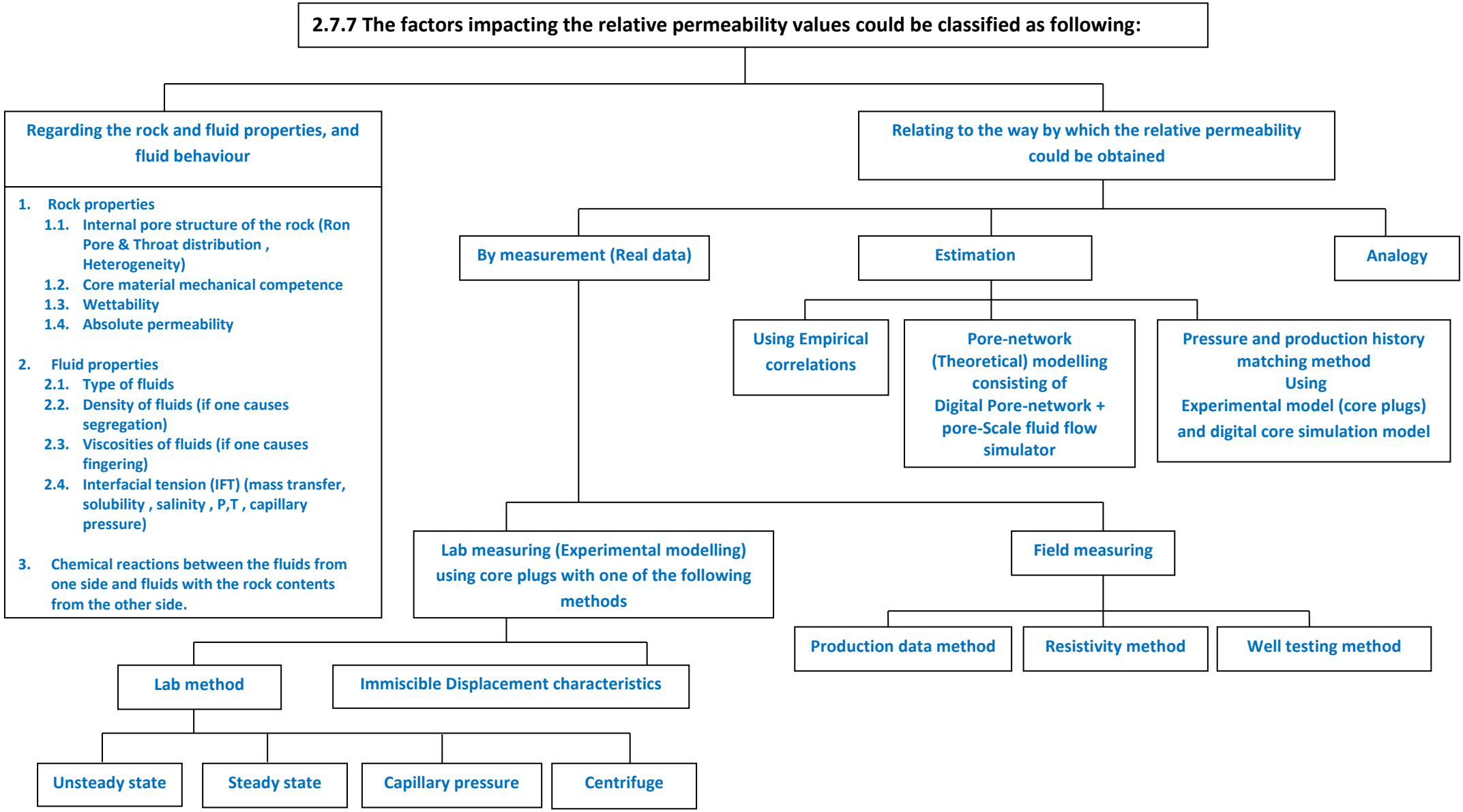
2.7.7 The factors impacting the relative permeability values could be classified as following:
Regarding the rock and fluid properties, and fluid behaviour
1. Rock properties
1.1. Internal pore structure of the rock (Ron Pore & Throat distribution , Heterogeneity)
1.2. Core material mechanical competence
1.3. Wettability
1.4. Absolute permeability
2. Fluid properties
2.1. Type of fluids
2.2. Density of fluids (if one causes segregation)
2.3. Viscosities of fluids (if one causes fingering)
2.4. Interfacial tension (IFT) (mass transfer, solubility , salinity , P,T , capillary pressure)
3. Chemical reactions between the fluids from one side and fluids with the rock contents from the other side.
Relating to the way by which the relative permeability could be obtained
By measurement (Real data)
Estimation
Analogy
Using Empirical correlations
Pore-network (Theoretical) modelling consisting of Digital Pore-network + pore-Scale fluid flow simulator
Pressure and production history matching method Using Experimental model (core plugs) and digital core simulation model
Lab measuring (Experimental modelling) using core plugs with one of the following methods
Field measuring
Production data method
Resistivity method
Well testing method
Lab method
Immiscible Displacement characteristics
Unsteady state
Steady state
Capillary pressure
Centrifuge

References

ABACI, S., EDWARDS, J. S. & WHITTAKER, B. N. 1992. Relative permeability measurements for two phase flow in unconsolidated sands. *Mine Water and the Environment,* 11**,** 11-26.

ABE, A. A. 2005. *Relative Permeability and Wettability Implications of Dilute Surfactants at Reservoir Conditions.* Idaho State University, Idaho, USA.

ABU-KHAMSIN, S. A. 2004. Basic Properties of Reservoir Rocks. 96-99.

AHMADLOO, F., ASGHARI, K. & JAMALOEI, B. Y. 2009. Experimental and Theoretical Studies of Three Phase Relative Permeability. *SPE Annual Technical Conference and Exhibition.* New Orleans, Louisiana: Society of Petroleum Engineers.

AHMED, T. 2011. Resrvoir engineering handbook.

AL-DHAHLI, A. 2013. *PORE TO F I E LD SCALE MODE L L ING OF THRE E PHASE FLOW PROCE SSES IN HET EROGENEOUS RES ERVOIRS WITH ARB ITRARY WE TTAB I L I TY.*, Heriot-Watt.

AL-FATTAH, S. 2004. Equations for water/oil relative permeability in Saudi Arabian sandstone reservoirs. *Saudi Aramco Journal of Technology***,** 48-58.

AL-KHALIFAH, A. J. A. 1988. *Determination of absolute and relative permeability using well test analysis.*

AL-YASERI, A. Z. H. 2010. *Determination of Relative Permeability from Well Production by Consideration of Fluid Type, Formation Heterogeneity, and Skin Factor.* University of Oklahoma.

ASAR, H. & HANDY, L. L. 1988. Influence of Interfacial Tension on Gas/Oil Relative Permeability in a Gas-Condensate System. *SPE Reservoir Engineering,* 3**,** 257-264.

BACHU, S. & BENNION, B. 2008. Effects of in-situ conditions on relative permeability characteristics of CO2-brine systems. *Environmental Geology,* 54**,** 1707-1722.

BAKER, L. E. 1988. Three-Phase Relative Permeability Correlations. Society of Petroleum Engineers.

BENNION, B. & BACHU, S. 2008a. Drainage and Imbibition Relative Permeability Relationships for Supercritical CO2/Brine and H2S/Brine Systems in Intergranular Sandstone, Carbonate, Shale, and Anhydrite Rocks. *SPE Reservoir Evaluation & Engineering,* 11**,** 487-496.

BENNION, D. & THOMAS, F. Recent improvements in experimental and analytical techniques for the determination of relative permeability data from unsteady state flow experiments. SPE 10th Techncial Conference and Exposition, Port of Spain, Trinidad, 1991.

BENNION, D. B. & BACHU, S. 2007. Permeability and Relative Permeability Measurements at Reservoir Conditions for CO2-Water Systems in Ultra Low Permeability Confining Caprocks. *EUROPEC/EAGE Conference and Exhibition.* London, U.K.: Society of Petroleum Engineers.

BENNION, D. B. & BACHU, S. 2010. Drainage and Imbibition CO2/Brine Relative Permeability Curves at Reservoir Conditions for High-Permeability Carbonate Rocks. *SPE Annual Technical Conference and Exhibition.* Florence, Italy: Society of Petroleum Engineers.

BENNION, D. B., THOMAS, F. B., SCHULMEISTER, B. & MA, T. 2006. A Correlation of the Low and High Temperature Water-Oil Relative Permeability Characteristics of Typical Western Canadian Unconsolidated Bitumen Producing Formations. *Canadian International Petroleum Conference.* Calgary, Alberta: Petroleum Society of Canada.

BENNION, D. B., THOMAS, F. B., SCHULMEISTER, B. E. & MA, T. 2002. A Correlation of Water and Gas-Oil Relative Permeability Properties for Various Western Canadian Sandstone and Carbonate Oil Producing Formations. *Canadian International Petroleum Conference.* Calgary, Alberta: Petroleum Society of Canada.

BERG, S., OEDAI, S. & OTT, H. 2013. Displacement and mass transfer between saturated and unsaturated CO2–brine systems in sandstone. *International Journal of Greenhouse Gas Control,* 12**,** 478-492.

BLOM, S. M. P., HAGOORT, J. & SOETEKOUW, D. P. N. 2000. Relative Permeability at Near-Critical Conditions. *SPE Journal,* 5**,** 172-181.

BLUNT, M. J. & CHRISTIE, M. A. 1994. Theory of Viscous Fingering in Two Phase, Three Component Flow. *SPE Advanced Technology Series,* 2**,** 52-60.

BROOKS, R. H. & COREY, A. T. 1966. Properties of porous media affecting fluid flow.

BUCKLEY, J. S., MORROW, N. R., PALMER, C. & DASGUPTA, P. K. 2003. WETTABILITY AND IMBIBITION: MICROSCOPIC DISTRIBUTION OF WETTING AND ITS CONSEQUENCES AT THE CORE AND FIELD SCALES. *Other Information: PBD: 1 Feb 2003.*

BUCKLEY, S. E. & LEVERETT, M. C. 1942. *Mechanism of Fluid Displacement in Sands*.

BURDINE, N. T. 1953. *Relative Permeability Calculations From Pore Size Distribution Data*.

BUSCH, A. & MÜLLER, N. 2011. Determining CO2 /brine relative permeability and capillary threshold pressures for reservoir rocks and caprocks: Recommendations for development of standard laboratory protocols. *Energy Procedia,* 4**,** 6053-6060.

CASTANEDA G, J. O. 2008. *Estimation of relative permeability curves taking into account the poro-perm effect using artificial neural networks.* Msc project, Heriot - Watt university.

CAUDLE, B. H., SLOBOD, R. L. & BROWNSCOMBE, E. R. 1951. *Further Developments in the Laboratory Determination of Relative Permeability*.

CHALBAUD, C. A., LOMBARD, J.-M. N., MARTIN, F., ROBIN, M., BERTIN, H. J. & EGERMANN, P. 2007. Two Phase Flow Properties of Brine-CO2 Systems in a Carbonate Core: Influence of Wettability on Pc and kr. *SPE/EAGE Reservoir Characterization and Simulation Conference.* Abu Dhabi, UAE: Society of Petroleum Engineers.

CINAR, Y., MARQUEZ, S. & FRANKLIN M. ORR, J. 2007. Effect of IFT Variation and Wettability on Three-Phase Relative Permeability. *SPE Reservoir Evaluation & Engineering,* 10**,** pp. 211-220.

CLUFF, R. & BYRNES, A. Relative Permeability in Tight Gas Sandstone Reservoirs-The 'Permeability Jail'Model. SPWLA 51st Annual Logging Symposium, Perth, 2010.

COREY, A. T. 1954. The interrelation between gas and oil relative permeabilities. *Producers monthly,* 19**,** 38-41.

COREY, A. T., RATHJENS, C. H., HENDERSON, J. H. & WYLLIE, M. R. J. 1956. *Three-Phase Relative Permeability*.

COUNSIL, J. R. 1979. *Steam-water relative permeability.* Stanford University.

CROTTI, M. A. & ROSBACO, J. A. 1998. Relative Permeability Curves: The Influence of Flow Direction and Heterogeneities --- Dependence of End Point Saturations on Displacement Mechanisms. *SPE/DOE Improved Oil Recovery Symposium.* Tulsa, Oklahoma: Society of Petroleum Engineers.

DAKE, L. P. 1983. *Fundamentals of reservoir engineering*, Access Online via Elsevier.
DODDS, W. S., STUTZMAN, L. F. & SOLLAMI, B. J. 1956. Carbon Dioxide Solubility in Water. *Industrial & Engineering Chemistry Chemical & Engineering Data Series,* 1**,** 92-95.
DONALDSON, E. C., CHILINGARIAN, G. V. & YEN, T. F. 1985. *Enhanced Oil Recovery, I: fundamentals and analyses*, Access Online via Elsevier.
DULLIEN, F. A. 1991. *Porous media: fluid transport and pore structure*, Access Online via Elsevier.
FAYERS, F. J. & MATTHEWS, J. D. 1984. Evaluation of Normalized Stone's Methods for Estimating Three-Phase Relative Permeabilities. *Society of Petroleum Engineers Journal,* 24**,** 224-232.
GAWISH, A. & AL-HOMADHI, E. 2008. Relative permeability curves for high pressure, high temperature reservoir conditions. *Oil and Gas Business*.
GEFFEN, T. M., OWENS, W. W., PARRISH, D. R. & MORSE, R. A. 1951. *Experimental Investigation of Factors Affecting Laboratory Relative Permeability Measurements*.
GLOVER, P. 2011. *Formation Evaluation MSc Course Notes* [Online]. Available: http://www2.ggl.ulaval.ca/personnel/paglover/CD%20Contents/Formation%20Evaluation%20English/Chapter%2010.PDF 2011].
H., A. & HANDY, L. 1988. Influence of interfacial tension on Gas/oil relative permeability in a gas - condensate system.
HASSLER, G. L. 1944. METHOD AND APPARATUS FOB PERME. Google Patents.
HONARPOUR, M., KOEDERITZ, L. F. & HARVEY, A. H. 1982. Empirical Equations for Estimating Two-Phase Relative Permeability in Consolidated Rock. *Journal of Petroleum Technology,* 34**,** 2905-2908.
HONARPOUR, M. & MAHMOOD, S. M. 1988. Relative-Permeability Measurements: An Overview. *Journal of Petroleum Technology,* 40**,** 963-966.
HONARPOUR, M. M., KOEDERITZ, F. & HERBERT, A. 1986. *Relative permeability of petroleum reservoirs*.
HUSTAD, O. S. & HANSEN, A. A consistent correlation for three phase relative permeabilities and phase pressures based on three sets of two phase data. 8th European Symposium on Improved Oil Recovery, 1995.
HUSTAD, O. S. & HOLT, T. 1992. Gravity Stable Displacement of Oil by Hydrocarbon Gas After Waterflooding. *SPE/DOE Enhanced Oil Recovery Symposium.* Tulsa, Oklahoma: 1992 Copyright 1992, Society of Petroleum Engineers Inc.
JENKINS, C., AL-SHARIF, S., HARRIS, R., WEISGRAM, J. & MICHEL, D. 2004. Forty Years of Improved Oil Recovery: Lessons from Low-Permeability Turbidites of the East Wilmington Field, California. *SPE International Petroleum Conference in Mexico.* Puebla Pue., Mexico: Society of Petroleum Engineers.
JOHNSON, E. F., BOSSLER, D. P. & NAUMANN, V. O. 1959. *Calculation of Relative Permeability from Displacement Experiments*.
JOSENDAL, V. A., SANDIFORD, B. B. & WILSON, J. W. 1952. *Improved Multiphase Flow Studies Employing Radioactive Tracers*.
JURGAWCZYNSKI, M. 2007. *Predicting absolute and relative permeabilities of carbonate rocks using image analysis and effective medium theory.* Imperial College.

KALAM, Z., OBEIDA, T. & AL MASAABI, A. Acceptable water-oil and gas-oil relative permeability measurements for use in reservoir simulation models. Society of Core Analysis Conference Paper SCA, 2007. 1-12.
KJOSAVIK, A., RINGEN, J. K. & SKJÆVELAND, S. M. 2000. Relative Permeability Correlation for Mixed-Wet Reservoirs. *SPE/DOE Improved Oil Recovery Symposium.* Tulsa, Oklahoma: Society of Petroleum Engineers.
KOPP, A., CLASS, H. & HELMIG, R. 2009. Investigations on CO2 storage capacity in saline aquifers: Part 1. Dimensional analysis of flow processes and reservoir characteristics. *International Journal of Greenhouse Gas Control,* 3**,** 263-276.
KRAUSKOPF, K. B. & BIRD, D. K. 1967. *Introduction to geochemistry,* McGraw-Hill New York.
KREVOR, S. C. M., PINI, R., ZUO, L. & BENSON, S. M. 2012. Relative permeability and trapping of CO2 and water in sandstone rocks at reservoir conditions. *Water Resources Research,* 48**,** W02532.
LEVERETT, M. C. & LEWIS, W. B. 1941. *Steady Flow of Gas-oil-water Mixtures through Unconsolidated Sands*.
LEVINE, J. 2011. Relative Permeability Experiments of Carbon Dioxide Displacing Brine and Their Implications for Carbon Sequestration.
LI, K. 2008. A New Method for Calculating Two-Phase Relative Permeability from Resistivity Data in Porous Media. *Transport in Porous Media,* 74**,** 21-33.
LI, K. & HORNE, R. N. 2006. Comparison of methods to calculate relative permeability from capillary pressure in consolidated water-wet porous media. *Water Resources Research,* 42**,** W06405.
LIU, Q., SHEN, P. & WU, Y.-S. 2008. Characterizing two-phase flow relative permeabilities in chemical flooding using a pore-scale network model.
LONGERON, D. G. 1980. Influence of Very Low Interfacial Tensions on Relative Permeability. *Society of Petroleum Engineers Journal,* 20**,** 391-401.
LOOMIS, A. G. & CROWELL, D. C. 1961. Relative permeability studies: gas-oil and water-oil systems. Bureau of Mines, San Francisco, Calif.(USA). San Francisco Petroleum Research Lab.
M. SAEEDI & POOLADI-DARVISH, M. 2007. Revisiting the Drainage Relative Permeability Measurement by Centrifuge Method Using aForward-backward Modelling Scheme.
MALONEY, D., DOGGETT, K. & TOMUTSA, L. 1997. THREE-PHASE RELATIVE PERMEABILITY CHARACTERISTICS OF A DOLOMITE ROCK PLUG.
MENZIES, A. J. 1982. *Flow characteristics and relative permeability functions for two phase geothermal reservoirs from a one dimensional thermodynamic model.* Stanford University.
MORSE, R., TERWILLIGER, P. & YUSTER, S. 1947. Relative permeability measurements on small core samples. *Oil Gas J,* 46**,** 109.
MÜLLER, N. 2011. Supercritical CO2-Brine Relative Permeability Experiments in Reservoir Rocks—Literature Review and Recommendations. *Transport in Porous Media,* 87**,** 367-383.
NKENCHO, E. E. 2010. *The predictive abilities of pore scale network models for the modelling of relative permeability and capillary pressures of two-phase mixed-wet systems.* Msc project, Heriot - Watt university.
NORDBOTTEN, J., CELIA, M. & BACHU, S. 2005. Injection and Storage of CO2 in Deep Saline Aquifers: Analytical Solution for CO2 Plume Evolution During Injection. *Transport in Porous Media,* 58**,** 339-360.

OBIORA EBUKA, E. 2010. <*Review of how relative permeability is measured expermentally for use in numerical simulation.pdf*>. Msc project., Heriot - Watt university.
OKASHA, T. M., FUNK, J. J. & AL-ENEZI, S. M. 2003. Wettability and Relative Permeability of Lower Cretaceous Carbonate Rock Reservoir, Saudi Arabia. *Middle East Oil Show*. Bahrain: Society of Petroleum Engineers.
OSOBA, J. S., RICHARDSON, J. G., KERVER, J. K., HAFFORD, J. A. & BLAIR, P. M. 1951. *Laboratory Measurements of Relative Permeability*.
PETROWIKI Measurements of relative permeability and capillary pressure.
PIRSON, S. J. 1977. *Oil reservoir engineering*, McGraw-Hill.
PIRSON, S. J. & BOATMAN, E. M. 1964. *Prediction of Relative Permeability Characteristics Of Intergranular Reservoir Rocks from Electrical Resistivity Measurements*.
PISTONE, S. 2011. *The significance of co2 solubility in deep subsurface environments.*, Stanford University.
POPE, G. A., WU, W., NARAYANASWAMY, G., DELSHAD, M., SHARMA, M. M. & WANG, P. 2000. Modeling Relative Permeability Effects in Gas-Condensate Reservoirs With a New Trapping Model. *SPE Reservoir Evaluation & Engineering,* 3**,** 171-178.
PURCELL, W. R. 1949. *Capillary Pressures - Their Measurement Using Mercury and the Calculation of Permeability Therefrom*.
RICHARDSON, J. G., KERVER, J. K., HAFFORD, J. A. & OSOBA, J. S. 1952. *Laboratory Determination of Relative Permeability*.
ROSE, W. 1987. *Relative Permeability (1987 PEH Chapter 28).*
ROSENTHAL, O. 2010. *Determination of three phase relative permeabilities for tertiary gas injection.*
SIGMUND, P. M. & MCCAFFERY, F. G. 1979. An Improved Unsteady-State Procedure for Determining the Relative-Permeability Characteristics of Heterogeneous Porous Media (includes associated papers 8028 and 8777). *Society of Petroleum Engineers Journal,* 19**,** 15-28.
SKAUGE, A., HAASKJOLD, G., THORSEN, T. & AARRA, M. 1997. Accuracy of gas-oil relative permeability from two-phase flow experiments. *Soc. Core Analyst,* 9707.
SORBIE , K., PICK UP, G. & MACKAY, E. 2005. *Reservoir Simulation.*, Institute of petroleum engineering, heriot - Watt university.
SPIVAK, A. & CHIMA, C. M. 1984. Mechanisms of Immiscible CO2 Injection in Heavy Oil Reservoirs, Wilmington Field, CA. *SPE Enhanced Oil Recovery Symposium.* Tulsa, Oklahoma: 1984 Copyright 1984 Society of Petroleum Engineers of AIME.
STANDING, M. 1975. Notes on relative permeability relationships. *Proc., University of Trondheim, NTH, Norway*.
STONE, H. 1973. Estimation of three-phase relative permeability and residual oil data. *J. Pet. Technol.;(United States),* 12.
TIAB, D. & DONALDSON, E. C. 2011. *Petrophysics: theory and practice of measuring reservoir rock and fluid transport properties*, Gulf professional publishing.
TORCASO, M. A. & WYLLIE, M. R. J. 1958. *A Comparison of Calculated krg/kro Ratios With a Correlation of Field Data*.
VAN DIJKE, M. I. J., MCDOUGALL, S. R. & SORBIE, K. S. 2001a. Three-Phase Capillary Pressure and Relative Permeability Relationships in Mixed-Wet Systems. *Transport in Porous Media,* 44**,** 1-32.

VAN DIJKE, M. I. J. & SORBIE, K. S. 2003. Pore-scale modelling of three-phase flow in mixed-wet porous media: multiple displacement chains. *Journal of Petroleum Science and Engineering,* 39**,** 201-216.

VAN DIJKE, M. I. J. & SORBIE, K. S. 2007. Consistency of three-phase capillary entry pressures and pore phase occupancies. *Advances in Water Resources,* 30**,** 182-198.

VAN DIJKE, M. I. J., SORBIE, K. S. & MCDOUGALL, S. R. 2001b. Saturation-dependencies of three-phase relative permeabilities in mixed-wet and fractionally wet systems. *Advances in Water Resources,* 24**,** 365-384.

WELGE, H. J. 1952. *A Simplified Method for Computing Oil Recovery by Gas or Water Drive*.

WYLLIE, M. & GARDNER, G. 1958. The generalized Kozeny-Carman equation. *World Oil,* 146**,** 210-213.

WYLLIE, M. R. J. 1951. *A Note on the Interrelationship Between Wetting and Nonwetting Phase Relative Permeability*.

YUQI1, D., BOLAJI, O. B. & DACUN, L. 2004. Literature Review on Methods toObtain Relative Permeability Data.

Chapter 3

CO_2 relative permeability

3.1. CO_2 relative permeability concept

The absolute permeability is generally a capacity measure for the medium to transmit one fluid through it but when two fluids or more exist in the medium, the transmit capacity (of the rock) for each fluid separately is called effective permeability, which is affected by fluid saturation and wetting characteristics of that fluid. The summation of effective permeabilities (of all fluids) is equal to absolute permeability.

To represent the percentage of effective permeability for a certain fluid to absolute permeability, an additional term has been created and defined as relative permeability, which is calculated by dividing effective permeability by absolute permeability.

$$\mathbf{k_{relative}} = \frac{\mathbf{k_{effective}}}{\mathbf{k_{absolute}}} \qquad \text{Eq. 3.1}$$

Since our study is for injection of CO_2 as supercritical gas in deep saline aquifer, the relative permeability of both CO_2 and brine will be as following:

$$k_{rw} = \frac{k_w}{k_{abs}} \qquad \text{Eq. 3.2}$$

$$k_{rco_2} = \frac{k_{co_2}}{k_{abs}} \qquad \text{Eq. 3.3}$$

Where k_w = effective permeability to brine for a given water saturation.

Where k_{co2} = effective permeability to CO_2 for a given CO_2 saturation.

Since the effective permeability values range from zero to k_{ab}, the relative permeability values will be from zero to one.

The summation of relative permeabilities is always a little less than or equal to 1.

3.2. CO_2 relative permeability importance

In multi-phase flow, the concept of CO_2 relative permeability is fundamental when predicting the following:

- Spatial and temporal distribution of CO_2 saturation and trapping.
- CO_2 migration plume during CO_2 injection (field-scale).
- Injection pressure and rate.

Relative permeability curves to CO_2 and brine can be measured in the laboratory, but the validity of using laboratory-measured relative permeability curves to describe the reservoir is subject to a number of uncertainties.

3.3. CO_2 relative permeability during drainage and Imbibition processes for CO_2-Brine system

When CO_2 is being injected into saline aquifer, it starts penetrating the aquifer formation and form plumes around the wellbore, the plumes movie inside the aquifer with velocity called plume velocity. Brine always exists in the aquifer as a wetting phase whereas CO_2 is the non-wetting phase.

When CO_2 injection starts, its saturation goes up rapidly to form a continuous and mobile phase. The saturation of CO_2 at this point is called critical gas saturation. At this critical gas saturation, the CO_2 starts to displace the brine. During displacement of brine by CO_2, the CO_2 will spread through brine and cuts the continuous phase of brine. With continuation of CO_2 injection, the saturation of brine decreases to a minimum value and called as irreducible or connate water saturation in which the brine becomes discontinuous and immobile phase. The brine relative permeability at this point will be zero. This process could be represented in the lab as drainage processes.

The maximum relative permeability value of CO_2 during drainage is called CO_2 endpoint relative permeability.

If the injection is suspended, the brine enters into formation as influx from adjacent layers. Its saturation would increase to form a continuous and mobile phase at critical brine saturation, and then starts to displace the CO_2. During the displacement of CO_2 by brine, the brine will spread through CO_2 and cuts the continuous phase of CO_2. As brine water saturation keeps increasing, the saturation of CO_2 decreases to a minimum value,

called residual gas saturation in which the CO_2 becomes discontinuous and immobile phase. The CO_2 relative permeability at this point will be zero. These processes could be represented in the lab as Imbibition processes (Figure 3.1).

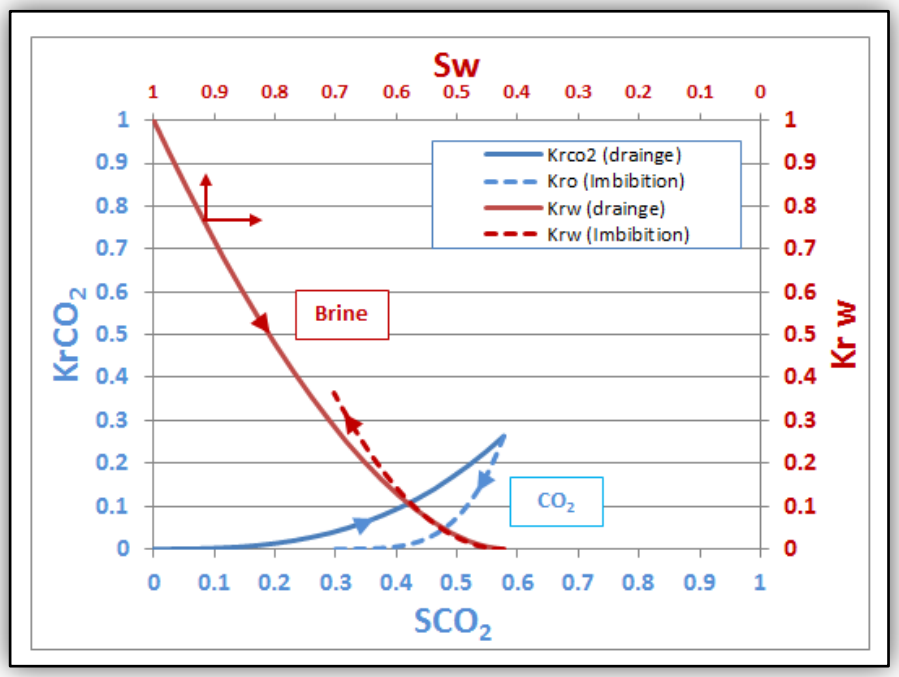

Figure 3.1: CO_2 relative permeability curves (Drainage and Imbibition) for CO_2-Brine system

3.4. Source of CO_2 relative permeability data

3.4.1. Lab measurement (real data)

If the system is CO_2-Brine, the first laboratory procedure is to saturate the core with brine, and then start injecting CO_2. The saturation of CO_2 goes up to form a mobile phase at **Critical CO_2 saturation** ① and then starts to displace brine. During CO_2 injection the relative permeability of CO_2 and brine are measured. The CO_2 injection should continue until brine relative permeability equals zero. The saturation of CO_2 at this point will be high (but < 100%) and the saturation of brine will be minimum (**irreducible or connate water saturation**①). At this irreducible water saturation (S_{wirr}) only gas can flow; this procedure is called primary drainage and could be identified as the process of measuring CO_2 relative permeability when the brine saturation decreases from 100%.

After that, brine injection is resumed. The saturation of brine goes up to form a mobile phase at **critical brine saturation** and then starts to displace CO_2 from the core. During brine injection the relative permeability of brine and CO_2 are measured. The brine injection should continue until CO_2 relative permeability equals zero. At this point, the saturation of brine will be high (but < 100%), while the saturation of CO_2 will be minimum (**residual gas saturation**). At residual gas saturation (S_{gr}) only brine can flow. This procedure is called primary imbibition and could be identified as the process of measuring brine relative permeability when the CO_2 saturation decreases from high saturation level in the presence of irreducible brine water saturation.

The third procedure is injecting CO_2 again into the core. The saturation of CO_2 goes up to form a mobile phase at **critical CO_2 saturation ②** and then starts to displace brine. During CO_2 injection the relative permeability of CO_2 and brine are measured. The CO_2 injection should continue until brine relative permeability equals zero. The saturation of CO_2 at this point will be high (but < 100%) and the saturation of brine will decline to a minimum value (**irreducible or connate brine saturation②**). This procedure is called secondary drainage and could be defined as the process of measuring CO_2 relative permeability when the brine saturation decreases from high saturation level in the presence of residual CO_2 saturation (Figure 3.2, Figure 3.3).

As mentioned before, critical saturation is the minimum saturation value required to form a mobile phase for both CO_2 and brine. Theoretically, for non-wetting phase (CO_2) the **critical Co2 saturation ②** is equal to **residual gas saturation**, but they are not identical since **critical Co_2 saturation ②** is measured in the direction of increasing saturation (secondary drainage), while **residual gas saturation** is measured in the direction of reducing saturation (primary imbibition).

As for wetting phase (brine), the **critical brine saturation** is greater than **irreducible or connate brine saturation①**, and it's owing to the fact that brine (at irreducible saturation) occupies the smaller pores where the capillary forces (resistant to flow) are the greatest, and to start moving, extra amounts of brine should be added to **irreducible brine saturation ①** in order to overcome the effect of high capillary forces. As an additional result, it has been found that the **critical brine saturation** is relatively higher than **critical saturation** for CO_2 which occupies the larger pores with small capillary pressure and the least difficult to flow.

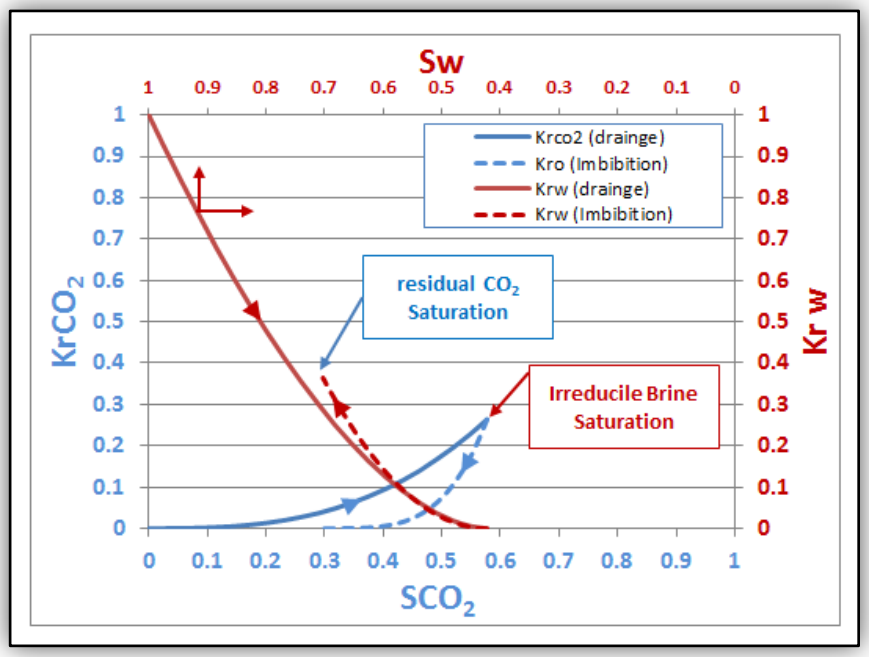

Figure 3.2: Irreducible and Residual saturations

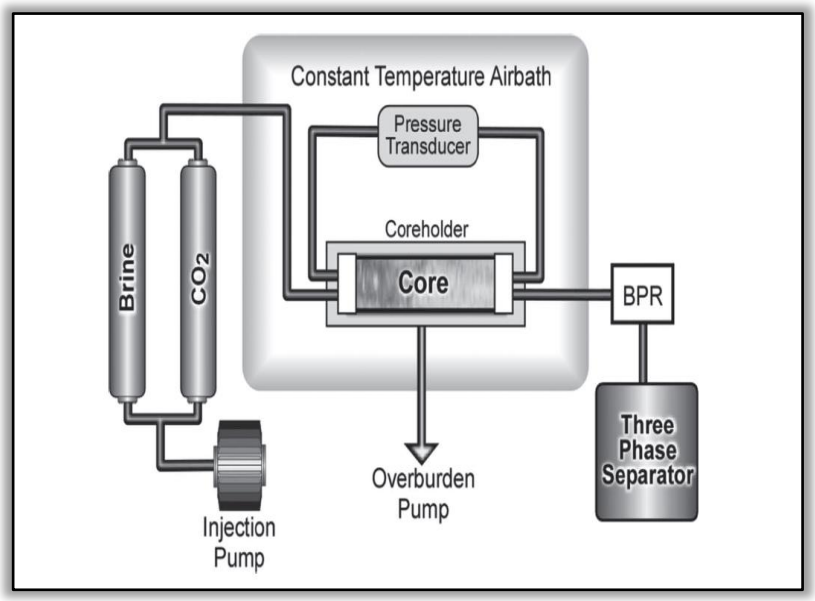

Figure 3.3: Experimental apparatus used for CO_2 relative permeability

Challenges facing the measurement of CO_2 relative permeability in labs

Since the unsteady state method is used to measure the CO_2 relative permeability in brine system, all challenges mentioned in the previous chapter will be present here, but what I would like to add to this matter is that in 1991, Bennion and Thomas (1991) presented a simple correction technique for Johnson-Bossler-Naumann (JBN) calculations concerning the capillary pressure; this correction includes incrementally increasing the fluid injection rate after starting drainage process then measuring the change in endpoint permeability and doing the following:

- If the endpoint permeability stays constant, it is safe to assume that capillary effects are negligible.
- If the endpoint permeability increases or decreases with increasing injection rate, then there is a simple correction technique wherein a nonlinear model is fit to the data and relative permeability curves are scaled to fit the corrected endpoint permeabilities.

3.4.2. By using correlations to estimate relative permeability values of CO_2 and Brine:

This method is usually used when it is not possible to measure CO_2 relative permeability in the Lab; there are many correlations in literature used to estimate relative permeability values of CO_2 as following:

A) Corey's Correlations (Ahmed, 2011)

A.1) **Corey (independent saturations)**

In this model, the wetting and non-wetting phase relative permeabilities are assumed to be independent of the saturations of the other phases; consequently, the correlation requires only a single suite of gas/water-relative permeability data.

$$k_{rg} = \left[\frac{S_g}{1-S_{iw}}\right]^2 \left[1 - \left(\frac{1-S_g-S_{iw}}{1-S_{iw}}\right)^2\right] \quad \text{Eq. 3.4}$$

$$k_{rw} = \left[\frac{S_w - S_{iw}}{1-S_{iw}}\right]^4 \quad \text{Eq. 3.5}$$

A.2) **Corey (Generalized) (Associates, 2014)**

This is similar to the Corey's correlation but developed for a wider range of rock and wettability characteristics. This correlation can be used to change the endpoints of water-gas relative permeability curves while still retaining the shape of the curves.

$$K_{rg} = K_{rg_{(Wir)}} \left[\frac{S_g - S_{gr}}{1 - S_{gr} - S_{wir}} \right]^{ng} \qquad \text{Eq. 3.6}$$

$$K_{rw} = K_{rw_{(gr)}} \left[\frac{S_w - S_{wir}}{1 - S_{gr} - S_{wir}} \right]^{nw} \qquad \text{Eq. 3.7}$$

Where:

$K_{rg(wir)}$ = gas endpoint relative permeability at irreducible water saturation.

K_{rwgr} = water endpoint relative permeability at residual gas saturation.

S_{gr} = residual gas saturation, S_{wir} = irreducible water saturation.

n_g = Corey's gas exponent , n_w = Corey's water exponent.

B) Pirson's Correlations (Water – wet rocks) (Ahmed, 2011)

B.1) **Pirson's Correlation for k_{rw}**

$k_{rw} = \sqrt{S_w^*}\ S_w^3$ (for Drainge and Imbibition) Eq. 3.8

B.2) **Pirson's Correlation for k_{rg}**

$$k_{rg} = \left[1 - \left(\frac{S_w - S_{wc}}{1 - S_{wc} - S_g}\right)\right]^2 \quad \text{(For Imbibition)} \quad \text{Eq. 3.9}$$

$$k_{rg} = (1 - S_w^*)\left[1 - (S_w^*)^{0.25}\ \sqrt{S_w}\ \right]^{0.5} \quad \text{(For Drainage)} \quad \text{Eq. 3.10}$$

Where:

$$S_w^* = \frac{S_w - S_{wc}}{1 - S_{wc}} \quad \text{Eq. 3.11}$$

S_w = brine water saturation

S_g = gas saturation

C) Van Genuchten correlation and Corey (Pruess et al., 2001)

$$k_{rg} = (1 - \hat{S})^2 \ (1 - \hat{S}^2) \qquad \text{Eq. 3.12}$$

$$\hat{S} = \frac{S_w - S_{wr}}{1 - S_{wr} - S_{gr}} \qquad \text{Eq. 3.13}$$

$$k_{rw} = \sqrt{S^*} \left[1 - \left(1 - [S^*]^{\frac{1}{m}}\right)^m\right]^2 \qquad \text{Eq. 3.14}$$

$$S^* = \frac{S_w - S_{wr}}{1 - S_{wr}} \qquad \text{Eq. 3.15}$$

Where:

S_w = Brine water saturation

S_{wr} = Irreducible water saturation

S_{gr} = residual gas saturation

m = exponent

3.5. Importance of CO_2 relative permeability

The relative permeability and residual gas saturation decisively affect injection and storage parameters; these parameters (for instance, the injectivity or the amount which could be injected) depend completely on CO_2 relative permeability, so CO_2 relative permeability and residual gas saturation are considered as the most important elements of CO_2 displacement characteristics.

3.6. CO_2 relative permeability data

Very few laboratory experiments have been published on CO_2 -Brine systems, and for the study purposes, I've collected as much CO_2 – Brine relative permeabilities as possible and classified them in Appendix A.

Some researchers conducted experiments to measure relative permeability for CO_2-Brine system at in-situ conditions. They used core samples filled with brine. CO_2 had been injected firstly to get CO_2 relative permeability curves (drainage); after that, brine was re-injected to generate brine relative permeability (imbibition). The conducted experiments are as follows:

a) Bennion and Bachu (2005), Bennion and Bachu (2006a), Bennion and Bachu (2006c), Bennion and Bachu (2007), Bachu and Bennion (2008), Bennion and Bachu (2008a), Bennion and Bachu (2008b), Bennion and Bachu (2010), Bennion and Bachu (2006b) used sandstone and carbonate rock samples obtained from different formations in Wabamun Lake area in Alberta (Alberta basin, part of the Western Canada Sedimentary Basin), southwest of Edmonton western Canda.

b) Perrin and Benson (2010) measured, at reservoir conditions, the relative permeabilities of CO_2 -Brine system using Berea sandstone rock[2] and Otway sandstone sample from CO_2CRC- Otway project, Australia.

c) Krevor et al. (2012) used Berea sandstone samples in addition to three sandstone core plugs from different formations; one from the Paaratte formation in Southern Australia, and Mt. Simon sandstone in Illinois; the third one from Tuscaloosa massive sand in Alabama.

d) Akbarabadi and Piri (2013) conducted relative permeability experiments on CO_2 -Brine system at reservoir conditions over both of Berea sandstone rock samples.

The data collected (from the above studies) are tabled in the (appendix A).

[2] Core samples of sedimentary rock have been widely recognized by the petroleum industry, usually are being used to make comparisons with other studies conducted on different - source sandstone samples.

References

AHMED, T. 2011. Resrvoir engineering handbook.

AKBARABADI, M. & PIRI, M. 2013. Relative permeability hysteresis and capillary trapping characteristics of supercritical CO2/brine systems: An experimental study at reservoir conditions. *Advances in Water Resources,* 52**,** 190-206.

ASSOCIATES, F. 2014. *Relative Permeability Correlations* [Online]. Available: http://www.fekete.com/SAN/WebHelp/FeketeHarmony/Harmony_WebHelp/Content/HTML_Files/Reference_Material/Calculations_and_Correlations/Relative_Permeability_Correlations.htm.

BACHU, S. & BENNION, B. 2008. Effects of in-situ conditions on relative permeability characteristics of CO2-brine systems. *Environmental Geology,* 54**,** 1707-1722.

BENNION, B. & BACHU, S. 2005. Relative Permeability Characteristics for Supercritical CO2 Displacing Water in a Variety of Potential Sequestration Zones in the Western Canada Sedimentary Basin. *SPE Annual Technical Conference and Exhibition.* Dallas, Texas: Society of Petroleum Engineers.

BENNION, B. & BACHU, S. 2008a. Drainage and Imbibition Relative Permeability Relationships for Supercritical CO2/Brine and H2S/Brine Systems in Intergranular Sandstone, Carbonate, Shale, and Anhydrite Rocks. *SPE Reservoir Evaluation & Engineering,* 11**,** 487-496.

BENNION, D. & THOMAS, F. Recent improvements in experimental and analytical techniques for the determination of relative permeability data from unsteady state flow experiments. SPE 10th Techncial Conference and Exposition, Port of Spain, Trinidad, 1991.

BENNION, D. B. & BACHU, S. 2006a. The Impact of Interfacial Tension and Pore Size Distribution/Capillary Pressure Character on CO2 Relative Permeability at Reservoir Conditions in CO2-Brine Systems. *SPE/DOE Symposium on Improved Oil Recovery.* Tulsa, Oklahoma, USA: Society of Petroleum Engineers.

BENNION, D. B. & BACHU, S. 2006b. Supercritical CO2 and H2S—Brine Drainage and Imbibition Relative Permeability Relationships for Intergranular Sandstone and Carbonate Formations. *SPE Europec/EAGE Annual Conference and Exhibition.* Vienna, Austria: Society of Petroleum Engineers.

BENNION, D. B. & BACHU, S. 2006c. Dependence on Temperature, Pressure, and Salinity of the IFT and Relative Permeability Displacement Characteristics of CO2 Injected in Deep Saline Aquifers. *SPE Annual Technical Conference and Exhibition.* San Antonio, Texas, USA: Society of Petroleum Engineers.

BENNION, D. B. & BACHU, S. 2007. Permeability and Relative Permeability Measurements at Reservoir Conditions for CO2-Water Systems in Ultra Low Permeability Confining Caprocks. *EUROPEC/EAGE Conference and Exhibition.* London, U.K.: Society of Petroleum Engineers.

BENNION, D. B. & BACHU, S. 2008b. Correlations for the Interfacial Tension Between Supercritical Phase CO2 and Equilibrium Brines at In Situ Conditions. Society of Petroleum Engineers.

BENNION, D. B. & BACHU, S. 2010. Drainage and Imbibition CO2/Brine Relative Permeability Curves at Reservoir Conditions for High-Permeability Carbonate Rocks. *SPE Annual Technical Conference and Exhibition.* Florence, Italy: Society of Petroleum Engineers.

BERG, S., OEDAI, S. & OTT, H. 2013. Displacement and mass transfer between saturated and unsaturated CO2–brine systems in sandstone. *International Journal of Greenhouse Gas Control,* 12**,** 478-492.

DRIA, D. E., POPE, G. A. & SEPEHRNOORI, K. 1993. Three-Phase Gas/Oil/Brine Relative Permeabilities Measured Under CO2 Flooding Conditions. *SPE Reservoir Engineering,* 8**,** 143-150.

GHANBARI, S., AL-ZAABI, Y., PICKUP, G. E., MACKAY, E., GOZALPOUR, F. & TODD, A. C. 2006. Simulation of CO2 Storage In Saline Aquifers. *Chemical Engineering Research and Design,* 84**,** 764-775.

KREVOR, S. C. M., PINI, R., LI, B. & BENSON, S. M. 2011. Capillary heterogeneity trapping of CO2 in a sandstone rock at reservoir conditions. *Geophysical Research Letters,* 38**,** L15401.

KREVOR, S. C. M., PINI, R., ZUO, L. & BENSON, S. M. 2012. Relative permeability and trapping of CO2 and water in sandstone rocks at reservoir conditions. *Water Resources Research,* 48**,** W02532.

LEVINE, J. 2011. Relative Permeability Experiments of Carbon Dioxide Displacing Brine and Their Implications for Carbon Sequestration.

OKABE, H., TSUCHIYA, Y., MIHAMA-KU, H. & SHINJYUKU-KU, O. Experimental investigation of residual CO 2 saturation distribution in carbonate rock. International symposium of the society of core analysts, Abu Dhabi, UAE, 2008.

PENTLAND, C. H., EL-MAGHRABY, R., IGLAUER, S. & BLUNT, M. J. 2011. Measurements of the capillary trapping of super-critical carbon dioxide in Berea sandstone. *Geophysical Research Letters,* 38**,** L06401.

PERRIN, J.-C. & BENSON, S. 2010. An Experimental Study on the Influence of Sub-Core Scale Heterogeneities on CO2 Distribution in Reservoir Rocks. *Transport in Porous Media,* 82**,** 93-109.

PISTONE, S. 2011. *The significance of co2 solubility in deep subsurface environments.*, Stanford University.

PRUESS, K., XU, T., APPS, J. & GARCIA, J. 2001. Numerical Modeling of Aquifer Disposal of CO2. *SPE/EPA/DOE Exploration and Production Environmental Conference.* San Antonio, Texas.

SHI, J.-Q., XUE, Z. & DURUCAN, S. 2009. History matching of CO2 core flooding CT scan saturation profiles with porosity dependent capillary pressure. *Energy Procedia,* 1**,** 3205-3211.

SUEKANE, T., NOBUSO, T., HIRAI, S. & KIYOTA, M. 2008. Geological storage of carbon dioxide by residual gas and solubility trapping. *International Journal of Greenhouse Gas Control,* 2**,** 58-64.

VAN GENUCHTEN, M. T. 1980. A Closed-form Equation for Predicting the Hydraulic Conductivity of Unsaturated Soils1. *Soil Sci. Soc. Am. J.,* 44**,** 892-898.

ZUO, L., KREVOR, S., FALTA, R. & BENSON, S. 2012. An Experimental Study of CO2 Exsolution and Relative Permeability Measurements During CO2 Saturated Water Depressurization. *Transport in Porous Media,* 91**,** 459-478.

Chapter 4

Designing and applying an assessment package tool for $KrCO_2$ experiments.

4.1. Introduction

It is known that the CO_2 relative permeability is considered as one of the factors having a decisive effect on CO_2 flow properties either through (CGS) or (EOR) operations. These flow properties may include injectivity, CO_2 plume migration during the injection, displacement, saturation, trapping and sequestration. The CO_2 relative permeability could be measured in the lab using empirical models to get real data, or it could be calculated or estimated using empirical correlations or mathematical modelling[3]. The practical or experimental way (Lab or empirical model) is mostly preferred, which could be conducted in two ways: steady state or un-steady state methods. As a matter of fact, measuring CO_2 relative permeability is a complicated issue since there are wide differences in applied experimental setups whether the method used is steady state or un-steady state; also the ways used for interpretation are variant, and not to forget that each experiment carried out has characteristic conditions of temperature, pressure, rock type, and finally carrying out an experiment for CO_2 relative permeability usually faces many challenges and difficulties. One of these problems is attributed to small sample set not being representative of real reservoirs, and the other one is the essential correctness being done for the tests to simulate what happens in the reservoir.

All that mentioned will certainly impact the values and accuracy of CO_2 relative permeability data produced; therefore, it is not easy to compare the results and determine the cause of differences. Consequently, additional experiments are required to close this gap in CO_2 relative permeability knowledge. In this study, we are going to make a general review of CO_2 relative permeability experiments done between 1993 and 2013. The review includes standards for lab measurements and challenges facing experimental procedures. The study also looks forward to designing and applying an assessment package tool consisting of fundamental indicators to be used to verify the protocols and data resulting from CO_2 relative permeability experiments published. Furthermore, recommendations will be made to avoid errors in experimental procedures and resulting data. It is hoped that all that will prospectively help in determining lab measurements needed to be defined, and thus getting reliable CO_2 relative permeability data to be used for obtaining accurate prediction of the flow properties to CO_2 through (CGS) or (EOR). Finally, introducing some vital notices whereby the Co_2 relative

[3] Digital core or digital pore-network is being run through fluid flow simulator.

permeability curves could be read and interpreted correctly will be an additional target at the end of this chapter.

4.2. Assessment indicators to protocols and data resulting from CO_2 relative permeability experiments published

4.2.1. Type of method used

A) Un-steady state

Archer and Wong (1973) cited in Sigmund and McCaffery (1979) mentioned that using the conventional Johnson-Bossler-Naumann (JBN) methods for determining relative permeabilities from a water flood test could give invalid results for heterogeneous carbonate as well as for relatively homogeneous porous media having a mixed wettability. The error is observed as a stepwise or humped shape of water relative permeability curves mainly. The abnormal shapes of the relative permeability do not represent properties of the bulk of the core sample, and were attributed to the effect of water breakthrough ahead of the main flood front entering the JBN calculation. And not to forget that in (JBN) method calculations the effects of both capillary pressure and gravity are neglected. These simplifying assumptions reduce the accuracy of (JBN) method.

Consequently, using the numerical solution (simulations) proposed by Archer and Wong (1973) is obligatory in conjunction with the measurement of the relative permeability in the lab. According to Berg et al. (2013) and Sigmund and McCaffery (1979), this method used empirical model (core plug un-steady state experiment) and theoretical core model (simulation model) simultaneously to get the most representative CO_2 relative permeability for the targeted formation. This is done by adjusting the CO_2 relative permeability values applied in the simulator until the pressure and production data (produced from both empirical and theoretical models) have a good matching, but what is important is that it is possible to get more than one set of data (due to the impact of velocity), but the one which is considered as the most representative to the targeted formation must be unique, and it (unique data set) could be verified by comparing saturation and capillary maps drawn by the simulator with that obtained from CT scan or (NMR) imaging tools.

This approach is more favoured since the gravity and capillary pressure effects can be incorporated into the simulation (Pistone, 2011), and the effect of water breakthrough ahead of the main flood front is avoidable (Pistone, 2011).

Berg et al. (2013) confirmed that the un-steady method in fact cannot access the parts of the sample where water saturation is very low.

B) Steady state

The steady state technique is considered as a more representative technique to reservoir conditions since it includes capillary equilibrium and the calculations are simple as Darcy's law is the only calculations needed to be applied for each fluid. Moreover, the system saturation in steady state method is homogeneous. On the other hand, the un-steady state is considered to be the most realistic in matching water-gas displacement, for instance in the Brine–CO_2 system.

4.2.2. **Issues relating to the core properties.**

A) Core heterogeneity

In a homogeneous sample, both results whether coming from a steady state method or an un-steady state are the same, but in a heterogeneous one they are completely different. It is known that all samples have a degree of heterogeneity however small it is, and when applying an un-steady state method in heterogeneous cores, the displacing fluid will follow the heterogeneity paths instead of spreading uniformly all over the core, and as a result, the saturation is to be incomplete and the fluid does not flow the entire sample (Müller, 2011). Bennion and Bachu (2005) and Perrin et al. (2009) attributed the high irreducible brine saturation value at the end of drainage to heterogeneity impact. Sigmund and McCaffery (1979) developed an enhanced unsteady state test method to measure the relative permeability of heterogeneous carbonate core samples, and they added that the method can be applied to all porous rocks, regardless of the size, direction and distribution of the heterogeneities. However, Sigmund and McCaffery (1979) mentioned that the existence of large-scale heterogeneity like vugs, fractures, and stratification results in the derived relative permeability relations to be impacted by viscosity or mobility ratio and displacement rate.

Using the steady state method resolves the problem of core heterogeneity since both fluids are injected together and invade the pores at the same time, so the saturation will

be distributed uniformly throughout the sample and the relative permeability generated will represent an average to the relative permeability for each layer.

Sigmund and McCaffery (1979) remarked that heterogeneity is one of the most common reasons of uncertainties when turning core data into field scale. The 3D CT scan is necessary to verify whether there is heterogeneity or not.

B) Core material mechanical competence

Müller (2011) clarified that the core material mechanical competence may be very weak due to the origin of the rock (unconsolidated and friable rocks) or as a result of sampling or core retrieve technique (like side cores). This problem brings about incomplete fluid saturation, and consequently the fluid does not flow the entire sample.

C) Core absolute permeability

Fluid distribution along the core is affected by absolute permeability of the core.

D) Core size and orientation

The orientation, length and cross sectional area of the core are very important parameters in measuring CO_2 relative permeability. For instance, in horizontal experimental set ups, gravity force may lead to fluid segregation owing to density differences. All that results in CO_2 being more buoyant than other fluids and flowing at the top of core plug (Müller, 2011). Therefore, the vertical position to the core will help in getting rid of this problem.

4.2.3. Rock wettability altering due to the impact of supercritical CO_2

Chalbaud et al. (2007) and Chiquet et al. (2007) mentioned that if CO_2 is in a supercritical condition, it may impact the rock wettability specifications and convert it from strong brine-wet to either weak brine-wet or gas-wet.

4.2.4. Overburden stress, clay and fines content

Apart from the well-known parameters affecting the relative permeability, many researchers (Bennion and Thomas, 1991, Crotti and Rosbaco, 1998) confirmed that there is an effect of additional factors on the relative permeability curves, for instance, the overburden stress, clay and fines content. The samples are usually fired at 600^{o}C for 17 hours to steady clays and prevent any unwanted swelling or chemical reactions, but

impact of the other additional factors stays unavoidable, all that means there is still a long way to get an accurate method for obtaining true data.

4.2.5. **Solubility and IFT**

According to Müller (2011), when CO_2 is at a supercritical state, both brine and CO_2 may dissolve in each other, but it is generally known that CO_2 dissolves much more in water than does water in CO_2. In other words, the solubility degree of water in CO_2 is less than that of CO_2 in water. The solubility of water in CO_2 may cause formation dry-out near the injection well (Muller et al., 2009, Pruess and Müller, 2009).

Berg et al. (2013) argued that if the brine used is not saturated with CO_2 (un-equilibrated or un-saturated brine) and the CO_2 used is also not saturated with brine (un-equilibrated or un-saturated CO_2), the mass transfer between those non-equilibrated phases would be expected whenever the pressure changes, from field scale viewpoint and through CO_2 injection. This case corresponds to the flood front where fluids have not yet been fully saturated.

Therefore, to prevent the effect of mass transfer phenomenon on relative permeability data when un-steady state is applied, brine-saturated CO_2 is injected during drainage, and CO_2-saturated brine is injected throughout imbibition. In the field, this case is representative for regions located behind the flood front, particularly in the centre of the plume where fluids are fully equilibrated (Berg et al., 2013).

As for IFT, it is known that the IFT decreases as solubility rises, so comparison with similar relative permeability data is essential to ensure the effect of IFT.

4.2.6. **Viscosity ratio or mobility**

Unfavourable viscosity ratio leads the displacement to be inefficient, resulting in the irreducible and residual saturations to be higher than expected as a result of bypassing some parts of the core sample; the last one as well, causes the assumption of uniform saturation in dynamic displacement to be cancelled and leads to rapid CO_2 breakthrough at outlet point. Finally, all that mentioned will result in false data of relative permeability being produced. The CO_2 viscosity increases with increasing the pressure so the brine-to-CO_2 viscosity ratio will decrease as a result of CO_2 viscosity increasing under the impact of pressure. It is the same for IFT, which was found to decrease with increasing the pressure; therefore, both IFT and viscosity ratio have similar

dependencies on pressure, temperature and water salinity. Practically, there is no other method to change IFT value without having an impact on the viscosity ratio of CO_2-brine phases.

4.2.7. Partial or non-uniform fluid saturation - incomplete Brine or CO_2 displacement

Due to many reasons, the saturation of a fluid may not distribute uniformly all over the core sample, and as a result, the displacement with respect to other fluids will be incomplete. Below are some reasons of this problem.

A) Viscous fingering (the unstable flow)

Low viscous CO_2 cannot displace brine in a piston-like motion (the CO_2 does not contact the entire brine and bypasses some sections) and as a result viscous fingering occurs, which cancels out the assumption of uniform saturation in dynamic displacement, and causes the displacement to be inefficient. The irreducible and residual saturations are usually expected to very high. Furthermore, viscous fingering also leads to rapid CO_2 breakthrough at the outlet point. All that mentioned will result in false data of relative permeability being produced. To overcome this problem, the WAG (water alternating gas slugs) is applied. The idea of this technique is that the water slugs will lower the mobility of the CO_2 and lead to a more piston-like displacement with higher flood efficiencies.

B) Gravitational forces (phase segregation problems)

In horizontal experimental set ups, gravity force may lead to fluid segregation owing to density differences. All that results in CO_2 being more buoyant than other fluids flowing at the top of core plug (Müller, 2011).

4.2.8. Dominant viscous forces

It is known that in the reservoir conditions, the capillary and gravitational forces are the dominant forces, and to simulate these conditions in the lab, technicians need a very long time, and they usually face some complicated problems like capillary end effect; therefore, the customary solution is to make the viscous forces as dominant forces to generate relative permeability data in labs; this procedure could be carried out by applying high injection rates. However, Dake (1994) emphasized that the capillary and

gravitational forces have a considerable impact on relative permeability data, so these forces should be considered when making the calculations.

Generally, in both lab methods, if viscous forces are not dominant in the reservoir, only the end points will be useful and could be obtained only by injecting the displacing phase.

4.2.9. **Flow direction**

What is important in this matter is that if the core is extracted vertically from the well, it will not be logical to apply horizontal core flooding in the lab as the flow direction over the reservoir is to be perpendicular to the flow direction through the core in the lab.

4.2.10. **Interference between relative permeability data and capillary pressure data**

It is a fact that relative permeability and capillary pressure interfere with each other throughout the experiments; therefore, corrections must be made by using numerical simulation means which can calculate simultaneously both the relative permeability and the capillary pressure. Many simulation runs and data sets are necessary, as one simulation run cannot generate a unique solution using a single data set (Müller, 2011).

4.2.11. **Up-scaling laboratory results to reservoir conditions**

In general, the lab experiments are usually done on small core plugs, size ranging from 0.05 to 0.15m, whereas the grid-blocks of reservoir model used in the simulations could range from 0.1 to 1,000m. Therefore, the big question here is how a small piece of formation rock could be representative for the whole formation (Müller, 2011). Consequently, up-scaling laboratory data to reservoir conditions should be given special attention as it is fundamental to minimizing the uncertainty in the simulation results.

4.2.12. **Base permeability and relative permeability**

The relative permeability is effective permeability divided by base permeability. The base permeability could be absolute permeability measured by using air or CO_2-saturated brine permeability or permeability of CO_2 at irreducible brine saturation. The three types of base permeabilities are different from each other in value, so an excellent correlation among all these permeabilities must be present to avoid the problem relating to which permeability should be used (to generate the relative permeability).

4.2.13. **CO_2 reaction with the sample rock minerals**

The reactive effect of carbonic acid, resulting from dissolving of CO_2 in water, may lead to changing the internal pore structure of the core sample which appears as altering in the porosity and absolute permeability of the sample; therefore, in many cases the steady state method is not valid to generate relative permeability data in a brine–CO_2 system as it requires a very long time to get to capillary and saturation equilibrium. However, the produced water should, in case of doubt, be analysed to investigate the extent of salts and minerals dissolved.

4.2.14. **Capillary end effect (collection of wetting phase at the outlet)**

Müller (2011) argued that, although the good design of inlet and outlet could mitigate the capillary end effect considerably, the capillary end effect could not be completely prevented. (Berg et al., 2013) said that, in order to diminish the impact of the capillary end-effect on the relative permeability measurement, a long core must be used, and then the saturations, in addition to pressure drop, could be safely measured over the central section of the core away from inlet and outlet. According to Bennion and Bachu (2008a) the capillary end effects could be avoided by conducting a high-rate displacement.

4.2.15. **Saturations profile and measurement**

The fluids must flow through the entire core, not only parts, as the incomplete fluid saturation of the core always causes problems in interpreting data. Another important issue is that the core must not be dismounted from the holder to measure the saturation, as the dismounting results in changing the core's conditions. Therefore, the advanced methods must be applied to monitor the fluid saturation and record its profile along the core axis during the displacement, and they have to be applied as well to avoid the errors resulting from applying the old conventional methods (mass balance methods) in which the core sample is dismounted from the holder to estimate the saturations.

These advanced methods have been arranged subsequently from the old to the most recent and the most expensive (Glover, 2011):

- Computerized tomography (CT) scans.
- Nuclear magnetic scattering (NMR), which is a very new application and similar to CT scanning with increased resolution, but it is very expensive.
- Scanning electron microscope (SEM).

Although the advanced-methods mentioned produce a complete 3D saturation distribution map of fluids inside the core, but such saturation maps could also be obtained from the simulations; therefore, using more than one tool to get fluid saturations map is very important to get a confirmed picture of saturation distribution through the core.

The X-ray CT scanning, for instance, could give 3D pictures for CO_2 and brine saturations in real time and in-situ conditions, inside the core sample.

4.2.16. **Challenges relating to instruments or devices used in the experiments**

Using water baths to heat liquids to reservoir temperature before entering the core and using ovens to keep the core holder at reservoir temperature, in addition to applying high pressure to simulate pressure existing in the reservoir all will cause very high stress on the material of experiment devices particularly relating to connection pieces; also the corrosive nature of carbonic acid (resulting from CO_2 dissolving in the water) may lead the acid to attack the experiment's equipment (Müller, 2011); therefore, the parts of the experimental model used must be fully protected from any damage that may happen, since the damage however small will certainly impact the results.

Figure 4.1 summarized the assessment indicators to protect of KrCO2 experiment.

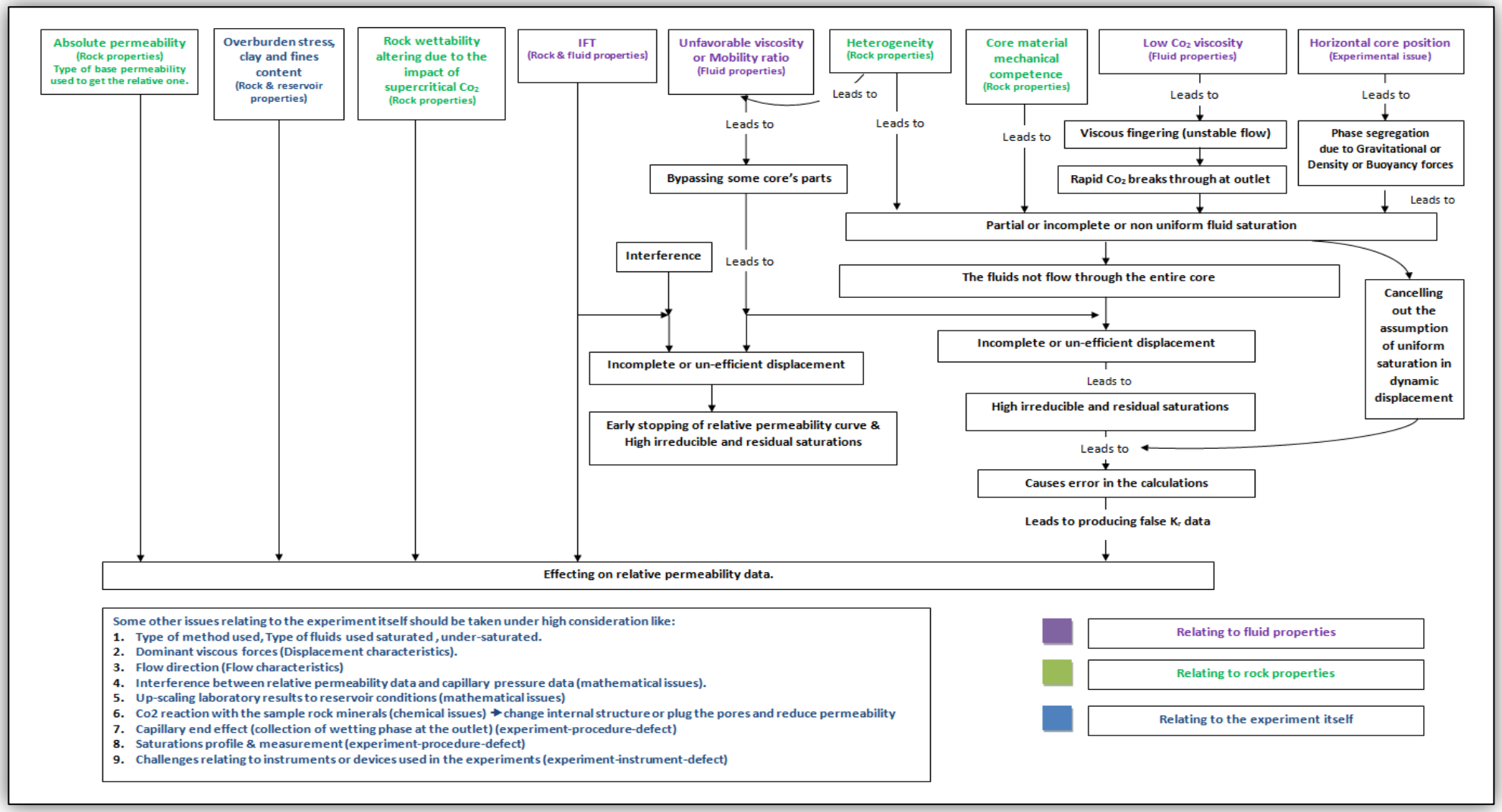

Figure 4.1: Assessment indicators to protocols of CO_2 relative permeability experiments

4.3. General review of CO_2 relative-permeability papers published depending on the assessment indicators mentioned earlier

In this section, a review is conducted and assessment of CO_2 relative-permeability papers published according to chronology, starting with the experiment conducted in 1993 to the one conducted in 2013.

Note: More information about the experiment data and CO_2 relative permeability values is available in (Appendix A).

4.3.1. [**Paper 1**] "Three-Phase Gas/Oil/Brine Relative Permeabilities Measured Under CO_2 Flooding Conditions (Dria et al., 1993)"

This steady-state experiment is considered as one of the early attempts to measure the relative permeability of three phases (gas, oil, brine) in dolomite long core.

A) The experimental protocol and procedures done:

- Tracer co-injection was used to measure the saturations.
- Heterogeneity was verified by using X-ray CT scan.
- The core sample was saturated with oil up to irreducible brine saturation while the gas saturation was zero, and then flooded firstly with water and later injected with gas.

B) The results:

The low endpoint of CO_2 relative permeability (Figure 4.2) denotes that the brine displacement by CO_2 was incomplete. As no saturation profiles are available, it is difficult to attribute the incomplete brine displacement to capillary end effects or to heterogeneity or to the horizontal setup.

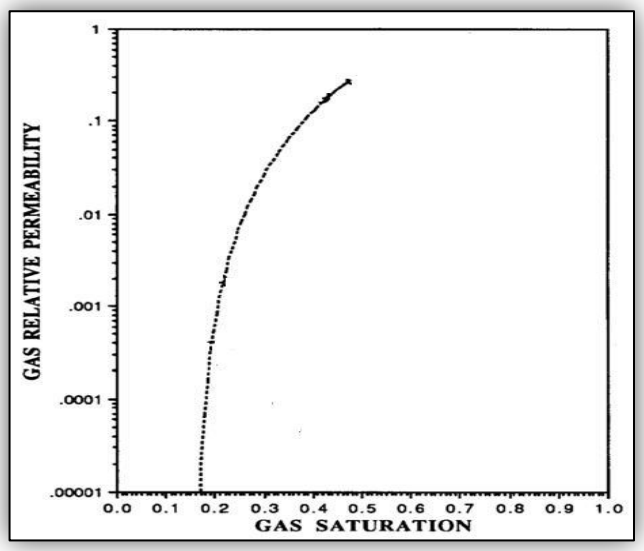

Figure 4.2: CO_2 relative permeability curve (Dria et al., 1993)

4.3.2. [**Paper 2**] "Relative Permeability Characteristics for Supercritical CO_2 Displacing Water in a variety of Potential Sequestration Zones in the Western Canada Sedimentary Basin by (Bennion and Bachu, 2005)"

In this, they introduced water-CO_2 relative permeability data for three sandstone and three carbonate formations in the Wabamun Lake area southwest of Edmonton in Alberta, western Canada.

A) The experimental protocol and procedures done:

- Un-steady-state method was applied.
- To avoid capillary end effect and verify the CO_2 endpoint relative permeability, they conducted multiple rate endpoint floods.
- In the displacement system (core container) all wetted surfaces were made from hast alloy or 316 stainless- steel to prevent corrosion.
- To include the impact of reservoir overburden pressure, the core sample(s) are placed in a flexible confining sleeve made up from lead. The flexibility of the sleeve allows transferring overburden stresses (generated by pressurizing non-damaging saline brine filling the annular space between the core holder and the core sleeve) to the core sample in an axial and radial mode.

- The pieces of the core holder (directly adjacent to the inflow and outflow ends) were equipped with radial distribution plates to make sure that fluid flow is uniformly distributed into and out of the sample.

- The oven (used to generate the reservoir temperature) consisted of a circulating air system to stabilise internal temperature.

- The saturation profile in the core was not verified by X-ray, neither by CT scan or any other method.

B) The results:

- There was an excellent correlation among all permeabilities measured such as: in–situ air permeability, CO_2-saturated brine permeability and the permeability of CO_2 at irreducible brine saturation. Consequently, there was no problem relating to which permeability should be used for generating the relative permeability.

- It has been noted that a poor correlation was remarked between the absolute permeability measured by using CO_2 and the maximum saturation of CO_2 obtained; this leads us to the fact that heterogeneity was a dominant factor controlling the displacement efficiency using CO_2.

- In these tests it was observed that the lowest permeability samples were having the highest values of endpoint relative permeability to CO_2 and higher CO_2 maximum-saturations. It is believed that this is due to better displacement efficiency in the tight, more homogeneous samples in contrast to the more heterogeneous higher permeability cores, where more bypassing of some sections of the core occurs owing to abnormal pore size distribution.

- The viscosity ratio between water and CO_2 has excellent correlation with both of maximum endpoint relative permeability and saturation to CO_2 (Figure 4.3). This excellent correlation is classically expected when accurate experimental results come out.

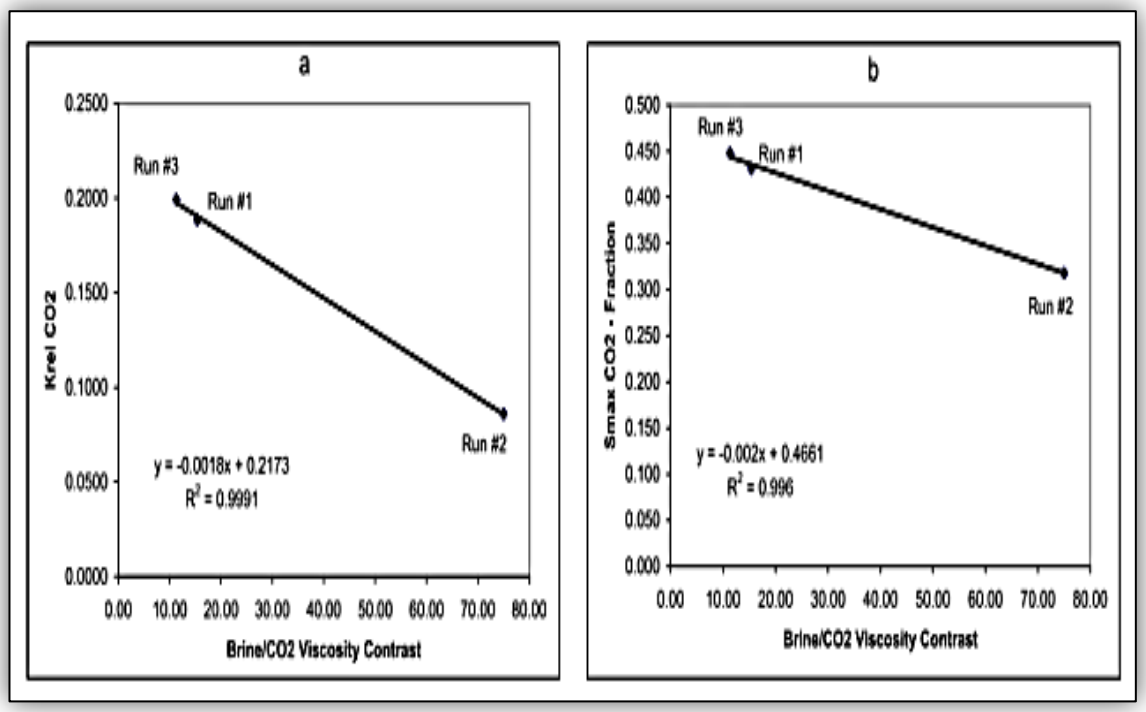

Figure 4.3: Viscosity ratio vs. both maximum saturation and endpoint relative permeability to CO_2 (Bennion and Bachu, 2005)

4.3.3. [**Paper 3**] "Impact of Interfacial Tension and Pore-Size distribution/Capillary Pressure Character on CO_2 Relative Permeability at Reservoir Conditions in CO_2-Brine systems (Bennion and Bachu, 2006a)"

A) The experimental protocol and procedures done:

- Un-steady-state method was applied.
- The equipment's specific details, procedures applied to conduct the relative permeability measurements and the corresponding results are explained by the authors in the previous paper (Bennion and Bachu, 2005) and were for seven sets of rock samples collected from three carbonate and three sandstone formations.
- The saturation profile in the core was not verified by X-ray, neither by CT scan or other methods.

B) The results:

- Strong inverse function was observed between CO_2-brine IFT and reservoir pressure (Figure 4.4).

- The absolute permeability was affected by pore characteristics (size and distribution) and increases with increasing median pore diameter (Figure 4.5).

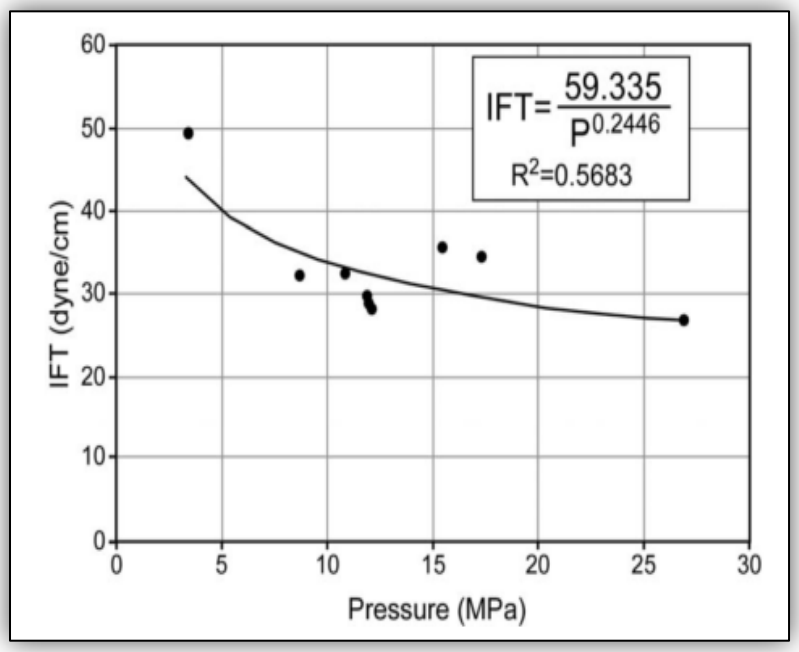

Figure 4.4: Variation of interfacial tension for CO_2-brine systems with pressure (Bennion and Bachu, 2006a)

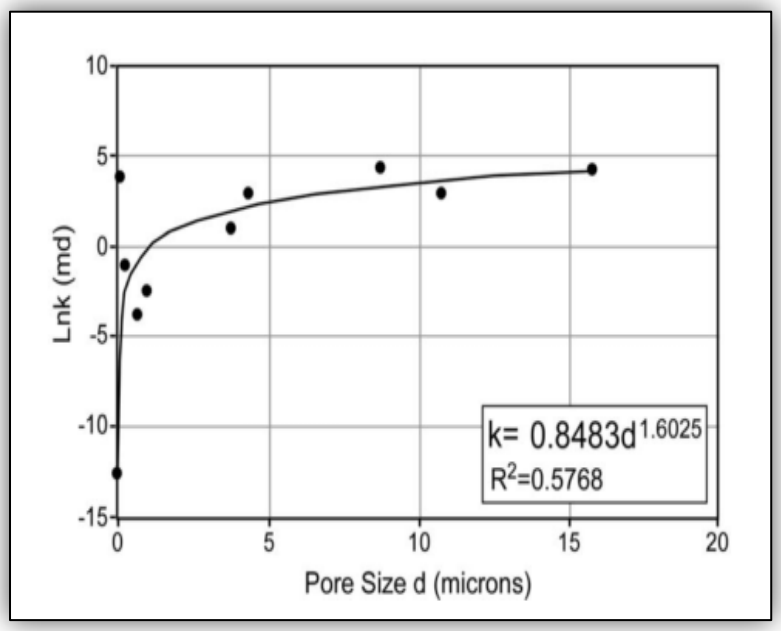

Figure 4.5: Relation between permeability to brine at in-situ conditions and median pore size (Bennion and Bachu, 2006a)

4.3.4. [**Paper 4**] "Supercritical CO_2 and H_2S-Brine Drainage and Imbibition Relative Permeability Relationships for Intergranular Sandstone and Carbonate Formations (Bennion and Bachu, 2006b)"

This paper is the third in series of CO_2-Brine relative permeability research program; the first paper (Bennion and Bachu, 2005) was for details relating to the geological setting and the equipment and procedures applied to measuring CO_2 relative permeability, and the second one (Bennion and Bachu, 2006a) was for the specific details of IFT and capillary pressure at reservoir conditions.

A) The experimental protocol and procedures done:

- Un-steady-state method was applied.
- In this set of experiments, pure H_2S was added as a displacement fluid apart from CO_2 to make comparative tests through samples extracted from Viking sandstone and Nisku carbonate formations, and due to the higher solubility and high ability of H_2S-brine system to react with rocks, the CO_2 experiments were carried out first. Then the core was cleaned and re-saturated to be ready for H_2S-based experiments. This could be considered as a defect in this research as the core's internal structure might have been changed after conducting the first test for CO_2.
- Since the H_2S a highly toxic and corrosive gas, special core-holder cells, pumps and displacement equipment (composed of Hast-alloy C or Titanium) were used and the tests were conducted in an automated explosion-proof isolation laboratory for safety purposes (Figure 4.6) (Bennion and Bachu, 2006b).

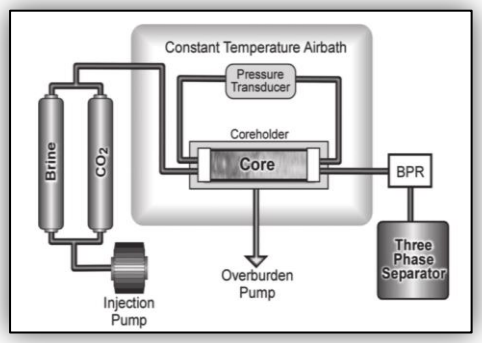

Figure 4.6: a schematic form of the laboratory experimental apparatus used to measure relative permeability of CO_2-brine and H_2S-brine systems (Bennion and Bachu, 2006b)

B) The results:

B.1) For both Viking and Nisku formations:

At the same in-situ conditions of temperature, pressure and salinity, the H_2S-Brine system (in both types of rocks) has lower IFT than that recorded for CO_2-Brine (approximately 35-40% of the CO_2-brine IFT values) (Table 4.1). This lower interfacial tension can be attributed to the high solubility degree of H_2S in brine in comparison to CO_2.

The reduction of IFT to H_2S-Brine system caused the H_2S-brine system capillary pressure to be smaller than that to CO_2-Brine system (Figure 4.7).

Formation Name	Formation type	Pressure (MPa)	Temperature (°C)	Brine salinity (ppm)	IFT to CO2-Brine (mN.m)	IFT to H_2S-Brine (mN.m)
Viking	sandstone	8.6	35	28,286	32.12	12.2
Nisku	carbonate	17.4	56	136,817	34.56	12.3

Table 4.1: In-situ characteristics of CO_2-Brine and H_2S-Brine systems in Viking and Nisku formations (Bennion and Bachu, 2006b)

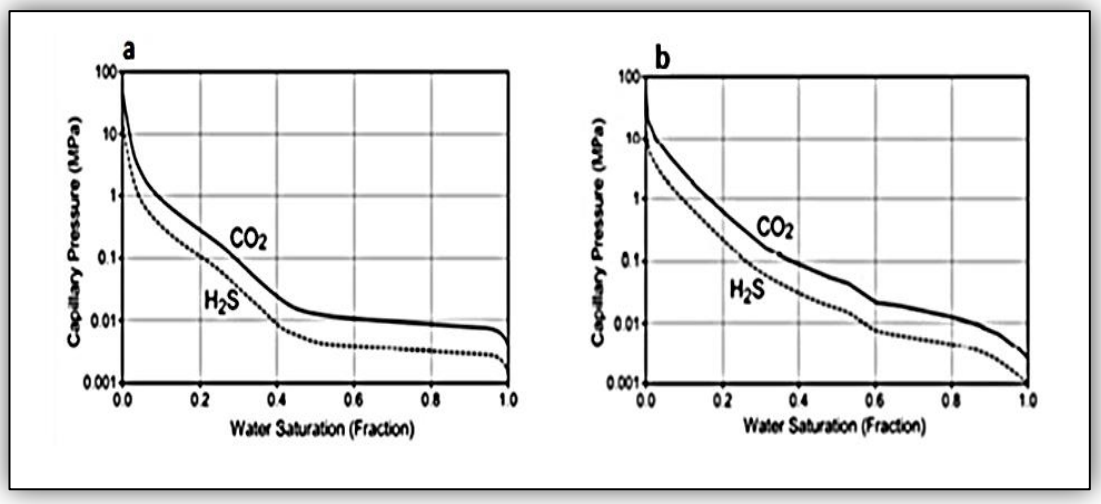

Figure 4.7: Capillary pressure curves for Co2-Brine and H_2S-Brine systems: a) in Viking (sandstone) formation, b) in Nisku (carbonate) formation (Bennion and Bachu, 2006b)

B.2) For Viking formation (sandstone rock) we have the following:

i. The hysteresis is slightly more in CO_2 than in H_2S (Figure 4.8), and it is compatible with the lower IFT of the H_2S-brine system (Table 4.1).

ii. For drainage (Figure 4.9a):

- The H_2S relative permeability values, in general, are higher than those for CO_2 which goes with the fact that the IFT of H_2S-Brine system is lower than that for CO_2- Brine system.

- In H_2S-Brine system, there are lower H_2S relative permeability and saturation endpoints; thus, the higher brine irreducible saturations in comparison to those for CO_2-Brine system are not all consistent with the lower IFT of H_2S-Brine system. And it suggests that the displacement efficiency was better in CO_2, as the higher mobility of the H_2S counteracting the lower IFT effect results in more macroscopic bypassing of the pore system.

iii. For Imbibition (Figure 4.9b)

- The Brine relative permeability values, in general, are lower in H_2S-Brine system than in CO_2-Brine system. This is not consistent with the lower IFT of H_2S-Brine system, and it is thought to be due to plugging some pore throats by precipitations produced from the aggressive chemical reaction of H_2S with rock materials (Figure 4.10), resulting in reducing the brine relative permeability.

- The residual H_2S saturation in the H_2S-Brine system was considerably lower than in the CO_2-Brine system. It is consistent with the expectation that with the lower IFT the capillary forces resisting displacement will be smaller (Figure 4.7a), resulting in a more reduction in residual-gas saturation.

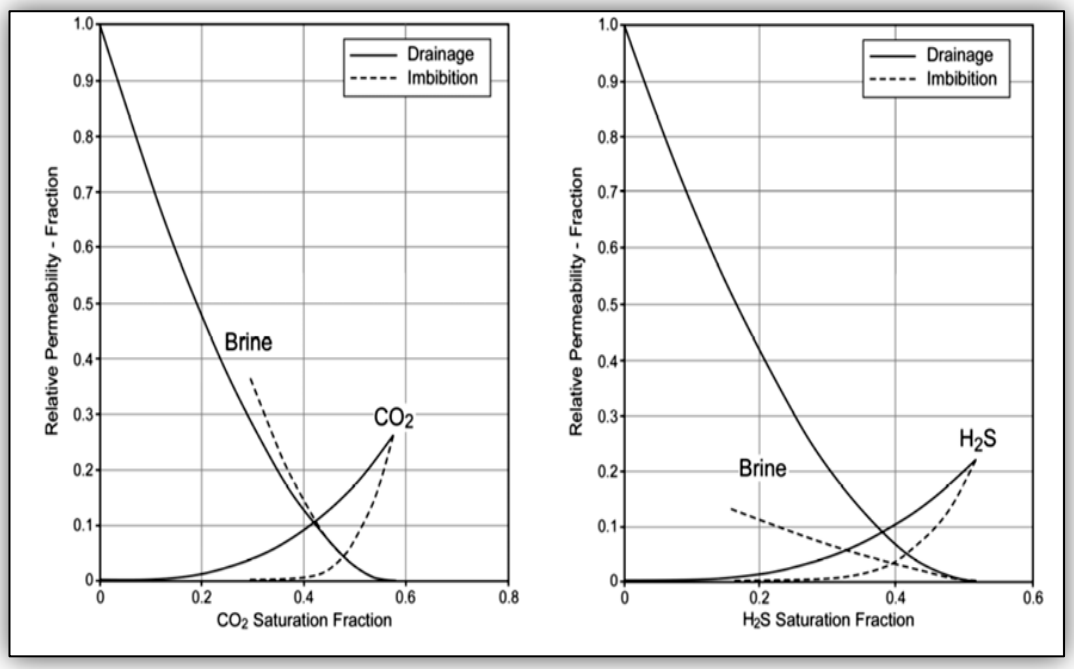

Figure 4.8: relative permeability for CO_2-brine and H_2S-brine systems in the sandstone Viking Formation (Bennion and Bachu, 2006b)

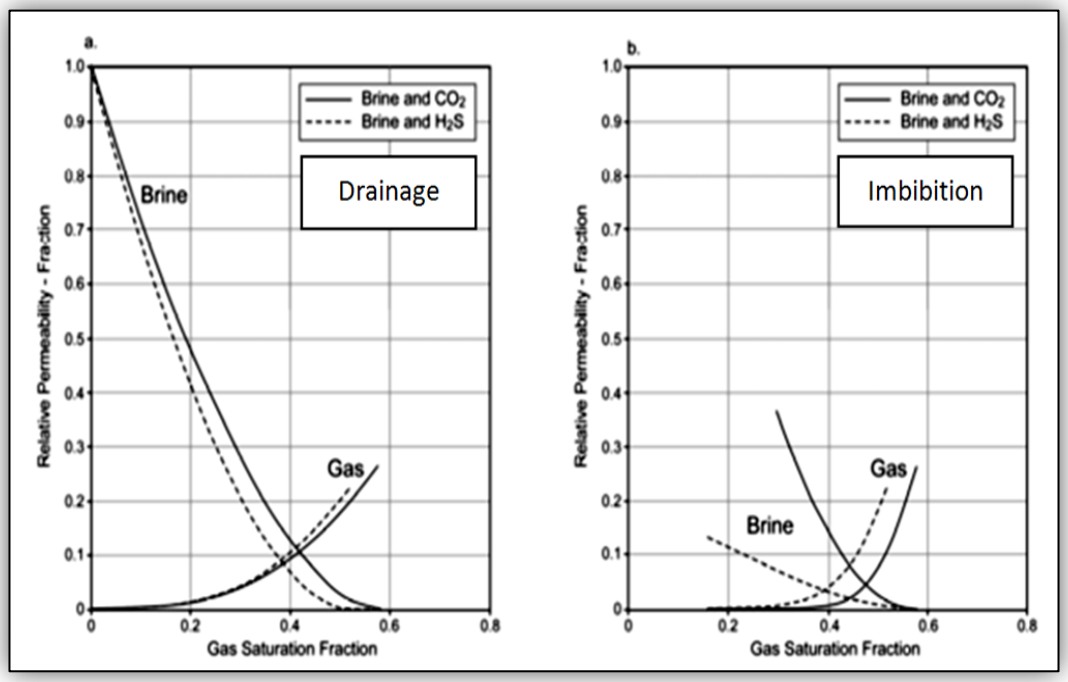

Figure 4.9: Comparison between relative permeability for CO_2-brine and H_2S-brine systems for: a) drainage in the Viking formation sand stone; b) imbibition in the Viking formation (Bennion and Bachu, 2006b).

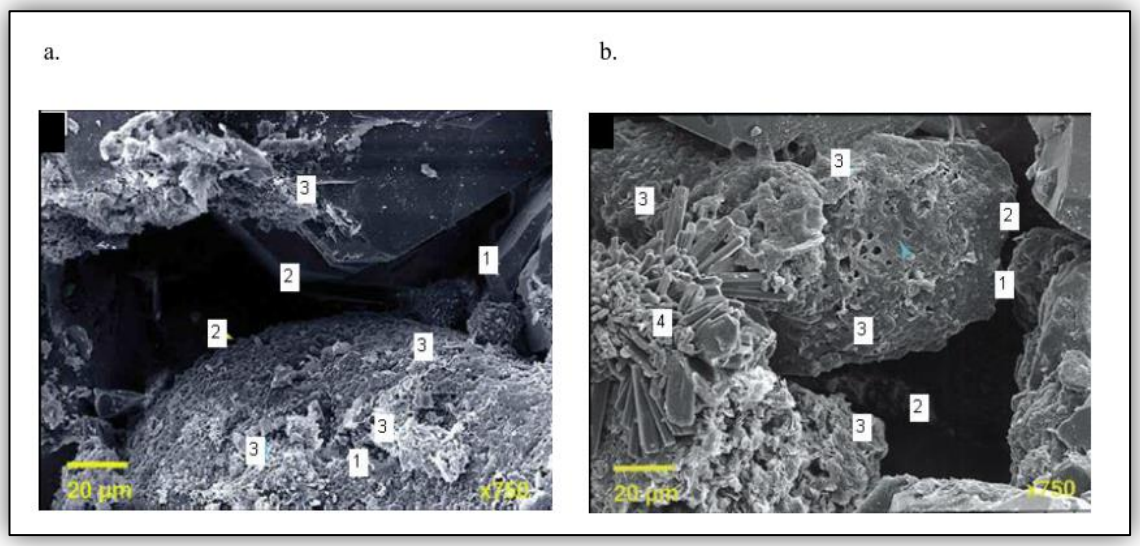

Figure 4.10: Scanning electron microscope (SEM) analysis of Viking Formation. Sand stone samples: a) pre-test, and b) post-test after flooding with CO_2 and H_2S. The numbers on the images indicate: (1) quartz overgrowths, (2) intergranular porosity (3) leached and migrated grain coating clays, and (4) blocking precipitated calcite crystal (Bennion and Bachu, 2006b).

B.3) For Nisku formation (carbonate rock) we have the following:

The hysteresis is again slightly more in CO_2 than in H_2S system (Figure 4.11), and it is in agreement with the lower IFT of the H_2S-brine system (Table 4.1).

i. For drainage (Figure 4.12c)

- The H_2S relative permeability values, in general, are higher than those for CO_2 which goes with the lower IFT of H_2S-Brine system, and it suggests that limited or no damage to the pore system was caused by H_2S reaction with Nisku carbonate matrix, and potentially even some permeability enhancement has been made (Figure 4.13).

- At the end of drainage, the endpoint relative permeability of H_2S is higher than that for CO_2, which is consistent with the lower IFT of H_2S-Brine system, and it suggests that the displacement efficiency was much better in H_2S drainage.

- For the H_2S-Brine system, there is lower H_2S endpoint saturation; thus, the higher brine irreducible saturation in comparison to CO_2-Brine system is not absolutely consistent with the lower IFT of H_2S-Brine system. This is thought to be due to the

bypassing effect coming from the higher mobility of the H_2S which is counteracting the lower IFT effect.

ii. For imbibition (Figure 4.12d), it is clear that the residual gas saturation in the H_2S-Brine system was higher than in the CO_2-Brine system (Figure 4.12d). This did not match the expectation as, when the IFT is lower, the capillary forces resisting displacement will be smaller (Figure 4.7b), resulting in the residual gas saturation value to be less. It may be that the higher mobility of the gas in the H_2S displacements is counteracting the lower IFT, resulting in more macroscopic bypassing of the pore system, leading to higher trapped-water saturations in the end.

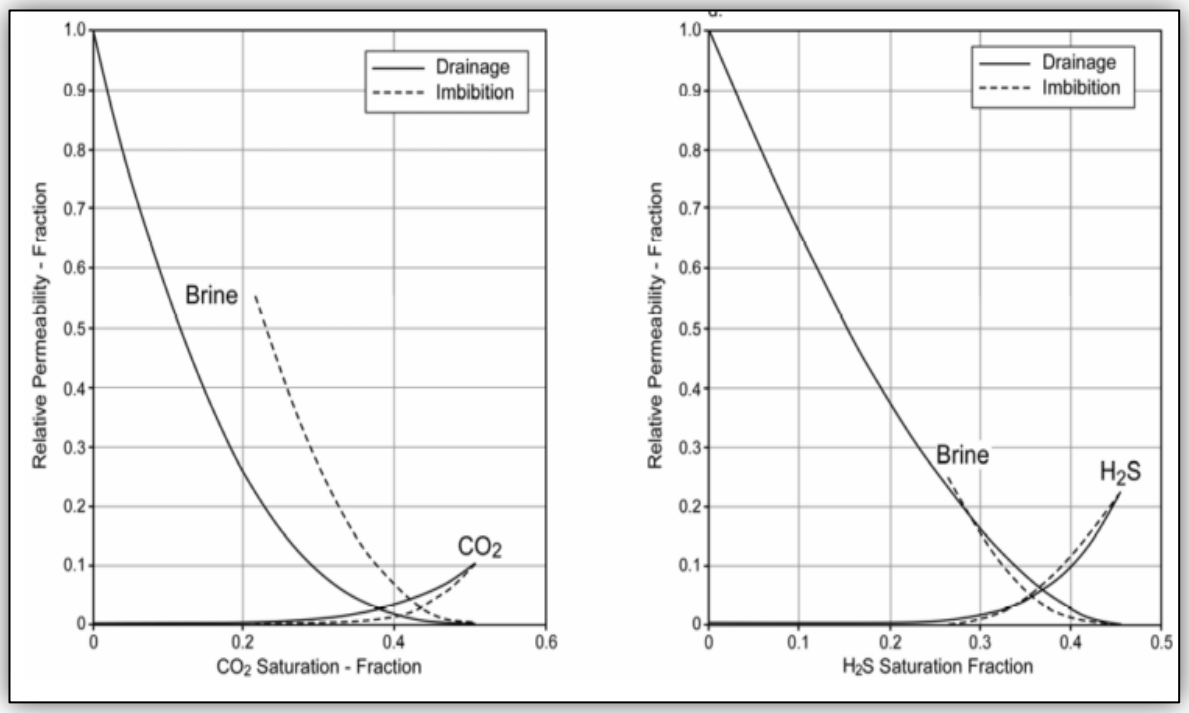

Figure 4.11: relative permeability for CO_2-brine and H_2S-brine systems in the carbonate Nisku Formation (Bennion and Bachu, 2006b)

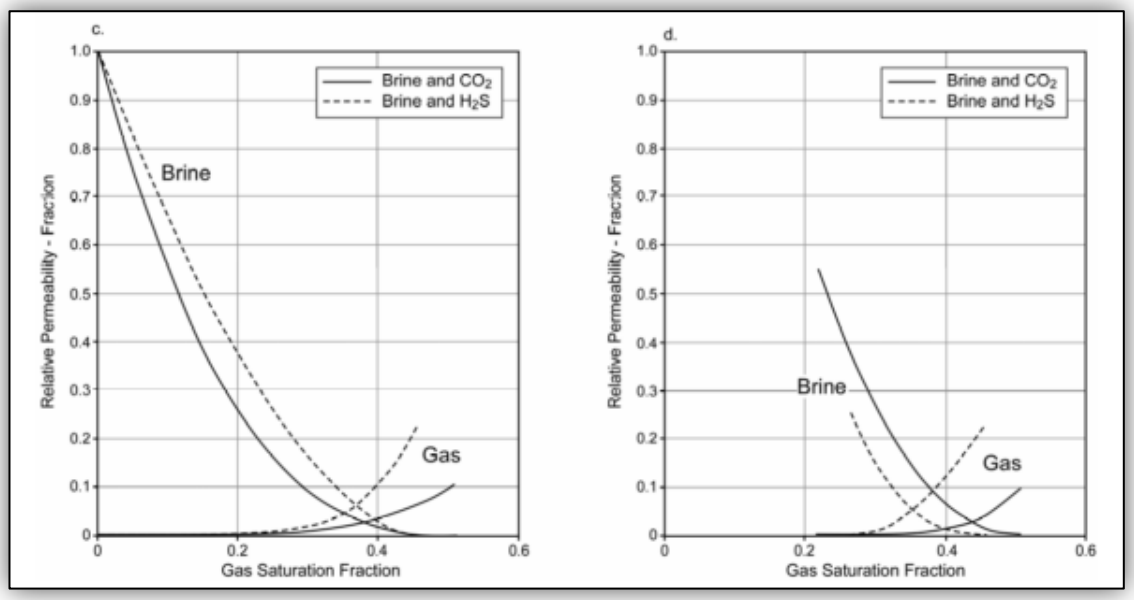

Figure 4.12: Comparison between relative permeability for CO_2-brine and H_2S-brine systems for: c) drainage in the Nisku Formation. Carbonate; d) Imbibition in Nisku formation Carbonate (Bennion and Bachu, 2006b)

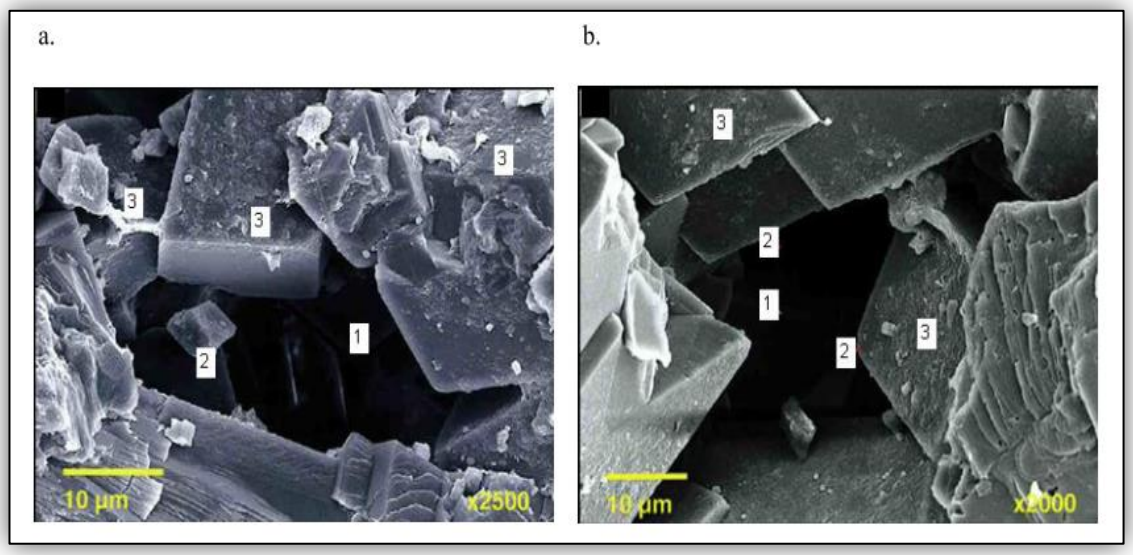

Figure 4.13: Petrographic SEM analysis of Nisku Formation. carbonate samples: a) pre-test, and b) post-test after flooding with CO_2 and H_2S. The numbers on the images indicate: (1) intergranular porosity, (2) dolomite cement, (3) residual trace drilling mud fines (Bennion and Bachu, 2006b)

By combining the drainage curves of CO_2 and H_2S and imbibition curves of the same gases in each type of rock tested (sandstone and carbonate) (Figure 4.14) we could see the following:

- For all cases, the gas relative permeability value for H_2S is greater than that for CO_2 (during both drainage and imbibition cycles) (Figure 4.14).

- According to Figure 4.14a and Figure 4.14c, in both rock types and at the end of drainage process it can also be remarked that the maximum gas saturation obtained with H_2S is slightly lower than that obtained with CO_2; in other words, the irreducible brine saturation for H_2S-Brine system is slightly higher than that for CO_2-Brine system. This is somewhat counterintuitive, as it would be expected that the lower-IFT H_2S system must be more effective at displacing the brine to a lower irreducible saturation than the CO_2 system; thus, the maximum gas saturation should be higher. The cause could be attributed to the fact that the higher mobility of the gas in H_2S displacements is working against the lower IFT, resulting in more macroscopic bypassing of the pore system, leading to higher trapped-water saturations in the end.

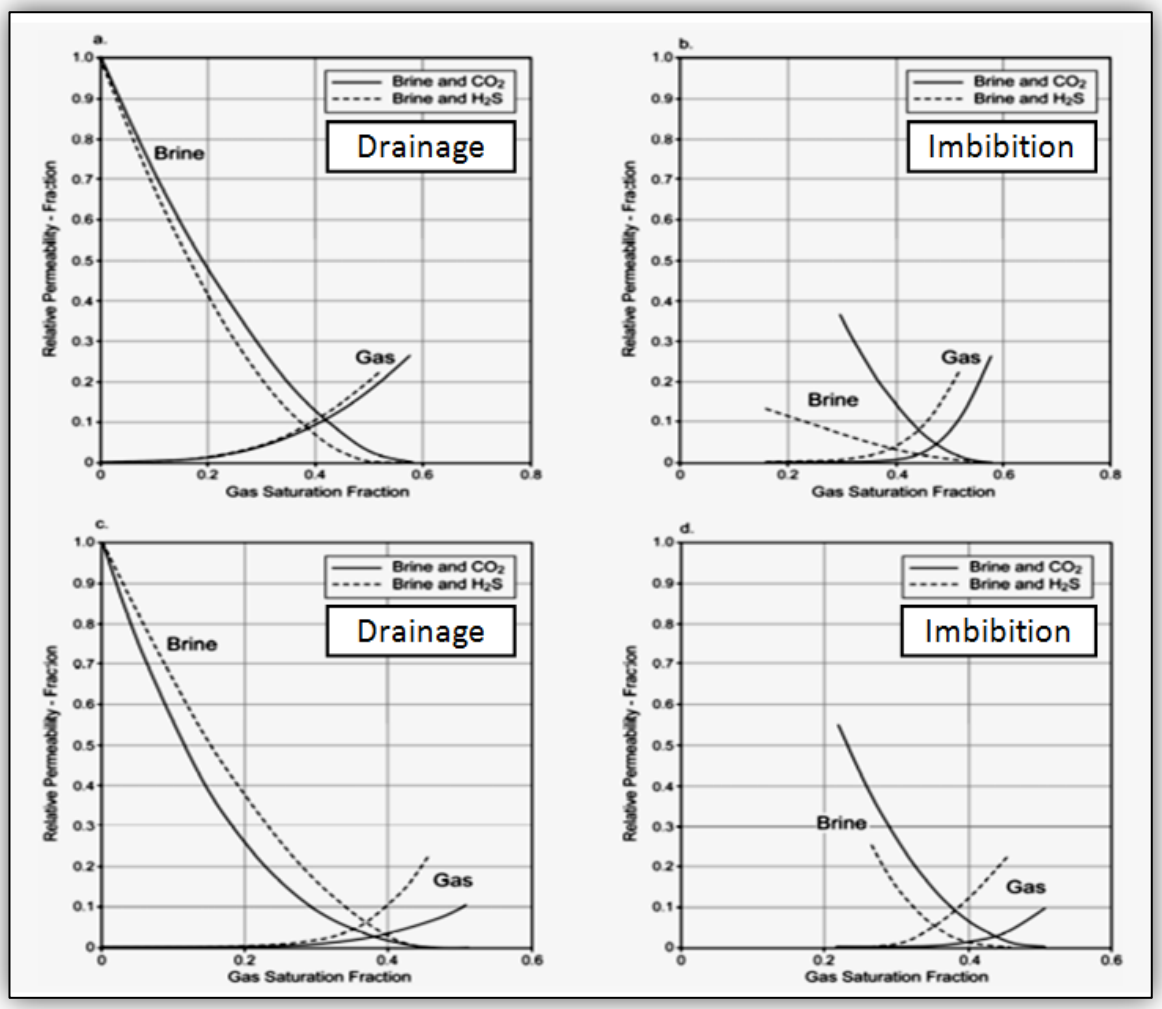

Figure 4.14: Comparison between relative permeability for CO_2-brine and H_2S-brine systems for: a) drainage in the Viking Formation sandstone; b) imbibition in the Viking Formation sandstone, c) drainage in Nisku formation carbonate; d) imbibition in the Nisku Fm. carbonate (Bennion and Bachu, 2006b)

4.3.5. [**Paper 5**] "Dependence on Temperature, Pressure, and Salinity of the IFT and Relative Permeability Displacement Characteristics of CO_2 Injected in Deep Saline Aquifers by (Bennion and Bachu, 2006c)"

This paper presented continuing results of a research study conducted by the authors to investigate the displacement characteristics of CO_2-brine systems at reservoir conditions for cases specific to the Alberta representative for intracratonic and foreland basins in North America.

More specifically, the experiment studied the effect of pressure, temperature and brine salinity on IFT of CO_2-Brine system and thus investigated the effect of interfacial tension on CO_2 relative permeability under the same conditions of temperature, pressure and brine salinity.

A) The experimental protocol and procedures done:

- Un-steady-state method was applied.
- A number of different core samples were selected depending on having a fairly wide pore throat size distributions (as opposed to "spike" type, narrow distribution) to each core, and the reason is that the sample with this type of pore distribution character would be better to illustrate the effect of interfacial tension variations on relative CO_2 permeability and residual saturations.
- The characteristics and in-situ conditions of the core plug used in this work are obtainable in the table below (Table 4.2):

Parameters	Value
Sample Depth (m)	1626.33
Net Overburden Pressure (kPa)	11,000
In-situ Temperature (°C)	43
In-situ salinity (ppm)	27,096
Sample Length (cm)	3.73
Sample Diameter (cm)	3.77
Flow Area (cm^2)	11.16
Displacement Rate (cm^3/hr)	10.0
Average Porosity (%)	15.3
Pore Volume (cm^3)	6.37

Table 4.2: Core plug Characteristics and in-situ conditions (Bennion and Bachu, 2006c)

B) The results:

- At the end of the drainage process, it can be clearly observed that both of the CO_2 endpoints to relative permeability and saturation increase as IFT decreases, evidently, as a result of pressure boost. At the end of the imbibition process, the saturation value of the trapped gas decreases as IFT declines with rising pressure.

- The variation in IFT of Brine-CO_2 system had been obtained by keeping salinity and temperature constant and varying only the pressure. However, the brine-to-CO_2 viscosity ratio varied as well due to the fact that the viscosity of CO_2 increases with increase in the pressure. Generally, IFT was found to decrease with increase in the pressure, and so the brine-to-CO_2 viscosity ratio will also decrease as a result of CO_2 viscosity increasing under the impact of pressure. Generally, both viscosity ratio and IFT have similar dependencies on temperature, pressure and water salinity, so, regardless of which one of these parameters is used, the variation is to appear at the same time in both the IFT and viscosity ratio. Practically, there is no other method to change IFT value without having an impact on the viscosity ratio of CO_2- brine phases.

  Through drawing, it is found that plotting the endpoints of relative permeability to CO_2 and brine in addition to maximum and trapped CO_2 saturations as a function of both IFT and viscosity ratio will produce identical trends as appear in Figure 4.15. Consequently, it is quite difficult as to whether the variations in displacement characteristics can be solely attributed to IFT effects or to viscosity ratio effects as well. But the researchers introduced an interpretation which indicates that the IFT was dominant instead of viscosity ratio, as follows:

  In the drainage process, it is recognized that as the pressure increases, the CO_2 viscosity will also increase; all that will affect the mobility of CO_2 and therefore its displacement efficiency negatively, and as a result, the irreducible to brine is expected to be higher, but it is not the case here as a very consistent reduction in irreducible water saturation occurred whenever the pressure increases (Figure 4.15 a). Consequently, we can say that the viscosity ratio is not dominant, and that will lead us to consider that IFT has much more effect than does the viscosity ratio.

  On the contrary, in imbibition, as the pressure increases, the CO_2 viscosity will also increase causing its mobility to be weaker and movement to be more difficult; all that will negatively affect brine displacement efficiency, and as a result, the residual CO_2 saturation at the end of drainage cycle is expected to be higher, but it is not the case here as the trapped gas saturation decreases with increase in the pressure (Figure 4.15 b), so we can say the viscosity ratio is in no way to be dominant, and alternatively the IFT, rather than the viscosity ratio, will play the main role.

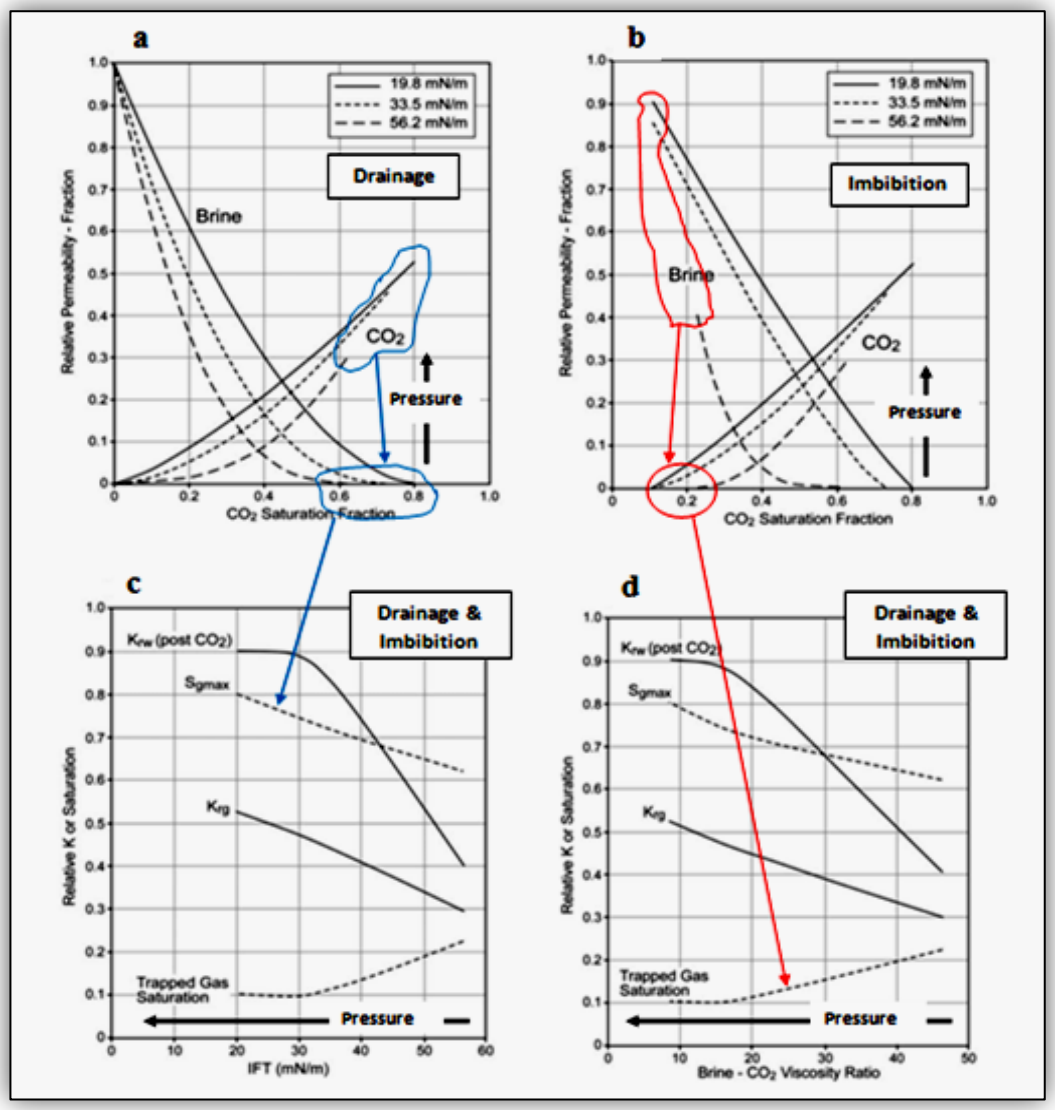

Figure 4.15: Endpoints of Kr_{CO2} and Kr_w, $S_{CO2(Max)}$, $S_{CO2(trapped)}$ Vs. IFT and viscosity ratio (Bennion and Bachu, 2006c)

4.3.6. [**Paper 6**] "Permeability and Relative Permeability Measurements at Reservoir Conditions for CO_2-Water Systems in Ultra Low Permeability Confining Caprocks (Bennion and Bachu, 2007)"

This paper presents results of experiments to measuring CO_2 and Brine relative permeabilities at full reservoir conditions in extensive low permeability Caprocks (Shale, anhydrite).

A) The experimental protocol and procedures done:

The general details of the equipment and procedures applied to conduct the experiments have been introduced by the authors in previous papers (Bennion and Bachu, 2005, Bennion and Bachu, 2006a).

- Un-steady-state method was applied.
- The 1.5 inch-OD core plug used was drilled from vertical full diameter core sections and mounted in the vertical-direction core-holder so that flow was parallel to natural bedding planes.
- They applied un-steady-state displacement with brine-vapour-saturated supercritical CO_2 through drainage process and CO_2-saturated brine over the imbibition; therefore, the mass transfer effect was completely under control.
- The researchers used history-matching method which includes theoretical model (core simulation) in addition to measurements (empirical modelling) synchronously.
- The offcut end sections from each test plug (removed when the sample was drilled from the parent full diameter core) were subjected to high pressure testing (mercury injection). These end cut sections represented the best approximation to the actual test samples, being removed directly from the ends of the tested samples themselves.

B) The results:

- As the permeability of Anhydrite sample was extremely low (less than 1 picoDarcy, or (10^{-12} Darcy), it was not possible to produce imbibition data for this rock type (Figure 4.16).

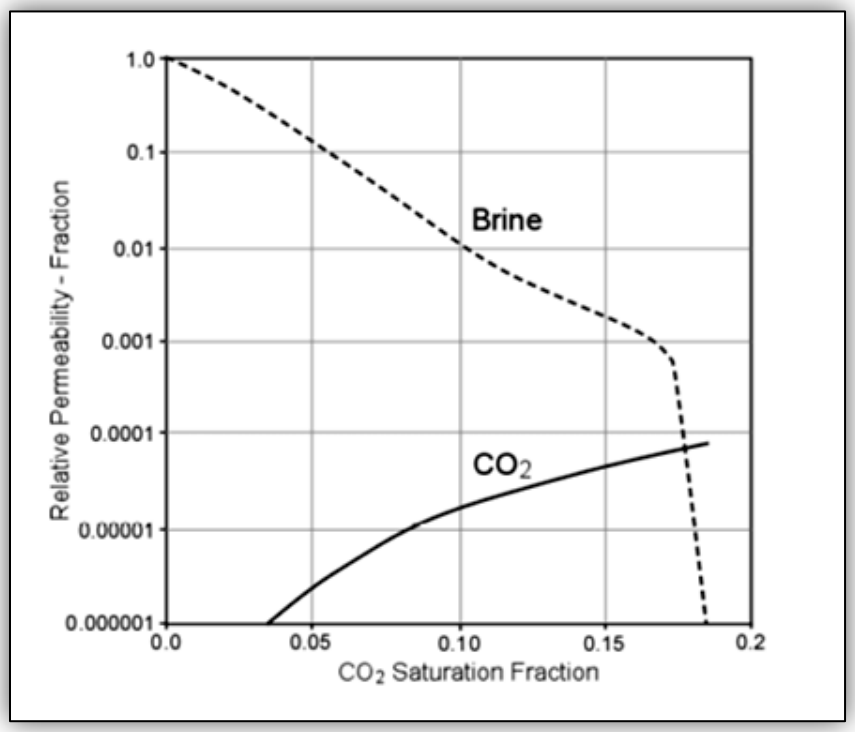

Figure 4.16: Drainage CO_2-brine relative permeability for Muskeg anhydrite Formation (Bennion and Bachu, 2007)

- In the shale rocks, the residual gas saturations had a strong reducing effect on the permeability to brine (Figure 4.17). This has two reasons: the first is the existence of the extremely small pores (high capillary resistance) in the samples tested, and the second is the high level of interference between CO_2 and brine.

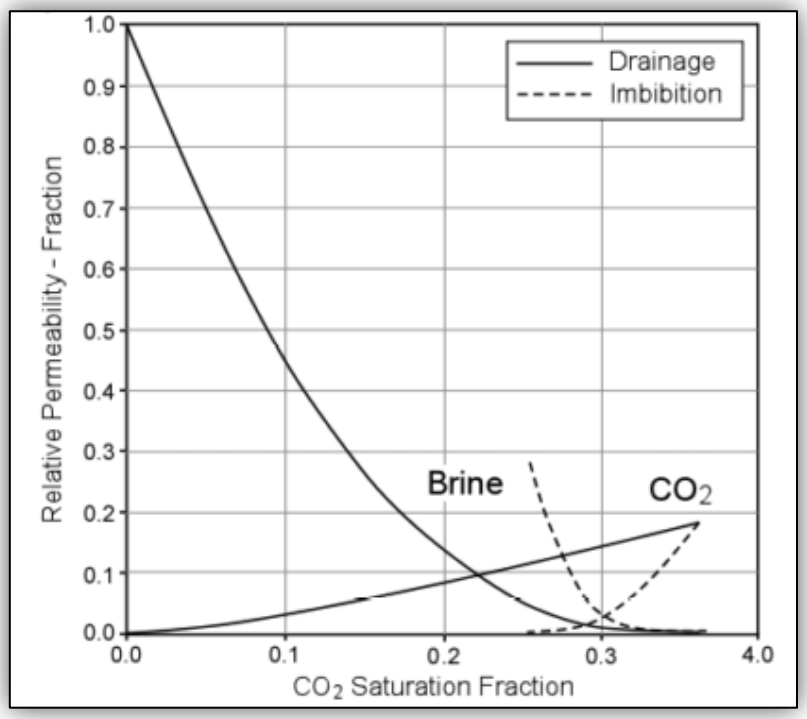

Figure 4.17: CO_2-brine relative permeability for Calmar shale formation (Bennion and Bachu, 2007)

4.3.7. [**Paper 7**] "Two Phase Flow Properties of Brine-CO_2 Systems in a Carbonate Core: Influence of Wettability on Pc and kr (Chalbaud et al., 2007)"

This paper focused on the un-steady state (USS) experiment to measure CO_2 relative permeability at reservoir conditions and different wettability types over carbonate (limestone) rock samples.

A) The experimental protocol and procedures done:

- Two types of wettability were applied: water-wet and intermediate-wet.
- All thermodynamic conditions including temperature, pressure and water salinity were the same for all experiments.
- Multi-rate experiments were conducted, and the saturation was monitored over in-situ conditions.
- Enhanced heterogeneous interpretation approach was conducted to the production data to obtain complete sets of relative permeability data.

- The sample was installed in a core holder horizontally positioned and exposed to X-rays.

- The saturation profiles were recorded over the whole test. This procedure is essential to observe the transient evolution and also to check the stabilization at the end of each step.

B) The results:

- The heterogeneity of the sample caused some fluctuations in the CO_2 stabilized saturation profiles (Figure 4.18).

- Although the CO_2 saturation was only at 80%, the relative permeability was extrapolated numerically until 100% (Figure 4.19).

- The relative permeability of CO_2 was the same whether the rock is intermediate-wet or water-wet although a different pressure profile was observed (Figure 4.20).

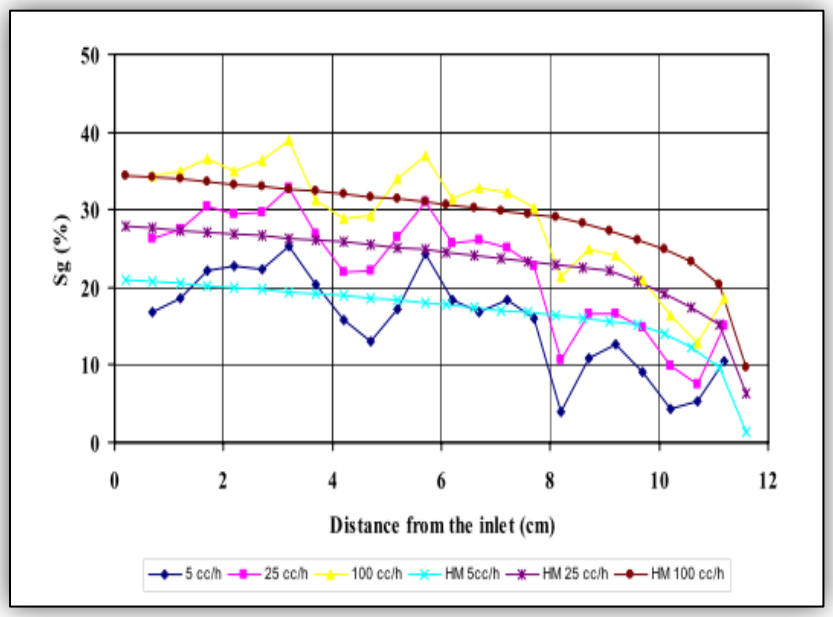

Figure 4.18: CO_2 saturation profile (Chalbaud et al., 2007)

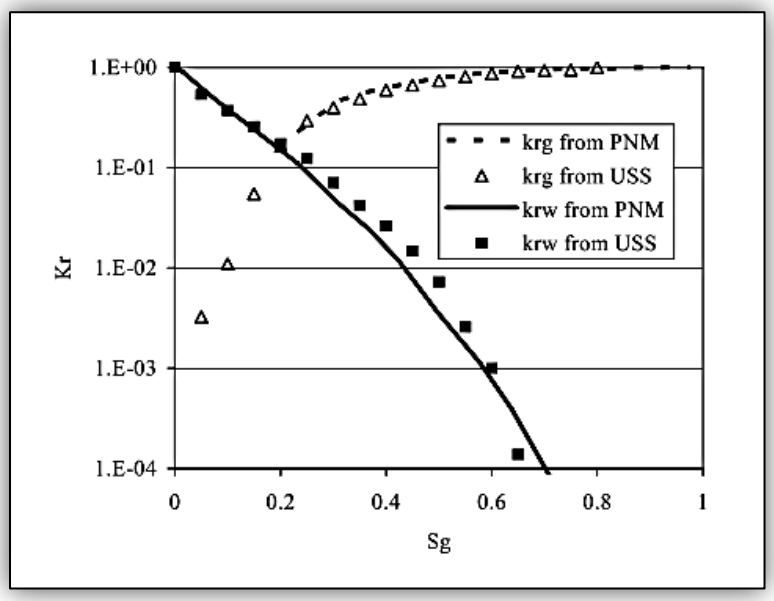

Figure 4.19: CO_2 saturation profile (Chalbaud et al., 2007)

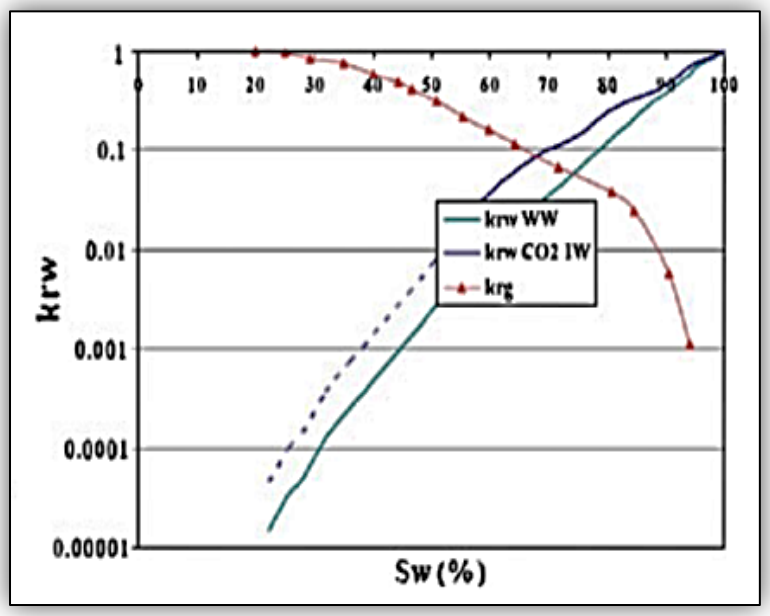

Figure 4.20: Relative permeability curves (Chalbaud et al., 2007)

4.3.8. [**Paper 8**] "Effects of in-situ conditions on relative permeability characteristics of CO_2-brine systems (Bachu and Bennion, 2008)"

This paper is a continuation of a series of tests to understand the relative permeability characteristics of CO_2-Brine system through a set of samples collected from deep sandstone and carbonate aquifers in the Wabamun Lake area southwest of Edmonton in Alberta (Table 4.3). In this paper, the authors studied the impact of in-situ conditions on certain relative permeability and other displacement characteristics in in-situ conditions.

Unit	Lithology	Depth (m)	Pressure (MPa)	Temperature (°C)	Salinity (mg/l)	IFT (mN/m)
Colorado Gp.	Shale	1,618	20.00	43	27,100	19.8
Cardium Fm. #1	Sandstone	1,627	20.00	43	27,100	19.8
Viking Fm. #1	Sandstone	1,240	8.60	35	28,300	32.1
Ellerslie Fm.	Sandstone	1,463	10.90	40	97,200	32.5
Wabamun Gp. #1	Carbonate	1,603	11.90	41	144,300	29.5
Calmar Fm.	Shale	1,566	12.25	43	129,700	27.6
Nisku Fm. #1	Carbonate	2,050	17.40	56	136,800	34.6
Cooking Lake Fm.	Carbonate	1,889	15.50	55	233,400	35.7
Basal Cambrian Fm.	Sandstone	2,734	27.00	75	248,000	27.0

Table 4.3: In-situ conditions for rock samples used (Bachu and Bennion, 2008)

A) The results:

- There is no correlation between pore size characteristics and porosity. This is expected because porosity is a measure of the volume of pores, while the pore size characteristic is a measure of the pore throat diameter and the fraction of total pore space represented by each diameter.

4.3.9. [**Paper 9**] "Drainage and Imbibition Relative Permeability Relationships for Supercritical CO_2-Brine and H_2S-Brine Systems in intergranular Sandstone, Carbonate, Shale, and Anhydrite Rocks (Bennion and Bachu, 2008a)"

This paper describes the details of experimental equipment and protocols used for a series of in-situ condition experiments to measure the supercritical-CO_2 and H_2S relative permeabilities in inter-crystalline sandstone, carbonate, shale, and anhydrite rocks from the Wabamun and Zama areas in Alberta, Canada (Table 4.4). The results are presented for each fluid and rock type.

Unit	Lithology	Depth (m)	Porosity (%)	Pressure (MPa)	Temperature (°C)	Salinity (mg/L)
Colorado Group	shale	1 618	4.4	20.00	43	27 100
Cardium Formation #1*	sandstone	1 627	15.3	20.00	43	27 100
Cardium Formation #2*	sandstone	1 620	16.1	20.00	43	27 100
Viking Formation #1*	sandstone	1 240	12.5	8.60	35	28 300
Viking Formation #2*	sandstone	1 342	19.5	8.60	35	28 300
Ellerslie Formation	sandstone	1 463	12.6	10.90	40	97 200
Wabamun Group #1*	carbonate	1 353	7.9	11.90	41	144 300
Wabamun Group #2*	carbonate	1 603	14.8	11.90	41	144 300
Calmar Formation	shale	1 566	3.9	12.25	43	129 700
Nisku Formation #1*	carbonate	2 050	9.7	17.40	56	136 800
Nisku Formation #2*	carbonate	1 953	11.4	17.40	56	136 800
Cooking Lake Formation	carbonate	1 889	9.9	15.40	55	233 400
Basal Cambrian Formation	sandstone	2 734	11.7	27.00	75	248 000
Muskeg Formation**	anhydrite	1 491	1.2	15.00	71	189 800

Table 4.4: In-situ conditions for rock samples used (Bennion and Bachu, 2008a)

A) The experimental protocol and procedures done:

- Un-steady-state method was applied.
- Petrographic investigation [scanning electron microscope (SEM) and X-ray diffraction] were used, which in turn gives a high credibility to results.
- The experimental procedures were applied depending on a variety of protocols published before (Felber, 2004, Goodlett et al., 1986, Honarpour and Mahmood, 1988, Jamaluddin et al., 1998, Kamath et al., 1998, Paterson et al., 1998, Prieditis et al., 1991, Rogers and Grigg, 2001).

- Many numerical-regression methods (Wellman et al., 2003, Toth et al., 2001, Sigmund and McCaffery, 1979, Archer and Wong, 1973, Mungan, 1972) were used to obtain the relative permeability curves and the Corey (1954) exponents optimized through the regression analysis.

B) The results:

- The first set of results was for the drainage displacement of brine by CO_2, Table 4.5, Figure 4.21. The results were also presented in Bennion and Bachu (2005).

Rock sample	K_{brine} at 100% saturation (md)	K_{rco2} at irreducible brine saturation	$S_{b\text{-}irr}$	Corey exponent to Brine	Corey exponent to CO_2
(a) Sandstone	2.7	0.3319	0.558	2.9	3.2
(b) Sandstone	0.376	0.1156	0.659	2.1	2.2
(c) Carbonate	0.018	0.5289	0.595	1.4	5.6
(d) Carbonate	66.98	0.1883	0.569	1.4	2.1
(e) Carbonate	45.92	0.1768	0.330	2.8	1.1
(g) Carbonate	65.3	0.0685	0.476	1.4	5.6
(g) Sandstone	0.081	0.5446	0.294	1.8	5

Table 4.5: Endpoints and Corey exponents data for drainage displacement of brine by CO_2 (Bennion and Bachu, 2008a)

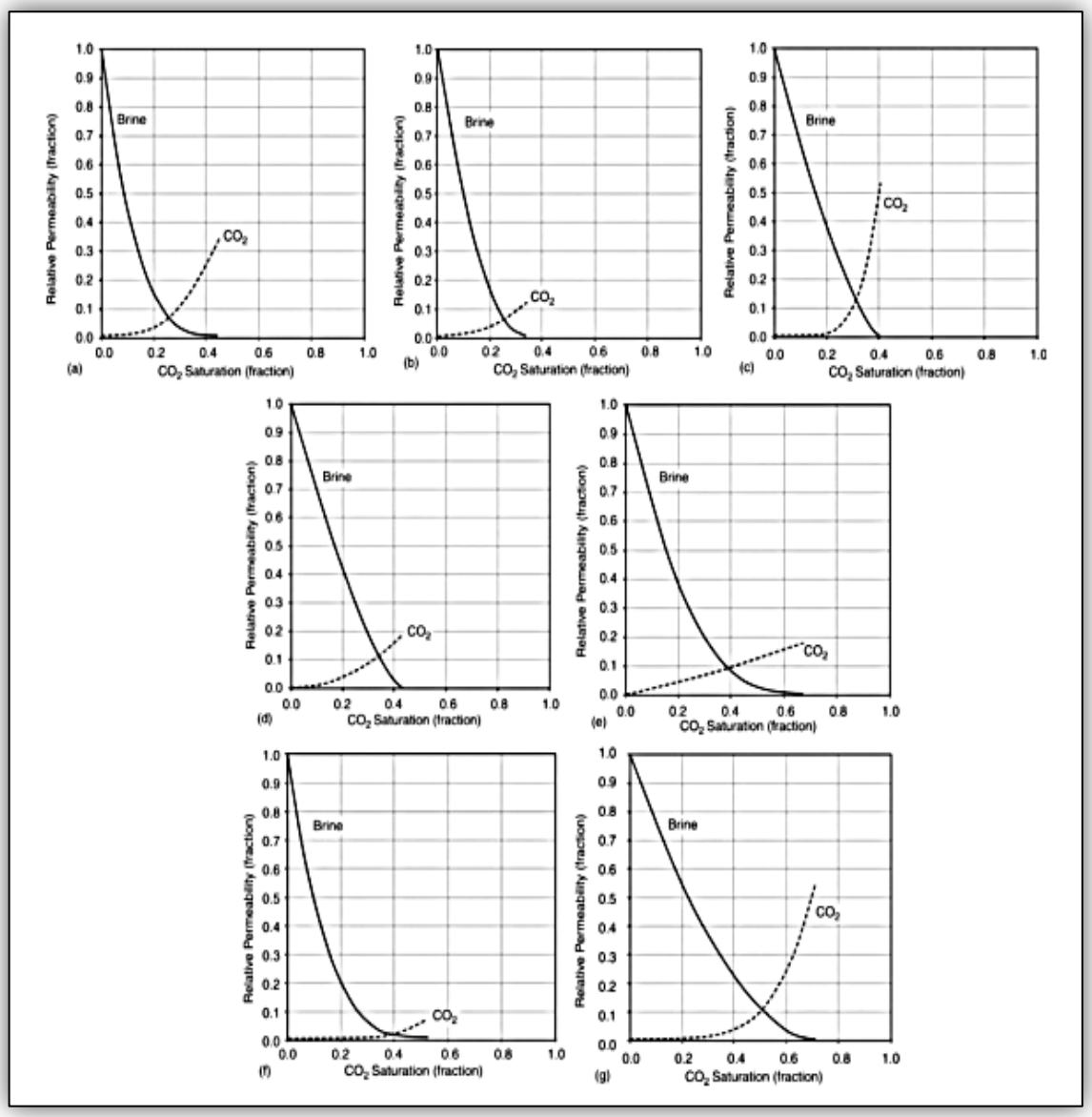

Figure 4.21: Relative permeability curves for data in Table 4.5 (Bennion and Bachu, 2008a)

- The second set of results were to the drainage (brine being displaced by CO_2) and imbibition (CO_2 being displaced by brine), (Table 4.6, Table 4.7, Figure 4.22). The results were presented as well in (Bennion and Bachu, 2006a, Bennion and Bachu, 2007, Bennion and Bachu, 2006b, Bennion and Bachu, 2006c)

Rock sample	K_{brine} at 100% saturation (md)	K_{rco2} at irreducible brine saturation	$S_{b\text{-}irr}$	Corey exponent to Brine	Corey exponent to CO_2
(a) Sandstone	21.72	0.2638	0.423	1.7	2.8
(b) Carbonate	21.02	0.0999	0.492	2.7	4.6
(c) Sandstone	0.356	0.526	0.197	1.3	1.7
(d) Sandstone	21.17	0.129	0.425	1.2	1.3
(e) Shale	0.0000788	0.0148	0.605	6.5	2.6
(f) Anhydrite	0.000354	0.0000828	0.815	6.6	2.7

Table 4.6: Endpoints and Corey exponents data for drainage displacement of brine by CO_2 (Bennion and Bachu, 2008a)

Rock sample	K_{brine} residual gas saturation	$S_{CO2\text{-}irr}$	Corey exponent to Brine	Corey exponent to CO_2
(a) sandstone	0.365	0.297	2.1	4
(b) Carbonate	0.5500	0.218	2.1	4.4
(c) sandstone	0.9050	0.102	1.2	1.2
(d) sandstone	0.267	0.253	1.9	4.5
(e) Shale	0.0024	0.349	4.3	3.5
(f) Anhydrite	tstm	0.180	n/a	n/a

Table 4.7: Endpoints and Corey's exponent data for imbibition displacement of CO_2 by brine (Bennion and Bachu, 2008a).

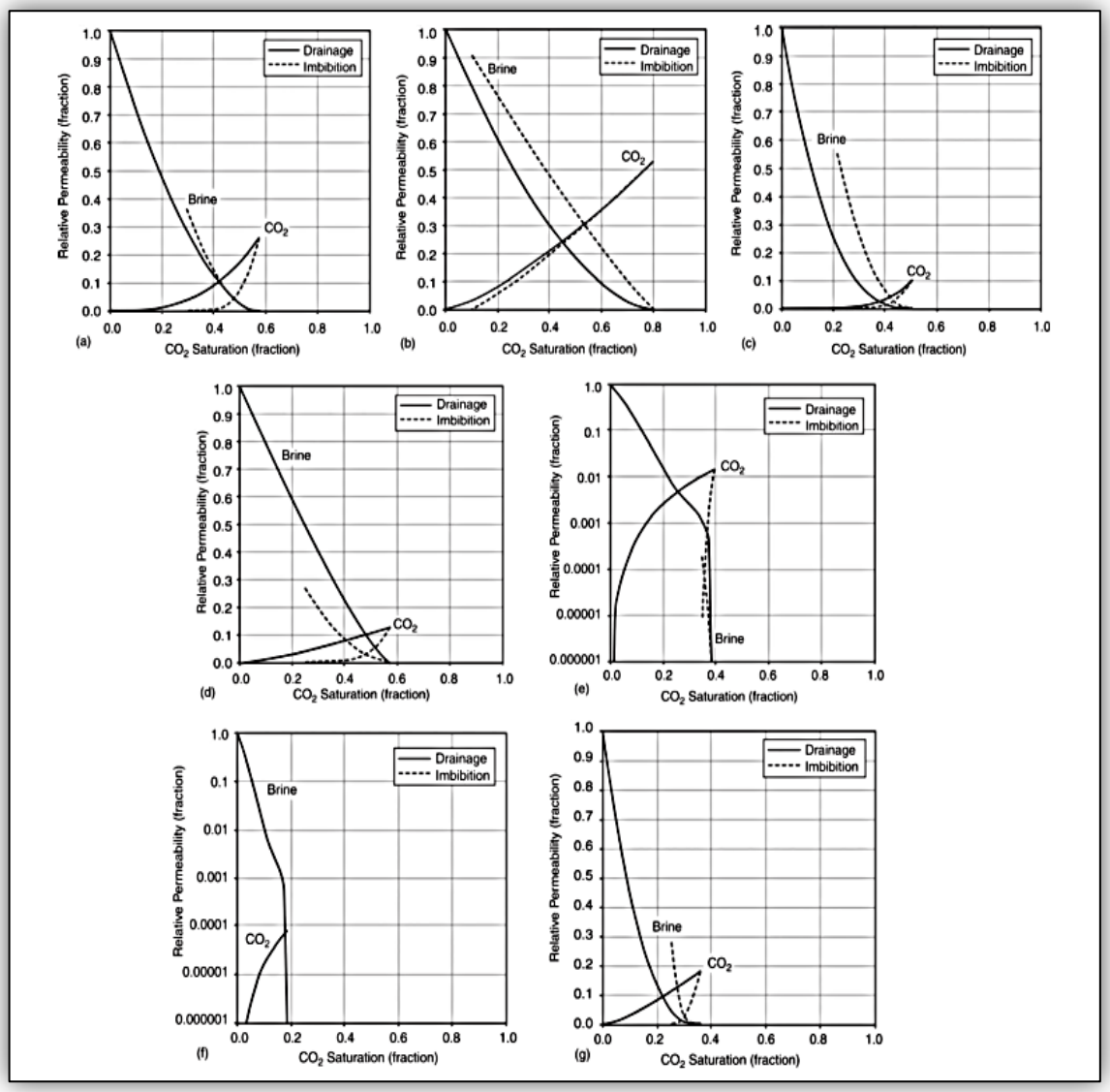

Figure 4.22: Relative permeability curves for data in (Table 4.6, Table 4.7) Bennion and Bachu (2008a)

- High-rate displacement was conducted to avoid the capillary end effects.
- For both of drainage and imbibition processes the interference effects were more significant in the CO_2 phase than for the brine phase (curves of the relative permeability were more concave in the CO_2 phase).
- The curve-concavity degree (Corey exponents) of CO_2 relative permeability is greater in imbibition than for drainage, indicating more multiphase interference effects through the imbibition.
- The interference was found to be affected by the median pore size (pore characteristics), as the bigger median pore size generally leads to relative

permeability curves to be less-concave, indicating a reduction in multiphase interference effects.

4.3.10. [**Paper 10**] "Core-scale experimental study of relative permeability properties of CO_2 and brine in reservoir rocks (Perrin et al., 2009)"

This paper summarized the results of core-scale steady-state relative permeability experiments on two different rock samples (sandstone from the Otway Basin/Australia and fired Berea sandstone**)** through a range of flow rates. The experimental results were compared with those obtained from core-flood simulations.

A) The experimental protocol and procedures done:

- The core was put in a sleeve and an aluminium core holder. This could be considered as a good step to protect the parts of experimental model (particularly connections pieces) from the effect of massive stress resulting from the high pressure and also from the corrosive impact of carbonic acid resulting from dissolving of CO2 in water, as aluminium core holder is not affected by both of them.

- The back pressure, also called pore pressure, is always at least 200 psi below the overburden pressure value in order to avoid any leakage through the Teflon sleeve surrounding the core.

- They used X-ray CT Scan to monitor the fluid saturation along the core during the displacement and avoiding dismounting the core from the holder to measure the saturations.

- To obtain the drainage relative permeability curves, CO_2 and brine were co-injected in different percentages (fractional flows) through full-saturated-brine core; the fractional flows were calculated from the (Eq. 4.1).

$$f_{CO2} = \frac{FR_{CO2}^{T_{res}^{o},P_{res}}}{FR_{CO2}^{T_{res}^{o},P_{res}} + FR_{Brine}^{T_{res}^{o},P_{res}}} \quad \text{(Perrin et al., 2009)} \qquad \text{Eq. 4.1}$$

FR = flow rate.

- Measuring porosity and CO_2 saturation at the sub-core scale

The X-ray CT scanner was used to create 3-D porosity and saturation maps. To obtain a porosity map, two sets of images were needed: the dry-core images, and the brine-saturated-core images at the reservoir conditions (Eq. 4.2).

$$\Phi = \frac{CT_{brine}^{sat} - CT_{dry}}{CT_{brine} - CT_{air}}$$ (Perrin et al., 2009) Eq. 4.2

CT = absorption coefficient

To obtain the saturation map, three sets of pictures are needed: the brine-saturated core images, CO_2-saturated core images at reservoir conditions and the experimental images (Eq. 4.3).

$$S_{Co2} = \frac{CT_{exp} - CT_{brine}^{sat}}{CT_{Co2}^{sat} - CT_{brine}^{sat}}$$ (Perrin et al., 2009) Eq. 4.3

- Numerical Methods

The multi-phase flow simulator "TOUGH2 MP" with the ECO_2N fluid property module was used to simulate the laboratory experiments. TOUGH2 MP is the multiprocessor version of TOUGH2, while the ECO_2N was an addition designed for applications in geologic sequestration of CO_2 in saline aquifers. It includes a comprehensive description of the thermodynamics and thermo-physical properties of H_2O-NaCl-CO_2 mixtures (Perrin et al., 2009).

B) The results:

B.1) Fixed flow rate (2mL/min) drainage in a heterogeneous sample from the Otway Basin. The saturations simulate the porosity features map, so low CO2 saturations were at low porosity layers, whereas at the higher porosity regions the CO2 saturations had higher magnitudes (Figure 4.23 a, b). There were no clear signs of gravity override of the CO2 phase (Figure 4.24).

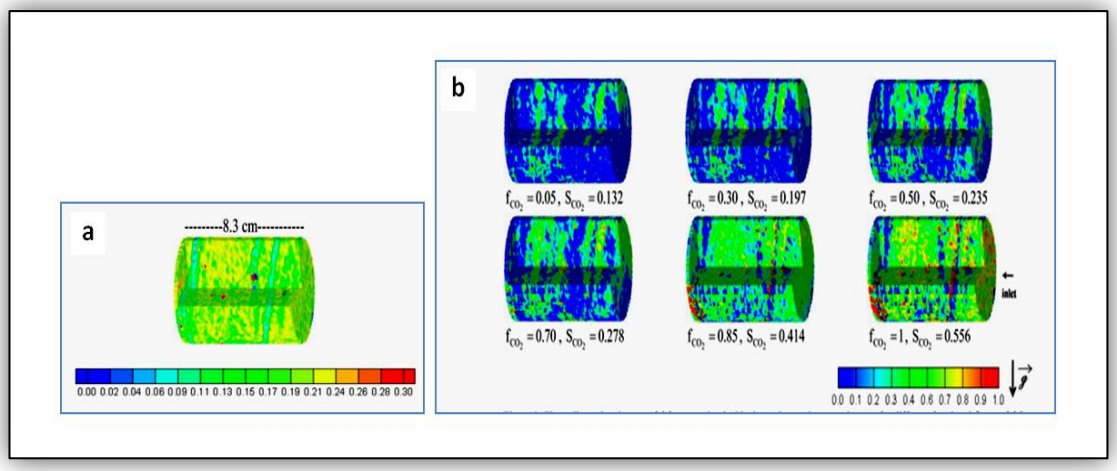

Figure 4.23: a) 3D porosity view, b) 3D CO_2 saturation maps for different fractional flows and fixed flow rate (2mL/min) (Perrin et al., 2009)

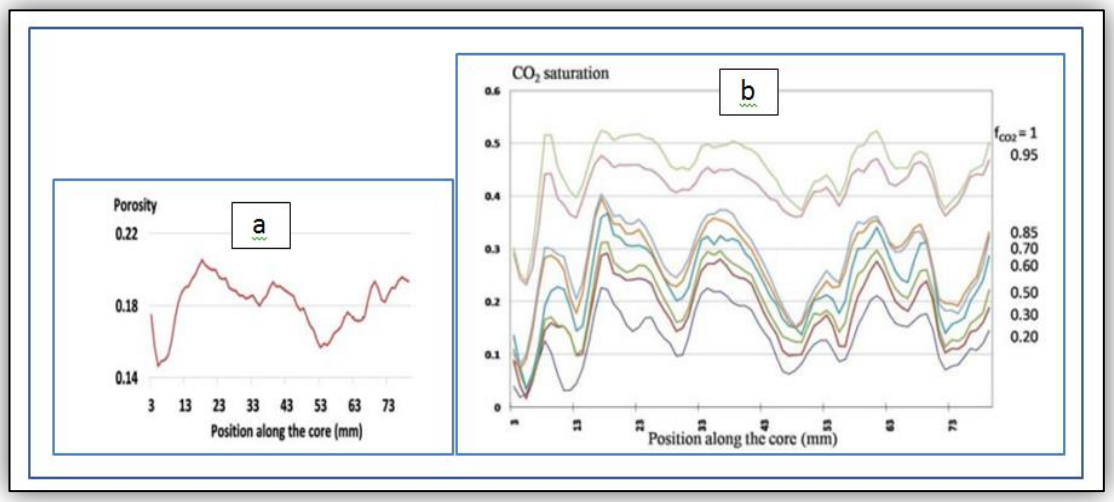

Figure 4.24: a) Porosity profile along the core, b) CO_2 saturation profiles along the core for different fractional flows (Perrin et al., 2009)

The high irreducible brine saturation (Figure 4.25) was attributed to the sub core-scale heterogeneities as observed and mentioned in previous studies (Bennion and Bachu, 2005, Benson et al., 2005) cited in Perrin et al., (2009).

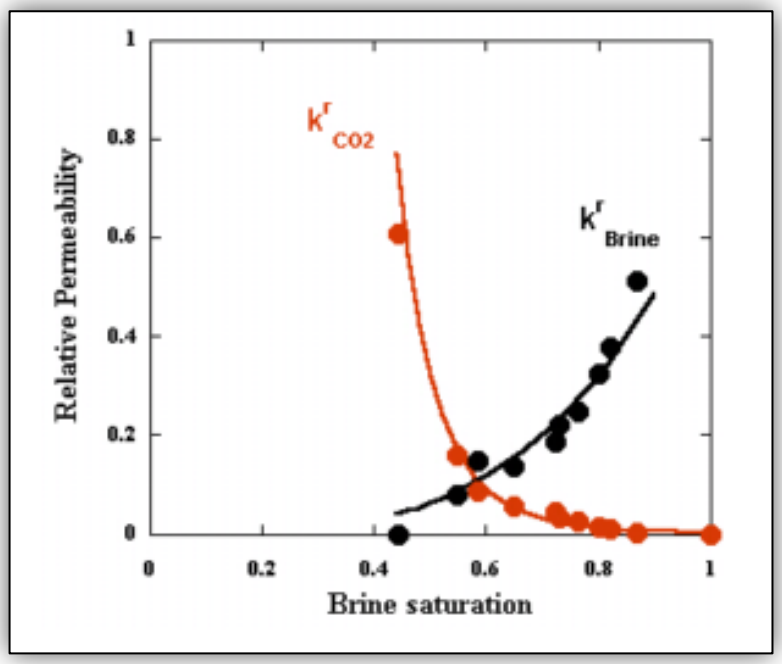

Figure 4.25: Relative permeability curves for drainage displacement (Perrin et al., 2009)

B.2) Drainage in heterogeneous Berea sandstone

Relative permeability experiments have been carried out during drainage. Three different total flow rates have been used: 2.6 mL/min; 1.2 mL/min; and 0.5 mL/min.

Furthermore, in this case, there is a strong relation between saturation distributions and porosity and this is attributed to the impact of capillary barriers created by the low porosity layers (Figure 4.26a, b).

Although the porosity of the Berea sandstone seemed to be very homogenous along the core axes, the incomplete gas saturation was clear at all flow rates (Figure 4.26:). While the core turned 180^{o}, the brine saturation picture did not change, which confirms the incomplete fluid replacement. The brine and CO_2 saturations in Berea sandstone were dependent on injection rate, for instance, at the highest injection rate (2.6 ml/min) the S_{wirr} = 57%, whereas at 0.05ml/min the S_{wirr} equalled 73%.

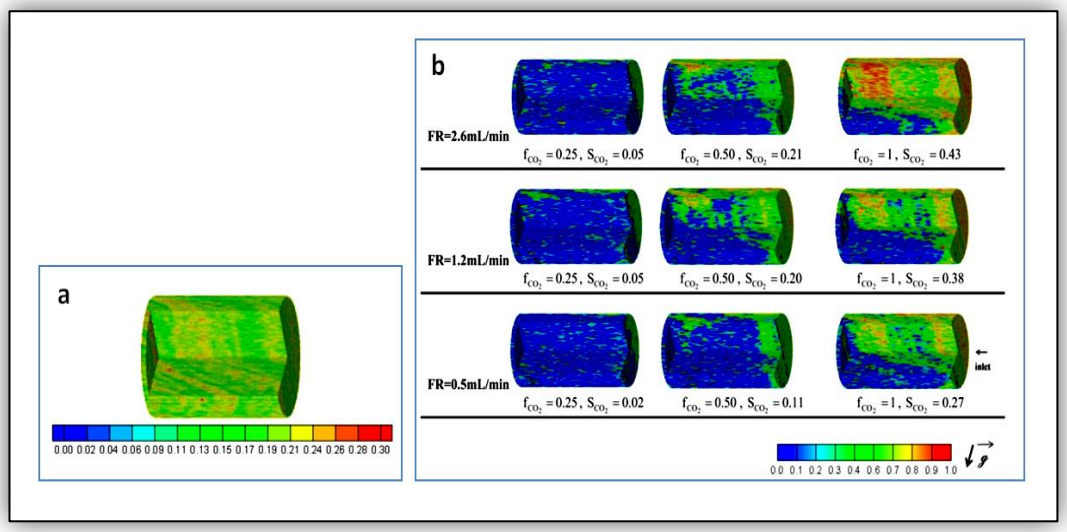

Figure 4.26: a) 3D porosity view, b) 3D CO_2 saturation maps for different fractional flows at three different flow rates (0.5,1.2,2.6 mL/min) (Perrin et al., 2009)

The CO_2 average saturation has a direct function with both flow rate and fractional flow, as appears in (Figure 4.27), whereas, for drainage, the CO_2 relative permeability values go up when the CO_2 flow rate increases (Figure 4.28).

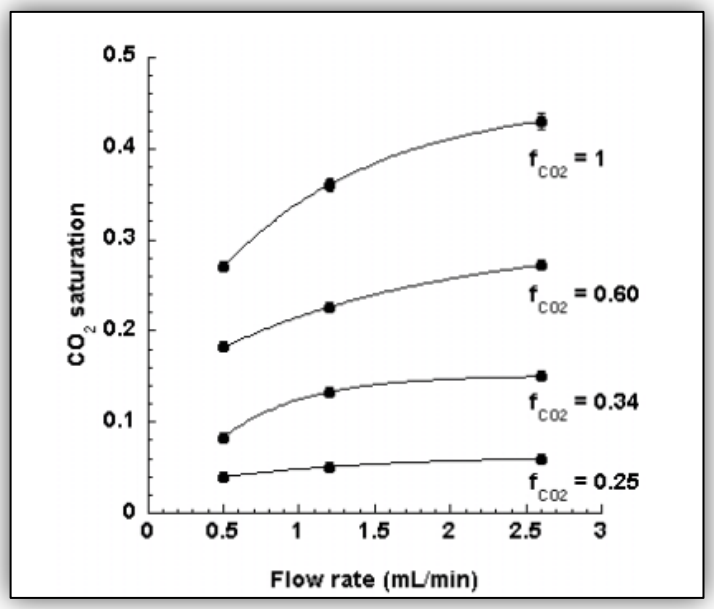

Figure 4.27: CO_2 saturation as a function of CO_2 flow rate and fractional flow (Perrin et al., 2009)

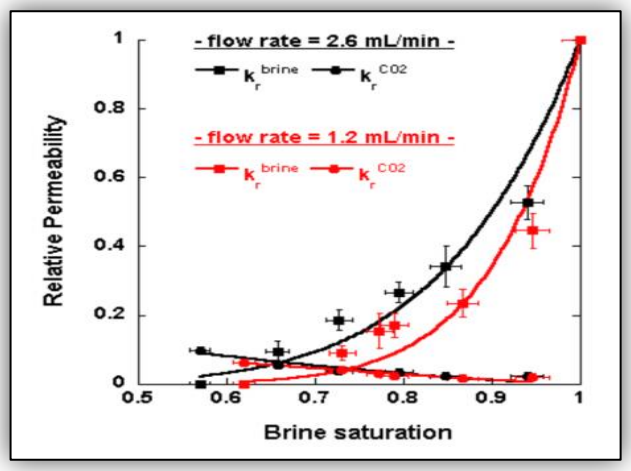

Figure 4.28: The influence of CO_2 flow rate on its relative permeability (Perrin et al.,-2009)

The case of (Fractional Flow CO_2 = 0. 50, flow rate = 1.2 mL/min) has been simulated with the multi-phase flow simulator TOUGH2 MP. The simulator has been provided with porosity maps extracted from X-ray CT scanner and permeability maps prepared using Carman-Kozeny equation. However, bypass of the lower part of the core which had been observed in the experiments was not simulated. This may be due to the fact that the approaches used for estimating the relative permeability maps are still being assessed and thus, they may lead the results to be not confirmable to experimental ones (Figure 4.29).

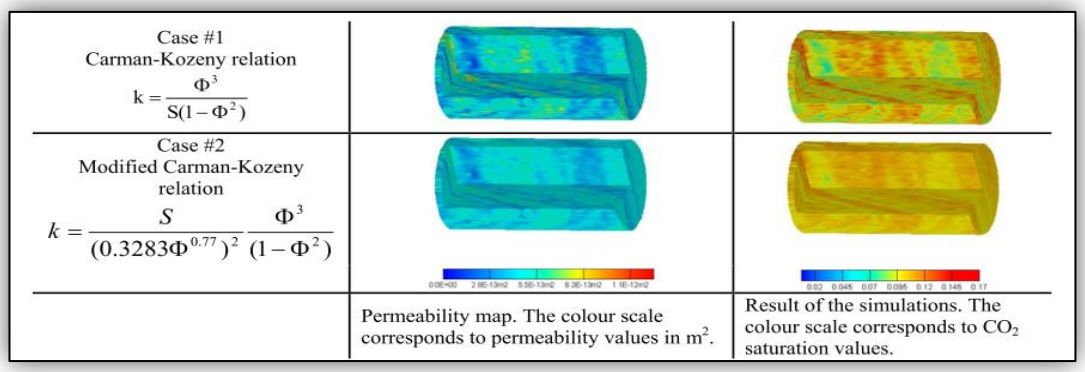

Figure 4.29: Permeability maps obtained from the Carman-Kozeny. Right: Results of the simulations (Perrin et al., 2009)

B.3) As a conclusion to this paper, we can say that although they applied experimental procedures in a good way, the results appeared to be heavily influenced by sample heterogeneity.

4.3.11. [**Paper 11**] "Drainage and Imbibition CO_2/Brine Relative Permeability Curves at Reservoir Conditions for High-Permeability Carbonate Rocks (Bennion and Bachu, 2010)"

This paper introduced a new set of high-pressure-temperature relative permeability measurements (drainage and imbibition) for reservoir carbonate rocks (limestone and dolomite) with higher absolute permeability values than those applied in the previous work that had been done by the authors (Bennion and Bachu, 2008a). And as it is a series of studies done by the same authors to measure the Kr_{Co2}, the experimental methodology was described previously in (Bennion and Bachu, 2005, Bennion and Bachu, 2008a).

Unit & Sample	Lithology	Depth (m)	Pressure (kPa)	Temperature (ºC)	Salinity (mg/l)	IFT** (mN/m)
Wabamun #3*	limestone	660.89	11,900	41	144,300	29.5
Nisku #3*	dolomite	1179.5	17,400	56	136,800	34.6
Grosmont	dolomite	502.04	11,900	41	144,300	34.2
Morinville Leduc	dolomite	1185.12	11,400	40	103,701	33.1
Redwater Leduc	limestone	957.27	9,200	36	106,069	35.1
Cooking Lake #3*	dolomite	1186.95	15,500	55	233,400	35.7
Slave Point	dolomite	1373.9	18,800	43	129,145	29.5
Winnipegosis	dolomite	1139.68	8,730	36	320,847	45.3

Table 4.8: In-situ conditions for rock samples from the Alberta basin used in the analysis of relative permeability and displacement characteristics of CO2.

A) The results:

A.1) As to CO_2 flow characteristics, Kopp et al. (2009), cited in Bennion and Bachu (2010), argued that the dimensional analysis brought out that the CO_2 flow in an aquifer is controlled by the interaction between the gravitational force (buoyancy) and viscous forces which oppose the flow. Nordbotten et al. (2005), cited in Bennion and Bachu (2010), introduced a term Γ (dimensionless Gravitational Number) representing the ratio between buoyancy (gravity) and viscous forces.

$$\Gamma = \frac{2\pi(\rho_{Brine}-\rho_{CO2})\,k_{rBrine}\,kB^2}{\mu_{Brine}\;Q} \quad \text{(Bennion and Bachu, 2010)} \qquad \text{Eq. 4.4}$$

Where Q is the injection rate, B is aquifer thickness, k_r is relative permeability, k is absolute permeability, ρ is density and μ is viscosity.

A.2) Valuation of relative permeability characteristics for carbonate rocks

- As in Table 4.9 the carbonate rock samples are classified into three groups according to the absolute permeability: Low k (<10 mD), Mid k (10-100 mD) , High k (>100 mD).

- At the end of drainage (Table 4.9b), the CO_2 performance in High-k samples was the worst, recording the minimum CO_2 endpoint relative permeability (0.0774) and maximum brine irreducible saturation (0.572). This bad performance of CO_2 (although the cores were classified as High-k) cannot be attributed to the interference phenomenon since the median pore size of the High-k samples was much higher than that for the Low-k cores (Table 4.9a) that produced the best CO_2 relative permeability characteristics; thus, heterogeneity (internal core structure) is most likely to be the reason behind that. It is similar to High-k samples compared with Mid-k cores through the imbibition (Table 4.9c), as the first one has lower brine endpoint relative permeability and higher CO_2 residual saturation although the median pore size in High-k cores was higher than that in Mid-k cores (Table 4.9a).

- According to Table 4.9b,c, the Corey exponent values for CO_2 at drainage process were always higher than those for the brine at the end of imbibition, which means brine (through imbibition) was displacing CO_2 in a better mobility or viscosity ratio displacement mode than did CO_2 over drainage, and thus, as expected that the process is to be more efficient when brine displacing CO_2.

a

Rock Group	% Micro Porosity	% Meso Porosity	% Macro Porosity	Median Pore Size (μm)	Porosity (%)	Threshold Capillary Pressure (kPa)
Low k	71.38	8.98	19.63	0.60	12.33	354.90
Mid k	22.87	10.60	66.52	8.36	11.85	32.17
High k	14.70	9.03	76.3	16.4	13.4	16.77

b

Rock Group	k_{brine} @100% saturation (mD)	$k_{r\ CO2}$ @ irreducible brine saturation	$S_{b\text{-}irr}$	Corey Model parameter for brine	Corey Model parameter for CO_2
Low k	2.05	0.4346	0.487	1.80	4.18
Mid k	54.65	0.1238	0.519	2.22	3.69
High k	293.13	0.0774	0.572	1.71	4.55

c

Rock Group	$k_{r\ brine}$ @ irreducible gas saturation	$S_{CO2\text{-}irr}$ (trapped gas)	Corey Model parameter for brine	Corey Model parameter for CO_2
Low k	0.1074	0.335	3.67	2.92
Mid k	0.6162	0.157	3.12	2.89
High k	0.3621	0.232	1.98	2.41

Table 4.9: Carbonate rock groups: a) Pore size distribution, b) relative permeability characteristics (drainage), c) relative permeability characteristics (imbibition) (Bennion and Bachu, 2010).

- Depending on the pre- and post-test CAT scans (Figure 4.30) of the core sample, the carbonic acid seemed to have reacted with the rock minerals. This reaction caused some variation in the pore structure, and possibly affecting the relative-permeability displacement behaviour of CO_2 and brine in such systems.

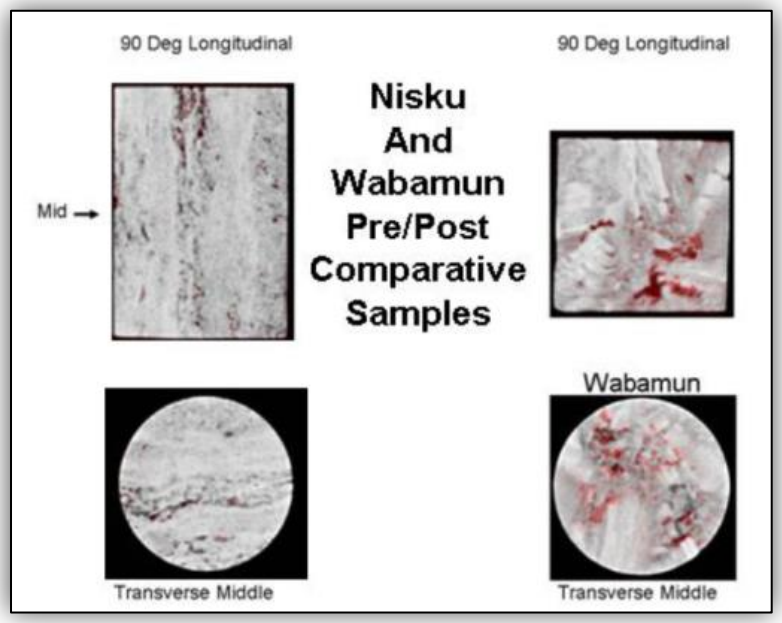

Figure 4.30: Comparison of pre- and post-test CAT-scan images of carbonate cores showing very little difference (Nisku #3, left) and significant differences (Wabamun #3, right) (Bennion and Bachu, 2010).

4.3.12. [**Paper 12**] "Relative Permeability Experiments of Carbon Dioxide Displacing Brine and their Implications for Carbon Sequestration (Levine, 2011)"

Experiments were carried out with synthetic and natural rock cores to measure CO_2 endpoint relative permeability rather than the entire relative permeability curve and at in-situ salinities, pressures, and temperatures and at different CO_2 conditions (supercritical and liquid).

A) The experimental protocol and procedures done:

The technique of Ramakrishnan and Cappiello (1991) was used. This is a steady state technique and apart from most steady state techniques which attempt to establish a uniform saturation throughout the core, this technique depends on establishing a monotonically decreasing saturation at capillary equilibrium throughout the core.

The advantage of this method is being relatively simple in both design and measuring CO_2 endpoint relative permeability without capillary end effect errors by exploiting the capillary end effect rather than avoiding it. In other words, it incorporates end effects by fitting relative permeability to the slope between two measured points taken at high flow rates, enabling a true measurement of drainage relative permeability at endpoint saturation despite the presence of saturation and pressure gradients in the core.

B) The results:

The values of CO_2 endpoint relative permeability obtained were around 0.35-0.4. These values indicate that the rock was not strongly water-wet, but might be either weakly or intermediately water-wet.

4.3.13. [**Paper 13**] "Relative permeability and trapping of CO_2 and water in sandstone rocks at reservoir conditions (Krevor et al., 2012)"

The steady state method was used to measure CO_2 relative permeability for CO_2-water system in four sandstone rock types at 50° C and 9 MPa pore pressure. The four sandstone samples are Berea, which is a homogeneous rock and shares with the Paaratte rock as being high permeability rocks, while Mt. Simon is a low permeability rock.

A) The experimental protocol and procedures done:

- The core was in a horizontal position.
- CO_2 distribution and saturation profile was observed using X-ray CT scan. This procedure is important to make sure that the results were not affected by heterogeneity, capillary end effects and fluid segregation.

B) The results:

- The relative permeability curves generated for the four samples are illustrated in Figure 4.31 with best-fit Corey curves depending on variables listed in Table 4.10. For all cases, kr_{Co2} at S_{wirr} was assumed to be 0.95, and the irreducible water saturation was considered to be 20% as it was measured in other past experiments.
- The impact of rock structure is more obviously observed in Tuscaloosa sandstone compared with other rocks (Figure 4.31).
- For drainage through all the samples, the irreducible water saturations were so high with recording values at least 40%. That negatively affects CO_2 relative

permeability to become considerably low. Bennion and Bachu (2008a) attributed this phenomenon to the impact of interfacial tension, while Müller (2011) referred it back to the influence of heterogeneity, capillary end effects and fluid segregation. As the impact of all these factors is absent, the researchers suggested that CO_2 saturations are controlled by maximum capillary pressure; therefore, low endpoint CO_2 permeabilities and saturations must not be taken as the endpoint values unless sufficient high capillary pressures were achieved in the experiment.

- Generally, all CO_2 relative permeability curves fit very well with the general characteristics of drainage displacement in strong water–wet rocks.

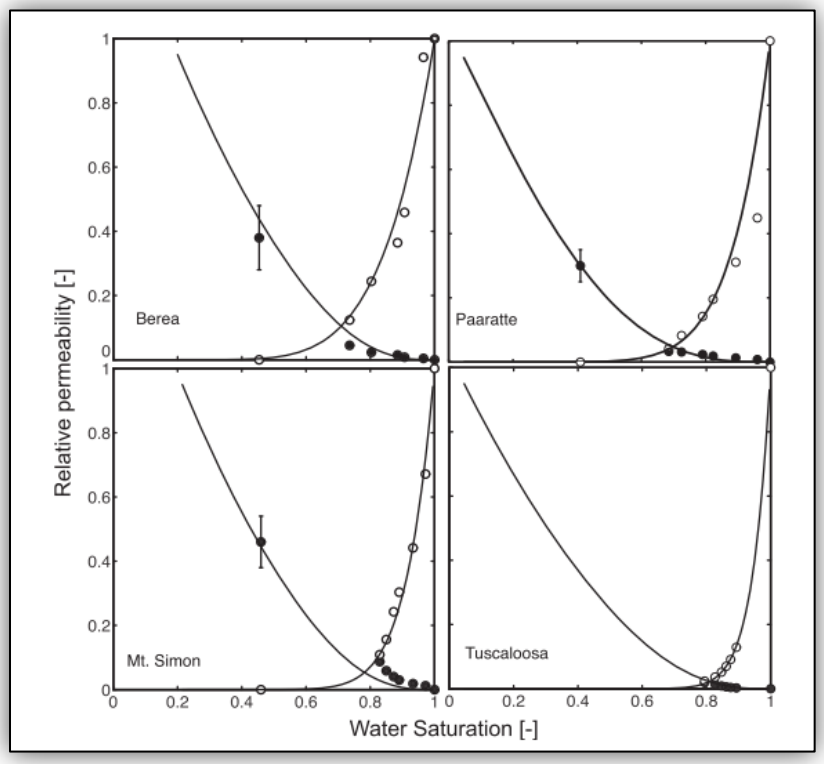

Figure 4.31: Solid circles refer to CO_2 relative permeability while water relative permeability was indicated by open circles. Solid black lines are best fit Brooks-Corey curves with best-fit parameters provided in Table 4.10

Name	$S_{CO_2,max}$	$k_{r,CO_2,max}$	N_w	N_{CO_2}
Berea	0.55	0.38	6	5
Paaratte	0.59	0.3	8	2
Mt. Simon	0.54	0.46	9	4
Tuscaloosa	0.46	–	17	4

[a] $k_{r,CO_2}(S_{wi})$ is assumed to be 0.95 for the fitting.
$S_{w,irr} = 0.2$. for the Berea sample

Table 4.10: Endpoint relative permeability, maximum saturations and best-fit Corey exponents for CO_2 and water in these experiments

4.3.14. [**Paper 14**] "An Experimental Study of CO_2 Ex-solution and Relative Permeability Measurements During Co_2-Saturated Water Depressurization (Zuo et al., 2012)"

Several experiments had been applied to measure the relative permeability of the ex-solved CO_2 under a wide range of depressurization (from 12.41 - 2.76 MPa) over three high permeable Berea sandstone samples and one sample of Mount Simon low permeability sandstone.

A) The experimental protocol and procedures done:

- Both rapid and slow depressurizations are applied to measure ex-solved CO_2 relative permeability from CO_2-saturated water.
- This type of CO_2 relative permeability has been measured for the first time.
- X-ray CT scanning was conducted for measuring porosity and CO_2 saturation synchronizing with monitoring saturation profile.
- The experimental setup was used for these experiments and designed to execute steady-state measurements of CO_2-water system relative permeability (Perrin and Benson, 2010). Modifications had been made on the empirical model to accommodate the special nature of these experiments.
- Measurements of ex-solved CO_2 relative permeabilities depended on depressurization method, in which the CO_2 was withdrawn from only one end of

the core. The calculation depended on a simple mathematical derivation. Tang and Firoozabadi (2003), cited in Zuo et al. (2012), mentioned that it is a multiphase modification of Darcy's Law, and assuming constant rock and fluid properties with no significant CO_2 saturation gradient across rock sample as extra assumption.

B) The results:

- The validity of no significant CO_2 saturation gradient was verified by observations of the saturation.
- The ex-solved CO_2 demonstrated different relative permeability compared with that obtained from steady-state drainage relative permeability measurements in the same cores; the ex-solved CO_2 relative permeability recorded very low values even when the Co_2 saturation was 40%. This reduction of relative permeability could be related to discontinuity of the ex-solved CO_2 phase.
- With no flow at the upstream boundary, and gradually increasing to 100% flow at the downstream boundary, the question which comes up here is: could the measurements be unduly biased by heterogeneities in the core?
- Although the rock composition of the cores consisted mainly of quartz, and small amounts of feldspar, calcite, siderite, and dolomite which could react with carbonic acid producing soluble salts and minerals, and although permeability measurements before and after demonstrated a difference in the values, the produced water was not analysed to check the extent of salts and minerals dissolved.

4.3.15. [**Paper 15**] "Relative permeability hysteresis and capillary trapping characteristics of supercritical CO_2-brine systems: An experimental study at reservoir conditions (Akbarabadi and Piri, 2013)"

Seven sets of steady-state drainage and imbibition full-recirculation flow experiments were conducted in three different sandstone rock samples, high- and low-permeability Nugget and Berea sandstones at reservoir conditions to generate a comprehensive group of relative permeability hysteresis curves.

A) The experimental protocol and procedures done:

- Throughout the steady-state experiments, super critical CO_2 and brine were co-injected with monotonically increasing or decreasing fractional flows to perform drainage and imbibition processes.

- At the end of each imbibition cycle, the researchers conducted in-situ dissolution of trapped CO_2 by injection of hundreds of brine pore volumes to get to $S_{wi} = 1$.
- In each cycle, a different level of S_{wi} was made, resulting in generating different-saturation-span relative permeability curves.

B) The results:

- As Figure 4.32 shows, the average initial brine saturation was relatively low and about 0.525.
- Over drainage process, the brine relative permeability displayed a very rapid decline accompanied by decrease in brine saturation (Figure 4.33). This is attributed to well connecting of brine elements being invaded by super-critical CO_2, resulting in significant reduction in brine hydraulic conductivity.

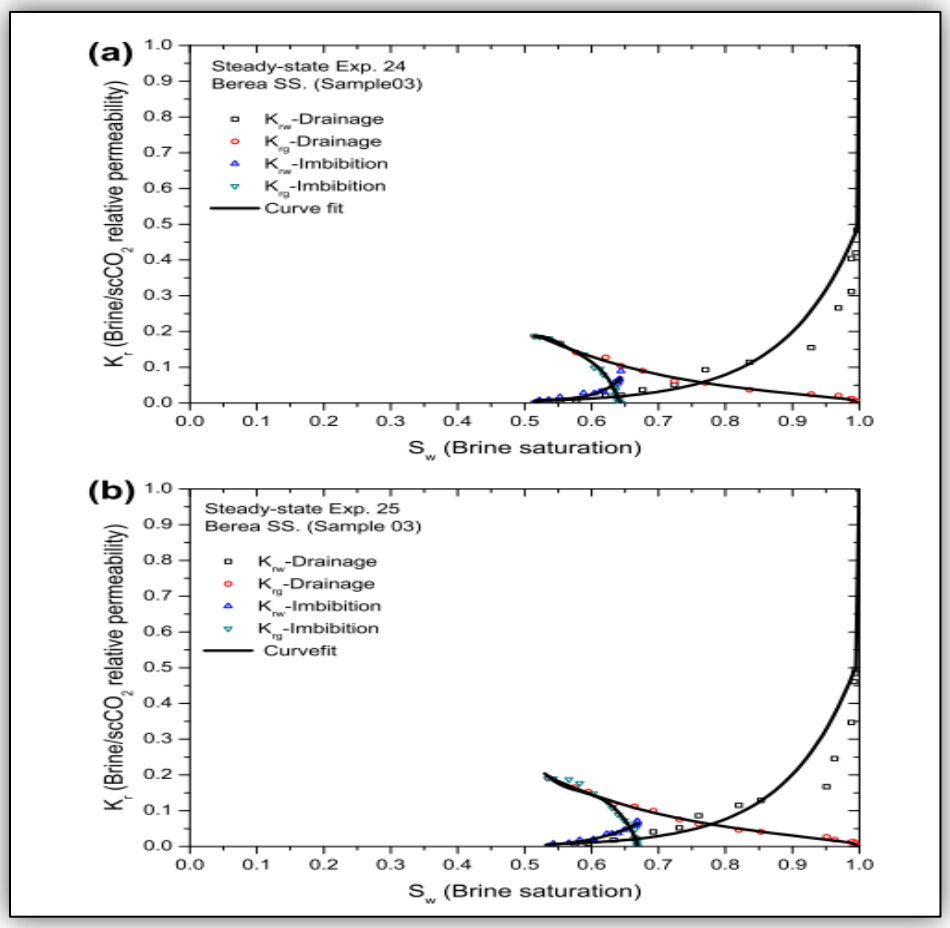

Figure 4.32: Full-cycle steady-state drainage and imbibition relative permeabilities for Berea sandstone core (Sample 3) generated by two separate experiments performed with identical fractional flow

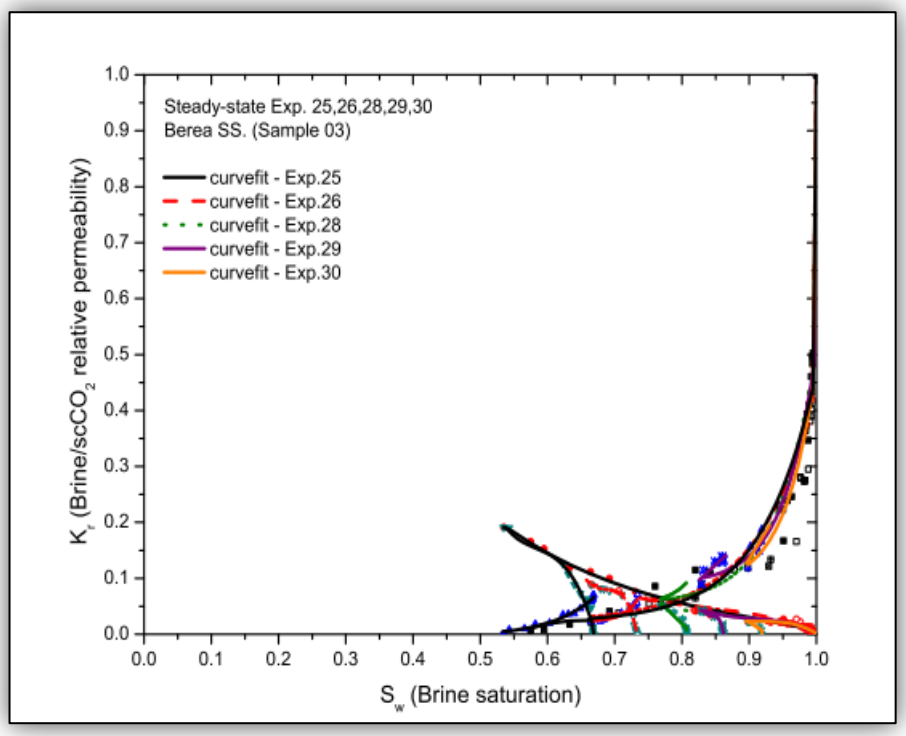

Figure 4.33: Steady-state drainage and imbibition relative permeabilities for Berea sandstone core (Sample 3) generated in this study

4.4. Recommendations to avoid errors in experimental procedures and data resulted

a. Select appropriate measurement protocol.

b. Having a vertical setup can mitigate the problems of horizontal setup like fluids segregation considerably.

c. Using X-ray CT scan and/or NMR methods to verify the core homogeneity and monitoring saturation profile during flooding (Müller, 2011).

d. Before doing measurement on the core-plugs of targeted formation, select another appropriate core samples so that:

- It can resist alter owing to the corrosive nature of carbonic acid.
- Getting homogenous as much as possible, for instance using the homogenous quartz sandstone or artificial core plug like Berea sandstone, sintered ceramics or glass would be optimal. These materials allow X-ray penetration during the core flood.

As long as the experimental protocol is successfully established, the measurements on the core-plugs of targeted formation could be applied-with reasonable confidence, even if they are heterogeneous cores (Müller, 2011).

e. Try to keep the same parameters like temperature, pressure, CO_2 saturation, and fluid velocity when applying different cores for the targeted formation.

f. Do monitoring and if possible quantify the changes in permeability and porosity distribution throughout the core due to reaction between CO_2 and rock material. This could be done by repeating the measurement after finishing the experiment.

g. Thermodynamic fluid behaviour for (mutual solubility, diffusion) should be taken into consideration when dealing with data resulted.

h. It is known that using a single laboratory method is not always sufficient; therefore, applying more than one way is essential for obtaining a good representative data for the rock.

i. Care should be taken on how the absolute or base permeability (reference permeability) was measured, whether it is by air or it is considered as the effective permeability to CO_2 at irreducible water.

4.5. Important notes about reading and interpreting the CO_2 relative permeability curves

Before going to read and interpret the CO_2 relative permeability curves, a few proactive steps must be considered and summarized in the following:

- A small step should be taken to make sure that there is not a partial or non-uniform fluid saturation (Figure 4.34) recorded while measuring the relative permeability. This task could be achieved by making a quick look on CT scan images obtained during the experiment running. This protective measure is very important as the incomplete fluid saturation leads to cancelling out the assumption of uniform saturation in dynamic displacement which necessarily in turn will produces an error in relative permeability data produced or renders it false (Figure 4.34).

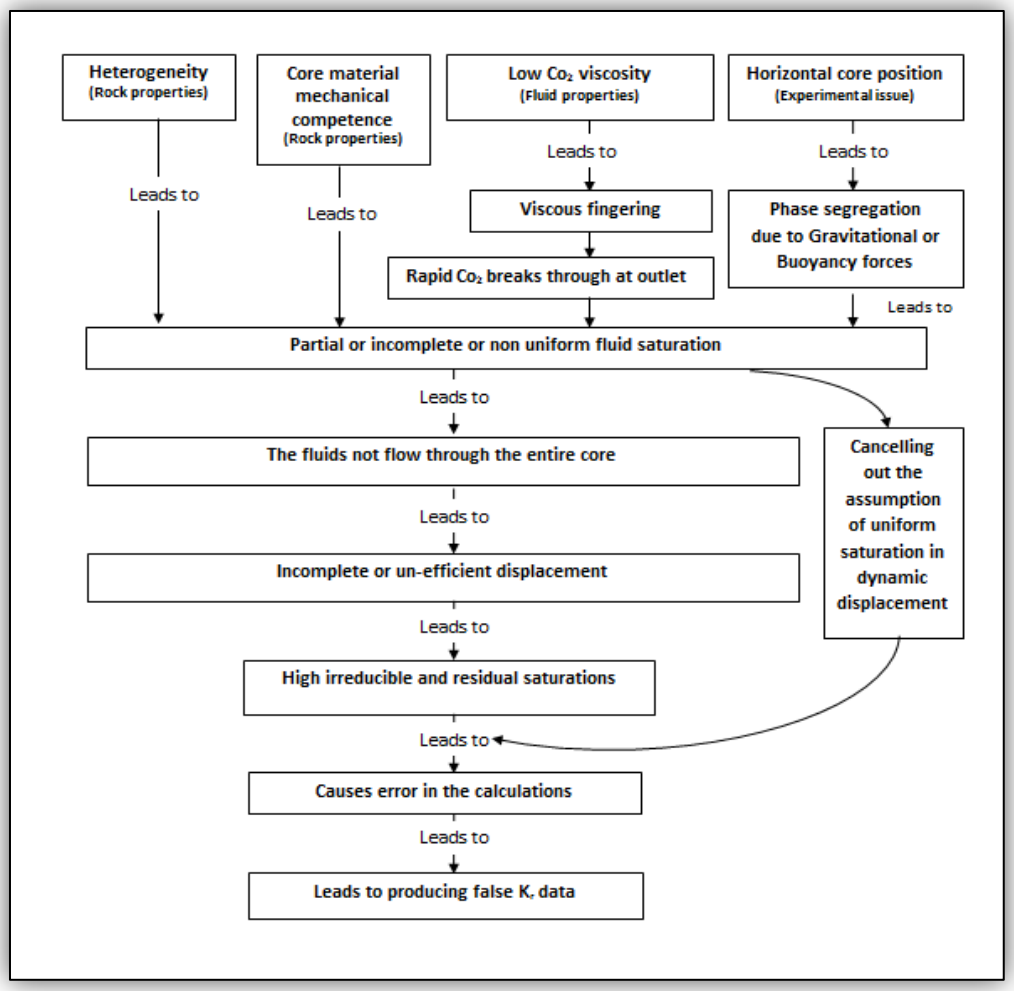

Figure 4.34 : Partial or non-uniform fluid saturation (causes and results)

- Petrographic SEM (Scanning Electron Microscope analysis) must be conducted to check if any pore throats were plugged by precipitations produced from the aggressive chemical reactions, which leads to the relative permeability and porosity being decreased. Repeating the measurements of permeability and porosity must be applied after the experiment is finished, as an additional procedure for certainty. The following (Figure 4.35) gives an example for the pore media before being plugged (a) and after plugging (b).

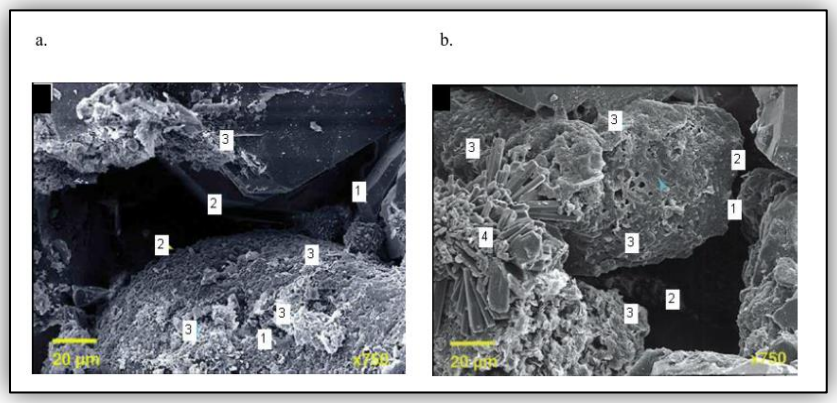

Figure 4.35: Electro-microscope Petrography: a) pre-test, and b) post-test

- Complete record of pressure, temperature and salinity must be enclosed to predict the impacts on the IFT and viscosity/Mobility ratio subsequently on the relative permeability.

- Fluids saturation degree must be well known, as the mass transfer would be expected if unsaturated - CO_2-brine system or unsaturated-brine-CO_2 system are in used. The mass transfer raises the solubility, which makes the IFT decrease.

- The wettability type and intensity should be measured before and after conducting the experiment.

- Another issue must be considered before reading and interpreting the CO_2 relative permeability curves; the low endpoint CO_2 saturations and permeabilities should not be taken as the endpoint values unless it is clearly shown that sufficiently high capillary pressures were achieved in the experiment.

Reading and interpreting the CO_2 relative permeability curves could be done depending on some of its characteristics such as:

4.5.1. The general shape of the curve

The general shape of CO_2 relative permeability curve is mainly affected by two factors as follows:

A) The interference leads the curve to be in concave shape, and as the interference is more intensive, the concavity (curvature degree) will be more severe (Figure 4.36).

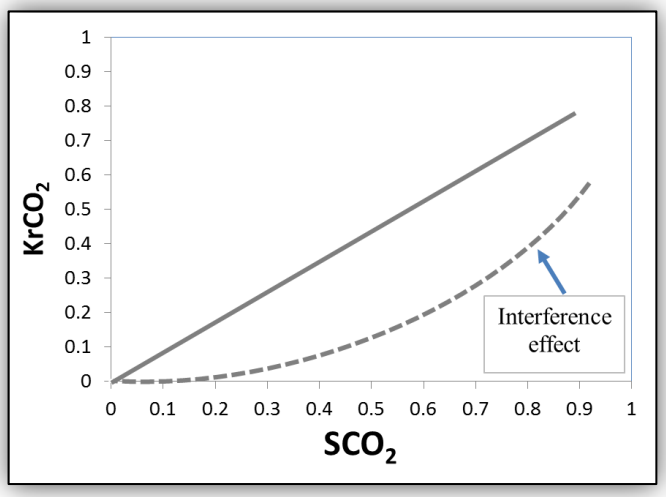

Figure 4.36: Impact of interference on CO_2 relative permeability values curve

B) The core's internal pore structure (pores and throat distribution investigated in the following chapter) will appear in two modes; the first is the normal pore and throat distributions that will produce a regular curve shape, whereas the abnormal distributions (the second) results in the curve shape to be almost vertical; the viscous fingering as well leaves a very similar impact (Figure 4.37).

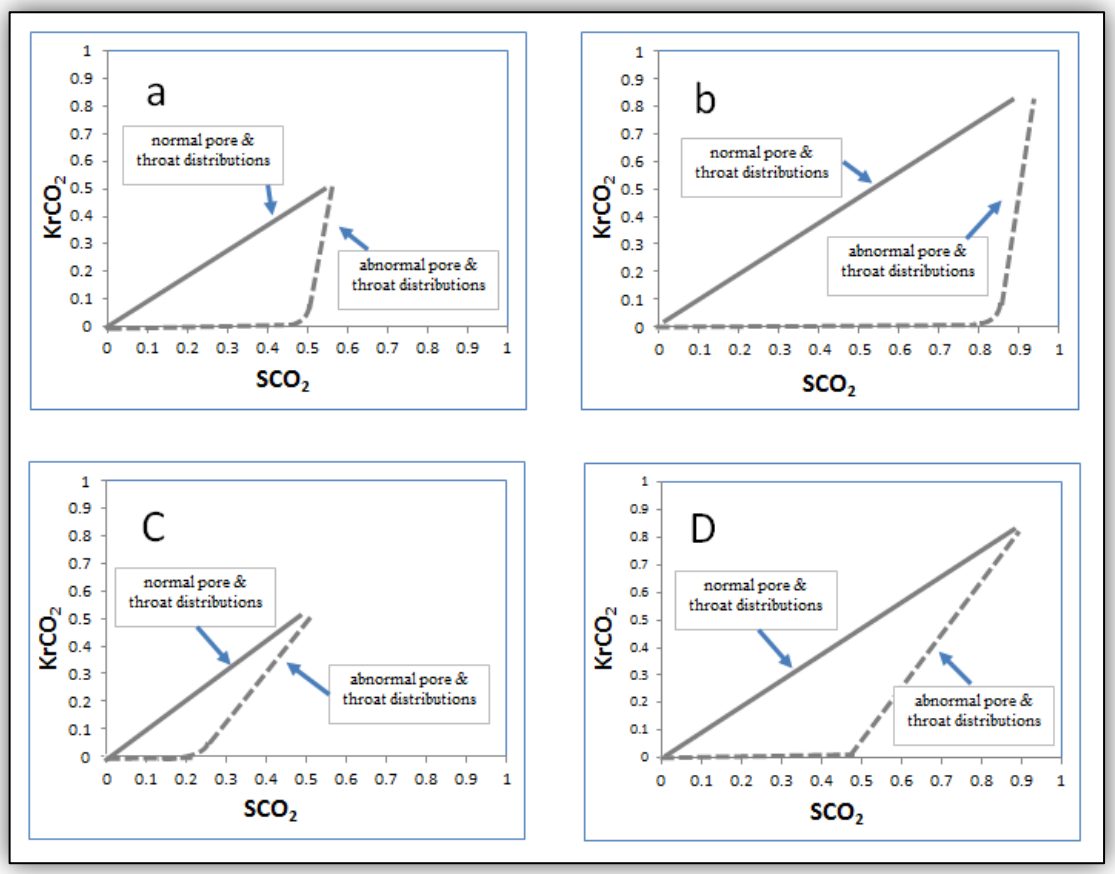

Figure 4.37: Impact of core's internal pore structure on CO_2 relative permeability values curve

The Corey exponent is a measure of curve concavity (curvature), which may refer to the impact of interference phenomena or core's internal pore structure (heterogeneity), but it has been identified that the Corey's exponent refers more to interference than to core's internal pore structure. Furthermore, the interference was found to have inverse function with the median pore size (pore characteristics), so the bigger median pore size leads generally to less-concave relative permeability curves, which indicates a reduction in multiphase interference effects (Bennion and Bachu, 2008a).

4.5.2. The values of the curve

A) The CO_2 relative permeability general values

Looking to the CO_2 relative permeability values individually, it had been found that the general values of the relative permeability curve are impacted by IFT (Figure 4.38). generally, the IFT produces a resistance to displacement, resulting in the number of invaded throats (responsible on generating relative permeability data) to be smaller, whereas a very high IFT may lead to incomplete or inefficient displacement which in turn results in early stopping of relative permeability curve. As the IFT is a function of pressure, temperature, salinity, solubility and mass transfer, the CO_2 relative permeability may suddenly get improved which means there is mass transfer which leads the IFT to be lower.

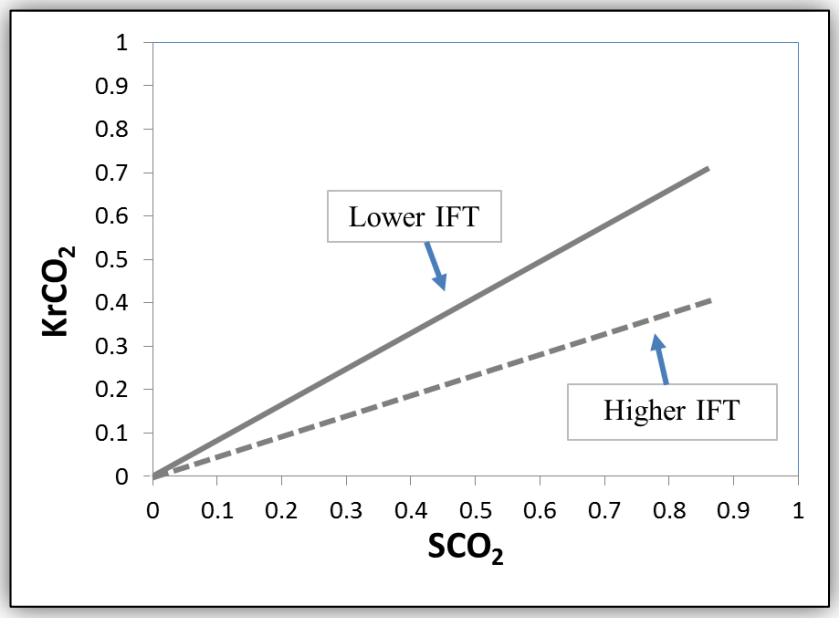

Figure 4.38: Impact of IFT on relative permeability values curve

B) The maximum or endpoints (CO_2 relative permeability and saturations) and the minimum (irreducible or residual) saturations

Avoiding the existence of viscous fingering, phase segregation and pore-throat plugging by undesirable chemical reactions, the maximum or endpoints (CO_2 relative permeability and saturations) and the minimum (irreducible or residual) saturations are affected by interference, internal rock structure (pore capillary pressure), IFT, mobility of CO_2 and wettability. More information about these factors follows:

i. Impact of interference and heterogeneity (internal core structure)

Both interference and heterogeneity (internal core structure) may result in CO_2 endpoint relative permeability being very low for example (0.0774) and the brine irreducible saturation to be very high, but if the median-pore-size is high (less effect of interference) it means heterogeneity is the main factor that caused unfavourable results.

ii. Synchronized impact of IFT, CO_2 mobility and pressure applied

- When applying an increasing pressure, it is not possible to attribute the low brine irreducible saturation to the impact of CO_2 viscosity since whenever the pressure increases the CO_2 viscosity will also increase. All that will negatively impact the mobility of CO_2 and thus negatively impact the general displacement efficiency as well, and as a final result, the brine irreducible saturations are expected to be higher with increasing pressure. Consequently, when applying an increasing pressure, the low irreducible saturations obtained must be attributed to the IFT depending on the fact that, the lower IFT the smaller capillary forces resists the displacement, resulting in more reduction in irreducible or residual saturations, which conforms with the case here.

- Although the IFT is low in some systems, it is observed that the CO_2 relative permeability is low and the brine irreducible saturation is quite high. Evidently, this is not consistent with the lower IFT as when the IFT is lower the capillary forces resisting displacement will be smaller, resulting in brine irreducible saturation value to be less. Therefore, the problem in this case could be attributed to CO_2 mobility which was high and counteracting the lower IFT effect, resulting in the displacement efficiency not being optimum owing to more macroscopic bypassing of the pore system.

Additional important notes:

In some studies, particularly those dealing with digital pore-network models or cores, the following conceptions are frequently used:

a. The endpoint (maximum) saturation value is an indicator to number of invaded pores (mainly) and throats, and particularly behind the outlet. In other words, the major part of endpoint saturation value comes from invading pores (in the first place) and throats, and mainly behind the outlet.

b. The endpoint (maximum) relative permeability value is an indicator to the number of throats invaded at outlet (percent of absolute permeability).

c. As pores and throats are connected and feed each other, the saturation value gives an idea about the size distribution of invaded and un-invaded throats when converting the saturation concept to pressure.

d. If the SCO_2-endpoint is much higher than $KrCO_2$-endpoint, it means that the throat distribution quality in vertical direction to flow is much better than that with flow direction.

References

AKBARABADI, M. & PIRI, M. 2013. Relative permeability hysteresis and capillary trapping characteristics of supercritical CO2/brine systems: An experimental study at reservoir conditions. *Advances in Water Resources,* 52**,** 190-206.

ARCHER, J. S. & WONG, S. W. 1973. Use of a Reservoir Simulator To Interpret Laboratory Waterflood Data. *Society of Petroleum Engineers Journal,* 13**,** 343-347.

BACHU, S. & BENNION, B. 2008. Effects of in-situ conditions on relative permeability characteristics of CO2-brine systems. *Environmental Geology,* 54**,** 1707-1722.

BENNION, B. & BACHU, S. 2005. Relative Permeability Characteristics for Supercritical CO2 Displacing Water in a Variety of Potential Sequestration Zones in the Western Canada Sedimentary Basin. *SPE Annual Technical Conference and Exhibition.* Dallas, Texas: Society of Petroleum Engineers.

BENNION, B. & BACHU, S. 2008a. Drainage and Imbibition Relative Permeability Relationships for Supercritical CO2/Brine and H2S/Brine Systems in Intergranular Sandstone, Carbonate, Shale, and Anhydrite Rocks. *SPE Reservoir Evaluation & Engineering,* 11**,** 487-496.

BENNION, D. & THOMAS, F. Recent improvements in experimental and analytical techniques for the determination of relative permeability data from unsteady state flow experiments. SPE 10th Techncial Conference and Exposition, Port of Spain, Trinidad, 1991.

BENNION, D. B. & BACHU, S. 2006a. The Impact of Interfacial Tension and Pore Size Distribution/Capillary Pressure Character on CO2 Relative Permeability at Reservoir Conditions in CO2-Brine Systems. *SPE/DOE Symposium on Improved Oil Recovery.* Tulsa, Oklahoma, USA: Society of Petroleum Engineers.

BENNION, D. B. & BACHU, S. 2006b. Supercritical CO2 and H2S—Brine Drainage and Imbibition Relative Permeability Relationships for Intergranular Sandstone and Carbonate Formations. *SPE Europec/EAGE Annual Conference and Exhibition.* Vienna, Austria: Society of Petroleum Engineers.

BENNION, D. B. & BACHU, S. 2006c. Dependence on Temperature, Pressure, and Salinity of the IFT and Relative Permeability Displacement Characteristics of CO2 Injected in Deep Saline Aquifers. *SPE Annual Technical Conference and Exhibition.* San Antonio, Texas, USA: Society of Petroleum Engineers.

BENNION, D. B. & BACHU, S. 2007. Permeability and Relative Permeability Measurements at Reservoir Conditions for CO2-Water Systems in Ultra Low Permeability Confining Caprocks. *EUROPEC/EAGE Conference and Exhibition.* London, U.K.: Society of Petroleum Engineers.

BENNION, D. B. & BACHU, S. 2008b. Correlations for the Interfacial Tension Between Supercritical Phase CO2 and Equilibrium Brines at In Situ Conditions. Society of Petroleum Engineers.

BENNION, D. B. & BACHU, S. 2010. Drainage and Imbibition CO2/Brine Relative Permeability Curves at Reservoir Conditions for High-Permeability Carbonate Rocks. *SPE Annual Technical Conference and Exhibition.* Florence, Italy: Society of Petroleum Engineers.

BENSON, S. M., TOMUTSA, L., SILIN, D., KNEAFSEY, T. & MILJKOVIC, L. 2005. Core scale and pore scale studies of carbon dioxide migration in saline formations.

BERG, S., OEDAI, S. & OTT, H. 2013. Displacement and mass transfer between saturated and unsaturated CO2–brine systems in sandstone. *International Journal of Greenhouse Gas Control,* 12**,** 478-492.

CHALBAUD, C. A., LOMBARD, J.-M. N., MARTIN, F., ROBIN, M., BERTIN, H. J. & EGERMANN, P. 2007. Two Phase Flow Properties of Brine-CO2 Systems in a Carbonate Core: Influence of Wettability on Pc and kr. *SPE/EAGE Reservoir Characterization and Simulation Conference.* Abu Dhabi, UAE: Society of Petroleum Engineers.

CHIQUET, P., BROSETA, D. & THIBEAU, S. 2007. Wettability alteration of caprock minerals by carbon dioxide. *Geofluids,* 7**,** 112-122.

COREY, A. T. 1954. The interrelation between gas and oil relative permeabilities. *Producers monthly,* 19**,** 38-41.

CROTTI, M. A. & ROSBACO, J. A. 1998. Relative Permeability Curves: The Influence of Flow Direction and Heterogeneities.

DAKE, L. 1994. The Practice of Reservoir Engineering, 1994. Elsevier, Amsterdam.

DRIA, D. E., POPE, G. A. & SEPEHRNOORI, K. 1993. Three-Phase Gas/Oil/Brine Relative Permeabilities Measured Under CO2 Flooding Conditions. *SPE Reservoir Engineering,* 8**,** 143-150.

EGERMANN, P., CHALBAUD, C. A., DUQUERROIX, J. & LE GALLO, Y. 2006. An Integrated Approach to Parameterize Reservoir Models for CO2 Injection in Aquifers. Society of Petroleum Engineers.

FELBER, B. J. 2004. Selected U. S. Department of Energy EOR Technology Applications. Society of Petroleum Engineers.

GLOVER, P. 2011. *Formation Evaluation MSc Course Notes* [Online]. Available: http://www2.ggl.ulaval.ca/personnel/paglover/CD%20Contents/Formation%20Evaluation%20English/Chapter%2010.PDF 2011].

GOODLETT, G. O., HONARPOUR, M. M., CHUNG, F. T. & SARATHI, P. S. 1986. The Role of Screening and Laboratory Flow Studies in EOR Process Evaluation. Society of Petroleum Engineers.

HONARPOUR, M. & MAHMOOD, S. M. 1988. Relative-Permeability Measurements: An Overview. *Journal of Petroleum Technology,* 40**,** 963-966.

JAMALUDDIN, A. K. M., BENNION, D. B., THOMAS, F. B. & CLARK, M. A. 1998. Acid/Sour Gas Management in the Petroleum Industry. Society of Petroleum Engineers.

JEAN-CHRISTOPHE PERRIN, M. K., CHIA-WEI KUO, & BENSON, L. A. S. M. 2008. Core- and pore-scale experimental study of relative permeability properties of CO2 and brine in reservoir rocks.

JOHNSON, E. F., BOSSLER, D. P. & NAUMANN, V. O. 1959. *Calculation of Relative Permeability from Displacement Experiments*.

KAMATH, J., NAKAGAWA, F. M., BOYER, R. E. & EDWARDS, K. A. 1998. Laboratory Investigation of Injectivity Losses During WAG in West Texas Dolomrites. Society of Petroleum Engineers.

KOPP, A., CLASS, H. & HELMIG, R. 2009. Investigations on CO2 storage capacity in saline aquifers: Part 1. Dimensional analysis of flow processes and reservoir characteristics. *International Journal of Greenhouse Gas Control,* 3**,** 263-276.

KREVOR, S. C. M., PINI, R., ZUO, L. & BENSON, S. M. 2012. Relative permeability and trapping of CO2 and water in sandstone rocks at reservoir conditions. *Water Resources Research,* 48**,** W02532.

LEVINE, J. 2011. Relative Permeability Experiments of Carbon Dioxide Displacing Brine and Their Implications for Carbon Sequestration.

MATHIAS, S. A., GLUYAS, J. G., GONZÁLEZ MARTÍNEZ DE MIGUEL, G. J., BRYANT, S. L. & WILSON, D. 2013. On relative permeability data uncertainty

and CO2 injectivity estimation for brine aquifers. *International Journal of Greenhouse Gas Control,* 12**,** 200-212.

MÜLLER, N. 2011. Supercritical CO2-Brine Relative Permeability Experiments in Reservoir Rocks—Literature Review and Recommendations. *Transport in Porous Media,* 87**,** 367-383.

MULLER, N., QI, R., MACKIE, E., PRUESS, K. & BLUNT, M. J. 2009. CO2 injection impairment due to halite precipitation. *Energy Procedia,* 1**,** 3507-3514.

MUNGAN, N. 1972. Relative Permeability Measurements Using Reservoir Fluids.

NORDBOTTEN, J., CELIA, M. & BACHU, S. 2005. Injection and Storage of CO2 in Deep Saline Aquifers: Analytical Solution for CO2 Plume Evolution During Injection. *Transport in Porous Media,* 58**,** 339-360.

OKABE, H., TSUCHIYA, Y., MIHAMA-KU, H. & SHINJYUKU-KU, O. Experimental investigation of residual CO 2 saturation distribution in carbonate rock. International symposium of the society of core analysts, Abu Dhabi, UAE, 2008.

PATERSON, L., PAINTER, S., ZHANG, X. & PINCZEWSKI, W. V. 1998. Simulating Residual Saturation and Relative Permeability in Heterogeneous Formations.

PENTLAND, C. H., EL-MAGHRABY, R., IGLAUER, S. & BLUNT, M. J. 2011. Measurements of the capillary trapping of super-critical carbon dioxide in Berea sandstone. *Geophysical Research Letters,* 38.

PERRIN, J.-C. & BENSON, S. 2010. An Experimental Study on the Influence of Sub-Core Scale Heterogeneities on CO2 Distribution in Reservoir Rocks. *Transport in Porous Media,* 82**,** 93-109.

PERRIN, J.-C., KRAUSE, M., KUO, C.-W., MILJKOVIC, L., CHAROBA, E. & BENSON, S. M. 2009. Core-scale experimental study of relative permeability properties of CO2 and brine in reservoir rocks. *Energy Procedia,* 1**,** 3515-3522.

PINI, R., KREVOR, S. C. M. & BENSON, S. M. 2012. Capillary pressure and heterogeneity for the CO2/water system in sandstone rocks at reservoir conditions. *Advances in Water Resources,* 38**,** 48-59.

PISTONE, S. 2011. *The significance of co2 solubility in deep subsurface environments.*, Stanford University.

PRIEDITIS, J., WOLLE, C. R. & NOTZ, P. K. 1991. A Laboratory and Field Injectivity Study: CO2 WAG in the San Andres Formation of West Texas. Society of Petroleum Engineers.

PRUESS, K. & MÜLLER, N. 2009. Formation dry-out from CO2 injection into saline aquifers: 1. Effects of solids precipitation and their mitigation. *Water Resources Research,* 45**,** W03402.

RAMAKRISHNAN, T. S. & CAPPIELLO, A. 1991. A new technique to measure static and dynamic properties of a partially saturated porous medium. *Chemical Engineering Science,* 46**,** 1157-1163.

ROGERS, J. D. & GRIGG, R. B. 2001. A Literature Analysis of the WAG Injectivity Abnormalities in the CO2 Process.

SCIENCES, S. O. E. 2013. *Relative Permeability Explorer* [Online]. Stanfod university. Available: https://pangea.stanford.edu/research/bensonlab/relperm/index.html.

SHI, J.-Q., XUE, Z. & DURUCAN, S. 2009. History matching of CO2 core flooding CT scan saturation profiles with porosity dependent capillary pressure. *Energy Procedia,* 1**,** 3205-3211.

SIGMUND, P. M. & MCCAFFERY, F. G. 1979. An Improved Unsteady-State Procedure for Determining the Relative-Permeability Characteristics of

Heterogeneous Porous Media (includes associated papers 8028 and 8777). *Society of Petroleum Engineers Journal,* 19**,** 15-28.

SUEKANE, T., NOBUSO, T., HIRAI, S. & KIYOTA, M. 2008. Geological storage of carbon dioxide by residual gas and solubility trapping. *International Journal of Greenhouse Gas Control,* 2**,** 58-64.

SURVEY, A. G. 2013. *Relative Permeability Data for Supercritical CO2 Displacing Water* [Online]. Alberta Geological Survey. Available: http://www.ags.gov.ab.ca/co2_h2s/wabamun/relative_permeability.html.

TANG, G.-Q. & FIROOZABADI, A. 2003. Gas- and Liquid-Phase Relative Permeabilities for Cold Production From Heavy-Oil Reservoirs.

TOTH, J., BODI, T., SZUCS, P. & CIVAN, F. 2001. Direct Determination of Relative Permeability from Nonsteady-State Constant Pressure and Rate Displacements. Society of Petroleum Engineers.

WELLMAN, T. P., GRIGG, R. B., MCPHERSON, B. J., SVEC, R. K. & LICHTNER, P. C. 2003. Evaluation of CO2-Brine-Reservoir Rock Interaction with Laboratory Flow Tests and Reactive Transport Modeling. Society of Petroleum Engineers.

YUQI1, D., BOLAJI, O. B. & DACUN, L. 2004. Literature Review on Methods toObtain Relative Permeability Data.

ZUO, L., KREVOR, S., FALTA, R. & BENSON, S. 2012. An Experimental Study of CO2 Exsolution and Relative Permeability Measurements During CO2 Saturated Water Depressurization. *Transport in Porous Media,* 91**,** 459-478.

Chapter 5

The Impact of Rock Pore Structure on CO_2 Relative Permeability.

5.1. Introduction

In most petroleum engineering literature, the relative permeability of CO_2 had been studied in terms of an individual case as for each formation separately, and all the research studies mentioned that the main factors affecting the CO_2 relative permeability are the saturation history, hysteresis, IFT and interference but with less degree.

As for a group of formations with different rock type (Figure 5.1), they mainly attributed the difference in CO_2 relative permeability curves to rock type parameter.

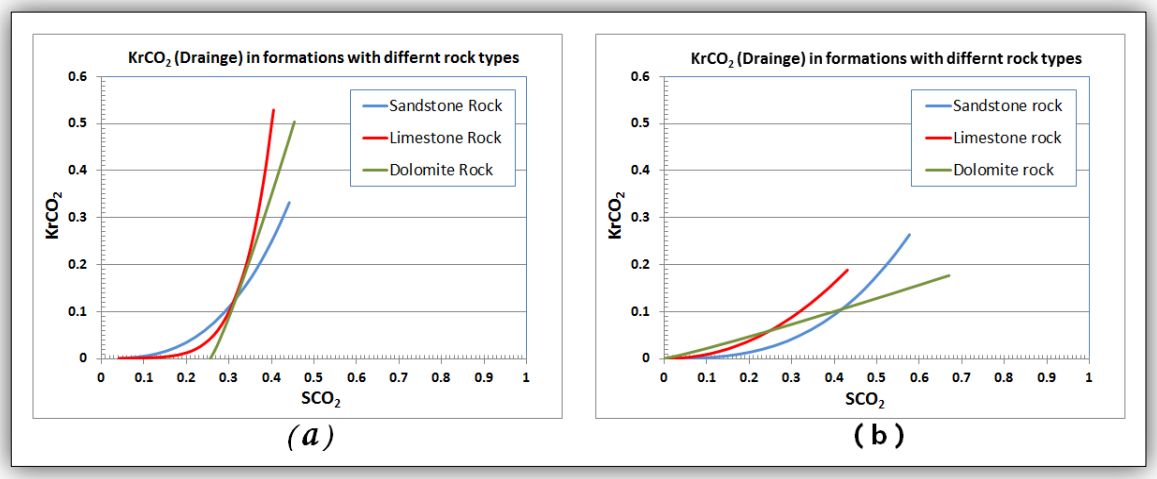

Figure 5.1: CO_2 relative permeability curves of formations with different rock types (Rerferences mentioned in paragraph (a) page 136)

However, it has been found that, even in a set of samples extracted from many formations with the same rock type or from a single formation and having the same capillary properties (wettability, IFT and viscosity) as well, there is diversity in CO_2 relative permeability curves as appears in Figure 5.2. The studies assumed that the rock pore structure or quality is the factor responsible for the disparity in this case, but no details of its cause and how it could be and how it results in producing variant CO_2 relative permeability curves for a set of formations with the same rock type or even for a set of samples taken out from the same formation were given. This research will introduce an upgraded conception as pore and throat distributions; this conception is to be used to interpret the difference in CO_2 relative permeabilities mentioned, and it is described in section 5.2.

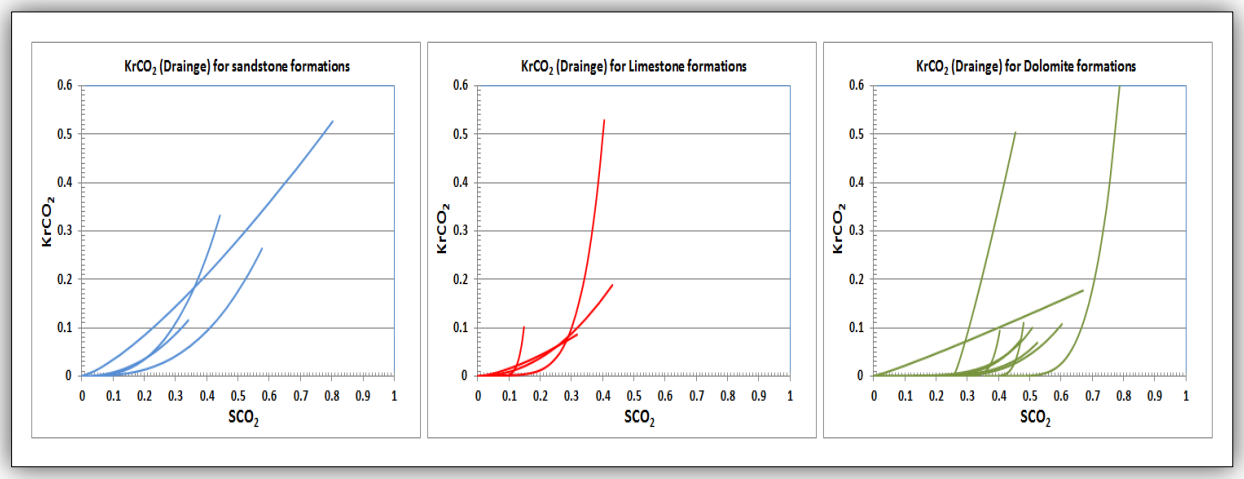

Figure 5.2: CO_2 relative permeability curves of formations with the same rock type (Sciences, 2013, Survey, 2013)

5.2. Upgrading the concept of pore size distribution

The rock consists of pores and throat (channels). The summation of cross sectional area of channels (throats) represents the absolute permeability, while the total volume of pores represents the porosity, so as an example, invading pores (filled with brine) by CO_2 produces the values of CO_2 saturation, whereas invading channels or throats will produce the values of CO_2 relative permeability.

Both throats and pores exist in the rock in variant sizes (Figure 5.3).

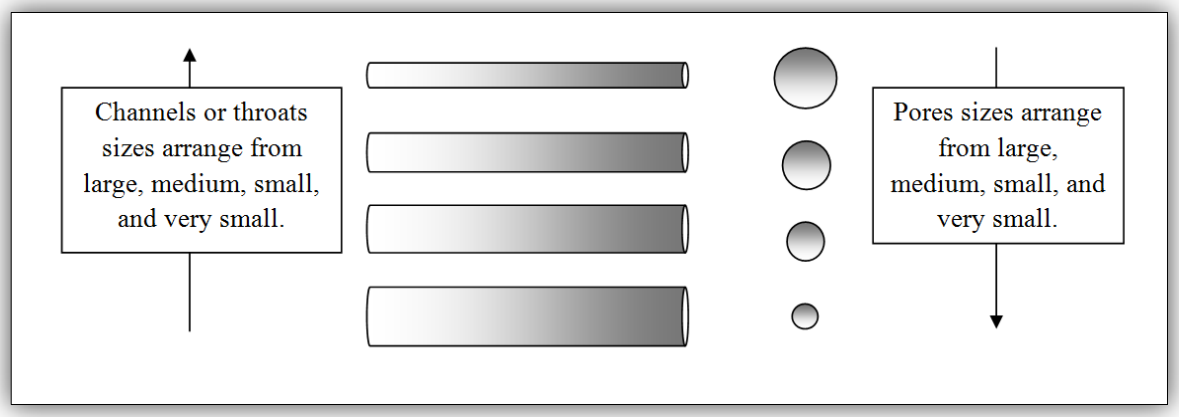

Figure 5.3: Different sizes of throats and pores

According to this principle, two types of distributions are suggested: pore size distribution and channel or throat size distribution, with fundamental concepts as shown in the next section.

5.2.1. **Throat size distributions:**

Throat size distribution is the percentage represented by each throat size in absolute permeability at the outlet part, not in the total number of throats[4]. If the percentages of throat size distribution are close to each other we can say there is a normal throat size distribution (Figure 5.4 a), but if some percentages are very high while others are very low, that means we have abnormal throat size distribution (Figure 5.4 b).

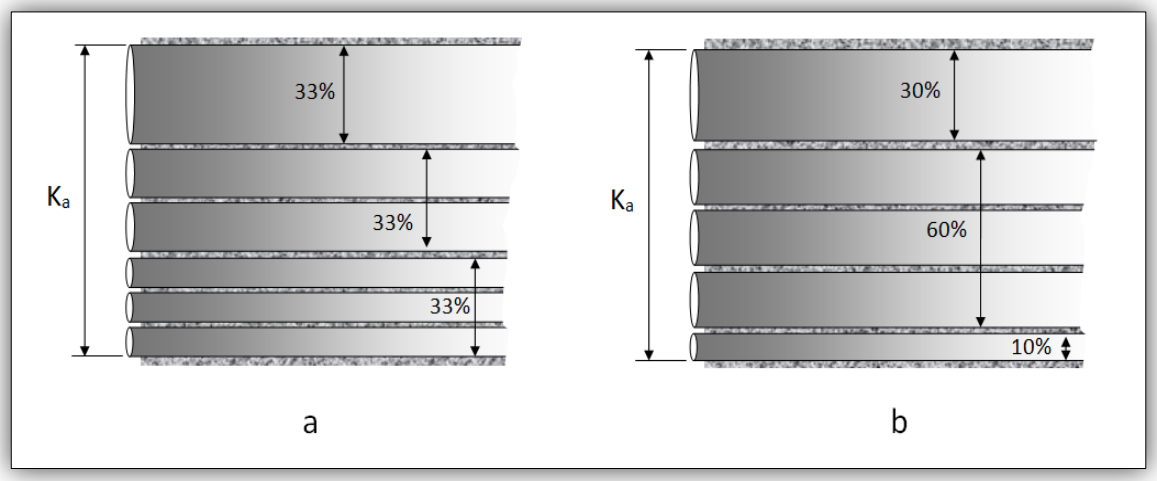

Figure 5.4: Throat size distribution

The importance of this conception being considered as a part of rock quality concept is that as percentage of large throats is high (in direction of flow) the fluids flow much more easily through it. At a certain point inside the rock, if the throat sizes in different direction are not close to each other, that means heterogeneity exists. Consequently, the throat size distribution should be verified in the direction of flow and in other directions (Figure 5.5).

[4] The old concept defines the pore size distribution as a measure of the pore throat diameter and the fraction of total pore space represented by each diameter. There is no relationship between porosity and pore size characteristics since porosity is a measure of the volume of the pores and pore size characteristics is a measure of pore diameter and distribution.

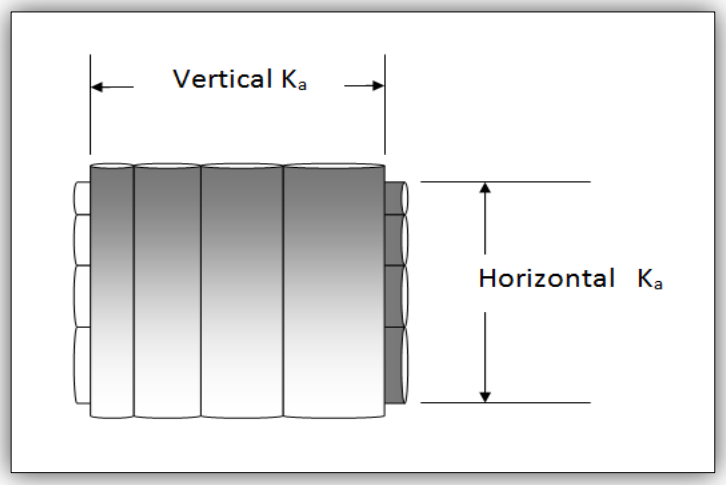

Figure 5.5: Importance of throat size distribution

5.2.2. **Pore size distributions:**

This is the percentage represented by each pore size in total porosity.

If the percentages of pore size distribution are close to each other, we can say there is a normal pore size distribution, but if some percentages are very high while others are very low, that means we have abnormal pore size distribution.

5.2.3. **Throats and pores connection.**

If the throats connect with pores and both of them have the same size, the system will appear as consisting of throats only (Figure 5.6 a): it's named a similar pore-throat connection, but if the connected throats and pores are in different sizes, there is a dissimilar pore-throat connection (Figure 5.6 b).

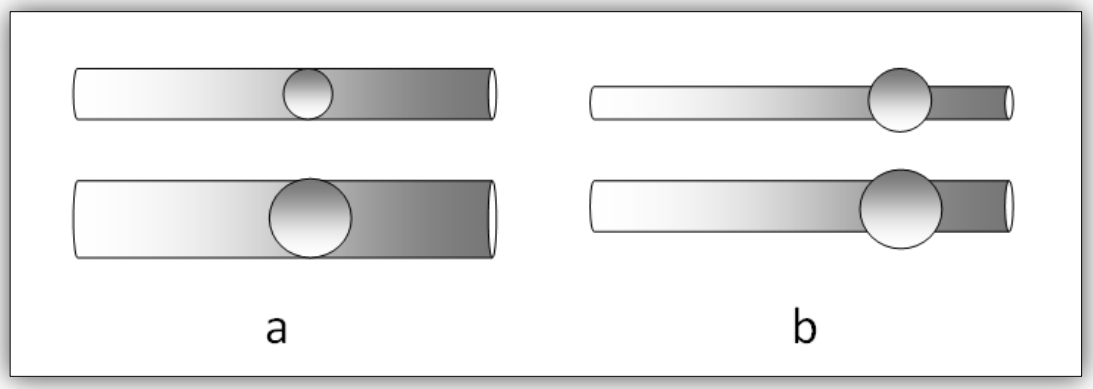

Figure 5.6: Throats and pores connection

It is admissible that the pores and throats are connected and feed each other; throat may be first and the pores next, and vice versa.

Therefore, and according to throats and pores distributions and connection concepts, this work will study the impact of these concepts on both relative permeability of CO_2 and the saturation accompanying it.

5.3. Normal pore size distribution and Normal throat size distributions with a similar pore-throat connection:

In this case, there is a normal pore size and normal throat size distributions with a similar pore-throat connection, the diameters of pores and throats are almost equal for the same degree of size distribution; in addition, the equal–diameter pores and throats are connected together (Figure 5.7). This system is called a **complete normal distribution–similar connection**. This case could be considered as we have a system consisting of throats only, **so it is a system of throat size distribution only**.

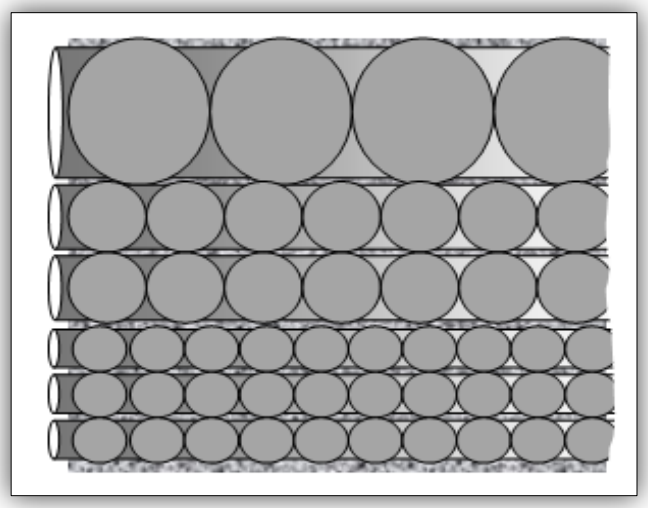

Figure 5.7: Complete normal distributions – similar connection

5.3.1. CO_2 Relative permeability progression and line shape through complete normal distributions – similar connection system:

In this system, the following could be expected:

A) Since the diameters of pores and throat are almost equal for the same degree of size distribution and connected to each other, for a certain size of pore and throat, the CO_2 invading will be instant and simultaneous in both pores and throats. Consequently, producing CO_2 saturation and relative permeability data occurs simultaneously; this also reflects the direct function between CO_2 saturation and relative permeability.

B) It can be admitted that brine capillary pressure (which represents the resistance force to invade the pores and throats by CO_2) has an inverse function with pore and throat diameter, which means as throat diameter or size decreases, the brine capillary pressure or resistance force increases. So, depending on information mentioned here and that from (A), it could be stated that the primary values of CO_2 relative permeability come from displacing the brine phase from the big throats, and the increase in CO_2 relative permeability is due to displacement of the brine from the other medium and small throats respectively.

C) As known, for a system with normal throat distribution, the percentages of throat size distribution in absolute permeability are very close to each other, and based on this information and that from (A & B) it's expected that the system produces a regular CO_2 relative permeability line with ordinary CO_2 relative permeability increase rate. Furthermore, some factors affect the shape and the general values of CO_2 relative permeability line; these factors are IFT, interference, and hysteresis, and their impact appears as follows: the $KrCO_2$ line shape takes the exponential function shape when interference has sensible value, whereas a depression in the general slope degree could be remarked in case of IFT. Disappearance of these factors returns the CO_2 relative permeability line to the straight line shape with 45° angle.

So, the KrCO2 develops as in (Figure 5.8), and that could be summarised as follows:

i. (Figure 5.8 a) represents a sample of normal distributions & similar connection and filled with brine.

ii. At the beginning, the CO_2 invades large pores and throats with low brine pressure to produce initial values of CO_2 saturation and relative permeability (Figure 5.8 b).

iii. After that, CO_2 invades medium pores and throats producing increase in CO_2 saturation and relative permeability (Figure 5.8 c).

iv. According to (Figure 5.8 d), invading small pores and throats introduces the final set of CO_2 saturation and relative permeability values; the most of CO_2 relative permeability lines never reach the point where relative permeability and saturation reach the unity, that's because there are very small pores and throats with very high brine pressure and cannot be occupied and invaded by CO_2.

v. The impact of IFT, interference could be apparent as depression and exponential in KrCO2 curve characteristics.

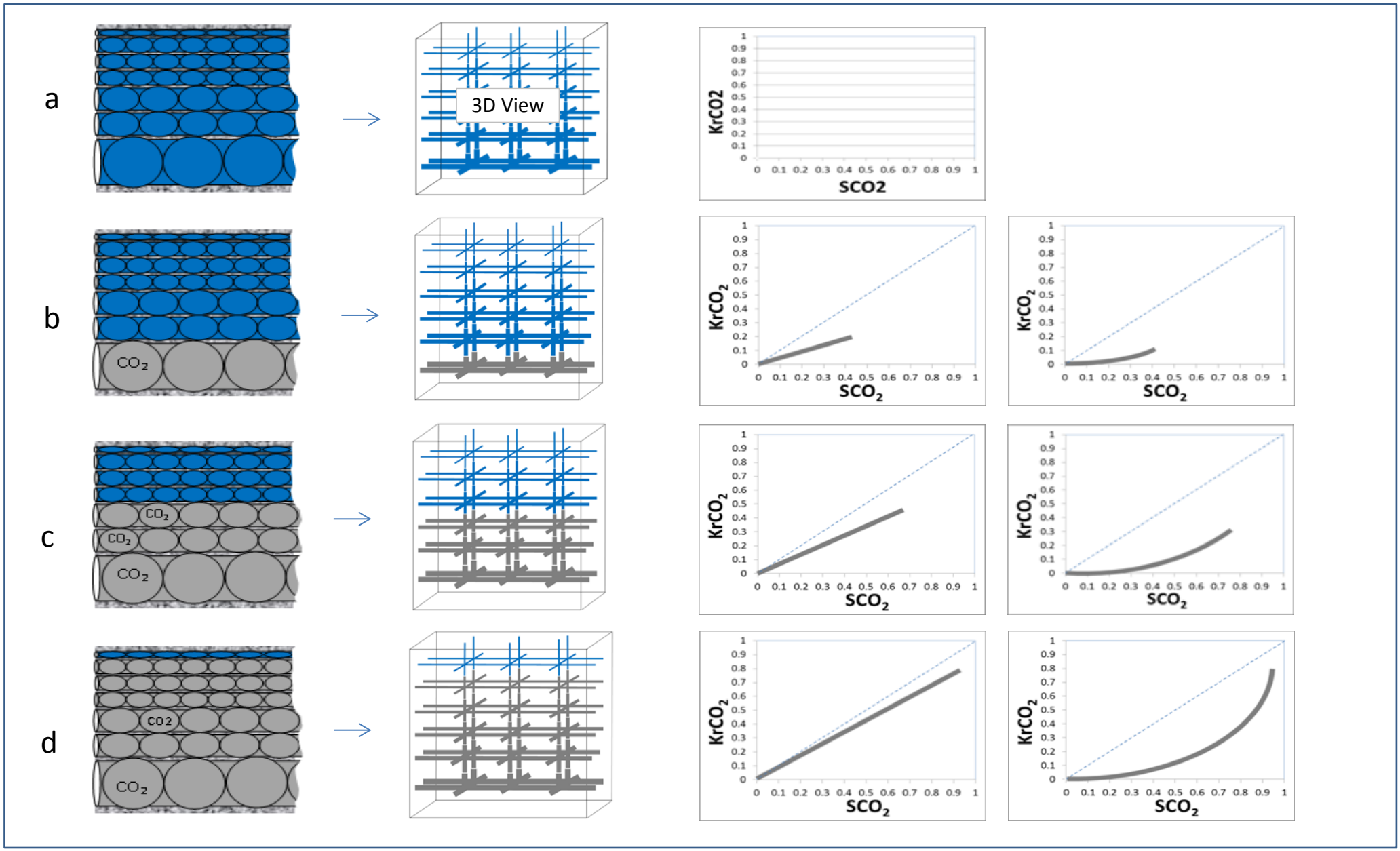

Figure 5.8: CO_2 Relative permeability progression and line shape

Experimentally, the CO_2 is withdrawn from the tank and injected with constant pressure. It immediately penetrates the large pores-throats where the brine pressure is low. After that, the CO_2 will accumulate in front of the core and its pressure increases until it becomes able to penetrate the smaller pores and throats. This phenomenon continues until CO_2 pressure reaches a maximum value and is not sufficient to invade more pore-throats which usually are very small with very high pressure. Then, the saturation of CO_2 will stop at a certain point, and to drive more CO_2 in the core the injection pressure at CO_2 tank should be raised.

5.3.2. Diffusion and flow pattern through complete normal distributions-similar connection system

According to the information mentioned, the CO_2 diffuses gradually and uniformly, consequently, the flow is expected to be laminar and to produce high injection rates.

5.3.3. Further understanding of the reason that CO_2 relative permeability decreases as IFT increases

As IFT is a phenomenon resulting from the repulsion forces between different molecules at the interface, it produces resistance to displace the brine by CO_2. All that will negatively impact CO_2 relative permeability by reducing the number of invaded throats (capillary channels), which generates the CO_2 relative permeability value.

5.3.4. The interference phenomenon

Interference is a phenomenon which negatively affects CO_2 relative permeability. This negative effect is due to the fact that in the ideal case CO_2 and brine flow separately, but in actual cases they mostly interfere with each other. Honarpour et al. (1986) mentioned that there are some other reasons that activate sharing flow of CO_2 and brine: part of the pore channels available may be reduced in size by the brine in the rock; some constrictions in a pore channel may be plugged completely by immobilized droplets of a fluid; some pore channels may become effectively plugged by adverse capillary forces if the pressure gradient is too low to push an interface through a constriction.

Interference is generally stronger when CO_2 saturation is decreased (imbibition) rather than being increased (drainage). The interference makes the sum of the relative permeabilities (for CO_2 and brine) always less than unity.

5.4. Abnormal distributions with dissimilar complicated connection system.

In this system either the throats or pores have abnormal distribution or both of them, in addition to dissimilar connections.

In this system, the following could be expected:

5.4.1. Relating to CO_2 relative permeability curve shape

A) In this system, the CO_2 saturation and relative permeability do not progress simultaneously, and in many cases the CO_2 relative permeability delays much after the CO_2 saturation starts to increase. This is of course due to dissimilar connections, and as a result, there is no permanent direct function between CO_2 saturation and relative permeability.

B) There is an irregular CO_2 relative permeability line (a nearly vertical line), which is because the relative permeability data are recorded at very close saturation values. It also indicates that the invaded throats' pressures and thus their sizes are very close to each other.

5.4.2. Relating to diffusion and flow pattern

According to the information above, the diffusion of CO_2 is never uniform; this disarranged diffusion produces turbulent flow which produces a dynamic skin and impedes the mobility of CO_2, and as a result, the injection rate will be mostly low.

Below are some criteria considered as basic principles to read the CO_2 relative permeability line:

a. The endpoint (maximum) saturation value is an indicator to number of invaded pores (mainly) and throats, and particularly behind the outlet. In other words, the major part of endpoint saturation value comes from invading pores (in first place) and throats, and mainly behind the outlet.

b. The endpoint (maximum) relative permeability value is an indicator to number of throats invaded at outlet (percent of absolute permeability).

c. As pores and throats are connected and feed each other, saturation value gives an idea about the size distribution of invaded and un-invaded throats when one convert the saturation concept to pressure.

d. If the SCO_2-endpoint is much higher than $KrCO_2$-endpoint, that means the throat distribution quality through vertical direction to flow is much better than that in flow direction.

Therefore, the CO_2 relative permeability progression and line shape could be introduced, depending on concepts mentioned, (A, B) in the rest section.

5.4.3. CO_2 relative permeability line shape in case of abnormal pore size distribution and abnormal throat size distributions with dissimilar connections.

To understand this better, the throat sizes are divided into four degrees: very large, large, medium, small, very small; the CO_2 relative permeability line shape is expected to be as following:

A) Case①, large and very small throats only at the outlet, with invasion only through the large ones (Figure 5.9).

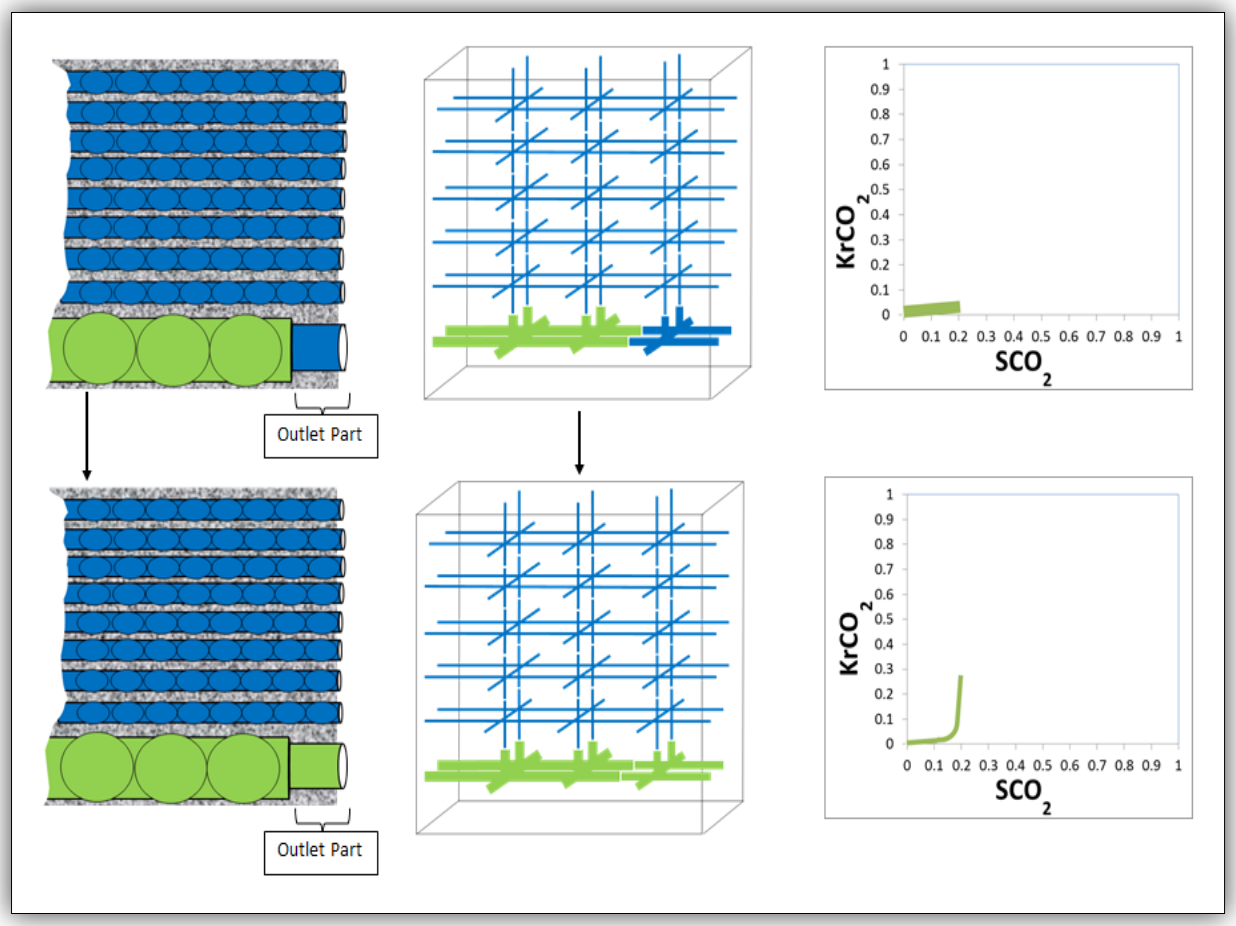

Figure 5.9: Case①, large and very small throats only at the outlet, with invading just through the large ones

From Figure 5.9, it could be remarked that there is delay in producing CO_2 relative permeability data due to dissimilar connection. The invading of throats ($KrCO_2$) started at very low CO_2 saturation (pressure) which means that the size of invaded throats was large. The vertical shape of $KrCO_2$ confirms that the throats invaded were of similar

size. Generally, a very small part of pore and throats are invaded (very small endpoints) as the rock consists mainly of very small throats and pores.

B) Case②, medium, small and very small throats only at the outlet, with invading only through the medium ones (Figure 5.10).

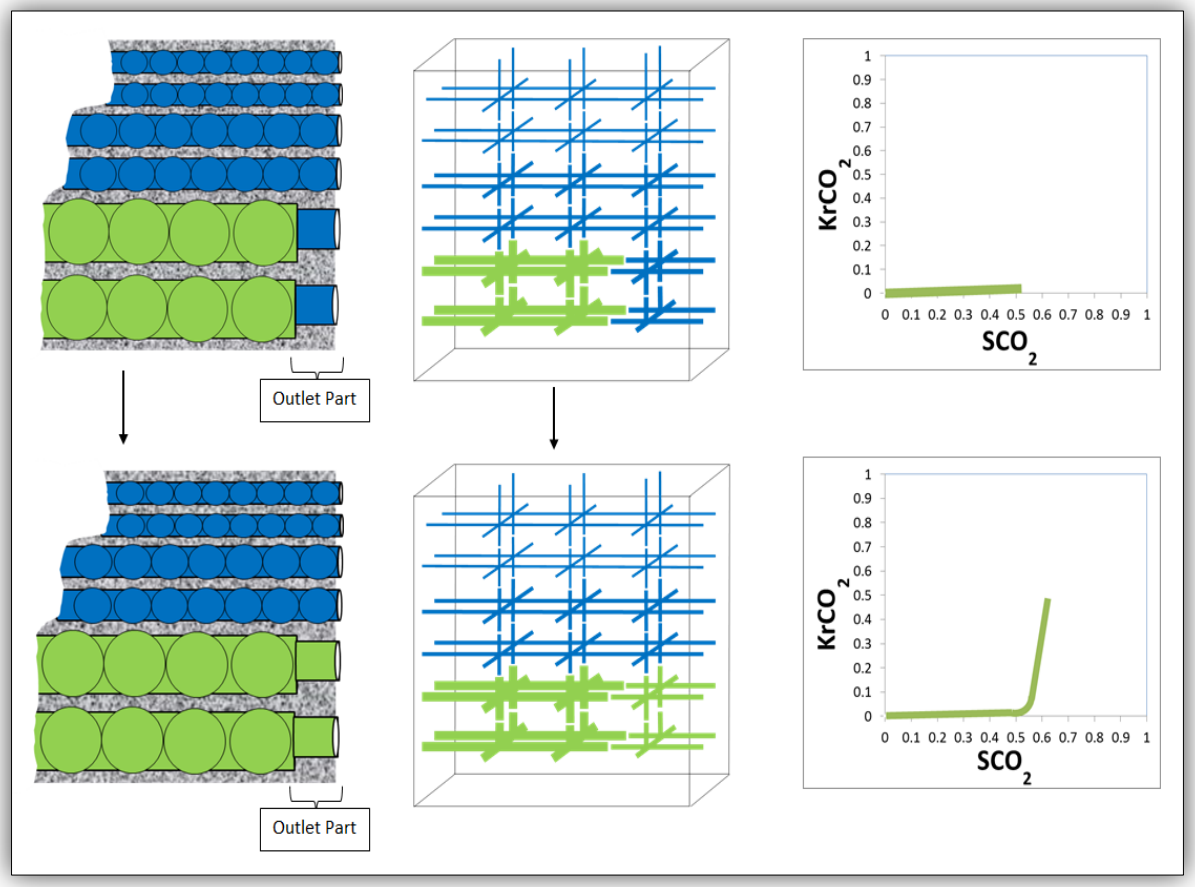

Figure 5.10: Case②, medium, small and very small throats only at the outlet, with invading only through the medium ones

The holdup of $KrCO_2$ data in Figure 5.10 is an indication of dissimilar connection. According to $KrCO_2$ and SCO_2 starting points, it could be that there are no large or very large throats at the outlet; what was there and actually invaded were throats with medium sizes. This size is applied to all invaded throats since the $KrCO_2$ curve shape is almost vertical. According to endpoint values, about a half percent of total pores and throats have been invaded.

Figure 5.11 is a special case of Case②. As there are few medium throats at the outlet (low quality of throat size), the endpoint of $KrCO_2$ is very low, which means that a very small number of throats have been invaded.

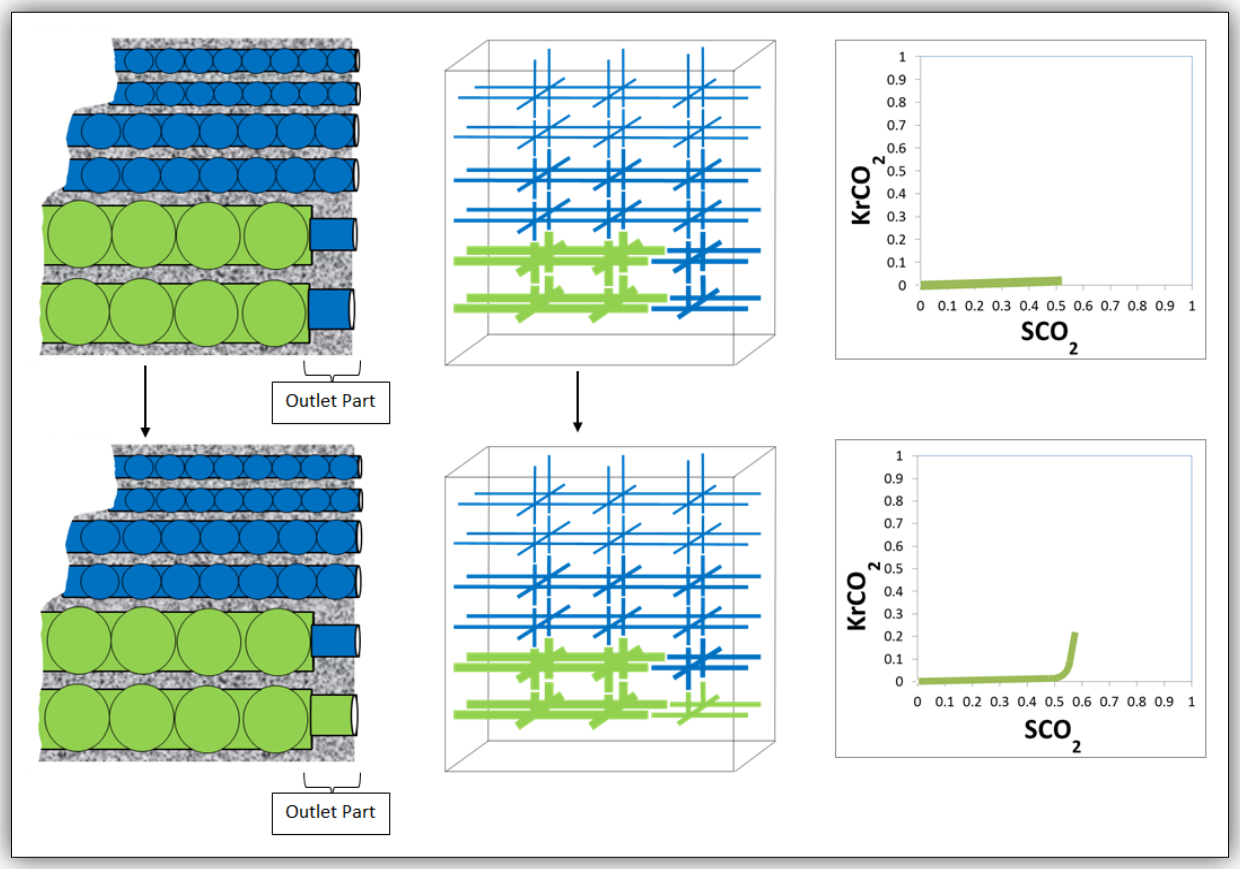

Figure 5.11: Case ② special state

C) Case③, only small and very small throats at the outlets, with invading merely through the small ones (Figure 5.12).

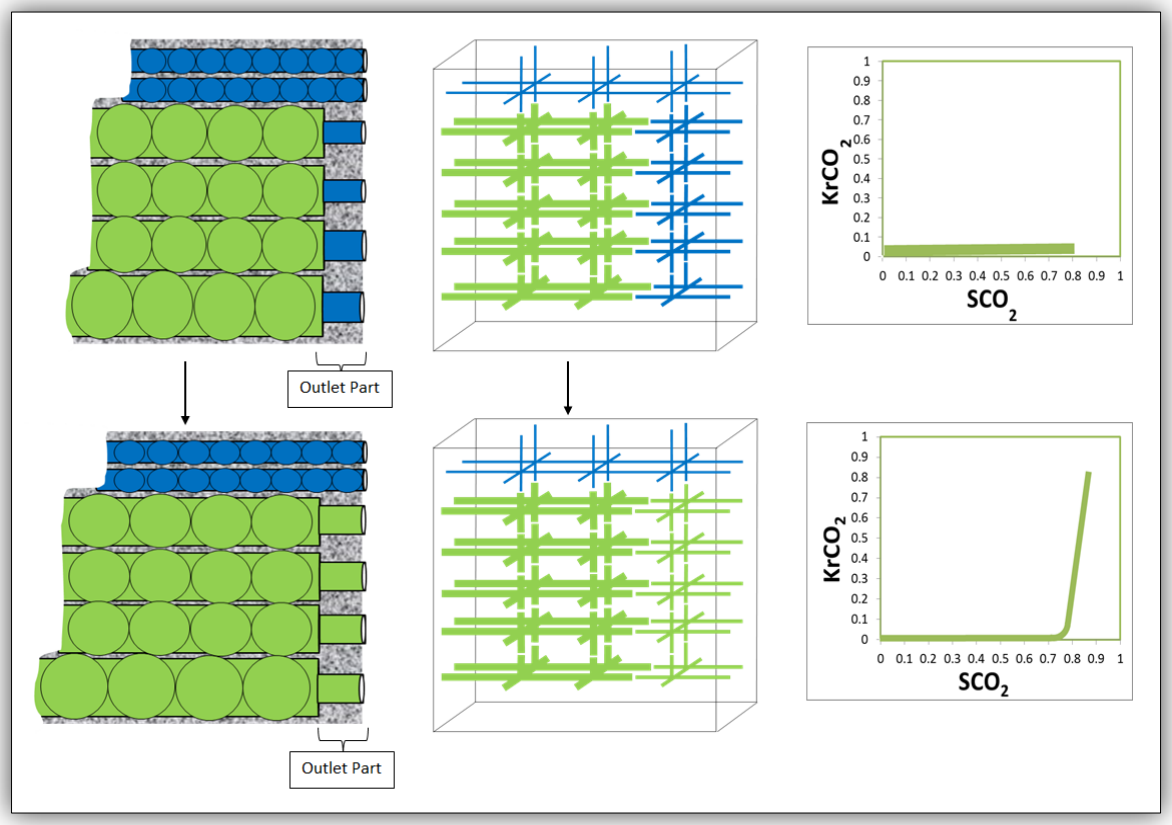

Figure 5.12: Case③, small and very small throats only at the outlets, with invading merely through the small ones

According to Figure 5.12, the delay in producing $KrCO_2$ data is clear (dissimilar connection). Based on CO_2 pressure (saturation) the invaded throats at outlet were small (with absence of large and medium throats) very similar in size as the $KrCO_2$ curve shape came out almost vertical. The major parts of total pores and throats were invaded.

Figure 5.13 is a special case of Figure 5.12. As there are few small throats (low quality of throat size), the endpoint of $KrCO_2$ is very low which means that a very small number of throats have been invaded at the outlet.

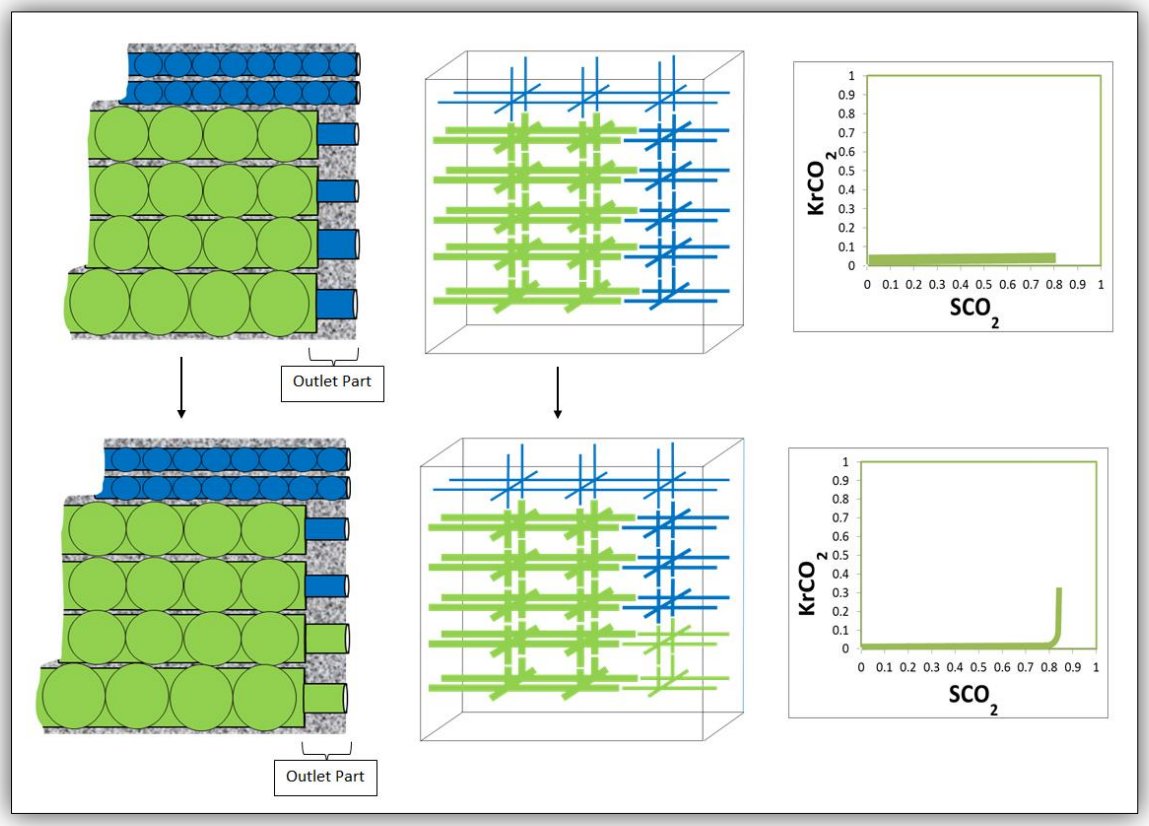

Figure 5.13: Case③ special state

D) Case ④, very small throats only at the outlets Figure 5.14

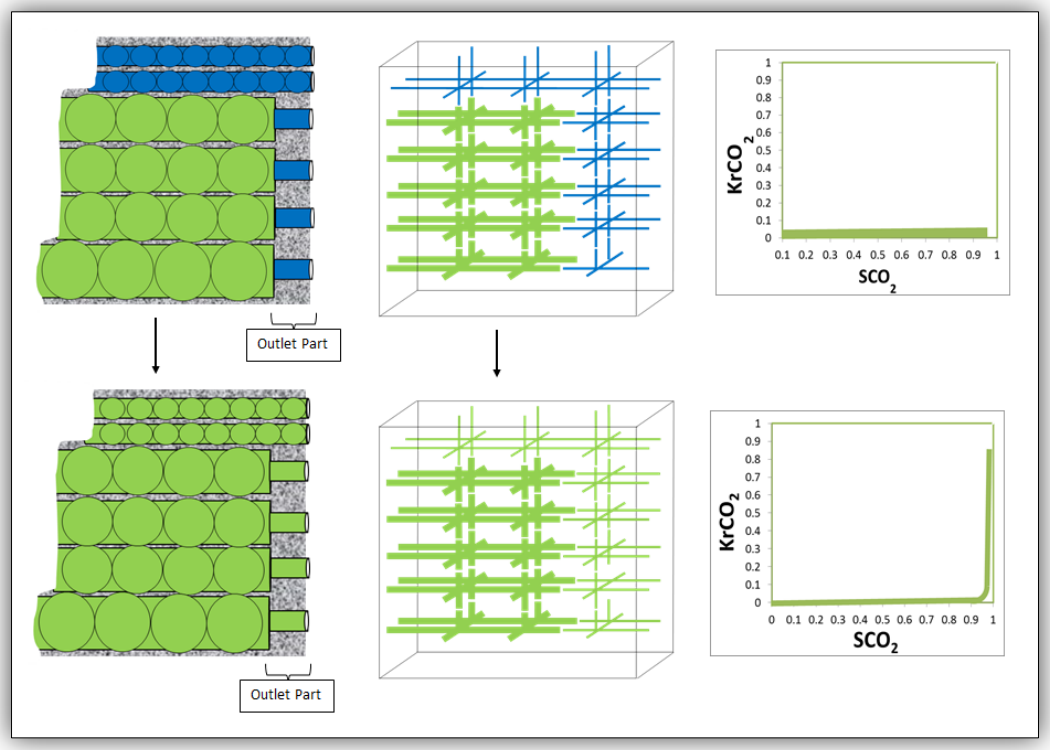

Figure 5.14: Case④, very small throats only at the outlets

Figure 5.14 illustrates that all invaded throats at the outlet were very small in size. This is confirmed by a very high saturation and vertical shape of the curve, and as a result, the $KrCO_2$ delayed much.

E) Case⑤, no very large throats at the outlet, with invading merely over the large and medium throats (Figure 5.15)

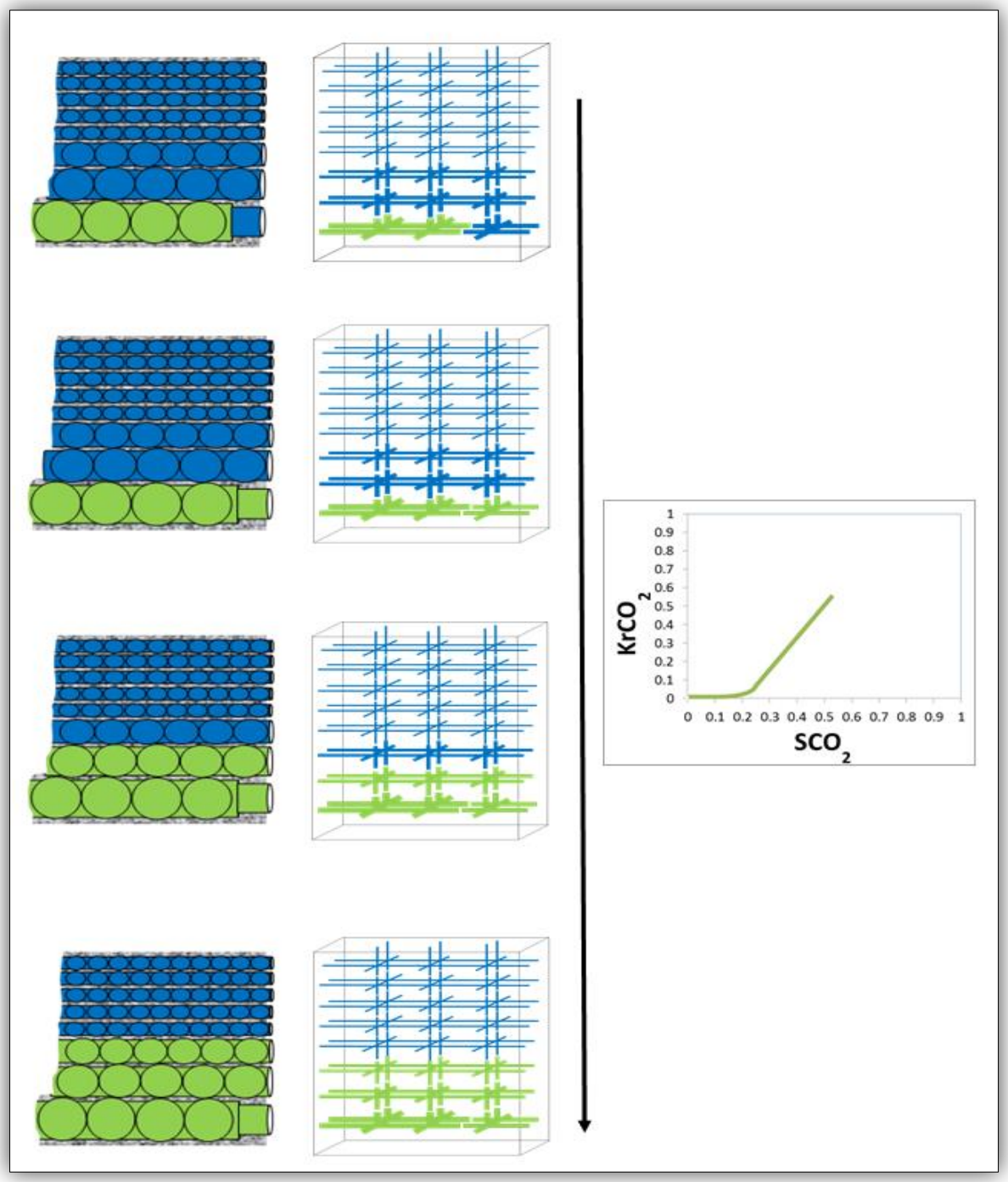

Figure 5.15: Case⑤, no very large throats at th e outlet, with invading merely over the large and medium throats

F) Case ⑥, no very large and large throats at the outlet, the invasion was merely through the medium and small throats (Figure 5.16)

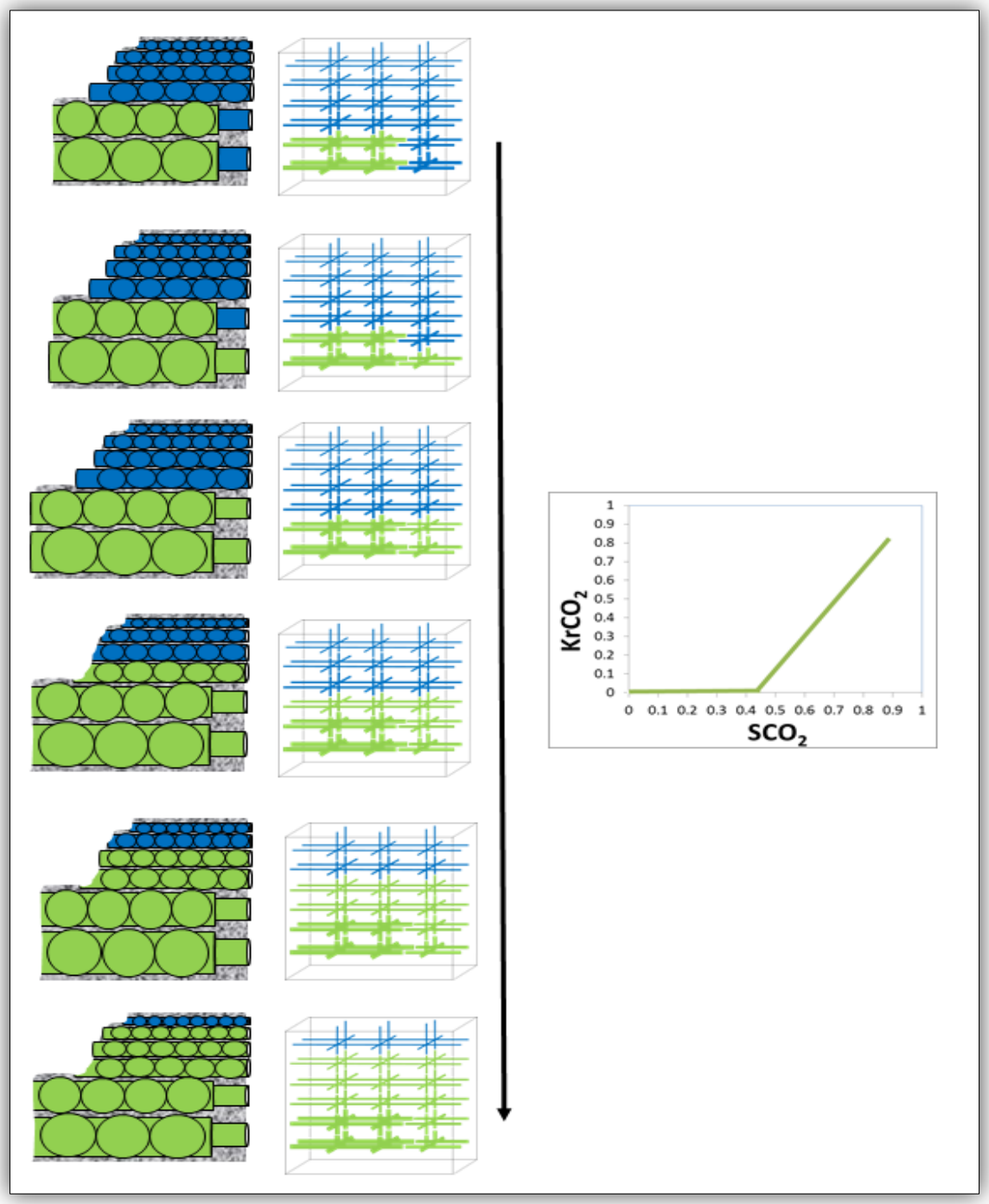

Figure 5.16: Case⑥, no very large and large throats at the outlet, the invading were merely through the medium small throats

In the next chapter, the concept of throat distribution as a main factor which impacts CO_2 relative permeability will be investigated.

References

HONARPOUR, M. M., KOEDERITZ, F. & HERBERT, A. 1986. *Relative permeability of petroleum reservoirs*.

SCIENCES, S. O. E. 2013. *Relative Permeability Explorer* [Online]. Stanfod university. Available: https://pangea.stanford.edu/research/bensonlab/relperm/index.html.

SURVEY, A. G. 2013. *Relative Permeability Data for Supercritical CO2 Displacing Water* [Online]. Alberta Geological Survey. Available: http://www.ags.gov.ab.ca/co2_h2s/wabamun/relative_permeability.html.

Chapter 6

Verification of the concept of throat distribution by using theoretical modelling (digital pores network + pore-scale fluid flow simulator)

6.1. Introduction

To verify the concept of throat distribution discussed in Chapter 5, the theoretical-Pore-scale modelling methodology is used. The reason for using this method instead of empirical or experimental model is due to the fact that there is no other way by which the impact of all parameters on $KrCO_2$, except the internal core structure, could be fixed, and as well to avoid the side effects of the interactions[5] (among the CO_2, brine and rock contents) on CO_2 relative permeability. Also, the lower cost and faster processing are advantages of applying theoretical modelling. In the next section, a concept of the theoretical-Pore-scale model in regard to its components will be provided.

6.2. Theoretical-Pore-scale model

Generally, the theoretical-pore-scale model usually consists of digital pore-network and pore-scale fluid flow simulator (Figure 6.1). Here is an explanation for each one of these two parts:

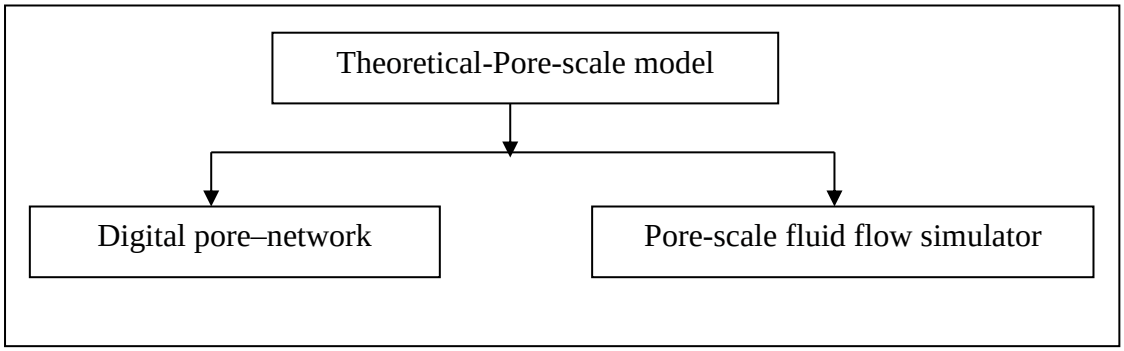

Figure 6.1: Theoretical-pore-scale model components

6.2.1. **Digital pore–network**

The pore-networks are commonly extracted from 3D digital images of porous media. There are three methods to obtain the 3D digital image of pore space:

A) Computed tomography (CT-Scan) imaging of core samples.

In this approach, the 3D digital rock is obtained by using computed micro-X-Ray computerized tomography (Figure 6.2). The micro-CT scan shows differences in the

[5] These interactions may impact everything, from the internal structure of the core up to all capillary properties, like wettability, IFT and viscosity ... etc. This has a considerable effect on $KrCO_2$.

density (attenuation) in the rock, like bone versus soft tissue in traditional medical X-rays (Rassenfoss, 2011, Baldwin et al., 1996, Jiang et al., 2007).

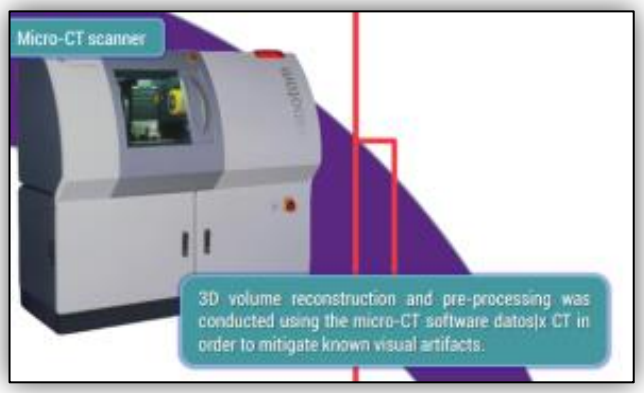

Figure 6.2: Computed tomography (CT)

B) Using 2D thin sections to reconstruct the 3D digital rock.

According to Okabe and Blunt (2004), Wu et al. (2006), and Jiang et al. (2007), this approach requires 2D thin section images which can be obtained, for example, by Scanning Electronic Microscope (SEM) and then using common 3D pore space reconstruction methods (Figure 6.3). This technique is widely done in two ways:

B.1) Process-based algorithms

B.2) Statistical methods

Many reconstruction approaches are applied as statistical methods, for instance, the multiple-point method (Okabe and Blunt, 2004) cited in (Dong and Blunt, 2009), and the five-point stencil method using a Markov chain Monte Carlo model, which reproduces typical patterns of the void space seen in 2D and consequently preserves the long-range connectivity (Dong and Blunt, 2009).

C) The rock image simulation

This method is summarized in simulating the packing of grains followed by the geological processes such as sedimentation, compaction, and digenesis by which sedimentary structures were formed (Dong and Blunt, 2009, Jiang et al., 2007, Øren and Bakke, 2002).

Once the 3D digital rocks are obtained, different types of algorithms can be used to extract pore-networks which are topologically and geometrically equivalent (Figure 6.3). The examples of these algorithms are presented below:

A) Medial axis based algorithm

The pore space topology is mathematically preserved by the medial axis. However, it is difficult to identify pores clearly. Clean-up processes need to be performed to remove trifling details on the skeleton due to the intrinsic sensitivity of the algorithm to noise in digitalized images (Dong and Blunt, 2009).

B) Maximum ball based algorithm

According to Dong and Blunt (2009), the maximal ball algorithm finds the largest inscribed spheres centered on each voxel of the image that just touch the grain or the boundary. Then, those included in other spheres are viewed as inclusions and removed; the rest are called maximal balls and describe the pore space without redundancy. Locally, the pores are identified by largest maximal balls while the smallest balls between pores are throats.

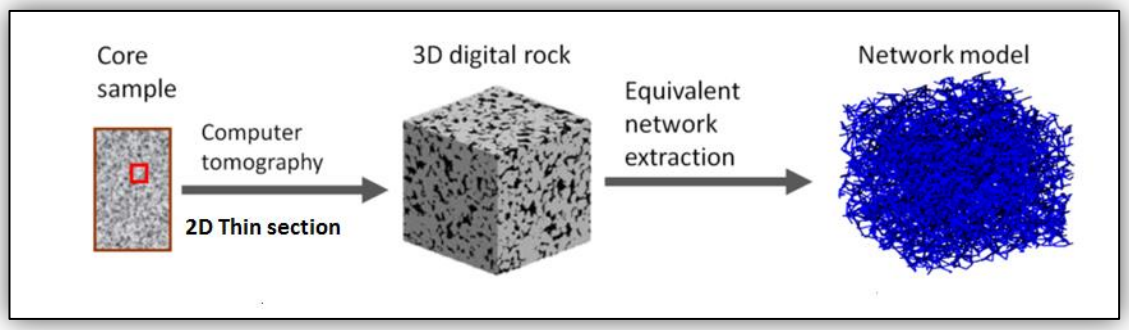

Figure 6.3: Steps of pore-network extraction

6.2.2. **Pore-scale fluid flow simulator**

Many Pore–scale fluid flow simulators are available in petroleum literature, one of which was designed by Heriot-Watt University (GUI version) and applied in this chapter (Figure 6.4 and Figure 6.5); other one was made by the Imperial College London (Dos version) and used in chapter 8.

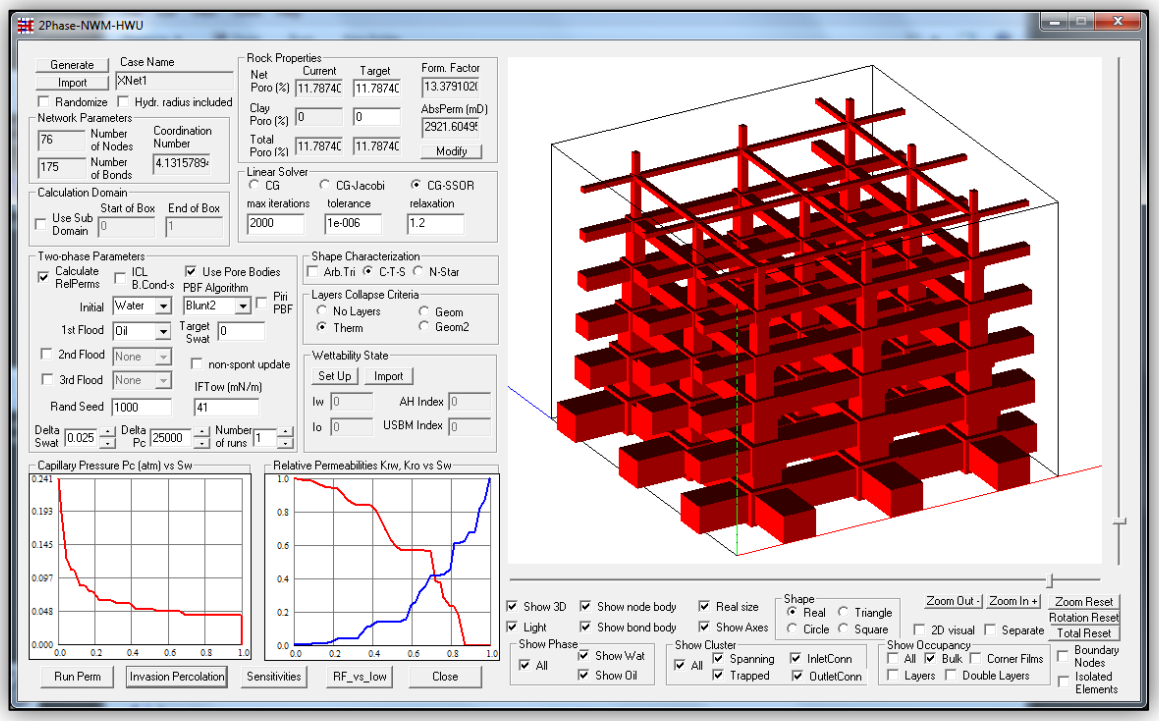

Figure 6.4: Heriot-Watt University's Pore–scale fluid flow simulator (Visual version) (Al-Dhahli, 2013, Ryazanov, 2011)

Here is a summary of theoretical pore-network model preparation steps.

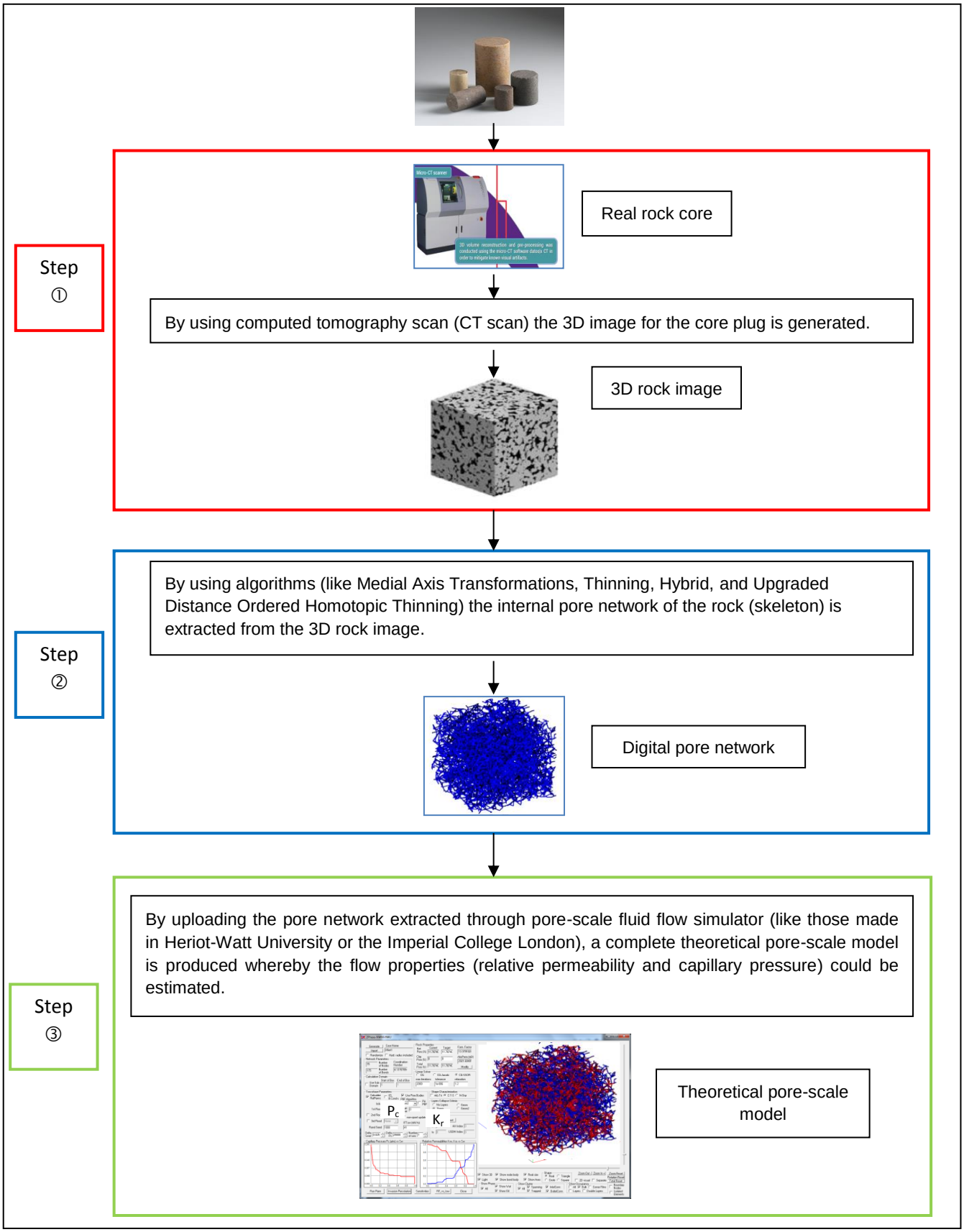

Figure 6.5: Summary of theoretical pore-scale model preparation steps

6.2.3. **Work done using theoretical Pore –scale model**

The author designed four digital pore-networks and loaded them into the pore-scale fluid flow simulator (designed by Heriot-Watt) to produce four different-structure pore-network models these represent different cases for core internal pore structure, and the results as following:

Model 1: It represents the case of normal pore size distribution and normal throat size distributions with a similar pore-throat connection (Figure 6.6).

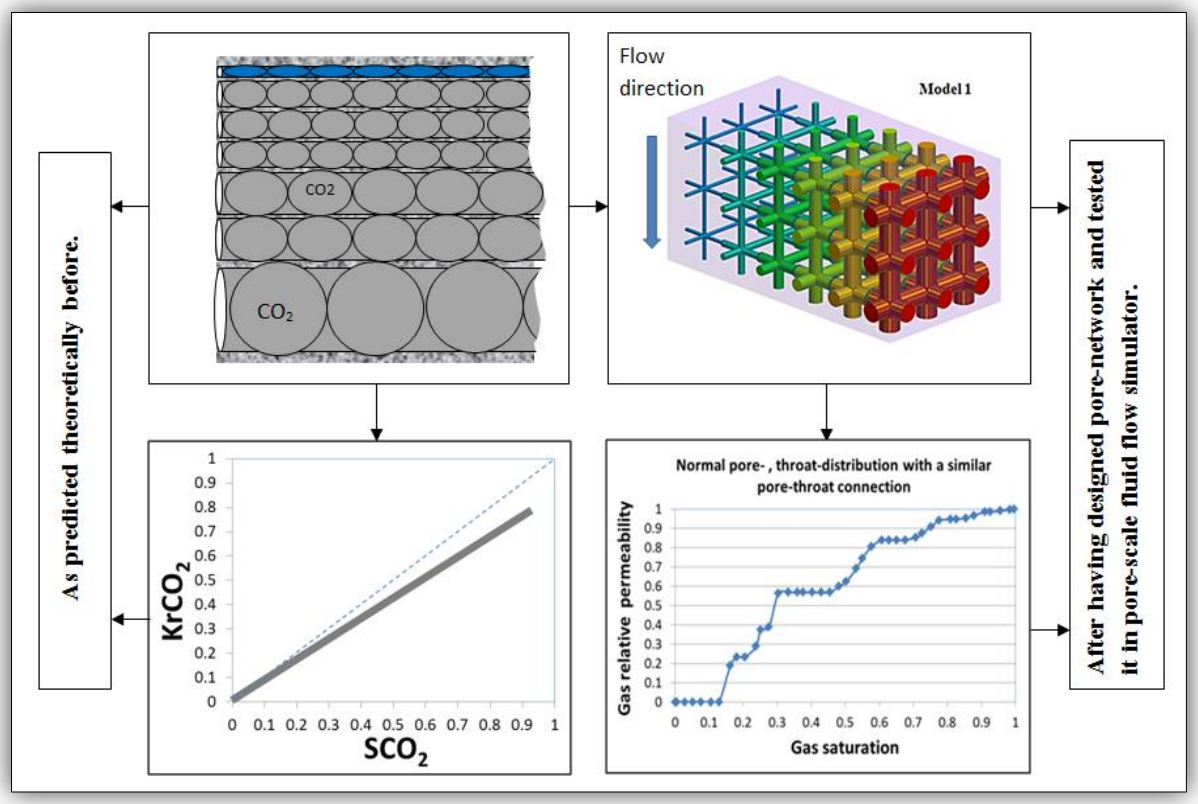

Figure 6.6: Pore network model represents the case of normal pore size distribution and normal throat size distributions with a similar pore-throat connection.

Model 2: It represents the case of abnormal pore and throat size distributions with dissimilar pore-throat connections (Case③), (Figure 6.7)

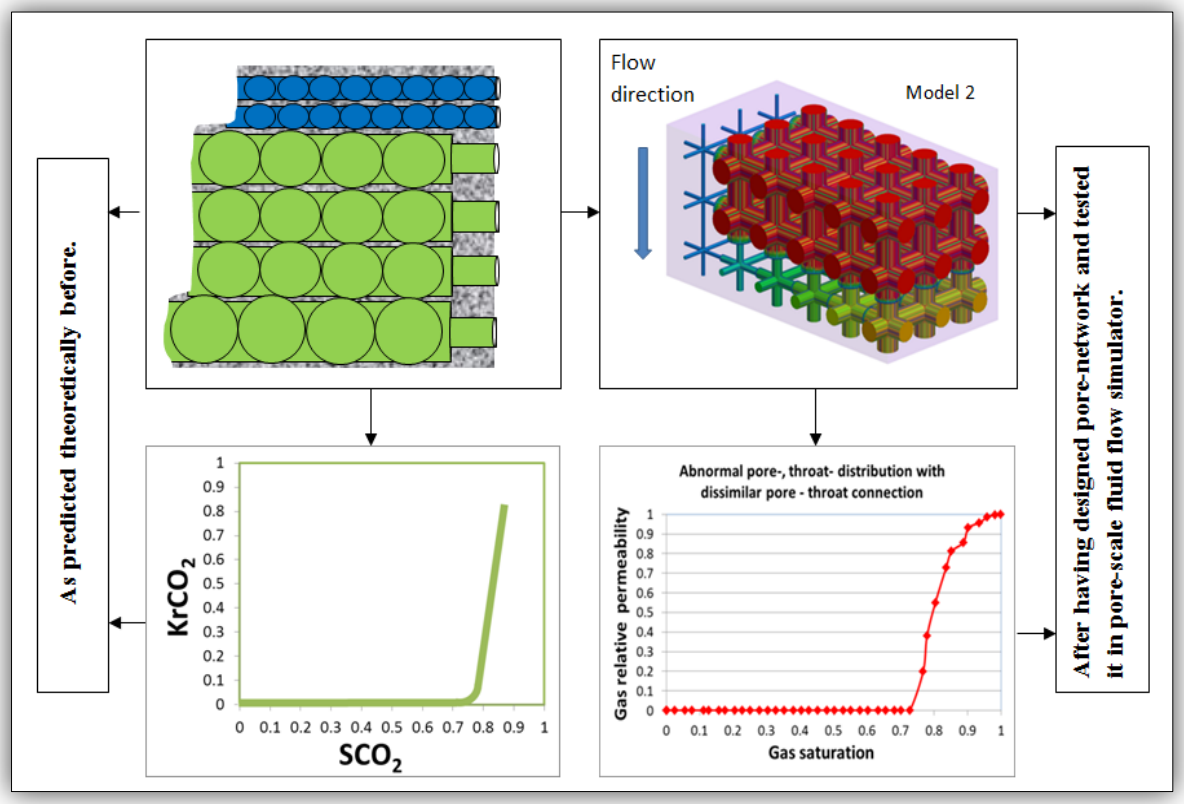

Figure 6.7: Pore network model corresponding to (Case③)

Model 3: It represents the case of abnormal pore and throat size distributions with dissimilar pore-throat connections (Case⑥), (Figure 6.8).

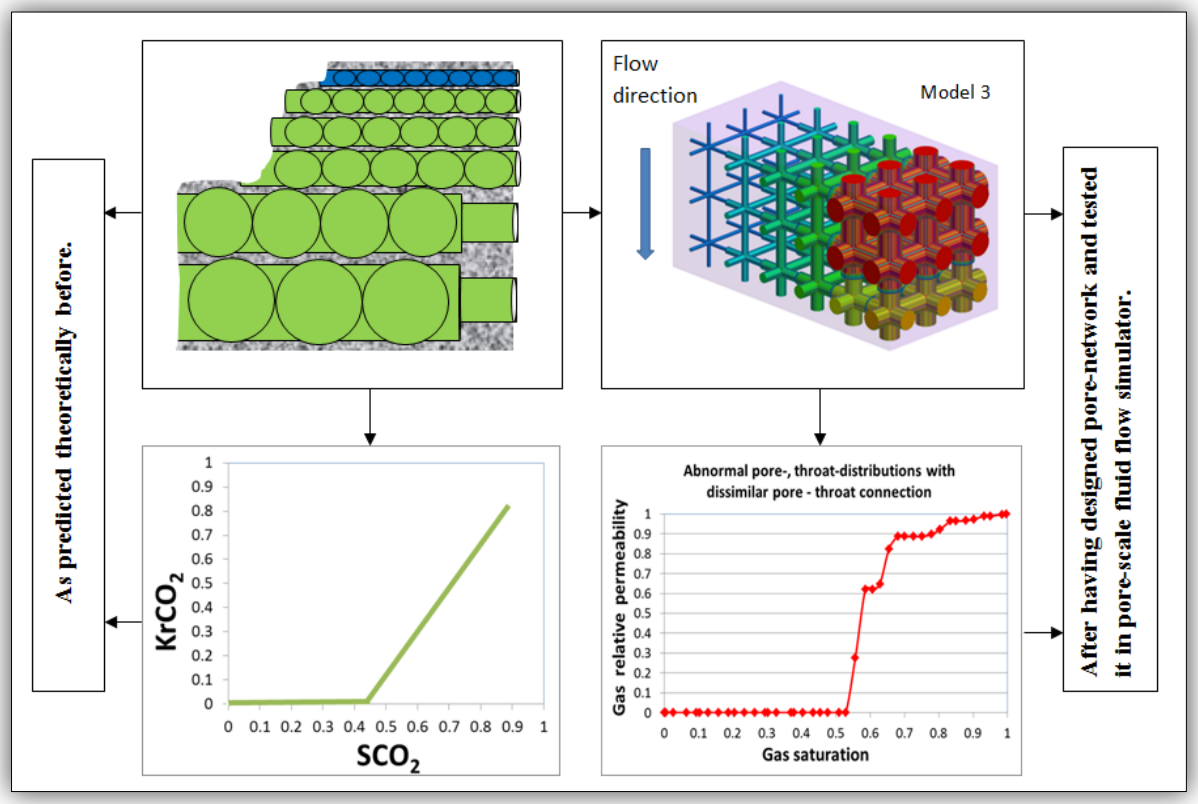

Figure 6.8: Pore network model corresponding to (Case⑥)

Model 4: It represents the case of abnormal pore and throat size distributions with dissimilar pore-throat connections (Case④), (Figure 6.9).

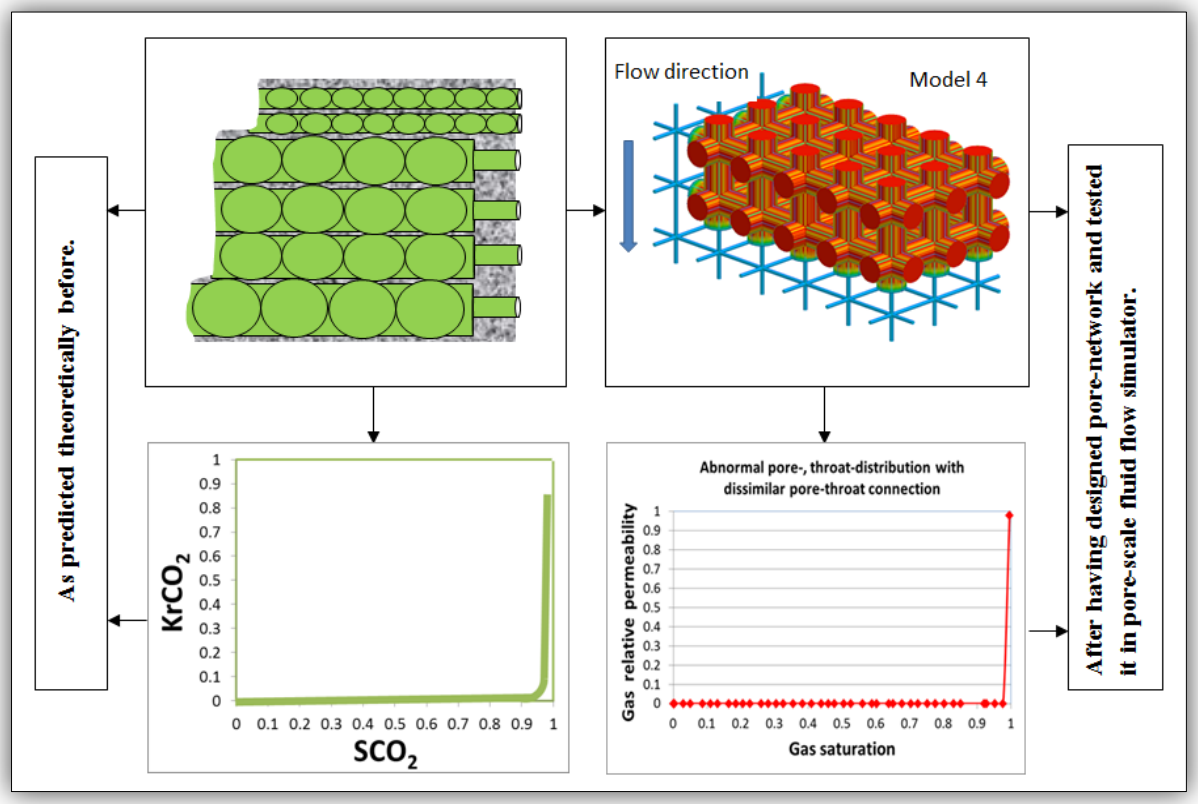

Figure 6.9: Pore network model corresponding to (Case④)

6.3. Applying the concept of throat distribution to CO_2 relative permeability Data in Appendix (A).

6.3.1. Sandstone formations

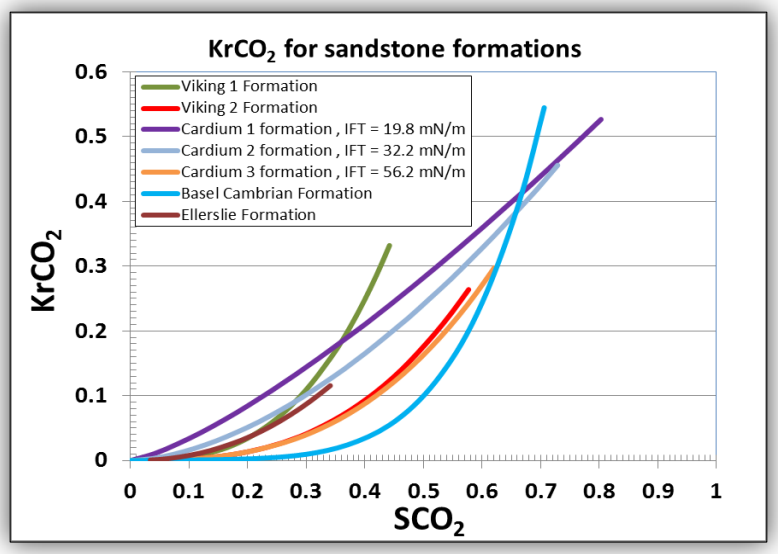

Figure 6.10: $KrCO_2$ (Drainage) for sandstone formations (Bennion and Bachu, 2005, Bennion and Bachu, 2006b, Bennion and Bachu, 2006c)

From Figure 6.11, extracted from Figure 6.10, the formation illustrates normal pore-throat distributions. The difference in curvature is due to the impact of IFT on $KrCO_2$ over drainage in a single formation (Cardium sandstone formation). All other factors affecting CO_2 relative permeability (apart from IFT and saturation history) are fixed because a single formation had been applied in this experiment, with the result that, as the IFT increases the increasing rate of CO_2 relative permeability declines to produce smaller CO_2 relative permeability value at the same CO_2 saturation point. This negative impact of interfacial tension on CO_2 relative permeability is due to the fact that, the interfacial tension produces resistance to displace the brine by CO_2, and as the interfacial tension becomes stronger, the CO_2 loses its mobility dramatically owing to increasing resistance. It is important to note that with raising the IFT, the endpoint relative permeability declines.

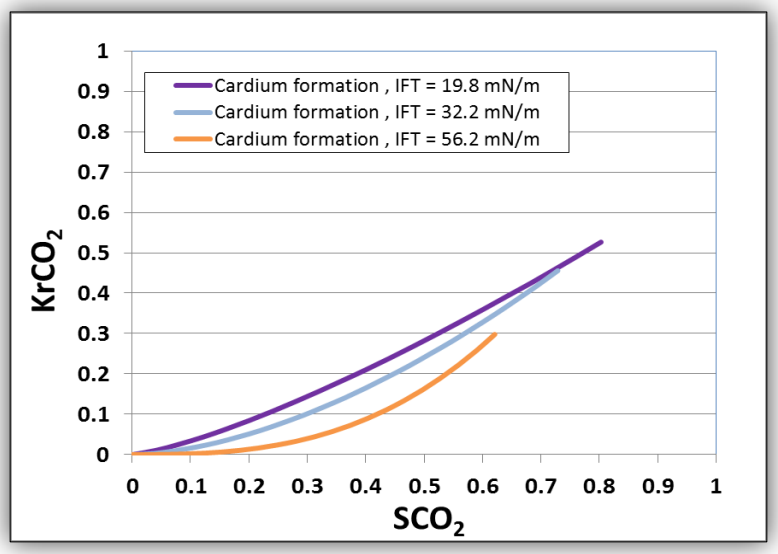

Figure 6.11: Effect of IFT on $KrCO_2$ during drainage for one formation (Cardium sand stone) (Bennion and Bachu, 2006c)

According to Figure 6.12, extracted from Figure 6.10, the Basel Cambrian and Viking 1 formations introduced abnormal throat size distribution, since the CO_2 relative permeability lines are near to vertical, but it is clearer in Basel Cambrian formation than in Viking 1 formation.

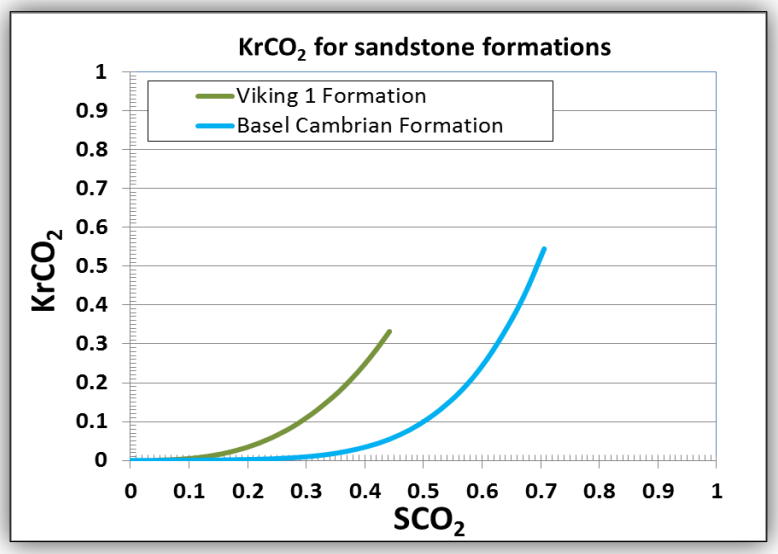

Figure 6.12: Abnormal throat size distribution in Basel Cambrian and Viking 1 formations (Bennion and Bachu, 2005)

According to Figure 6.13, extracted from Figure 6.10, both formations, Viking 2 and Ellerslie, introduced normal pore–throat distributions. The early stopping of CO_2 relative permeability data in Ellerslie formation may be due to insufficient CO_2 pressure, whereas the interference effect is clear in both formations.

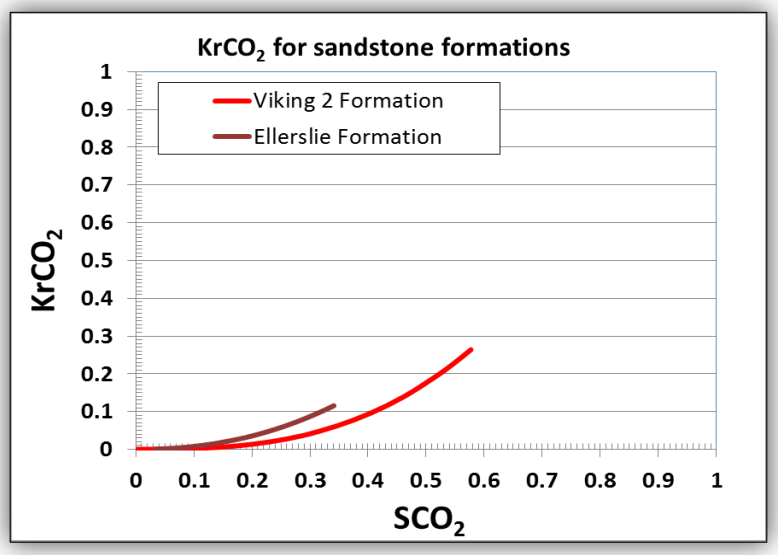

Figure 6.13: Normal throat size distribution in Viking 2 and Ellerslie formations (Bennion and Bachu, 2005, Bennion and Bachu, 2006b)

6.3.2. **Limestone formations**

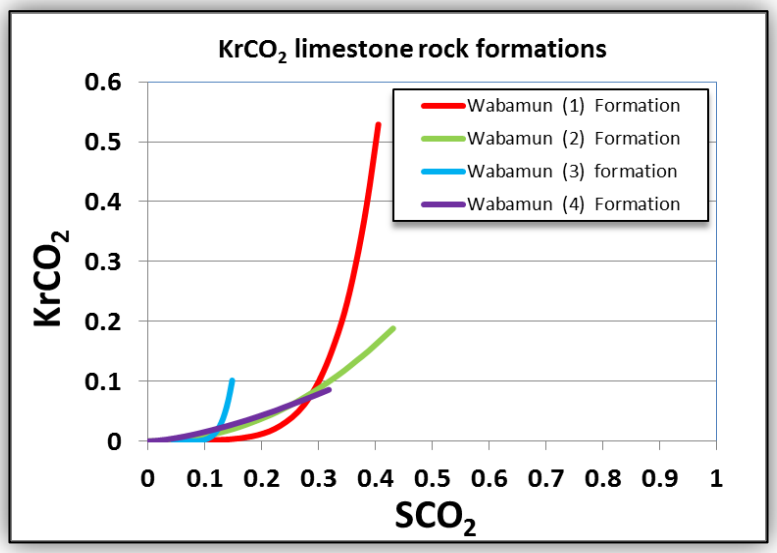

Figure 6.14: $KrCO_2$ (Drainage) for Limestone formations (Bennion and Bachu, 2010, Sciences, 2013)

As Figure 6.15, extracted from Figure 6.14, shows the two formations have normal pore-throat distributions, and due to low CO_2 pressure high interfacial tension the CO_2 relative permeability data stopped early in both formations. Furthermore, a slight effect of interference appeared in Vabamun (2) formation.

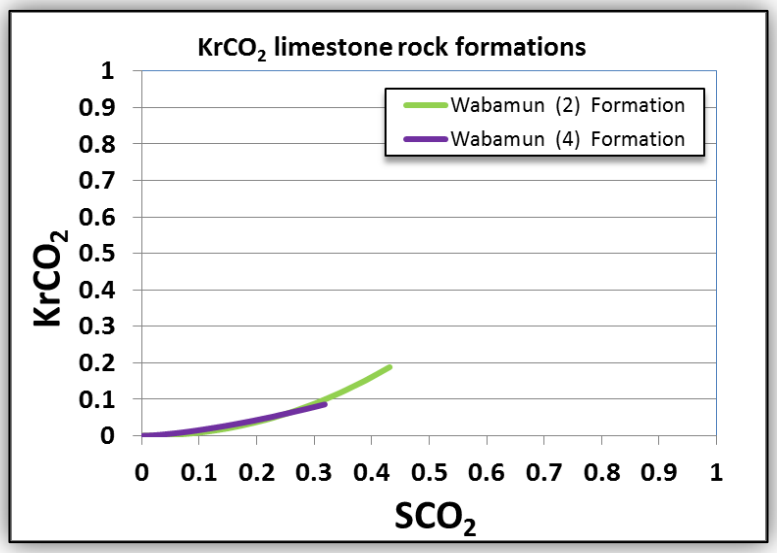

Figure 6.15: Normal throat size distribution in Vabamun (2 & 4) formations (Sciences, 2013)

According to Figure 6.16, extracted from Figure 6.14, both formations introduced abnormal pore-throat size distributions, since the CO_2 relative permeability lines are near to vertical.

Since only a small part of the total pores and throats had been invaded by CO_2 in Vabanum (3) formation, the CO_2 relative permeability is expected to be very low.

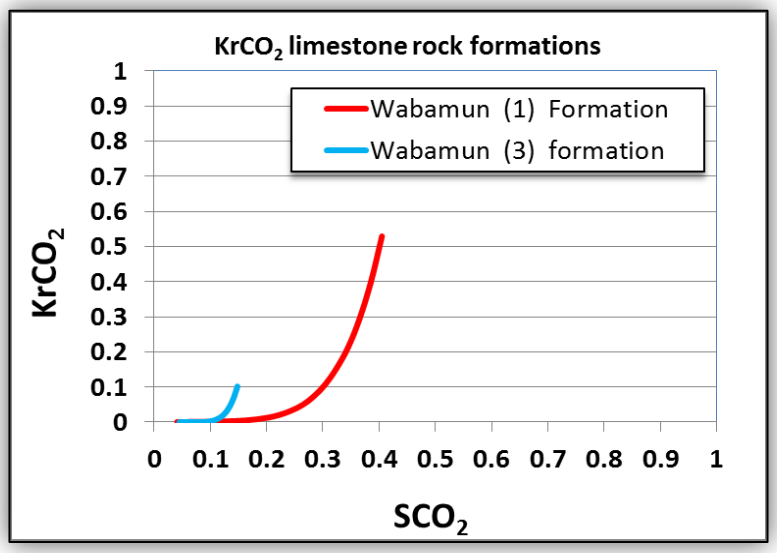

Figure 6.16: Abnormal throat size distribution in Vabanum (1, 3) formations (Bennion and Bachu, 2010, Sciences, 2013)

6.3.3. **Dolomite formations**

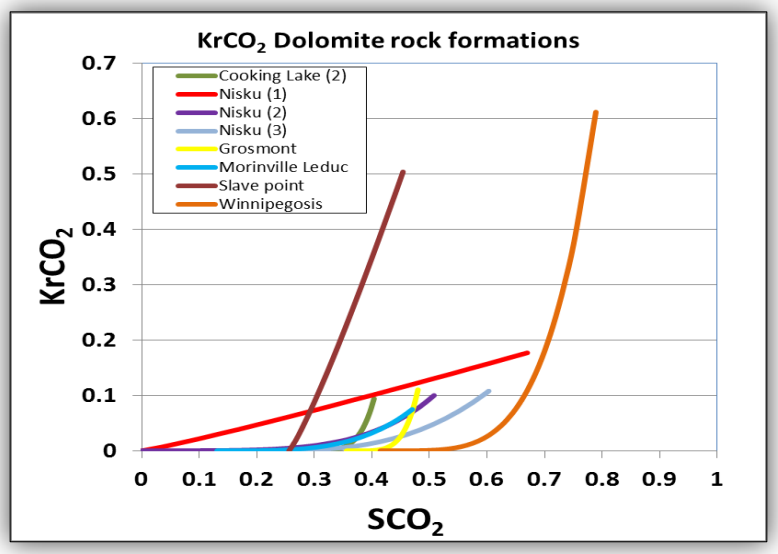

Figure 6.17: $KrCO_2$ (Drainage) for Dolomite formations (Bennion and Bachu, 2010, Survey, 2013)

Figure 6.18, extracted from Figure 6.17, illustrates that all formations showed abnormal pore-throat distributions. In addition, there are indications that the throat distribution quality through vertical direction to flow is much better than that in flow direction (horizontal) in formations Grosmont, Cooking Lake (2), as the endpoint of SCO_2 does not go with the endpoint of $KrCO_2$.

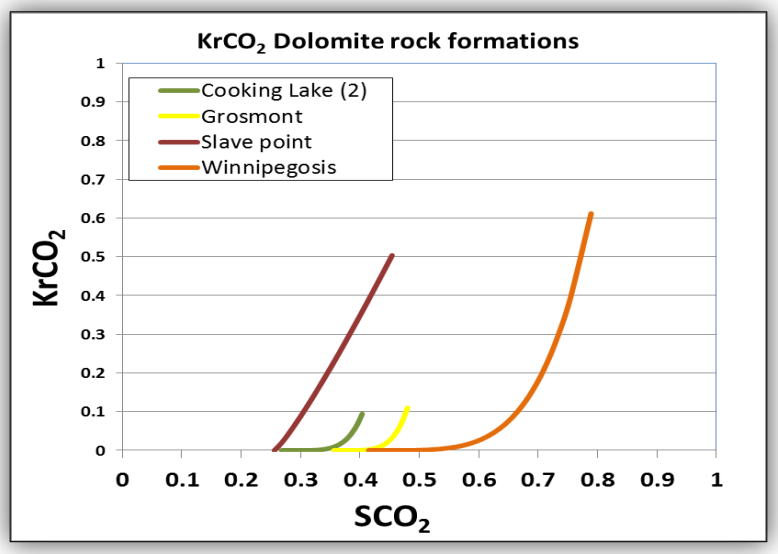

Figure 6.18: $KrCO_2$ (Drainage) for Dolomite formations (Bennion and Bachu, 2010)

Figure 6.19, extracted from Figure 6.17, shows that although the CO_2 relative permeability lines illustrated that there are normal Pore–throat distributions in all formations, the effect of very high interfacial tension is clear in all formations.

Except Nisku (1) formation, the interference effect is clear in all formations and appears obviously in line curvature.

In addition, there are indications that the throat size quality in the perpendicular direction (vertical) is much better than that in flow direction (horizontal) in all formations since the endpoint of SCO_2 does not go with the endpoint of $KrCO_2$.

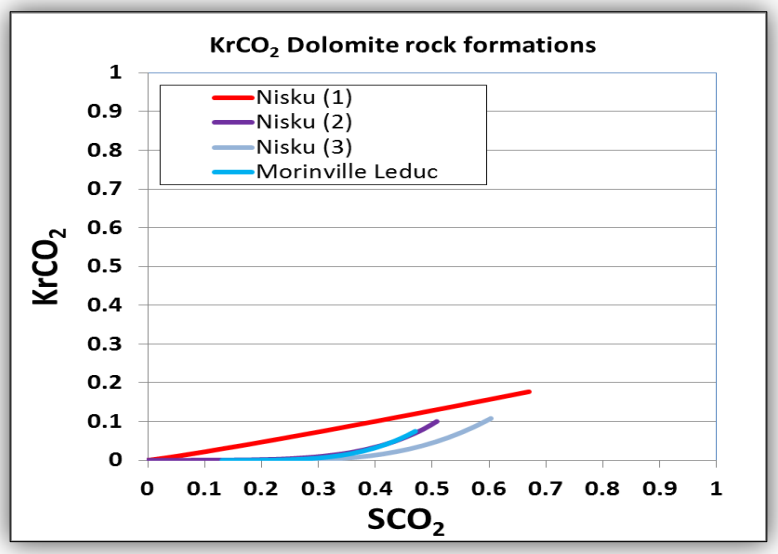

Figure 6.19: $KrCO_2$ (Drainage) for Dolomite formations (Bennion and Bachu, 2010, Survey, 2013)

6.4. Summary of the results

According to the information above, the pore and throat distributions concept has a decisive impact on the CO_2 relative permeability, and consequently, a disparity in CO_2 relative permeability curves is to be expected in even a set of formations with the same rock type or in samples extracted from a single formation, and even in case of developing the same other capillary properties as well.

References

AL-DHAHLI, A. 2013. *PORE TO F I E LD SCALE MODE L L ING OF THRE E PHASE FLOW PROCE SSES IN HET EROGENEOUS RES ERVOIRS WITH ARB ITRARY WE TTAB I L I TY.*, Heriot-Watt.

BALDWIN, C. A., SEDERMAN, A. J., MANTLE, M. D., ALEXANDER, P. & GLADDEN, L. F. 1996. Determination and characterization of the structure of a pore space from 3D volume images. *Journal of Colloid and Interface Science,* 181**,** 79-92.

BENNION, B. & BACHU, S. 2005. Relative Permeability Characteristics for Supercritical CO2 Displacing Water in a Variety of Potential Sequestration Zones in the Western Canada Sedimentary Basin. *SPE Annual Technical Conference and Exhibition.* Dallas, Texas: Society of Petroleum Engineers.

BENNION, D. B. & BACHU, S. 2006b. Supercritical CO2 and H2S—Brine Drainage and Imbibition Relative Permeability Relationships for Intergranular Sandstone and Carbonate Formations. *SPE Europec/EAGE Annual Conference and Exhibition.* Vienna, Austria: Society of Petroleum Engineers.

BENNION, D. B. & BACHU, S. 2006c. Dependence on Temperature, Pressure, and Salinity of the IFT and Relative Permeability Displacement Characteristics of CO2 Injected in Deep Saline Aquifers. *SPE Annual Technical Conference and Exhibition.* San Antonio, Texas, USA: Society of Petroleum Engineers.

BENNION, D. B. & BACHU, S. 2010. Drainage and Imbibition CO2/Brine Relative Permeability Curves at Reservoir Conditions for High-Permeability Carbonate Rocks. *SPE Annual Technical Conference and Exhibition.* Florence, Italy: Society of Petroleum Engineers.

DONG, H. & BLUNT, M. J. 2009. Pore-network extraction from micro-computerized-tomography images. *Physical review E,* 80**,** 036307.

JIANG, Z., WU, K., COUPLES, G., VAN DIJKE, M. I. J., SORBIE, K. S. & MA, J. 2007. Efficient extraction of networks from three-dimensional porous media. *Water Resources Research,* 43**,** W12S03.

OKABE, H. & BLUNT, M. 2004. Prediction of permeability for porous media reconstructed using multiple-point statistics. *Physical Review E,* 70.

ØREN, P.-E. & BAKKE, S. 2002. Process based reconstruction of sandstones and prediction of transport properties. *Transport in Porous Media,* 46**,** 311-343.

RASSENFOSS, S. 2011. Digital rocks out to become a core technology. *J Petrol Technol May***,** 36-41.

RYAZANOV, A. 2011. *Pore-Scale Network Modelling of Residual Oil Saturation in Mixed-Wet Systems.*, Heriot - Watt university.

SCIENCES, S. O. E. 2013. *Relative Permeability Explorer* [Online]. Stanfod university. Available: https://pangea.stanford.edu/research/bensonlab/relperm/index.html.

SURVEY, A. G. 2013. *Relative Permeability Data for Supercritical CO2 Displacing Water* [Online]. Alberta Geological Survey. Available: http://www.ags.gov.ab.ca/co2_h2s/wabamun/relative_permeability.html.

WU, K., VAN DIJKE, M. I., COUPLES, G. D., JIANG, Z., MA, J., SORBIE, K. S., CRAWFORD, J., YOUNG, I. & ZHANG, X. 2006. 3D stochastic modelling of heterogeneous porous media–applications to reservoir rocks. *Transport in Porous Media,* 65**,** 443-467.

Chapter 7

The impact of throat size distribution on CO_2 injection rate through brine aquifer formation (field scale).

7.1. Introduction

CO_2 injection in geologic formations (hydrocarbon reservoirs as well as aquifers) is increasingly considered as a method for increasing oil recovery and at the same time storing CO_2 in these formations to reduce the CO_2 emissions which are thought to be the main cause responsible for global warming or the greenhouse phenomenon.

As it is known, the CO_2 injection rate into geologic formations (either for EOR or storage process) is a main parameter, in addition to injection pressure, which controls the injection process. Furthermore, it is admissible that to minimize the injecting cost, the total injection time or the number of injecting wells or both of which should be minimum; this target could be achieved by increasing the injection rate.

Going further, if a certain amount of CO_2 is required to be injected, by increasing the injection rate the following issues could be logically expected:

- A fewer number of wells will be enough (to inject the same amount of CO_2 through the same period of time).
- Or, the time required (to inject the same amount of CO_2 through the same number of wells) will be less.

Basically, the injection rate could be raised by increasing the injection pressure, but this is always restricted and is not allowed to exceed the value of caprock entry and fracturing pressure. This value is usually considered as the starting value of injection pressure, in order to get the maximum rate and reduce injection time to minimum. Consequently, looking for other factors (not injection pressure) that affect injection rate becomes necessary, and according to Darcy's law, there is an effect of CO_2 relative permeability on the injection rate by changing this factor the injection rate could be increased; consequently, the injection time and number of wells could be considerably reduced, and a decline in the cost will appear. And it is admissible that each formation has specific CO_2 relative permeability data, and by changing the formation (where CO_2 will be injected) the ability of having variant options to CO_2 relative permeability (thus CO_2 injection rate) will be reachable. This will be very important particularly in the case of differentiating between two or more formations that have the same caprock entry and fracturing pressure since, in such a case, there is no opportunity to have variant options

to injection rate depending on injection pressure, while the potential to get a better injection rate depending on different CO_2 relative permeability data (coming from more than a single formation) will be high.

As mentioned earlier, the CO_2 relative permeability is a decisive parameter that controls the CO_2 injection rate. Mathias et al. (2013) also studied the impact of CO_2 relative permeability variance on injectivity estimations, (Burton et al., 2008) using data from Bennion and Bachu (2005) and found "a four-fold variation in injectivity when seven different CO_2-Brine permeability curves are used, holding all other reservoir [aquifer] parameters the same. Bennion and Bachu (2010) concluded that "quantifying the relative permeability curve is very important in determining achievable injection rate and therefore the well count for CO_2 geologic sequestration projects".

Darcy's law, of course, introduces the mathematical interpretation to the points mentioned, but what should not be overlooked here is that Darcy's law just introduces the CO_2 relative permeability as a single term which affects CO_2 injection rate and never goes beyond this term to parameters or factors that control the CO_2 relative permeability value and try to connect them with the CO_2 injection rate.

In this chapter, using simulation calculations and CO_2 relative permeability published and collected in the (appendix A), the author investigates the impact of the pore and throat distributions concept, which was mentioned and explained in chapter⑤, on one of the most common CO_2 injection parameters, i.e. the CO_2 injection rate.

7.2. Simulation work

A lot of packages in petroleum engineering are used to do reservoir numerical simulations. Some examples of these packages are Eclipse, STARS, GEM-GHG, TOUGH2. The Eclipse simulation package, which has been used in this study, in fact consists of two simulators: the Eclipse Black oil (E100) and Eclipse Compositional (E300). The Eclipse Black oil (E100) is fully implicit and is used for black oil simulation, whereas Eclipse Compositional (E300) is a simulator including a cubic equation of state and pressure-dependent permeability values in addition to Black oil calculations. There are some extra options which have been added to Eclipse Compositional (E300): these extra options are CO2STORE and GASWAT, CO2SOL (Class et al., 2009).

According to Class et al. (2009), the CO_2STORE option deals with issues relating to the solubility of CO_2 in water, and gives ability to compute the physical properties like viscosity density compressibility to both pure and impure CO_2 as a function of pressure and temperature. And what is important in terms of solubility is that the water dissolves into CO_2 and partitions it, and as result, the properties of CO_2 (density and viscosity) impacting its flow will change, which is similar to water, since CO_2 dissolves into water and partitions it causing change in water's density, viscosity and salinity. An additional important issue is that the mutual solubility calculations of CO_2 and water include a correction for salinity (Spycher and Pruess, 2005, Spycher et al., 2003) and its functionalities include describing dry-out and salt precipitation in addition to an incorporated speciation routine (Hurter et al., 2007).

The design of GASWAT option is to model gas phase/aqueous phase equilibrium by using a general Peng–Robinson equation of state, and compared with CO2STORE option, the GASWAT allows a multi-component gas phase which allows simulating CO_2 injection into depleted gas reservoirs. Another important issue is that GASWAT option always gives underestimated water solubility in CO_2 compared with the CO2STORE option.

The CO2SOL option was developed to model CO_2 enhanced oil recovery.

In this study, in order to investigate the effect of pore and throat distributions on CO_2 relative permeability and thus on CO_2 injection rate, an Eclipse 300 Model with CO2STORE option has been used. Eclipse 300 could be run in fully implicit (IMPES) or adaptive implicit (AIM) modes (Schlumberger, 2011). It tracks down chemical components in liquid and gas phases. As for CO2STORE option, this option calculates mutual solubility of H_2O and CO_2.

Since the model was used to study the effect of CO_2 relative permeability on injection and storage characteristics, some assumptions have been made as the following:

A) CO_2 is injected in supercritical phase.

B) The process throughout injection and after shut-in is isothermal.

C) Brine salinity is constant.

D) Dissolution of CO_2 in brine is assumed to be instantaneous.

E) Mineral trapping and solid precipitation are ignored (because they require a very long time).

F) Solid precipitation is neglected.

G) Boundary condition is used as closed tank.

Diffusion

Eclipse 300 uses two keywords (DIFFCGAS, DIFFCEAT) to calculate the normal diffusion coefficients (D_i). The calculation of these coefficients is done by using the following equation (Kiatsakulphan, 2009):

$$J_i = -c\, D_i \frac{\partial X_i}{\partial d} \qquad \text{Eq. 7.1}$$

Where:

J_i = molar flux of the component per unit area.

c = total molar concentration.

X_i = mole fraction of the component.

Di = Diffusion coefficient of the component.

$\frac{\partial}{\partial d}$ = the gradient in the direction of flow.

Fracture pressure gradient

To save the caprock condition, the injection pressure should be less than the caprock fracture pressure, which could be calculated by using fracture gradient equation as below (Kiatsakulphan, 2009):

$$P_f = \left[\frac{(P_o - P_p)\,\nu}{1-\nu}\right] + P_p \qquad \text{Eq. 7.2}$$

Where:

P_f = fracture gradient (kPa/m).

P_o = Overburden gradient (kPa/m).

P_p = Overburden gradient (kPa/m).

ν = Poisson's ratio.

Model specifications

A) Grid and Model dimensions:

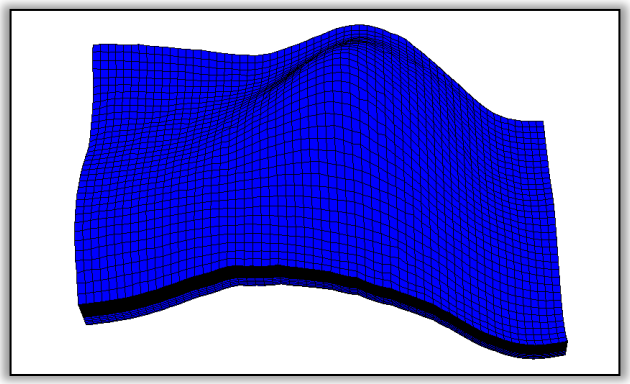

Figure 7.1: Grid and Model dimensions

NX = 110, ΔX = 400 meter

NY = 63, ΔY = 400 meter

NZ = 65, ΔZ = 0.345 – 21.19 meter

Total number of grids = 450,450 block

Model mean thickness = 7.69 meter for each layer.

First layer depth (TOPS) = 1211 meter.

B) Grid properties

Porosity = 0.158

PERMX = 233 mD

PERMY = 233 mD

PERMZ = 23.3 mD

Rock compressibility = 5.56×10^{-5}

C) Model temperatures

Depth (m)	^{o} C
500	26
1000	44
1500	62
2000	80

D) Number of injecting wells = 1

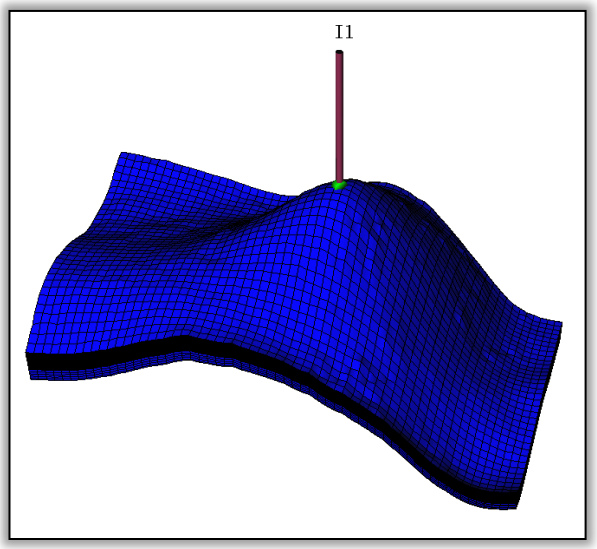

Figure 7.2: Number of injection wells

E) Perforation interval = 8 – 62 m

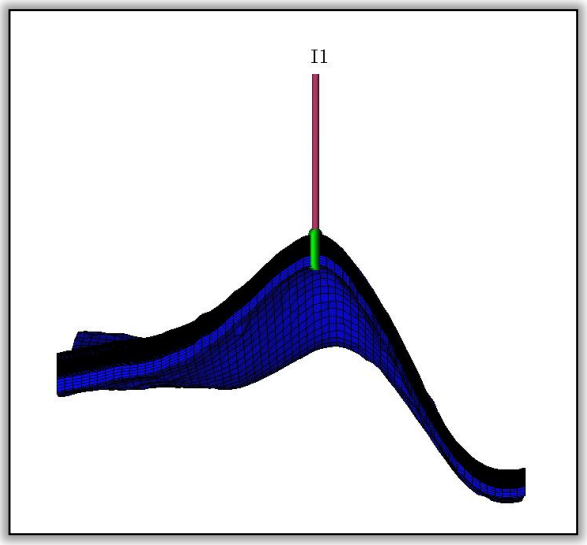

Figure 7.3: Perforation interval

F) Some of the Model outputs:

F.1) Average Field Pressure

F.2) Well bottom hole pressure of all wells

F.3) Field Average Gas Saturation

F.4) Field gas injection rate

F.5) Cumulative injected gas

F.6) Res Volume Injection Rate

F.7) Res Volume Injection Total

F.8) Field gas in-place [liquid and gas Phases]

F.9) Field gas in-place [liquid Phases]

F.10) Field gas in-place [GAS Phase]

F.11) CO_2 trapped (immobile) in gas phase

F.12) CO_2 ("carbon dioxide") mobile in gas phase

F.13) CO_2 dissolved in water phase

F.14) Well Gas injection rate for each well

F.15) Well Gas injection total for each well

G) General assumptions:

G.1) CO_2 is injected as the supercritical fluid phase to avoid two phase flow during injection in tubing.

G.2) Boundary condition is a closed tank.

H) Run Sample:

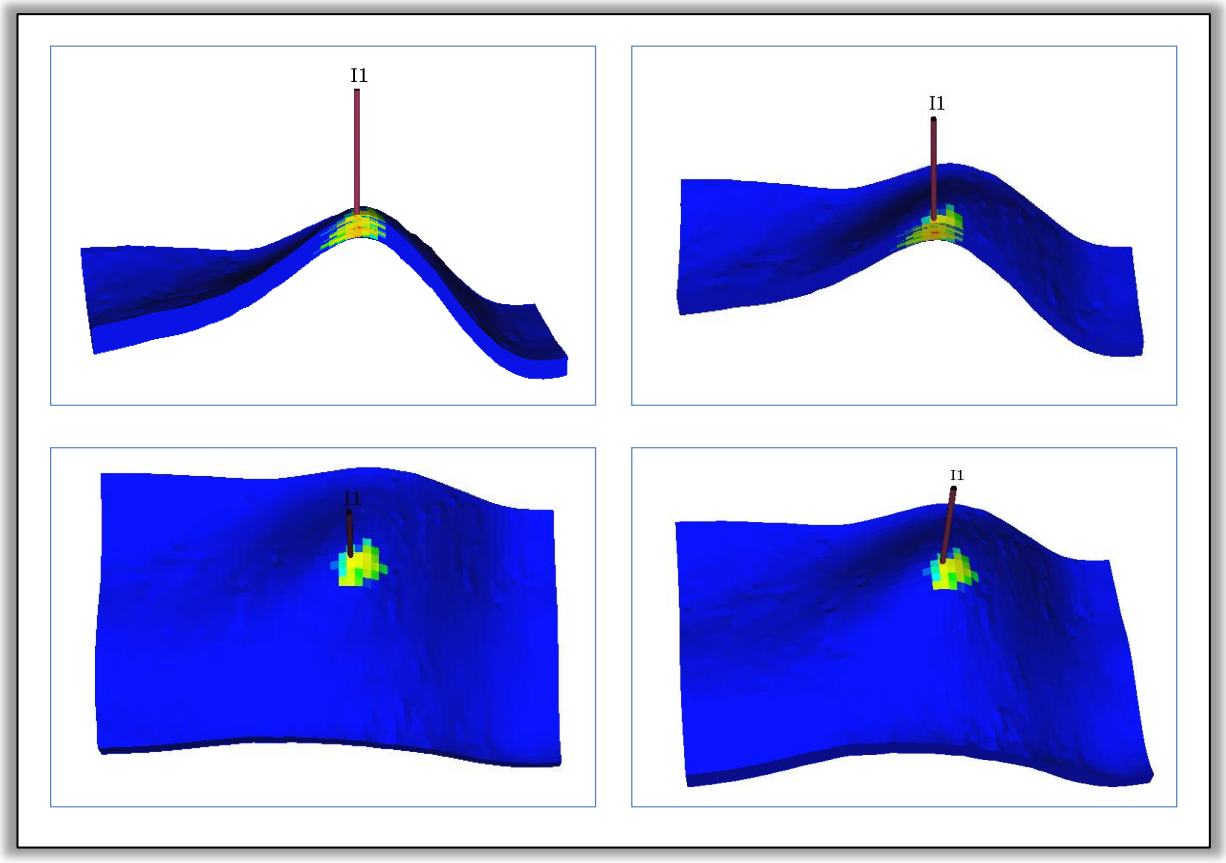

Figure 7.4: Eclipse model run sample

7.3. Results

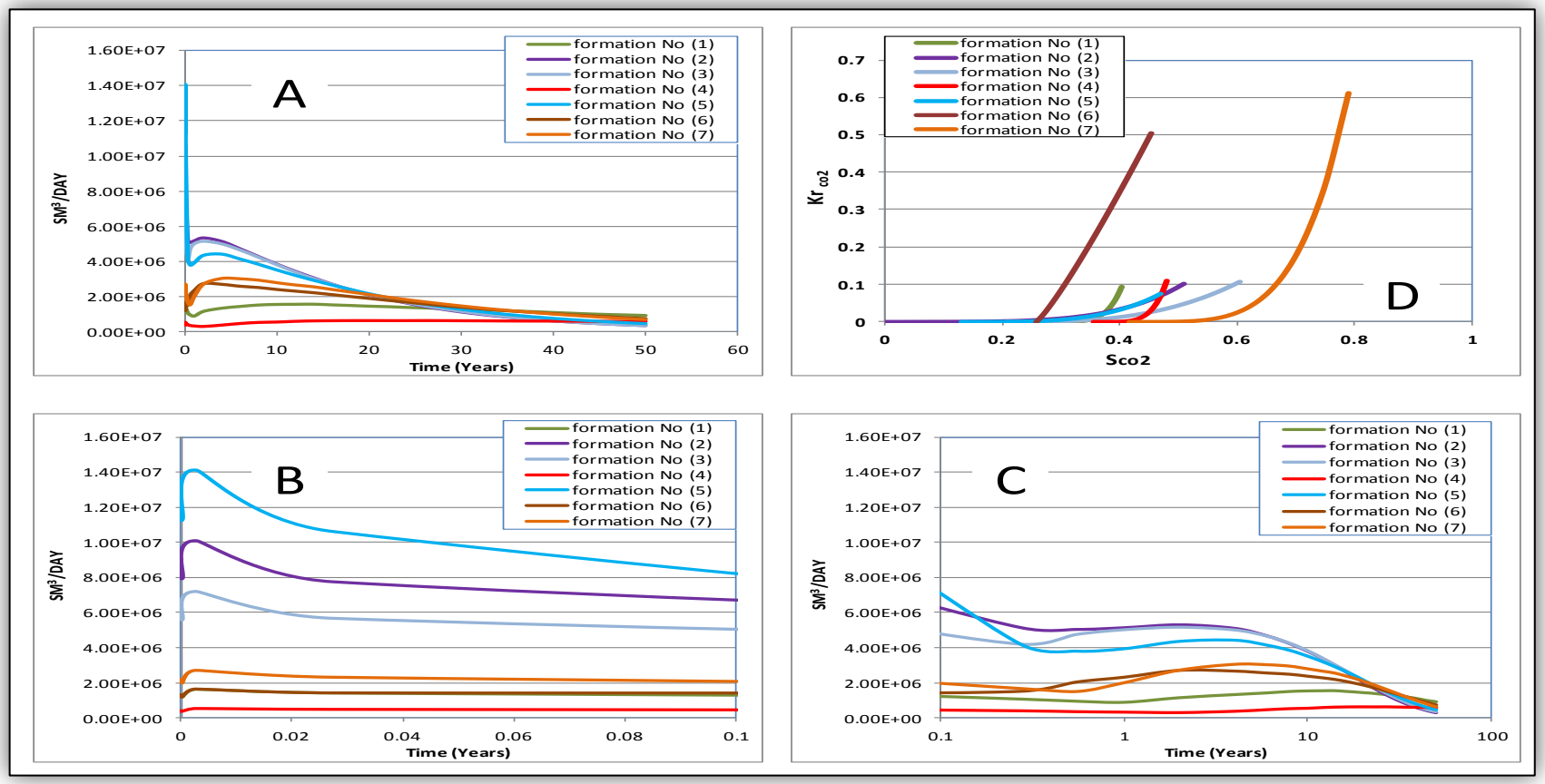

Figure 7.5: Impact of throat distributions on CO_2 injection rate

From Figure 7.5, a set of CO_2 relative permeability data (published and collected in the appendix A) used in the simulation, which is belonging to a group of different formations (1 - 7) and representing the normal and abnormal throat distribution concepts. The results concluded in the following:

Chart "A" in Figure 7.5 has been divided into two charts ("B" and "C"). Chart "B" represents early period of injection time (0 – 0.1 years), while Chart "C" introduces injection time from 0.1 to 50 years.

Chart "D" is CO_2 relative permeability curves for the same formations in Chart A.

According to charts B and C, It is remarkable that the group of **formations (5, 2, and 3)** produced much **higher injection rate** than did the group of **formations (1, 4, 6, and 7)**, and referring to graph D, the group of formations (5, 2, and 3) have normal pores and throat distributions, while in group of formations (1, 4, 6, and 7) there are abnormal throats distributions.

According to chart C, as for group of **formations (5, 2, and 3)**, it is clear that the injection rates in **formations (2 and 3)** are higher than that in **formation (5)**, and by going to chart D, we note that the **end point relative permeability** in formations (2 and 3) is a little higher than that in formation (5). The same could be remarked in formations group (1, 4, 6, and 7), as the injection rates are higher in formations (6 and 7) than others, which due to the fact that the first group (formations 6 and 7) has a much higher CO_2 endpoint relative permeability.

7.4. Summary of results

The best injection rates could be achievable in formations with normal pore–throat distributions, while the abnormal distributions of which produces poor injection rates due to impediment and turbulence impacts.

References

BENNION, B. & BACHU, S. 2005. Relative Permeability Characteristics for Supercritical CO2 Displacing Water in a Variety of Potential Sequestration Zones in the Western Canada Sedimentary Basin. *SPE Annual Technical Conference and Exhibition.* Dallas, Texas: Society of Petroleum Engineers.

BENNION, D. B. & BACHU, S. 2010. Drainage and Imbibition CO2/Brine Relative Permeability Curves at Reservoir Conditions for High-Permeability Carbonate Rocks. *SPE Annual Technical Conference and Exhibition.* Florence, Italy: Society of Petroleum Engineers.

BURTON, M., KUMAR, N. & BRYANT, S. L. 2008. Time-Dependent Injectivity During CO2 Storage in Aquifers. *SPE/DOE Symposium on Improved Oil Recovery.* Tulsa, Oklahoma, USA: Society of Petroleum Engineers.

CLASS, H., EBIGBO, A., HELMIG, R., DAHLE, H., NORDBOTTEN, J., CELIA, M., AUDIGANE, P., DARCIS, M., ENNIS-KING, J., FAN, Y., FLEMISCH, B., GASDA, S., JIN, M., KRUG, S., LABREGERE, D., NADERI BENI, A., PAWAR, R., SBAI, A., THOMAS, S., TRENTY, L. & WEI, L. 2009. A benchmark study on problems related to CO2 storage in geologic formations. *Computational Geosciences,* 13**,** 409-434.

HURTER, S., BERGE, J. G. & LABREGERE, D. 2007. Simulations for CO2 Injection Projects With Compositional Simulator. *Offshore Europe.* Aberdeen, Scotland, U.K.: Society of Petroleum Engineers.

KIATSAKULPHAN, M. 2009. *The effect of Grid resolution on the simulation of Co2 storage in deep saline aquifers.* . Heriot - Watt umiversity.

KONTOURIS, I. 2008. *Sensitivity study of Co2 EGR.* Msc project, Heriot - Watt umiversity.

KUMAR, A., NOH, M., POPE, G. A., SEPEHRNOORI, K., BRYANT, S. & LAKE, L. W. 2004. Reservoir Simulation of CO2 Storage in Deep Saline Aquifers. *SPE/DOE Symposium on Improved Oil Recovery.* Tulsa, Oklahoma: Society of Petroleum Engineers.

MATHIAS, S., GONZÁLEZ MARTÍNEZ DE MIGUEL, G., THATCHER, K. & ZIMMERMAN, R. 2011a. Pressure Buildup During CO2 Injection into a Closed Brine Aquifer. *Transport in Porous Media,* 89**,** 383-397.

MATHIAS, S., HARDISTY, P., TRUDELL, M. & ZIMMERMAN, R. 2009. Approximate Solutions for Pressure Buildup During CO2 Injection in Brine Aquifers. *Transport in Porous Media,* 79**,** 265-284.

MATHIAS, S. A., GLUYAS, J. G., GONZÁLEZ MARTÍNEZ DE MIGUEL, G. J., BRYANT, S. L. & WILSON, D. 2013. On relative permeability data uncertainty and CO2 injectivity estimation for brine aquifers. *International Journal of Greenhouse Gas Control,* 12**,** 200-212.

MATHIAS, S. A., GLUYAS, J. G., GONZÁLEZ MARTÍNEZ DE MIGUEL, G. J. & HOSSEINI, S. A. 2011b. Role of partial miscibility on pressure buildup due to constant rate injection of CO2 into closed and open brine aquifers. *Water Resources Research,* 47**,** W12525.

SCHLUMBERGER. 2011. *Eclipse technical description manual* [Online]. Available: file:///C:/ecl/2011.1/manuals/bookshelf.html.

SOHRABI, M., RIAZI, M., BERNSTONE, C., JAMIOLAHMADY, M. & CHRISTENSEN, N.-P. 2012. New Insights Into CO2 Injection and Storage in Saline Aquifers. *SPE Europec/EAGE Annual Conference.* Copenhagen, Denmark: Society of Petroleum Engineers.

SOTUMINU, O. 2007. *Numerical simulation of SAGD Wind-Down Process with Co2 Injection.* Msc project., Heriot - Watt umiversity.

SPYCHER, N. & PRUESS, K. 2005. CO2-H2O mixtures in the geological sequestration of CO2. II. Partitioning in chloride brines at 12–100°C and up to 600 bar. *Geochimica et Cosmochimica Acta,* 69**,** 3309-3320.

SPYCHER, N., PRUESS, K. & ENNIS-KING, J. 2003. CO2-H2O mixtures in the geological sequestration of CO2. I. Assessment and calculation of mutual solubilities from 12 to 100°C and up to 600 bar. *Geochimica et Cosmochimica Acta*, 67**,** 3015-3031.

WAHEIBI, H. 2008. *Simulation of Co2 flow in natural systems.* Msc project, Heriot - Watt umiversity.

Chapter 8

Investigating the difference between the relative permeabilities of CO_2 and other hydrocarbon gases (CH_4, C_2H_6) using theoretical pore-network model

8.1. Introduction

As it is known, relative permeability depends on many factors like rock and fluid properties, the method applied… etc. (Figure 8.1), and to show the difference in performance and relative permeability of CO_2 and other gases like hydrocarbon gases, all factors (impacting relative permeability) except the fluid type must be fixed.

If empirical or experimental methods are used (depending on real core plugs) to study the difference between CO_2 and other gases (regarding performance and relative permeability), there is a set of problems encountered. For instance, it is impossible to get two or more cores with the same internal structure (pore, throat and wettability distributions), and as a result, the difference in relative permeabilities of CO_2 and other gases (like CH_4 and C_2H_6) will be affected by the core's internal structure in addition to type of fluid injected. The additional problem (if using real cores) is the reactions among the injected gases and brine and the rock contents. These undesirable reactions must be avoided as they impact everything (from the internal structure of the real core to all capillary properties, like wettability, IFT and viscosity ... etc.), these have an extensive effect on the resulting relative permeabilities. Therefore, the substitute way (theoretical or mathematical modelling) should be applied, which consists of digital pore-network (digital core) filled with brine and pore-scale fluid flow simulator designed by the Imperial College[6]. By changing the properties of the injected gas, like viscosity, density and molecular weight ... etc., different types of gas was injected, to study the impact of gas type on the resulting relative permeabilities.

[6] Using Imperial College pore-scale fluid flow simulator was due to its ability to including the type of gas injected, where it was not available in the simulator designed by Heriot-watt University.

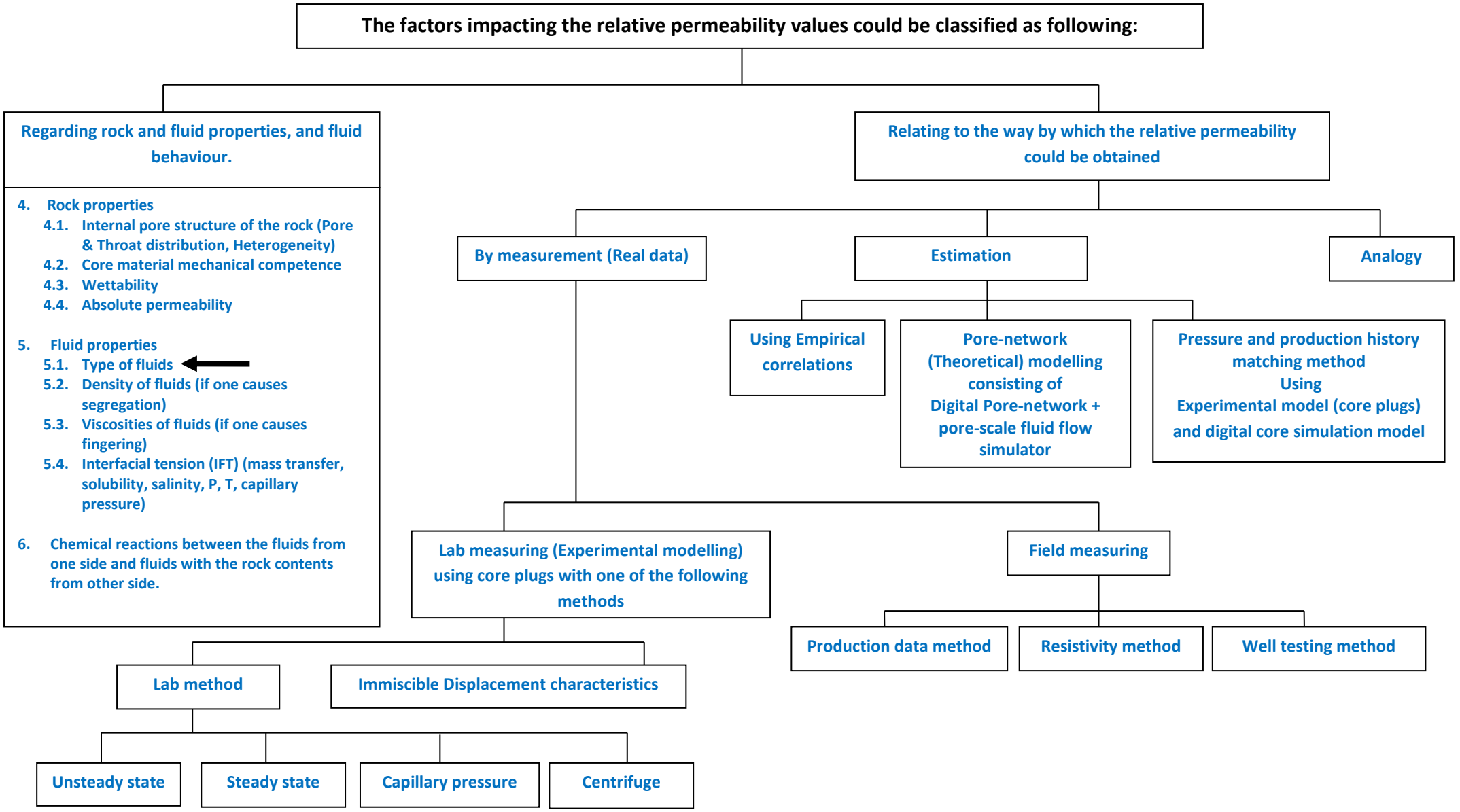

Figure 8.1: Factors impacting the relative permeability values, the type of fluid (targeted) is highlighted.

8.2. Theoretical Pore-scale model

As discussed in chapter 5, the theoretical pore-scale model consists of a synthetic digital pore-network and pore-scale fluid flow simulator. Here some information about the pore-network model used to achieve the target of this chapter.

8.2.1. **Pore-network model selection.**

As discussed in chapter 5, four different digital pore-networks were applied to investigate the impact of rock internal structure on CO_2 relative permeability curve shape. To achieve the target of this chapter, the digital pore-network used in the Model no ① (Figure 8.2) was used as this pore-network represents the most common internal structure of the real cores (normal pore and throat size distribution), thus producing the most common relative permeability and capillary pressure curves. The model was tested for oil and water in the drainage process and the results are illustrated in Figure 8.3.

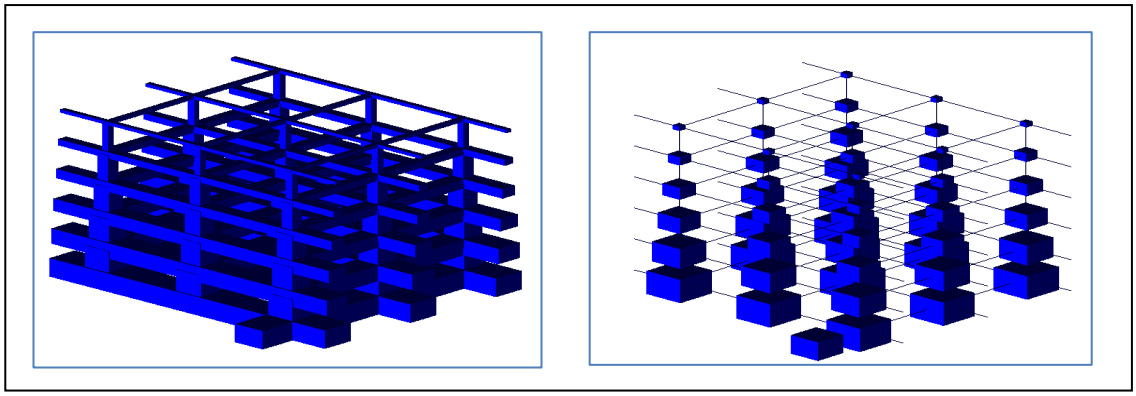

Figure 8.2: Normal pore and throat size distribution

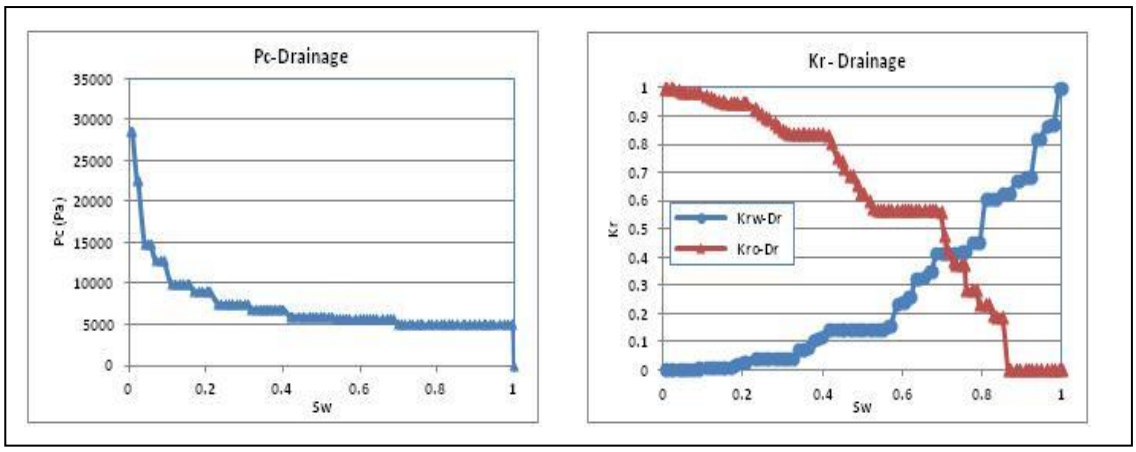

Figure 8.3: Capillary pressure and relative permeability curves for the model in Figure 8.2

Six digital pore-networks, with normal pore and throat distribution, have been modelled as in Figure 8.4 here:

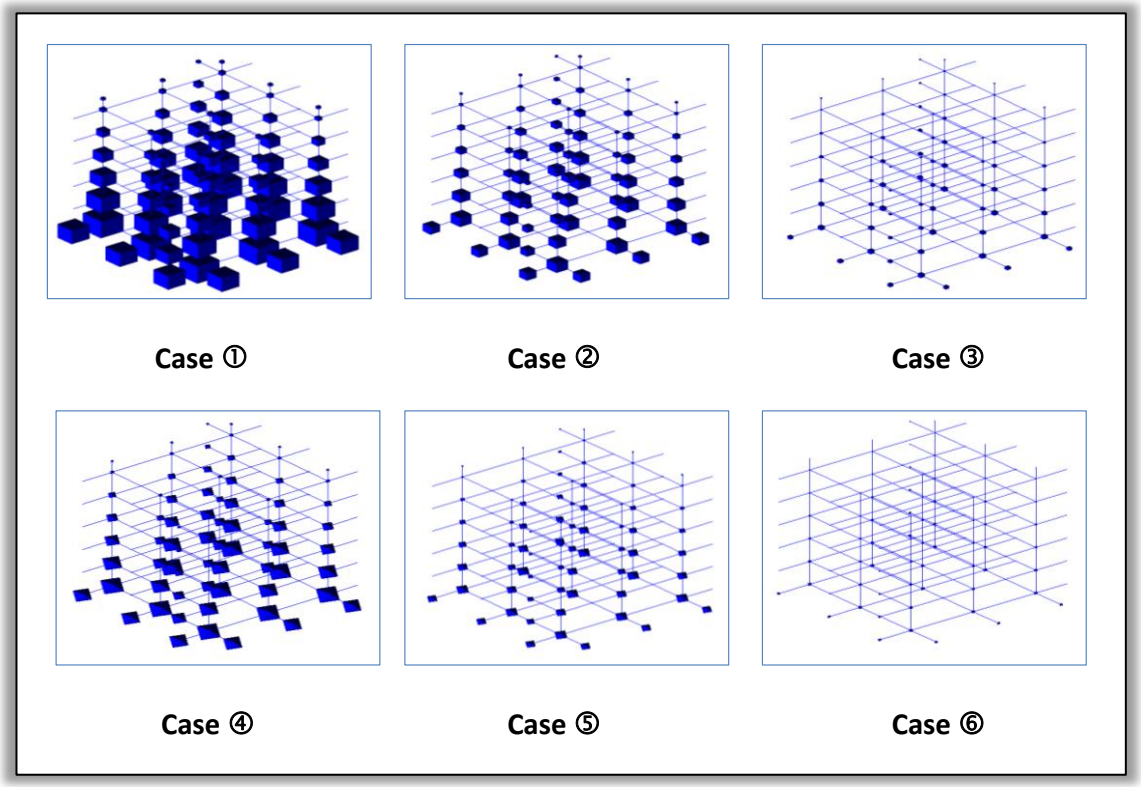

Figure 8.4: The six digital pore-networks with normal pore and throat distribution.

Shape Factor=0.06045 (Square)	Case1	Case2	Case3
Node and Bond Radius Range (μm)	3.16-22	2.16-12	1.1-4
Porosity (%)	11.787	11.787	11.79
AbsPerm (mD)	2921.6	243.91	3.317

Shape Factor=0.0481 (Triangle)	Case4	Case5	Case6
Node and Bond Radius Range (μm)	3.16-22	2.16-12	1.1-4
Porosity (%)	11.787	11.787	11.79
AbsPerm (mD)	4049.73	338.09	4.6

Table 8.1: Pore-space properties for the six pore-networks modelled.

As mentioned, there are two types of pore-shape: either square or triangular. Pore-network selected consisted of both types of pore-shape, as the triangular shape includes the wettability parameter. If the density of gas is considered, another code will be required. The small amount of data obtained is due to the fact that the pore-network used is too small (Figure 8.5), so another larger pore-network, with the same structure, was suggested to produce more data points (Figure 8.6).

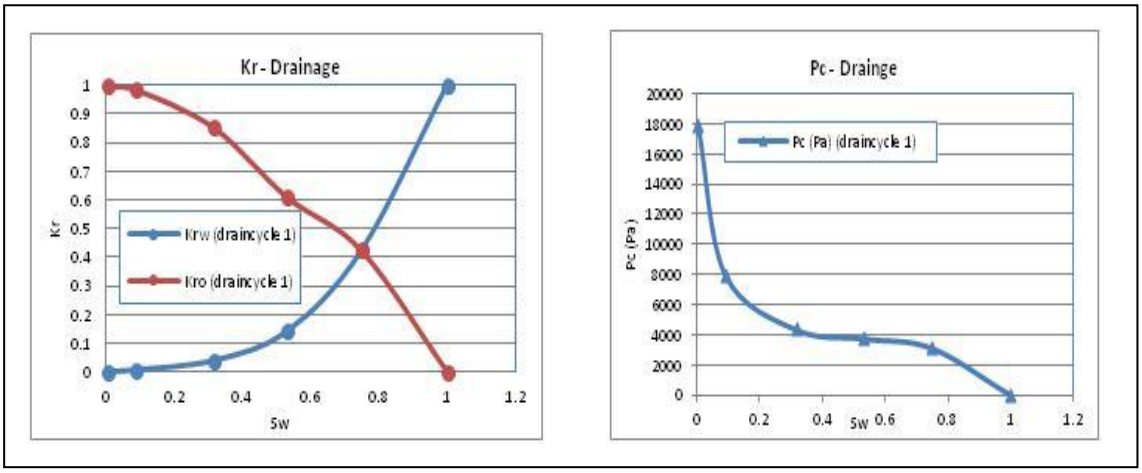

Figure 8.5: The Model's output data for the six pore-networks suggested.

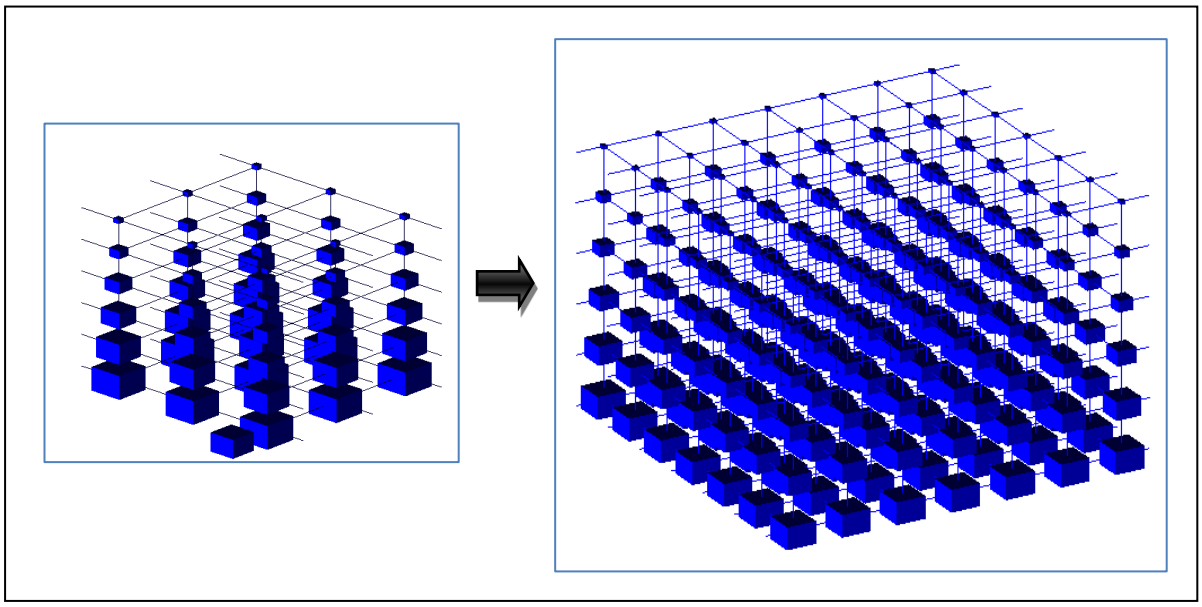

Figure 8.6: Upgrade the small pore-network to larger one.

8.2.2. **Pore-scale fluid flow simulator used**

A pore-scale fluid flow simulator designed by the Imperial College London (DOS version) (Valvatne, 2004), apart from that applied in chapter 5, has been used to make sensitivity tests for capillary pressure and relative permeability when a different type of gas is being injected each time.

A) Gases selected

Three gases (CO_2, CH_4, C_2H_6) were selected to investigate the effect of gas type on capillary pressure and relative permeability data.

B) Capillary pressure controlled system

The fluid flow simulator is assumed a capillary pressure controlled system rather than viscous force. This is because it is assumed that the flow has an infinitesimal flow rate so the pressure drop across the network due to friction forces between fluid layers is negligible.

So the capillary pressure which determines the fluid displacement equals:

$$Pc = \frac{2\sigma_{bg}\cos\theta_{bg}}{R} \qquad \text{Eq. 8.1}$$

Where:

σ_{bg} is the interfacial tension between brine and the gas.

θ_{bg} is the contact angle.

C) Wettability

It is known that θ_{bg} is different for drainage (receding) and imbibition (advancing), as illustrated in Figure 8.7 below, the receding (drainage) and imbibition (advancing) contact angles are correlated with the intrinsic contact angles which are considered as input data in fluid flow simulator.

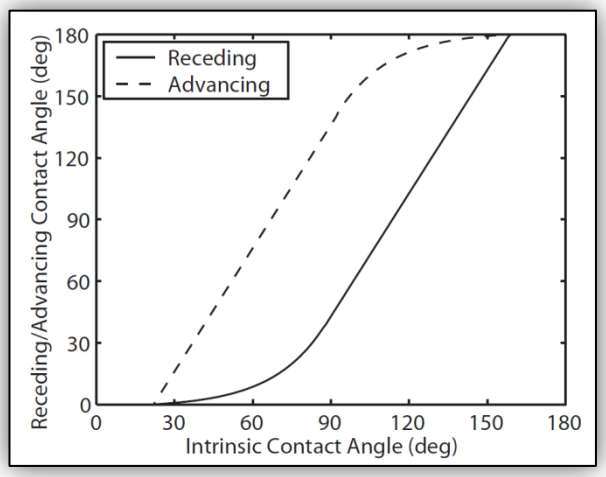

Figure 8.7: Relationship between receding and advancing contact angles on a rough surface, as a function of intrinsic contact angle measured at rest on a smooth surface (Morrow, 1975)

D) The interfacial tension (IFT)

Based on the equation $Pc = \frac{2\sigma_{bg}\cos\theta_{bg}}{R}$, the difference in the gases types is represented by the variance in the interfacial tension value (σ_{bg}) for each gas.

E) Displacement mechanisms

Although the displacement process for drainage and imbibition is set differently, in the drainage the displacement is almost simply determined by this equation, whereas in the imbibition process, it is more complicated as it is not just considering the piston-like process but also snap off. It will make the P_c in the imbibition process more sensitive to determine element (σ_{bg}).

F) Relative permeability calculations

When estimating the relative permeability, there is one important element which is the conductance. The conductance of phase P depends on the shape of the cross-section, for a circular cylinder of length L and radius R completely filled with phase P whose viscosity is μ_p, the conductance ($\boldsymbol{g}_p$) equals:

$$g_p = \frac{\pi R^4}{8\mu_p L} \qquad \text{Eq. 8.2}$$

8.2.3. Sensitivity Tests

Capillary pressure and relative permeability sensitivity tests were conducted for the gases (CO_2, CH_4, C_2H_6) to see the effect of different gases on capillary pressure and relative permeability data.

A) Sensitivity-test elements

A.1) Pore-network used

All sensitivity tests used the same pore-network model (Figure 8.8, Table 8.2) that was selected before, and as explained before in the introduction. All that, of course, was to avoid the impact of real-core internal structure on data produced when different real cores are being used.

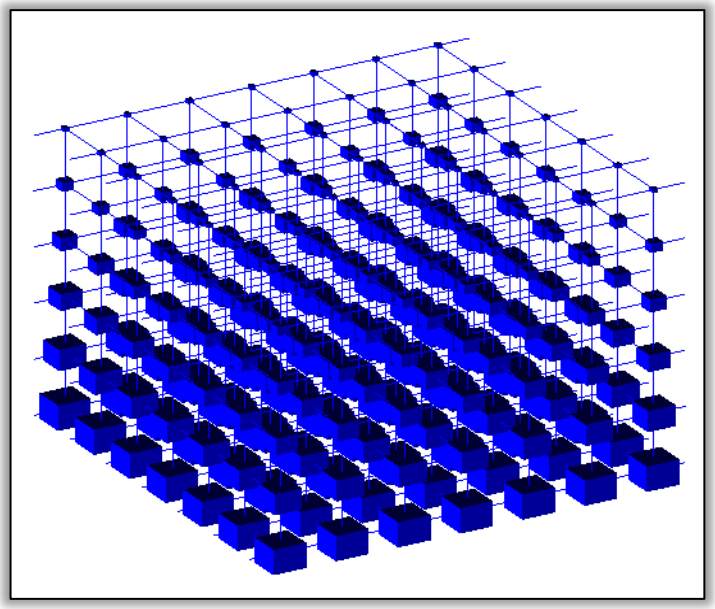

Figure 8.8: Model used in the sensitivity tests

Type of Gas	CO_2	CH_4	C_2H_4
Number of pores:	294	294	294
Number of throats:	833	833	833
Average connection number:	5.38095	5.38095	5.38095
Number of connections to inlet:	42	42	42
Number of connections to outlet:	42	42	42
Number of physically isolated elements:	0	0	0
Number of singlets removed:	0	0	0
Number of triangular shaped elements:	2	2	2
Number of square shaped elements:	1127	1127	1127
Number of circular shaped elements:	0	0	0
Median throat length to radius ratio:	4.20833	4.20833	4.20833
Net porosity:	0.12725	0.12725	0.12725
Clay bound porosity:	0	0	0
Absolute permeability (mD)	4428.67	4428.67	4428.67
Absolute permeability (m2)	4.37E-12	4.37E-12	4.37E-12
Formation factor:	7.69148	7.69148	7.69148

Table 8.2: The same specification of the model used for different gases

The contact angles for a receding process were between (0-5 degree) (strong water wet) and (0-50 degree) for advancing process, and the corresponding intrinsic contact angles were between (5 – 45 degree) as shown in Figure 8.9. The above contact angles selected had been applied with the same values for the three types of gases (CO_2, CH_4, C_2H_6).

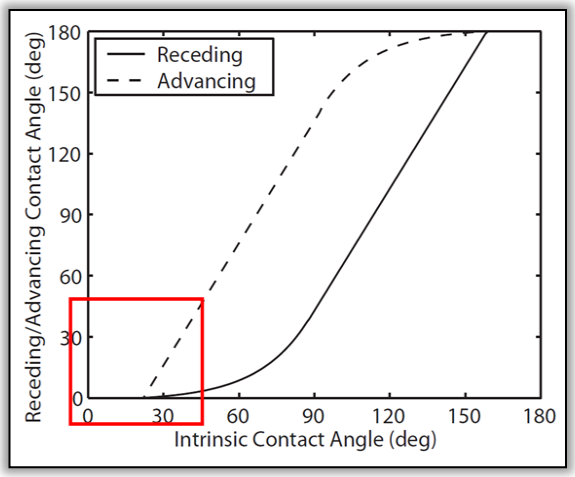

Figure 8.9: Contact angles ranges selected

The thermo-physical properties and (IFT) data of the gases applied in fluid simulator were collected from Technology (2011), and summarized as follows (Table 8.3 - Table 8.5):

A.2) Thermo-physical properties of carbon dioxide (CO_2).

Temperature (C º)	Pressure (bar)	Density (kg/m^3)	Viscosity (Cp)	Phase
25	60	190.61	0.018316	Vapour
Internal energy		U = 0 at 273.16 K for saturated liquid.		
Entropy		S = 0 at 273.16 K for saturated liquid.		
Critical temperature (T_c)		30.9782 ºC		
Critical pressure (P_c)		73.773 bar		
Critical density (D_c)		467.600 kg/m^3		
Normal boiling point		-78.40 ºC		

Table 8.3: Thermo-physical properties of carbon dioxide (CO_2)

A.3) Thermo-physical properties of Methane (CH_4)

Temperature (C º)	Pressure (bar)	Density (kg/m^3)	Viscosity (Cp)	Phase
25	60	43.024	0.012426	Supercritical
Internal energy		U = 0 at 273.16 K for saturated liquid.		
Entropy		S = 0 at 273.16 K for saturated liquid.		
Critical temperature (T_c)		-82.586 ºC		
Critical pressure (P_c)		45.992 bar		
Critical density (D_c)		162.66 kg/m^3		
Normal boiling point		-161.483 ºC		

Table 8.4: Thermo-physical properties of Methane (CH_4)

A.4) Thermo-physical properties of Ethane (C_2H_6)

Temperature (C º)	Pressure (bar)	Density (kg/m^3)	Viscosity (Cp)	Phase
25	60	135.84	0.016103	supercritical

Internal energy	U = 0 at 273.16 K for saturated liquid.
Entropy	S = 0 at 273.16 K for saturated liquid.
Critical temperature (T_c)	9.20 ºC
Critical pressure (P_c)	50.418 bar
Critical density (D_c)	214.2 kg/m^3
Normal boiling point	-103.771 ºC

Table 8.5: Thermo-physical properties of Ethane (C_2H_6)

- Interfacial tension (IFT) data between the gas and the brine obtained from Duchateau and Broseta (2012) (Table 8.6).

Gas type	CO_2	CH_4	C_2H_4
Interfacial tension (mN/m)	34	7.5	25.5

Table 8.6: Interfacial tension (IFT) data between the gas and the brine

B) Results

B.1) **Capillary pressure**

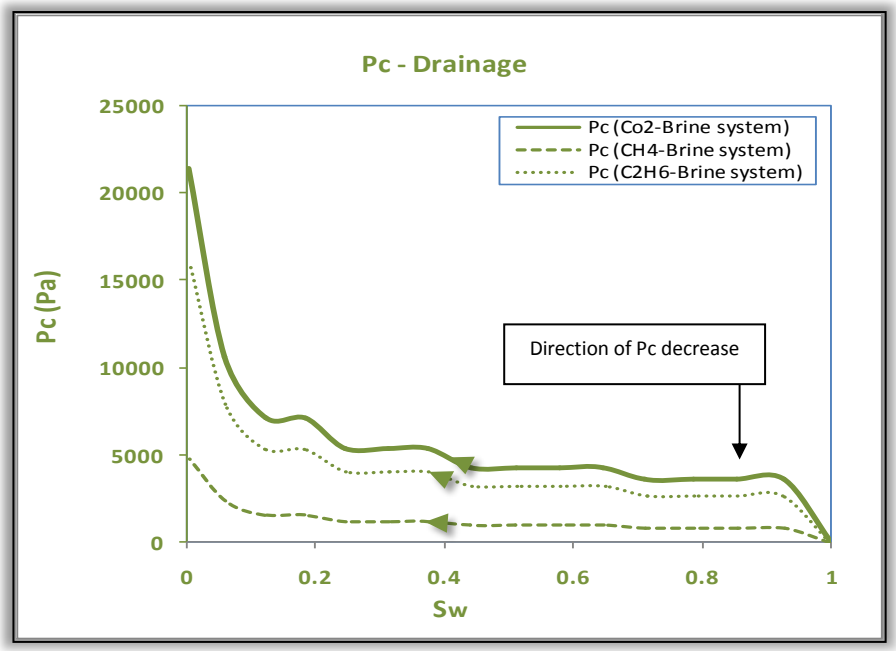

Figure 8.10: Capillary pressure data through drainage cycle for the gasses (CO_2, CH_4, C_2H_6)

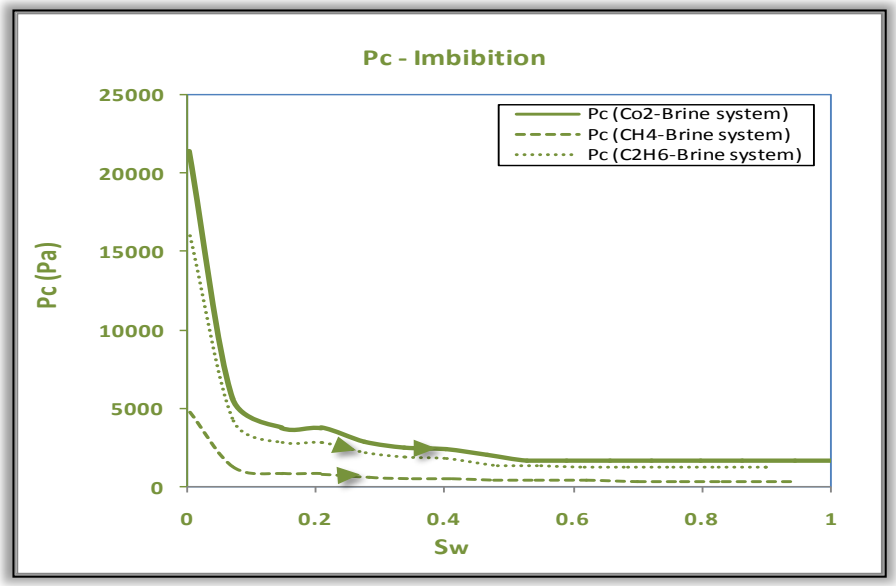

Figure 8.11: Capillary pressure data through imbibition cycle for the gasses (CO_2, CH_4, C_2H_6)

B.2) **Relative permeability**

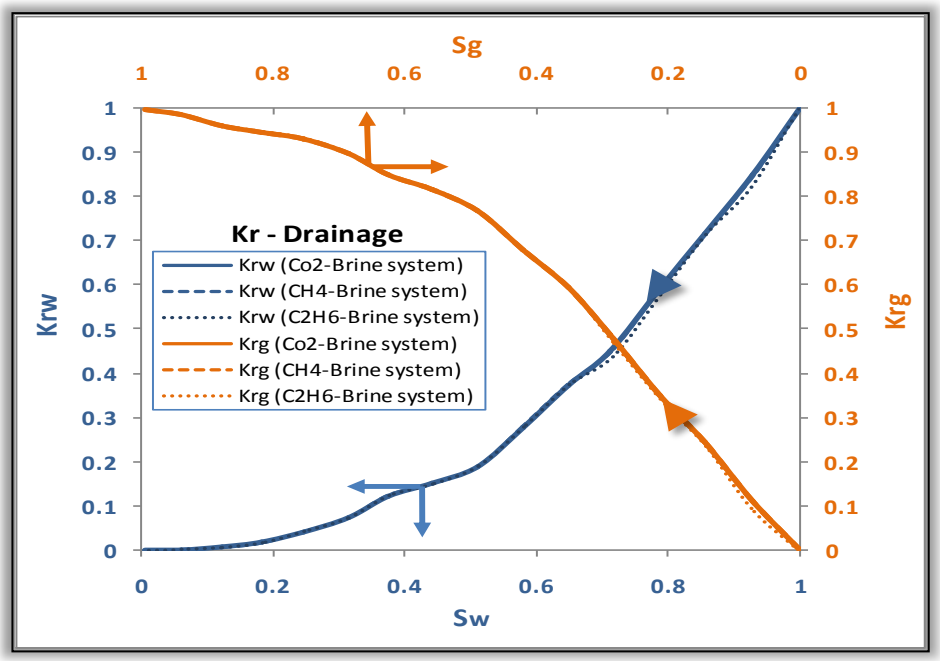

Figure 8.12: Relative permeability data for the gasses (CO_2, CH_4, C_2H_6) and brine through drainage cycle

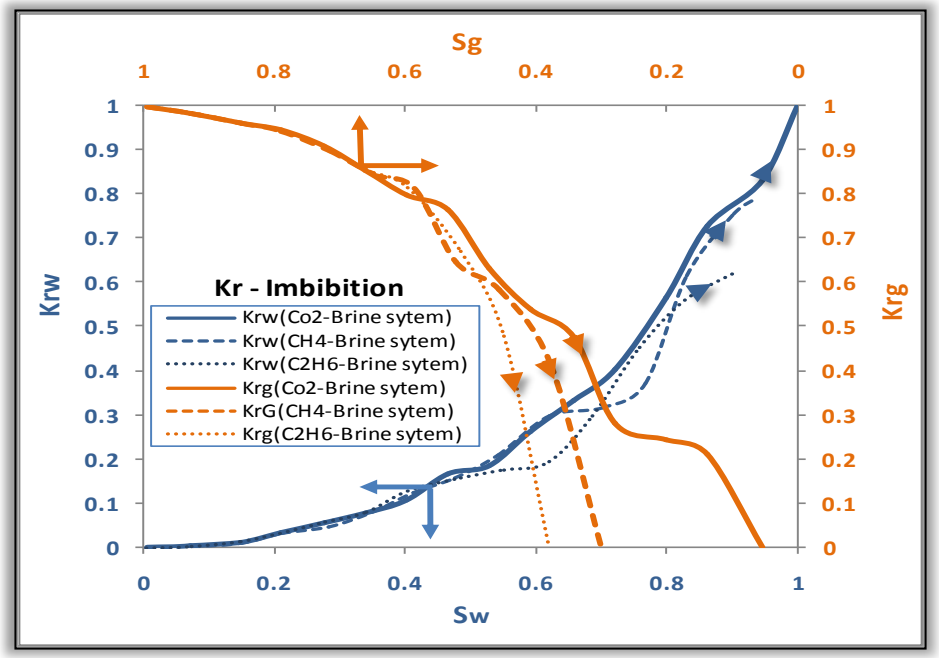

Figure 8.13: Relative permeability data for the gasses (CO_2, CH_4, C_2H_6) and brine through imbibition cycle

B.3) **Discussion of Results**

The difference in capillary pressures of the gases (CO_2, CH_4, C_2H_6), as appears in Figure 8.10 and Figure 8.11, was mainly caused by differences in the interfacial tension values of the gases applied, as predicted due to the capillary pressures are a strong function of interfacial tension.

As for the relative permeability charts we have the follows:

- In the drainage process (Figure 8.12), there is no effect of gas type on relative permeability curves, so all curves are identical.
- In the imbibition process (Figure 8.13), it is clear that the brine could not invade all pores and that is why the final saturations of all gases (CO_2, CH_4, C_2H_6) did get to zero. It is, of course, due to the fact that the viscosity of the brine is much higher than that for the gases, and the brine, consequently, could not efficiently penetrate the pores as the low viscous gases did. As for disparity in curves, we cannot attribute that to the difference in interfacial tension values, since the same values of IFT had been applied in both drainage and imbibition and no variation in data was observed during drainage. Consequently, the disparity in imbibition curves could be considered as a result of brine-gas viscosity ratios, which of course vary depending on the type of gas applied.

8.2.4. Modifying the bonds and nodes distribution in the selected pore-network to be random instead of uniform

It can be said here the imbibition results (Figure 8.13) were not quite convincing, which may due to the fact that the pores and throats in the applied model were uniformly distributed. As a matter of fact, this assumption does not exist in the real core or is at least very rare. Therefore, we suggested modifying the distribution of the bonds and nodes, in the used model, to be distributed randomly rather than uniformly.

Three different random distributions for the nodes and bonds (pores and throats) were modelled. The specifications of the three pore-network models, compared with the previous one with uniformly- distributed pores and throats, are as follows:

Node and Bond Radius Range (um)	Uniform 3.16 - 22	Random 2.16 - 18	Random 2.16 - 12	Random 1.1 - 4
Number of pores:	294	294	294	294
Number of throats:	833	835	834	837
Average connection number:	5.38095	5.39456	5.38776	5.40816
Number of triangular shaped elements:	2	949	956	991
Number of square shaped elements:	1127	129	143	109
Number of circular shaped elements:	0	53	31	33
Median throat length to radius ratio:	4.20833	5.97606	7.32009	15.6308
Net porosity:	0.12725	0.573719	0.396593	0.0903474
Clay bound porosity:	0	0	0	0
Absolute permeability (mD)	4428.67	4070.21	1276.53	32.7128
Absolute permeability (m2)	4.37E-12	4.02E-12	1.26E-12	3.23E-14
Formation factor:	7.69148	4.93014	7.43891	35.4818

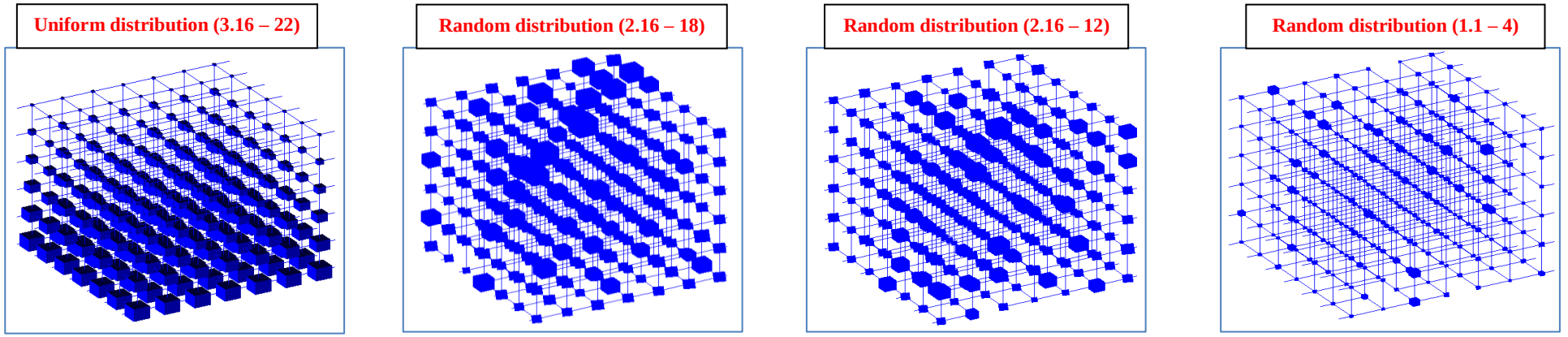

Table 8.7 : Three different random distributions in compared with the regular previous one.

A) Results

A.1) Pore-network with random nodes and bonds distribution (Radius Range 2.16 - 18 μm)

A.1.1) Capillary pressure

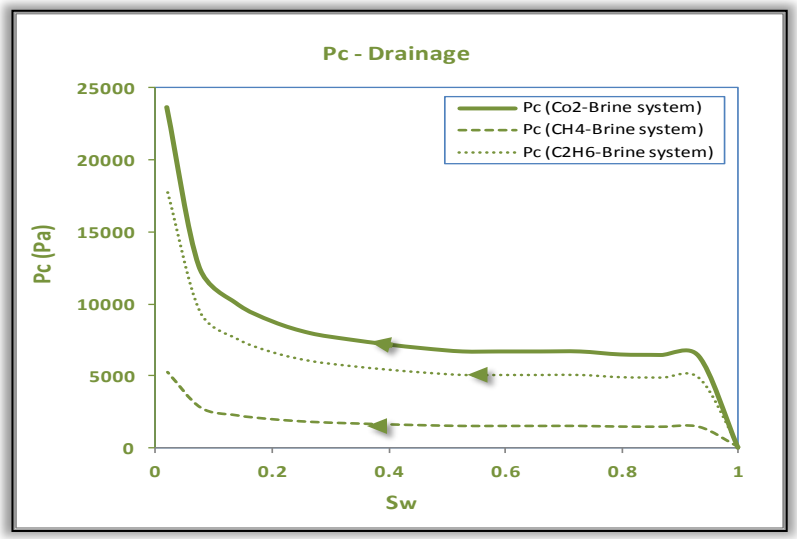

Figure 8.14: Capillary pressure data through drainage cycle to the gasses (CO_2, CH_4, C_2H_6) for pore-network with random (2.16-18) nodes and bonds distribution.

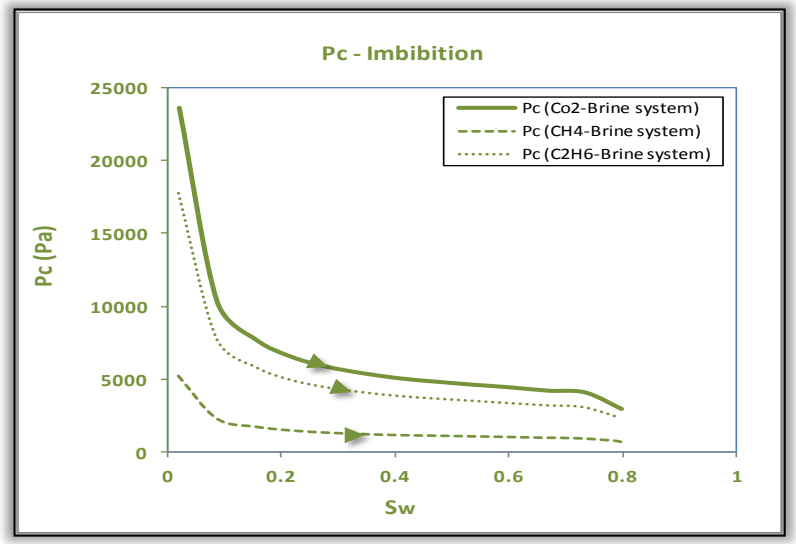

Figure 8.15: Capillary pressure data through the imbibition cycle to the gasses (CO_2, CH_4, C_2H_6) for pore-network with random (2.16 - 18) nodes and bonds distribution.

A.1.2) Relative permeability

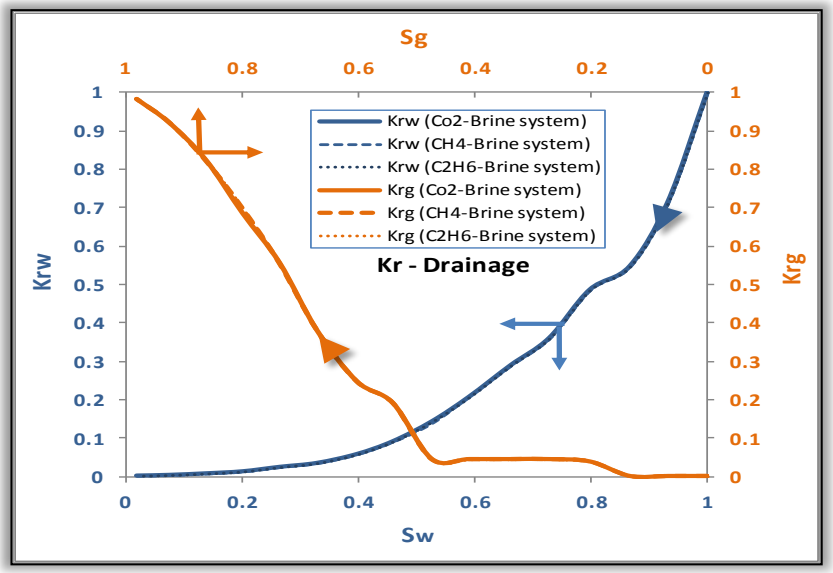

Figure 8.16: Relative permeability data to the gasses (CO_2, CH_4, C_2H_6) and brine through drainage cycle for pore–network with random (2.16 - 18) nodes and bonds distribution.

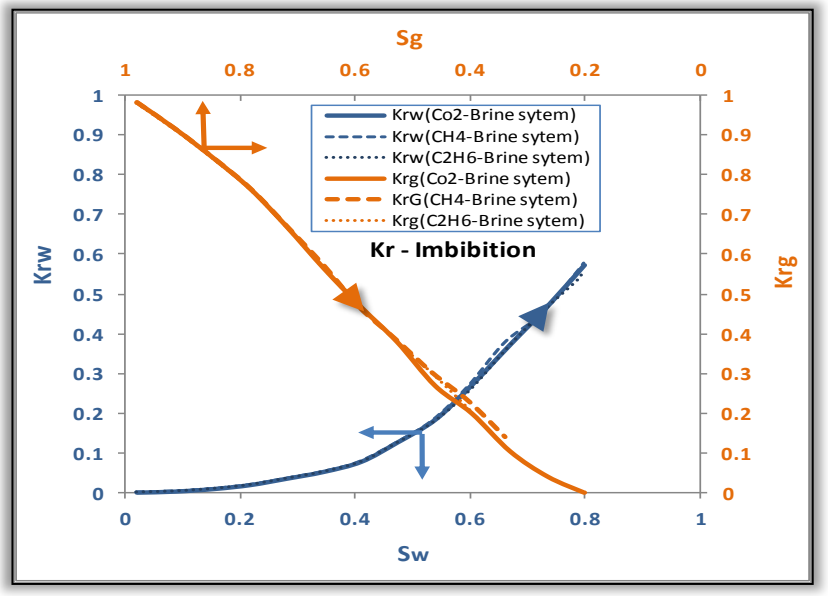

Figure 8.17: Relative permeability data to the gasses (CO_2, CH_4, C_2H_6) and brine through imbibition cycle for pore–network with random (2.16 - 18) nodes and bonds distribution

A.2) **Pore-network with random nodes and bonds distribution**

(Radius Range 2.16 - 12 μm)

A.2.1) Capillary pressure

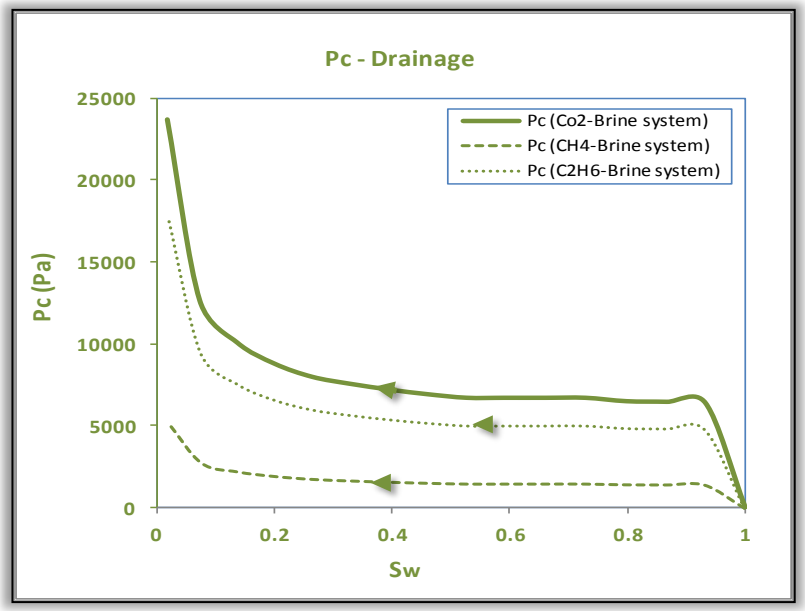

Figure 8.18: Capillary pressure data through drainage cycle to the gasses (CO_2, CH_4, C_2H_6) for pore–network with random (2.16-12) nodes and bonds distribution

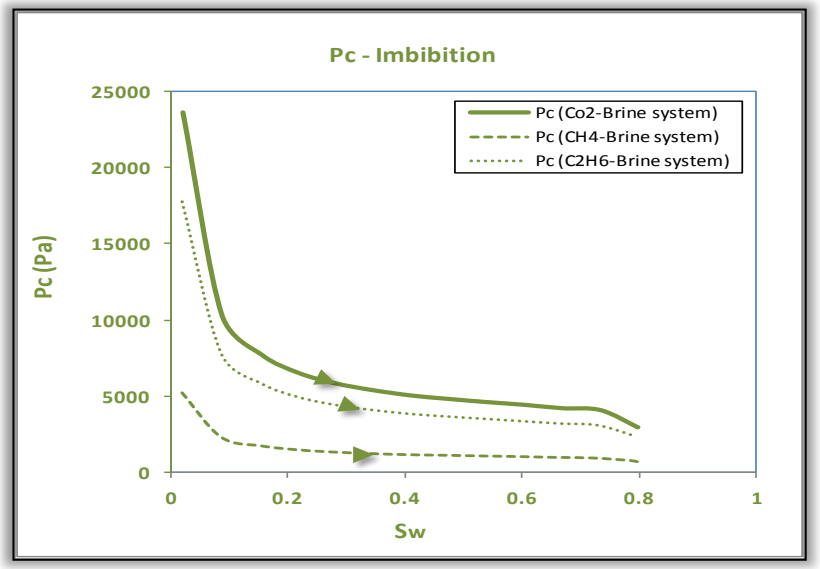

Figure 8.19: Capillary pressure data through imbibition cycle to the gasses (CO_2, CH_4, C_2H_6) for pore–network with random (2.16-12) nodes and bonds distribution

A.2.2) Relative permeability

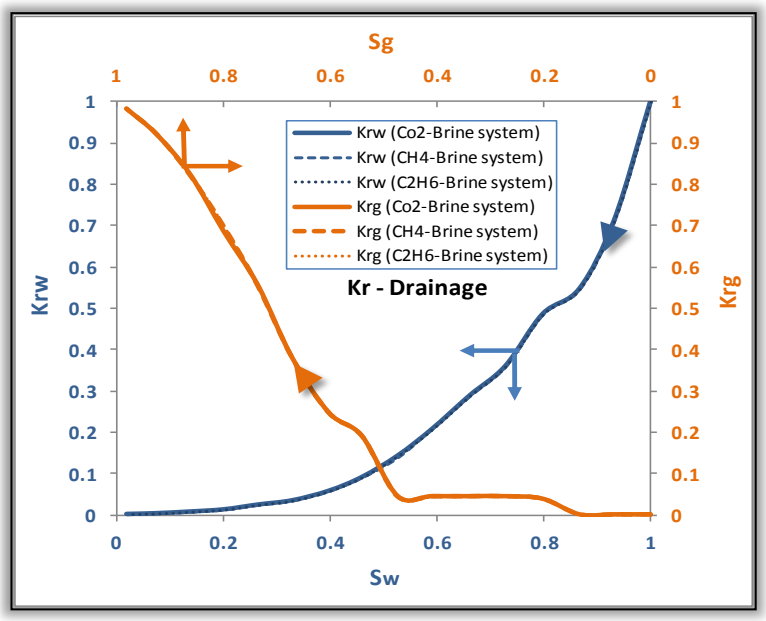

Figure 8.20: Relative permeability data to the gasses (CO_2, CH_4, C_2H_6) and brine through drainage cycle for pore–network with random (2.16 - 12) nodes and bonds distribution.

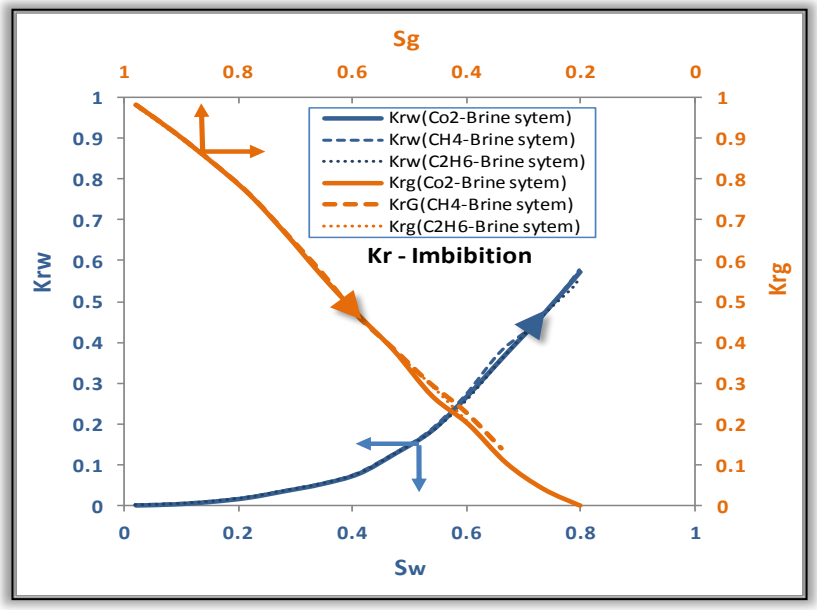

Figure 8.21: Relative permeability data to the gasses (CO_2, CH_4, C_2H_6) and brine through imbibition cycle for pore–network with random (2.16-12) nodes and bonds distribution

A.3) **Pore-network with random nodes and bonds distribution**

(Radius Range 1.1 - 4 μn)

A.3.1) Capillary pressure

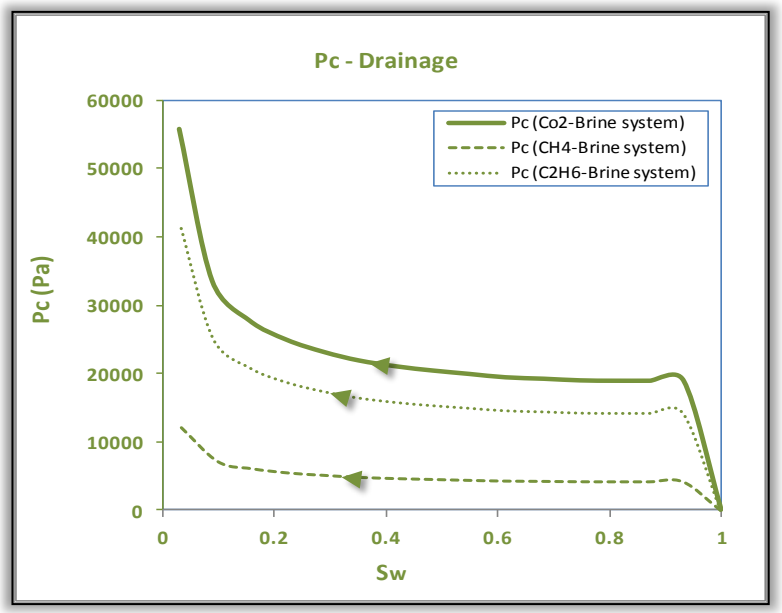

Figure 8.22: Capillary pressure data through drainage cycle to the gasses (CO_2, CH_4, C_2H_6) for pore-network with random (1.1-4) nodes and bonds distribution

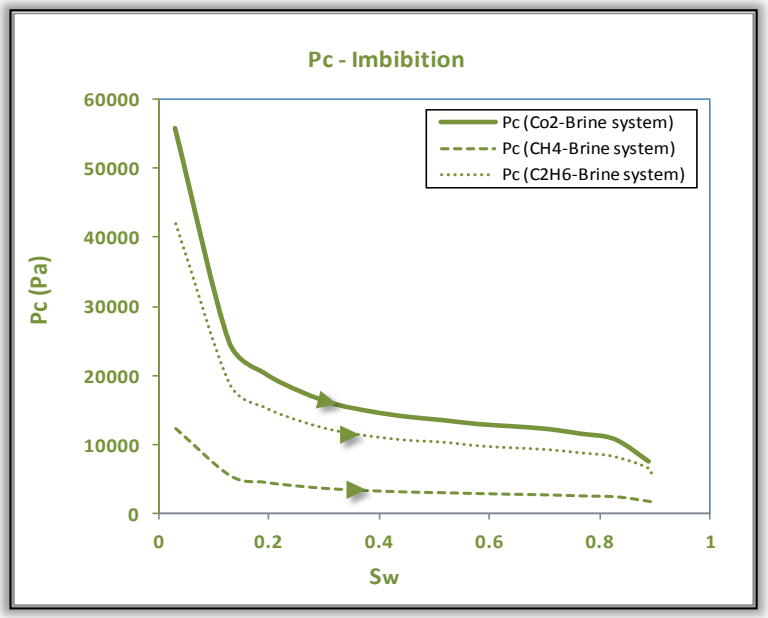

Figure 8.23: Capillary pressure data through imbibition cycle to the gasses (CO_2, CH_4, C_2H_6) for pore–network with random (1.1-4) nodes and bonds distribution

A.3.2) Relative permeability

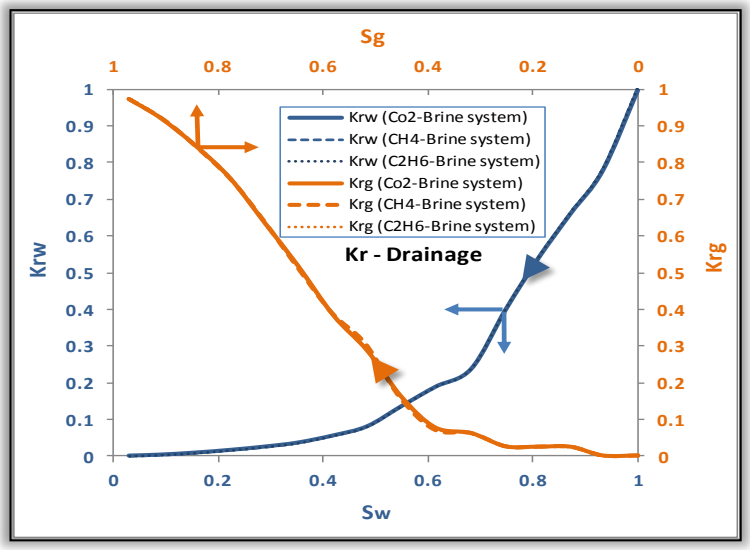

Figure 8.24: Relative permeability data to the gasses (CO_2, CH_4, C_2H_6) and brine through drainage cycle for pore-network with random (1.1-4) nodes and bonds distribution

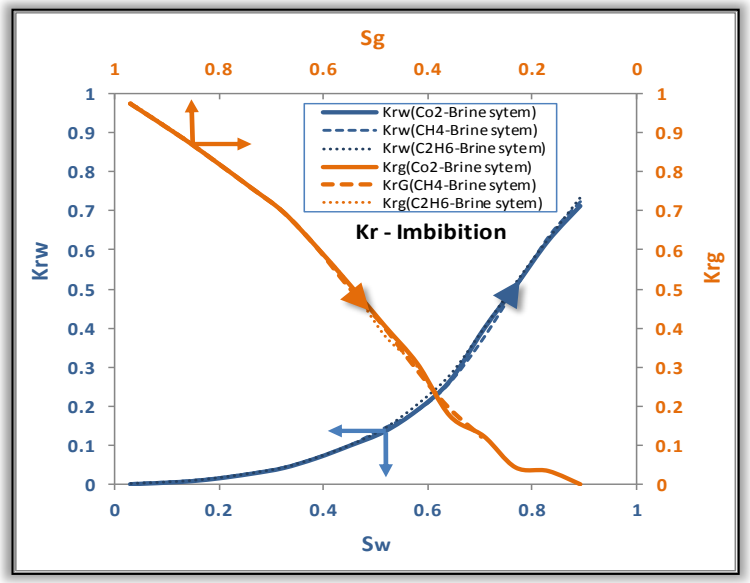

Figure 8.25: Relative permeability data to the gasses (CO_2, CH_4, C_2H_6) and Brine through Imbibition cycle for pore-network with random (1.1-4) nodes and bonds distribution

B) Discussion of results

According to the figures 8.17, 8.21 and 8.25, the variance in the gases/brine curves no longer existed, and consequently the curves difference in Figure 8.13 could be attributed to the fact that the uniform model used was far away from the real case that represents the real core samples.

8.3. General conclusion

The general conclusion which could be extracted from this chapter is that as long as all factors impacting the relative permeability (except the gas type) are fixed, no difference in relative permeability is made whatever type of gas is used (Figure 8.26) .

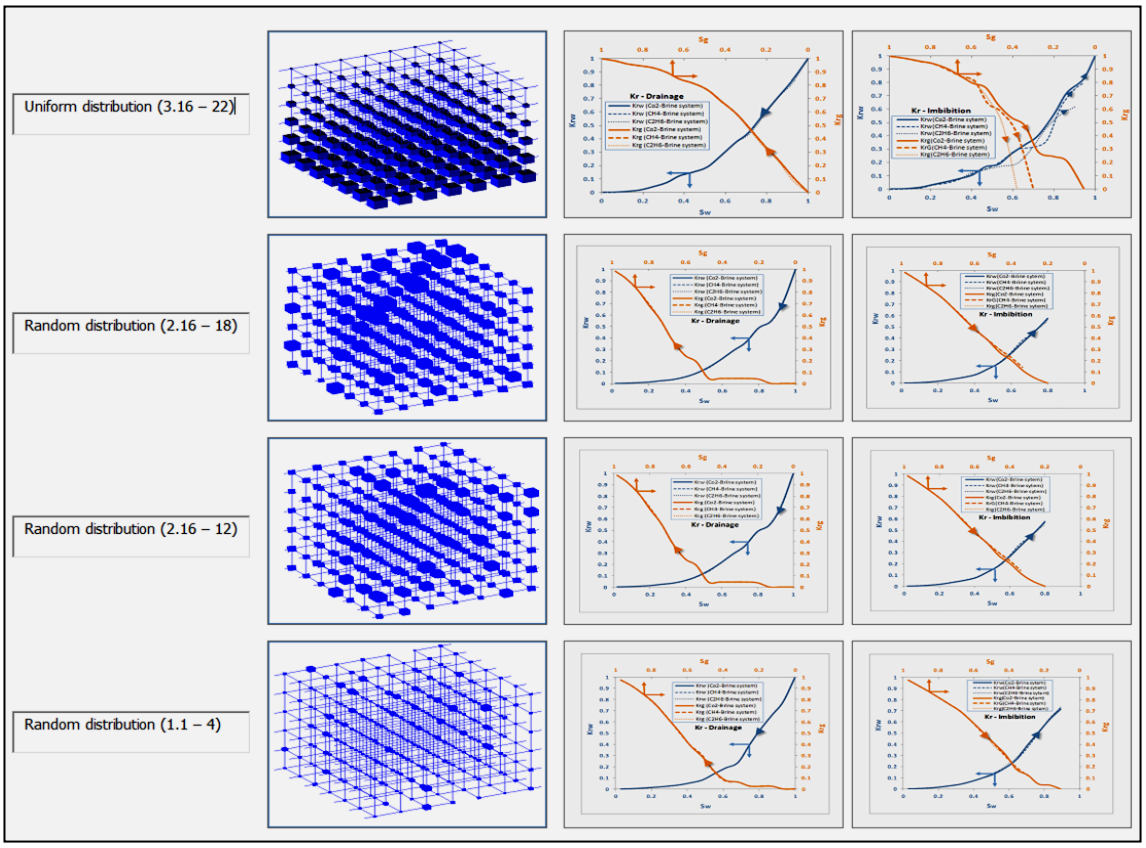

Figure 8.26 : Conclusion of final results

References

DUCHATEAU, C. & BROSETA, D. 2012. A simple method for determining brine–gas interfacial tensions. *Advances in Water Resources*, 42**,** 30-36.

MORROW, N. R. 1975. The Effects of Surface Roughness On Contact: Angle With Special Reference to Petroleum Recovery. *Journal of Canadian Petroleum Technology*, 14.

TECHNOLOGY, N. I. O. S. A. 2011. *Thermophysical Properties of Fluid Systems* [Online]. Available: http://webbook.nist.gov/chemistry/fluid/.

VALVATNE, P. H. 2004. *Pore-scale simulator* [Online]. IMPERIAL COLLEGE LONDON Available: http://www3.imperial.ac.uk/earthscienceandengineering/research/perm/porescalemodelling/software/two%20phase%20code PhD].

Chapter 9

Additional concepts and interpretations.

9.1. The effect of wettability distribution on CO_2 endpoint relative permeability

9.1.1. Introduction

Wettability may be represented by the contact angle formed among fluids and a flat solid surface or the angle formed between the fluids' interface and a glass capillary tube; as shown below, the angle is measured through the denser fluid.

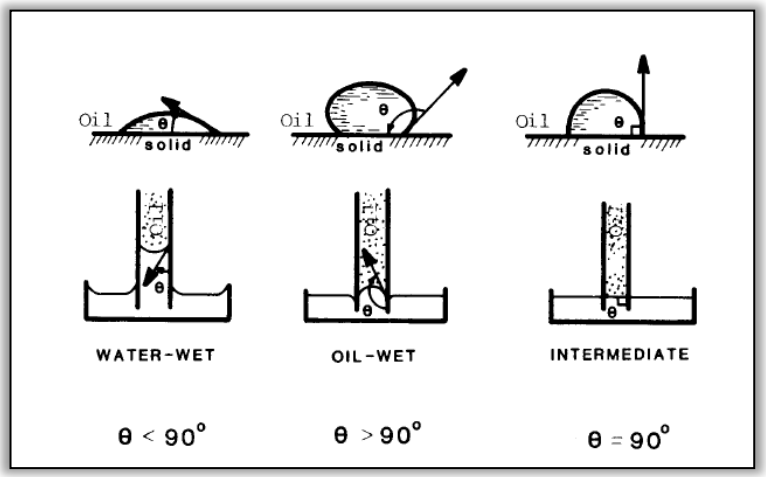

Figure 9.1: Different cases of contact angle (Honarpour et al., 1986)

The wettability of a porous medium is determined by a combination of all surface forces.

Where two liquids, oil and water, are in contact with a solid, the force exerted by water to spread laterally and displace oil (interfacial tension between water and oil) is opposed by the resultant of the solid and liquid forces (solid-oil and solid-water interfacial tensions). This difference in opposing forces is called the adhesion tension.

$$At = \sigma so - \sigma sw = \sigma wo \cos \theta wo \qquad \text{Eq. 9.1}$$

A_t is the adhesion tension.

From the above, we can refer to the wettability as adhesion tension with various intensity: strong, intermediate and weak.

9.1.2. **Difference in CO_2 endpoint relative permeabilities**

In some cases (Figure 9.2), it has been observed that there is different in CO_2 endpoint relative permeability although the used samples had been extracted from the same formation and showed almost identical throat distribution.

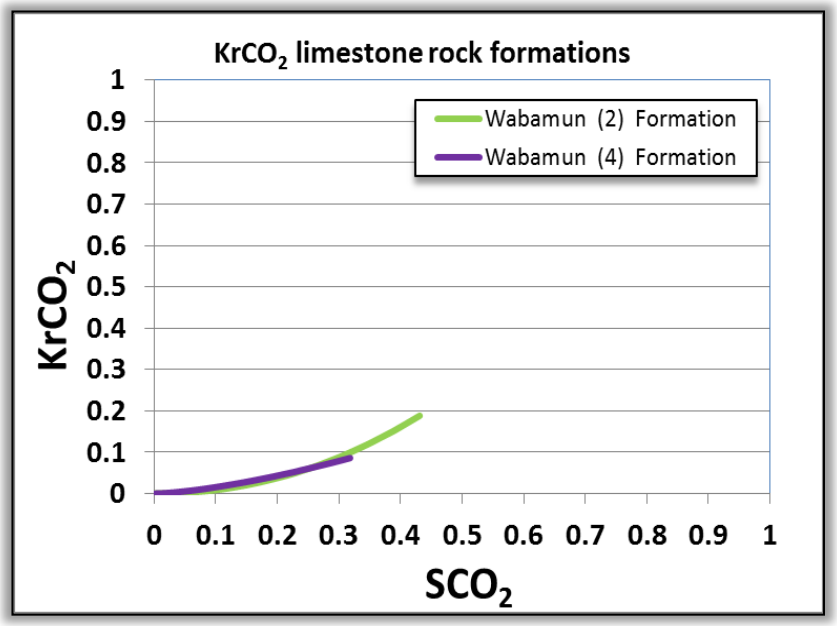

Figure 9.2: Different cases of contact angle (Sciences, 2013)

I attributed that difference to wettability distribution, explained below:

9.1.3. **Wettability distribution**

It is known that the wettability intensity is not equal throughout a single formation, but it may cover a broad spectrum (strong, intermediate, weak).

Therefore, wettability distribution is a new conception that gives an idea about the percentage of each intensity degree to wettability or adhesion tension in the whole rock formation.

9.1.4. **Wettability and relative permeability**

Based on Figure 9.3:

- There are two types of displacements; one for free layers and the other for adherent layers. And as a logical sequence, the displacement starts firstly in free layers and then for adherent layers.
- Since the adherent layers represent a small part of the total wetting phase, the main body to non-wetting phase relative permeability curve will be produced as a result of displacement in the free layers of wetting phase.

So wettability intensity could be identified in the following figures:

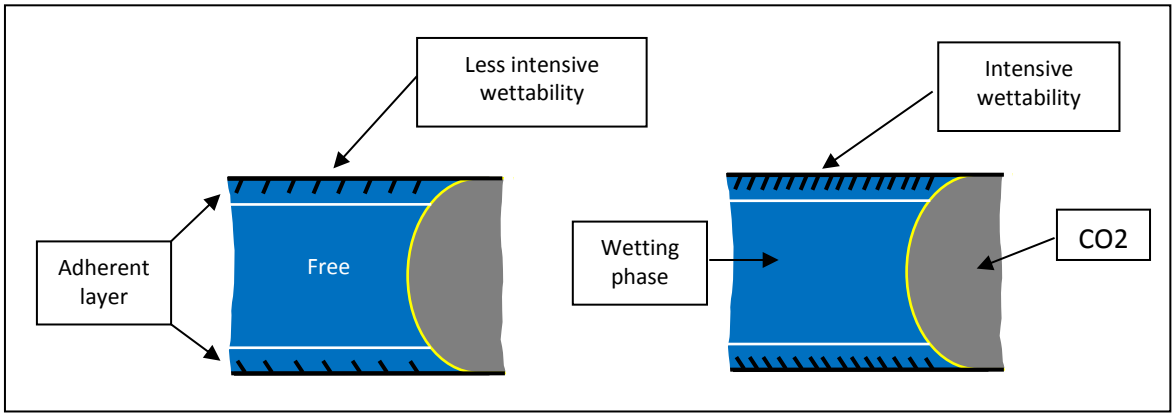

Figure 9.3: Different types of wettability intensity

According to above, the effect of wettability on the endpoint relative permeability values could be predicted as in the subsequent Figure 9.4 :

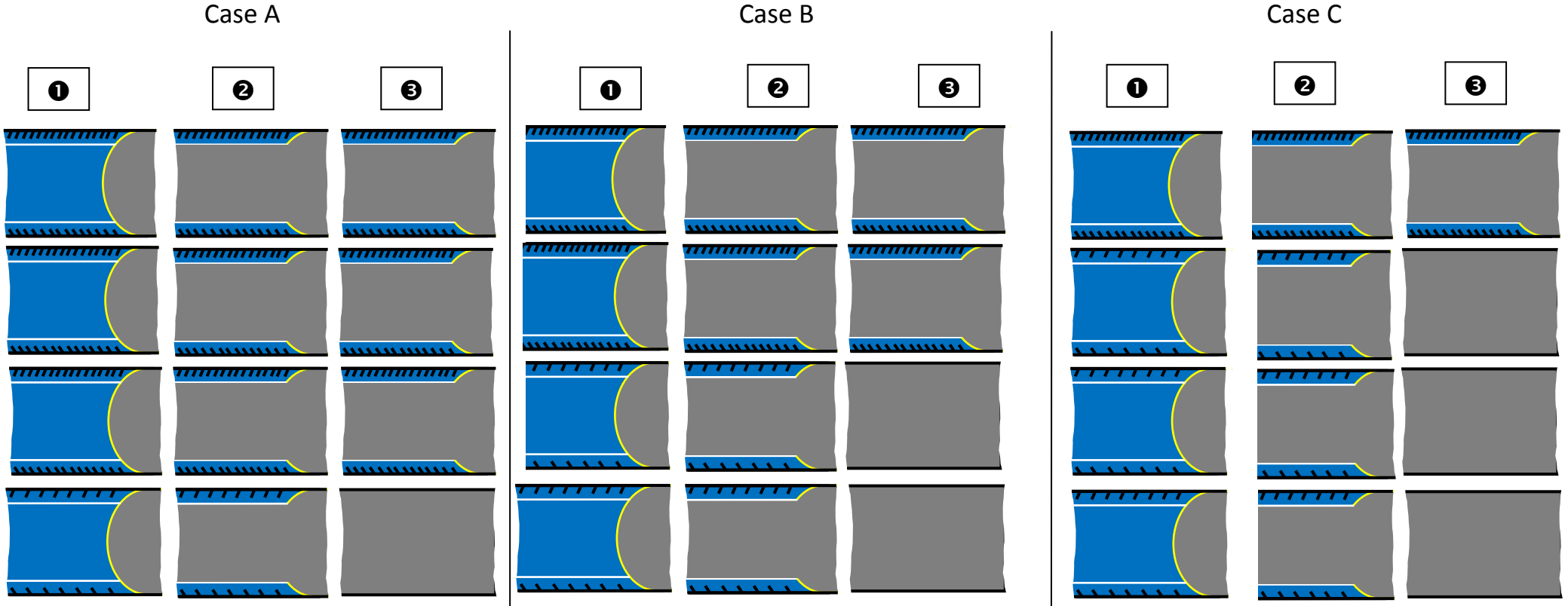

Column ❶ represents a case with majority of intensive wettability and before invading start. Column ❷ represents displacement of free layers that generates the main body to relative permeability curve, whereas the last figure in column ❸ represents extra displacement in adherent layers which raises the endpoint relative permeability.

Column ❶ less intensive wettability (last two figures), column ❸ represents extra displacement done in adherent layers which introduces more increase to endpoint relative permeability than that in case A.

Column ❶ represents a case with majority of less intensive wettability, column ❸ represents extra displacement done in adherent layers which adds more increase to endpoint relative permeability than that in case B.

Figure 9.4: The effect of wettability on the endpoint relative permeability values

9.1.5. **Conclusion**

The wettability distribution impacts mainly endpoint relative permeability value, in the last part of relative permeability curve.

9.2. The difference between relative permeabilities of CO_2 and other gases in terms of interfacial tension

9.2.1. Introduction

According to Asar and Handy (1988), in the gas-oil system, it was found that the relative permeability of gas starts to give values at very low IFT 0.82 mN/m; it also increases through a range of very low IFT values from 0.82 to 0.03 mN/m (Figure 9.5).

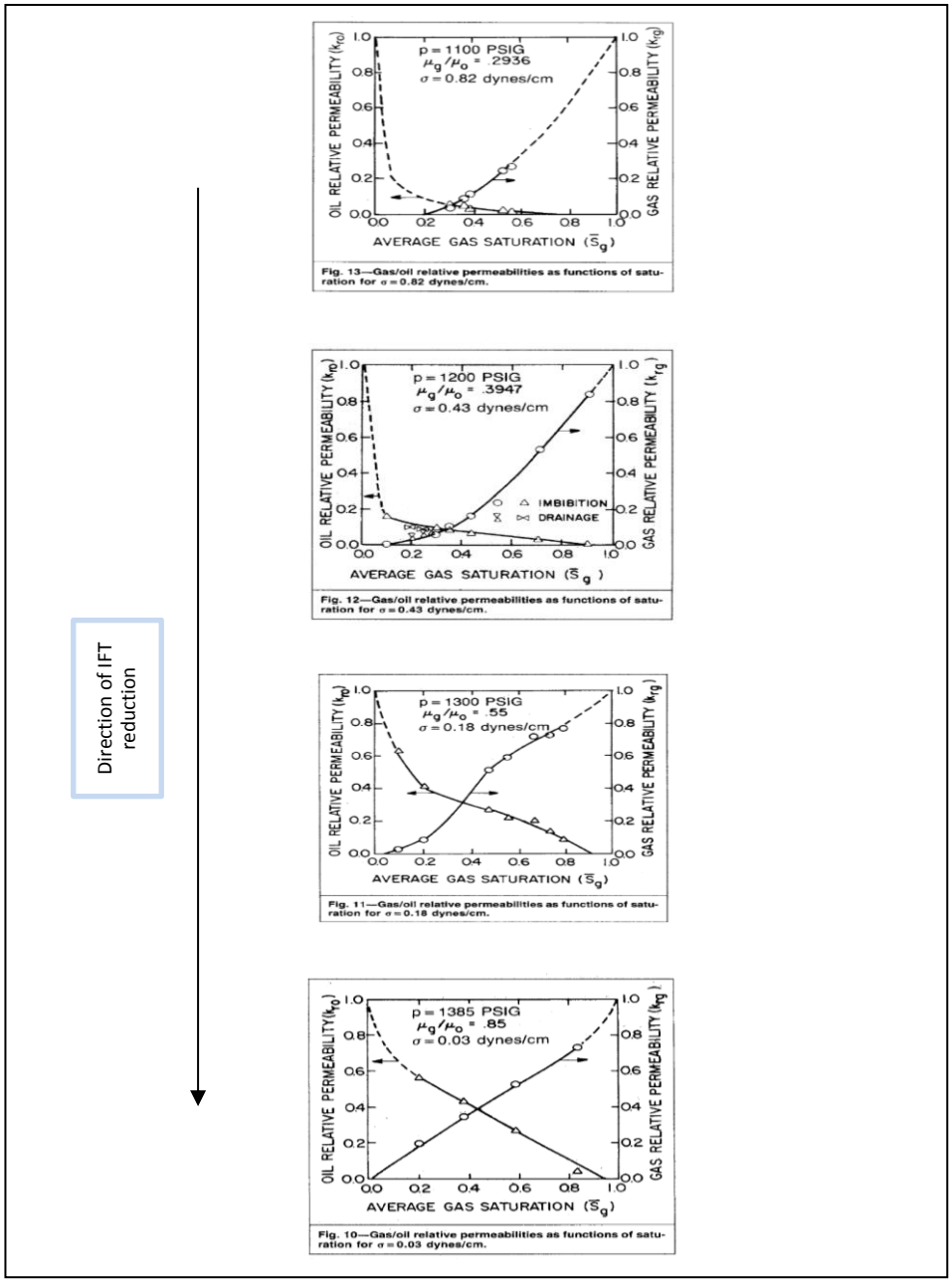

Figure 9.5: Effect of IFT on relative permeability values in gas-oil system (Asar and Handy, 1988)

On the other hand, in CO_2-Brine system (Bennion and Bachu, 2006c), it was found that the relative permeability of gas starts to give values at very high IFT 56.2 mN/m, and also increases through a range of very high IFT values from 56.2 to 19.8 mN/m (Figure 9.6).

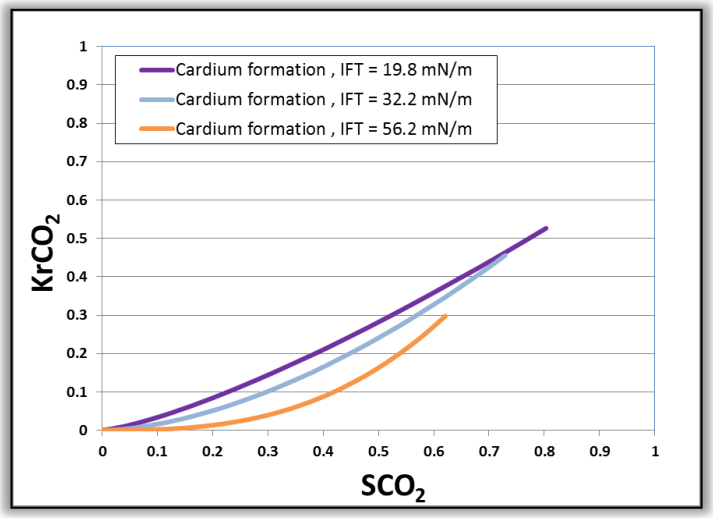

Figure 9.6: Effect of IFT on $KrCO_2$ during drainage for one formation (Bennion and Bachu, 2006c)

The question is why the relative permeability of gas in gas-oil system increases through a range of very low IFT, while in brine-gas system, the relative permeability of gas increases through a range of very high IFT, compared with that in gas-oil system.

The above phenomena could be interpreted section 9.2.2:

9.2.2. **The theory of displacement sequence:**

If a non-wetting phase is being injected to displace the wetting phase, it is known that the initial values of non-wetting phase relative permeability come from displacing the wetting phase from the big throats, and the increase in that relative permeability is due to displacing the wetting phase from the other medium and small throats respectively. This sequence in wetting phase displacing (according to throat size) is due to the fact that the resistance force against displacement (wetting phase capillary pressure) is greater as the throat size is smaller.

The wetting phase consists of many layers (multi-layer); the first layer is adherent on the throat wall, while the other is free and located in the centre of the throat. Since the resistance (particularly due to wettability force) in adherent layer is much greater than that in free layer, and according to displacement sequence mentioned in the previous paragraph, the displacing will be, firstly, for wetting phase free layer in large throat and then for free layer in medium and small throats. After that, the displacing will be for wetting phase adherent layer in big throats, then for medium and small throats respectively. The arrangement of displacing could be represented graphically (Figure 9.7).

A, B, and C are the initial cases of the pore channels (at the beginning of injection). No (1) represents the early values of non-wetting phase relative permeability, while (2) and (3) represent the increase in non-wetting phase relative permeability during the injection, whereas (4, 5), and (6) represent the last points in the range values of non-wetting phase relative permeability.

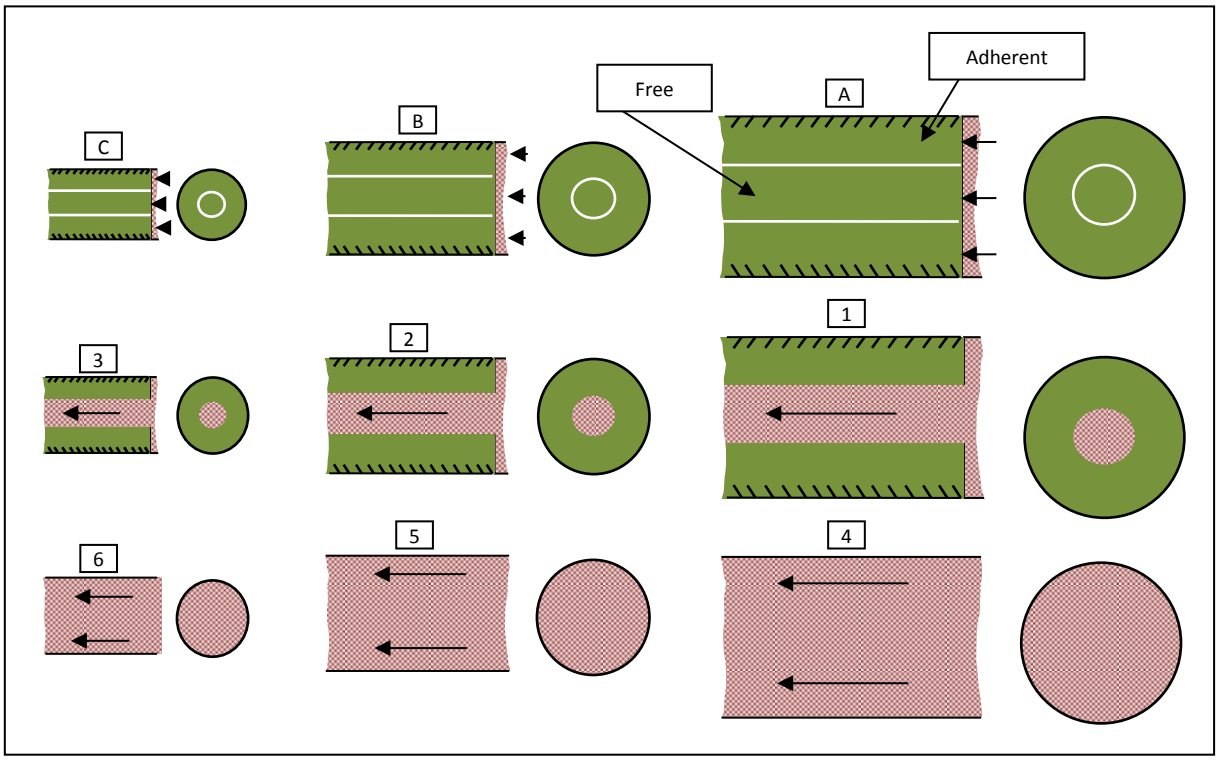

Figure 9.7: The theory of displacement sequence.

9.2.3. **Interfacial tension and non-wetting phase relative permeability during injection process.**

If non-wetting phase displaces the wetting phase by the effect of non-wetting phase mass pressure, it is known that the non-wetting phase will confront resistant forces. These forces are IFT (repulsion forces between different molecules at the interface) and wetting phase capillary forces that consist of:

A) Wetting phase pressure, which increases as wetting phase saturation goes up, and also increases as pores and throats diameter reduces.

B) Wetting phase wettability and weight forces

C) Wetting phase viscosity

In this case, the forces acting on the interface between the wetting and non-wetting phases are the pressures of both wetting and non-wetting phase, in addition to repulsion forces between different molecules at the interface.

The interfacial tension, as known, is the summation these forces[7], which produces resistance to displace the wetting phase by the non-wetting phase; therefore, as the value of interfacial tension increases, it means the wetting phase pressure is higher and higher, and as a result, the displacement of wetting phase by non-wetting phase will be more difficult. All that will negatively affect non-wetting phase relative permeability by reducing the number of invaded throats (capillary channels) that produce non-wetting phase relative permeability value.

[7] It is admissible that, at the interface, the mass pressures of both wetting and non-wetting phase are much greater than repulsion forces between different molecules.

9.2.4. So depending on information from paragraphs (9.2.2, 9.2.3), and as graphically presented in Figure 9.8 we can say that, in the system of gas-oil, the thickness of free layer is very high, so the major part of wetting phase pressure is concentrated in that free layer, and to displace this free layer (in order to produce non-wetting phase relative permeability), a high injection pressure should be applied. That leads the interfacial tension decreased to be very low as 0.82 mN/m. By contrast, in the system of Co_2-Brine, the thickness of free layer is very low, so the major part of wetting phase pressure concentrates in adherent layer rather than free layer; consequently, low injection pressure is enough to displace the wetting phase free layer, and as a result the interfacial tension decreases by a very small amount and stayes at a very high value as 56.2 mN/m. All that could be represented graphically below.

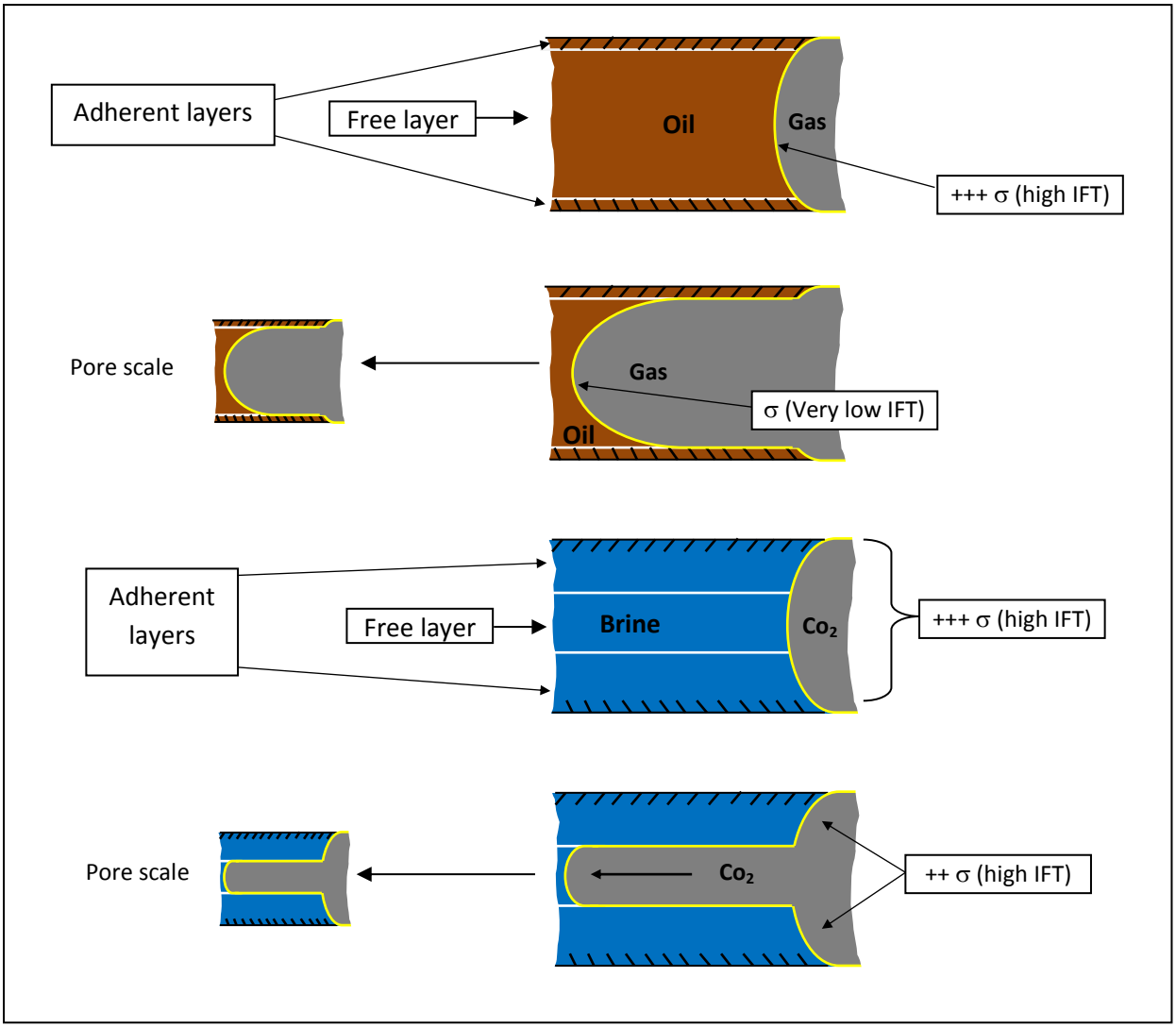

Figure 9.8: Interfacial tension and free layer during injection process (pore-scale)

References

ASAR, H. & HANDY, L. L. 1988. Influence of Interfacial Tension on Gas/Oil Relative Permeability in a Gas-Condensate System. *SPE Reservoir Engineering,* 3**,** 257-264.

BENNION, D. B. & BACHU, S. 2006c. Dependence on Temperature, Pressure, and Salinity of the IFT and Relative Permeability Displacement Characteristics of CO2 Injected in Deep Saline Aquifers. *SPE Annual Technical Conference and Exhibition.* San Antonio, Texas, USA: Society of Petroleum Engineers.

HONARPOUR, M. M., KOEDERITZ, F. & HERBERT, A. 1986. *Relative permeability of petroleum reservoirs*.

SCIENCES, S. O. E. 2013. *Relative Permeability Explorer* [Online]. Stanfod university. Available: https://pangea.stanford.edu/research/bensonlab/relperm/index.html.

Chapter 10

Conclusion and recommendation

1. The difference in pore and throat structures of the rock (rock quality), in terms of pore and throat distributions, very significantly impacts CO_2 relative permeability, and consequently, a variety in CO_2 relative permeability curves should be expected even for samples extracted from the same site with almost identical capillary properties.

   Based on the definition, a normal pore and throat distribution with similar connection produced a regular CO_2 relative permeability curve shape that appears as a diagonal line showing a clear direct relationship between the relative permeability and saturation data. The impact of some important factors like IFT and interference could be remarked obviously; for instance, the impact of IFT comes into sight as a depression in the slope degree to the general curve (Figure 10.1 a), while the exponential function shape is considered as a result of the interference parameter effect (Figure 10.1 b). Disappearance of these factors returns the CO_2 relative permeability line to straight line shape with 45° angle.

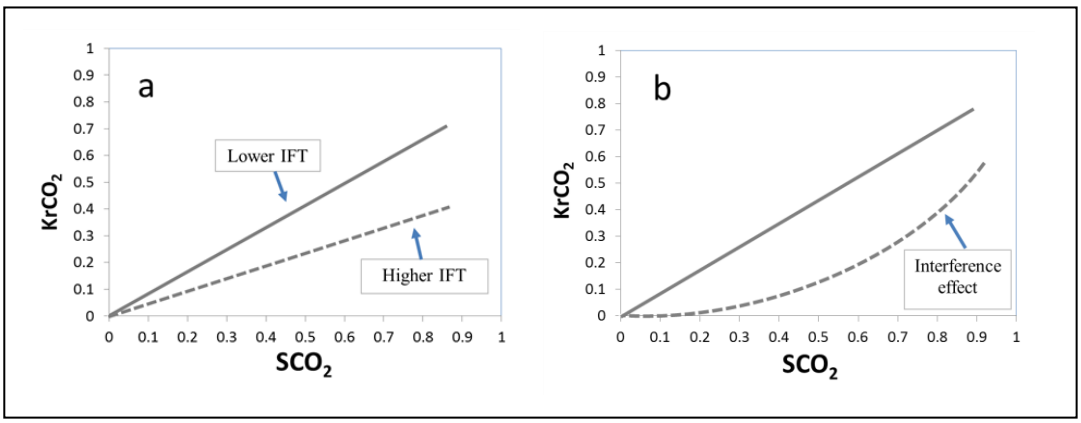

Figure 10.1: Normal pore and throat distributions with similar connection produced a regular CO_2 relative permeability curve shape; a) impact of IFT on $KrCO_2$ curve, b) interference effect on $KrCO_2$ curves.

By contrast, in the abnormal pore and throat distributions with dissimilar connection, the CO_2 relative permeability produced an irregular curve shape and is almost vertical (Figure 10.2). Furthermore, the impact of the factors including IFT and interference could not be evaluated easily.

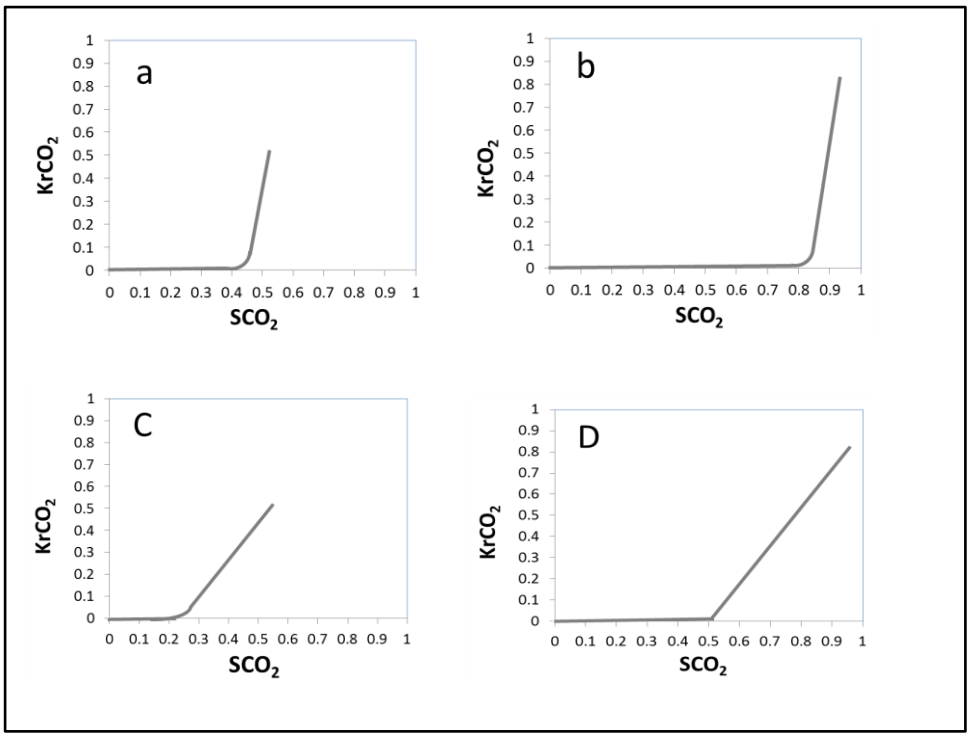

Figure 10.2: Abnormal pore and throat distributions with similar connection produced an irregular CO_2 relative permeability curve shape (almost vertical).

Generally, the concept presented (pore and throat distributions) will help considerably in reading, understanding and interpreting the CO_2 relative permeability curves, particularly in regard to those issues that had not been clarified adequately; for instance, Bennion and Bachu (2008a) mentioned that the Corey exponent is a measure of curve concavity (curvature), and they added that the curve concavity (curvature) may refer to the impact of interference phenomena or the heterogeneity effect. In the end, they concluded that it has been identified that the Corey's exponent refers more to interference than to heterogeneity, which matches exactly what had already been mentioned here in detail.

2. As known, the previous old concept of the pore size distribution was considered as a measure of pore throat diameter and the fraction of total-pore-space (porosity) represented by each diameter, whereas the new concept presented here as "pore and throat distribution" introduces a different meaning; for instance, the throat size distribution is a measure of throat diameter and the percentage of the absolute permeability at the outlet part represented by each throat size, and the same way in regard to the pore size distribution and porosity.

3. Reconsidering the factors[8] impacting on $KrCO_2$ (not the $KrCO_2$ itself) as the main reasons leading to CO_2 injection rate to be variant for a group of formations.

4. The results of this study will allow identification of rocks that would be more suitable for CO_2 injection (higher injection rate, thus lower time and cost) on the basis of the structure and distribution of the pores and throats of the rock, particularly in the formation where the injection rate could not be elevated by increasing the injection pressure due to restrictions in caprock's entry and fracturing pressures.

5. As known and as it appears in paragraph 2.7.7, the methods whereby the CO_2 relative permeability is measured are considered as one of the main factors impacting CO_2 relative permeability values, so designing and applying an assessment package tool (as suggested in this study) to verify the protocols and data measured, with recommendations to avoid errors, will help a lot in getting accurate data with high ability to represent the target formations.

6. As there are a lot of factors influencing the CO_2 relative permeability data (paragraph 2.7.7) whether they are measured or estimated, and as known, there is some disagreement or inconsistency in the literature about how these factors (in terms of their mechanisms) impact the CO_2 relative permeability and defining which of these factors has or have the major impact on CO_2 relative permeability, all that will affects the way by which the CO_2 relative permeability curve could be read and interpreted. The important notes mentioned in chapter 4 may help substantially in this matter and also to establish a widely acceptable way to read and interpret CO_2 relative permeability curves correctly.

7. In many cases, it has been confirmed that using empirical or experimental modelling will be absolutely illogical; consequently, the theoretical modelling, consisting of digital pore-network (digital core) and pore-scale fluid flow simulator, will be inevitable; furthermore the lower cost and faster processing are some of the advanced advantages of applying theoretical modelling, particularly in time-limited researches.

8. The wettability distribution is also a new concept that has been introduced as a factor which controls the magnitude of CO_2 endpoint relative permeability for rock samples having the same rock and capillary properties.

[8] Like pore and throat distribution.

Recommendation for future work

1. Studying other factors impacting CO_2 relative permeability by using the same technique, which depends on freezing the effect of all other factors except the one targeted for study, will introduce a very good addition to understanding the mechanisms of how each parameter impacts the CO_2 relative permeability and make it variant.

2. Extending the work mentioned in the last paragraph to include the impact on the CO_2 injection characteristics (injection rate for instance).

3. Using a real model for oil reservoirs whether depleted or under development for enhanced oil recovery, rather than the real aquifer model applied in this study.

4. Develop the assessment package tools used to verify the protocols and data measured in CO_2 relative permeability experiments, adding more recommendations to avoid errors, introduce more notes about how to read and interpret the CO_2 relative permeability curves in accurate mode; all that will help in creating something that could be adopted as a reference to all researchers interested in the CO_2 relative permeability discipline.

5. Studying widely the differences among the systems CO_2-Brine, CO_2-oil, CO_2-oil-Brine, in terms of capillary properties, must be given much attention.

Appendix

A) CO_2 relative permeability data published and collected

A.1) **Carbonate rock**

A.1.1) Dolomite

Cooking Lake (1) formation (Dolomite)

Drainage			
CO_2 Saturation Fraction	Krg	Water Saturation Fraction	Krw
0.000	0.0000	1.0000	1.0000
0.026	0.0000	0.9740	0.8432
0.052	0.0001	0.9480	0.7046
0.079	0.0001	0.9210	0.5828
0.105	0.0002	0.8950	0.4768
0.131	0.0002	0.8690	0.3851
0.157	0.0003	0.8430	0.3067
0.183	0.0005	0.8170	0.2403
0.210	0.0008	0.7900	0.1848
0.236	0.0014	0.7640	0.1391
0.262	0.0022	0.7380	0.1021
0.288	0.0034	0.7120	0.0727
0.314	0.0052	0.6860	0.0499
0.341	0.0077	0.6590	0.0329
0.367	0.0111	0.6330	0.0205
0.393	0.0157	0.6070	0.0120
0.419	0.0218	0.5810	0.0065
0.445	0.0297	0.5550	0.0032
0.472	0.0398	0.5280	0.0014
0.498	0.0526	0.5020	0.0005
0.524	0.0685	0.4760	0.0000

Imbibition			
Water Saturation Fraction	Krw	CO_2 Saturation Fraction	Krg

Formation Name	Lithology	Avg Porosity %	Ka (mD)	Depth (m)	Core length (cm)	Core diameter (cm)	Flow area (cm^2)	Temp (°C)	pore volume injected (cc)	Pore pressure (kPag)	Flow Rate [Ml/min]	Interfacial tension (mN/m)	Pc (kPa)	Salinity (mg/L)	Method used	Viscosity ratio μ_{brine} / μ_{Co2}
Cooking Lake (1)	Dolomite	9.9	645	1893	14.38	3.81	11.4	55	16.16	15400	-	35.74	11.1	233400	Unsteady state	15.43

Table A. 1: Relative permeability data for Cooking Lake (1) formation (Dolomite) (Bennion and Bachu, 2005, Bennion and Bachu, 2006a, Bachu and Bennion, 2008, Bennion and Bachu, 2008a, Sciences, 2013, Survey, 2013)

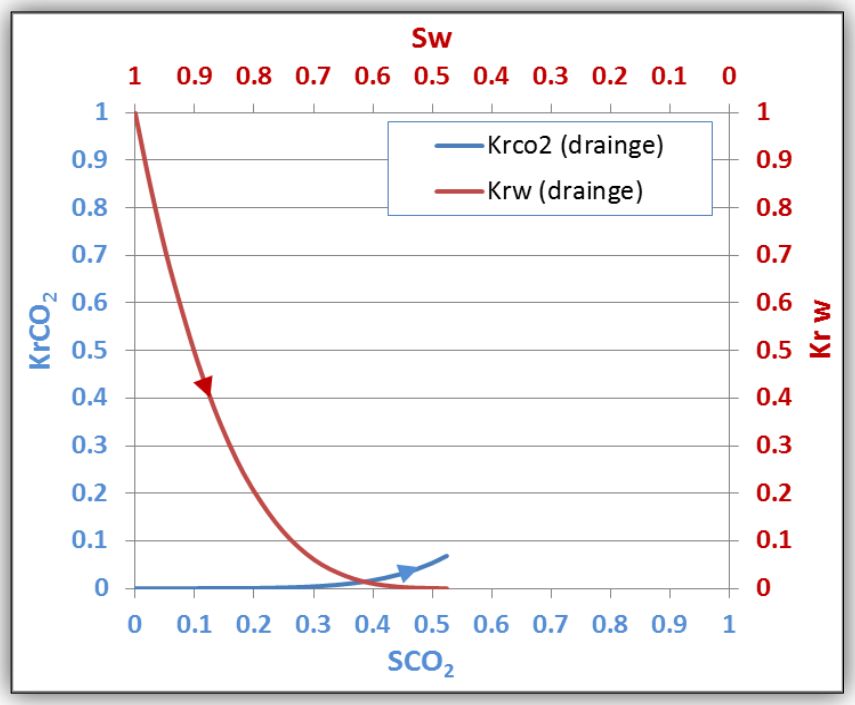

Figure A. 1: Relative permeability curves for Cooking Lake (1) formation (Dolomite) (Bennion and Bachu, 2005)

Cooking Lake (2) formation (Dolomite)

		Drainge		Imbibition	
S_{gr} =	0.268	ng =	5.44	ng =	1.15
S_{wir} =	0.5963	nw =	1.83	nw =	1.7
Krg (wir) =	0.094				
Krw (gr) =	0.0788				

Drainage

CO_2 Saturation Fraction	Krg	Water Saturation Fraction	Krw
0.0000	0.0000	1.0000	1.0000
0.0237	0.0000	0.9763	0.8952
0.0474	0.0000	0.9526	0.7957
0.0711	0.0000	0.9289	0.7015
0.0948	0.0000	0.9052	0.6127
0.1185	0.0001	0.8815	0.5295
0.1422	0.0003	0.8578	0.4517
0.1659	0.0007	0.8341	0.3796
0.1896	0.0015	0.8104	0.3133
0.2133	0.0029	0.7867	0.2528
0.2370	0.0052	0.7630	0.1982
0.2607	0.0087	0.7393	0.1497
0.2844	0.0140	0.7156	0.1074
0.3081	0.0216	0.6919	0.0716
0.3318	0.0323	0.6682	0.0425
0.3555	0.0471	0.6445	0.0205
0.3792	0.0669	0.6208	0.0059
0.4037	**0.0940**	**0.5963**	0.0000

Imbibition

Water Saturation Fraction	Krw	CO_2 Saturation Fraction	Krg
0.5963	0.0000	0.4037	**0.0940**
0.6042	0.0006	0.3958	0.0877
0.6121	0.0020	0.3879	0.0815
0.6200	0.0041	0.3800	0.0754
0.6279	0.0066	0.3721	0.0693
0.6358	0.0097	0.3642	0.0633
0.6437	0.0132	0.3563	0.0573
0.6516	0.0171	0.3484	0.0515
0.6595	0.0215	0.3405	0.0457
0.6674	0.0263	0.3326	0.0400
0.6753	0.0314	0.3247	0.0345
0.6832	0.0369	0.3168	0.0290
0.6911	0.0428	0.3089	0.0237
0.6990	0.0491	0.3010	0.0185
0.7069	0.0557	0.2931	0.0135
0.7148	0.0626	0.2852	0.0087
0.7227	0.0698	0.2773	0.0043
0.7320	**0.0788**	**0.2680**	0.0000

Formation Name	Lithology	Avg Porosity %	Ka (mD)	Depth (m)	Core length (cm)	Core diameter (cm)	Flow area (cm^2)	Temp (°C)	pore volume injected (cc)	Pore pressure (kPag)	Flow Rate [Ml/min]	Interfacial tension (mN/m)	Pc (kPa)	Salinity (mg/L)	Method used	Viscosity ratio μ_{brine} / μ_{Co2}
Cooking Lake (2)	Dolomite	9.9	645	1893	14.38	3.81	11.4	55	16.16	15400	-	35.74	11.1	233400	Unsteady state	

Table A. 2: Relative permeability data for Cooking Lake (2) formation (Dolomite), (Bennion and Bachu, 2010, Bennion and Bachu, 2006a, Bachu and Bennion, 2008, Bennion and Bachu, 2008a, Sciences, 2013, Survey, 2013)

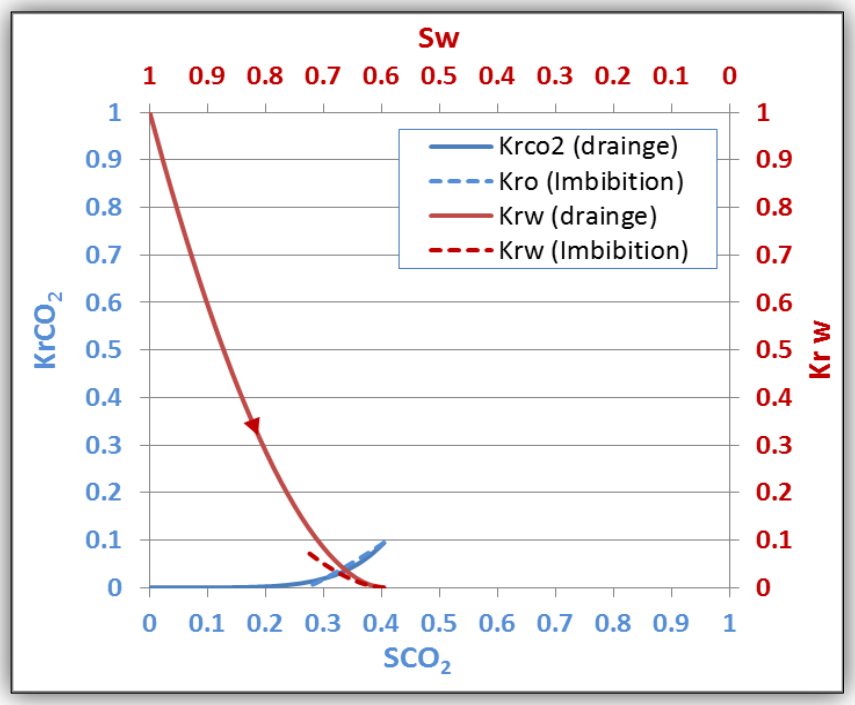

Figure A. 2: Relative permeability curves for Cooking Lake (2) formation (Dolomite), (Bennion and Bachu, 2010)

Nisku (1) formation (Dolomite)

Drainage			
CO_2 Saturation Fraction	Krg	Water Saturation Fraction	Krw
0.000	0.0000	1.0000	1.0000
0.034	0.0066	0.9660	0.8670
0.067	0.0141	0.9330	0.7461
0.101	0.0220	0.8990	0.6365
0.134	0.0302	0.8660	0.5380
0.168	0.0385	0.8320	0.4499
0.201	0.0471	0.7990	0.3719
0.235	0.0558	0.7650	0.3028
0.268	0.0646	0.7320	0.2428
0.302	0.0735	0.6980	0.1911
0.335	0.0825	0.6650	0.1471
0.368	0.0917	0.6320	0.1103
0.402	0.1008	0.5980	0.0801
0.435	0.1101	0.5650	0.0558
0.469	0.1195	0.5310	0.0370
0.502	0.1289	0.4980	0.0229
0.536	0.1383	0.4640	0.0129
0.569	0.1479	0.4310	0.0064
0.603	0.1575	0.3970	0.0026
0.636	0.1671	0.3640	0.0007
0.670	0.1768	0.3300	0.0000

Imbibition			
Water Saturation Fraction	Krw	CO_2 Saturation Fraction	Krg

Formation Name	Lithology	Avg Porosity %	Ka (mD)	Depth (m)	Core length (cm)	Core diameter (cm)	Flow area (cm^2)	Temp (°C)	pore volume injected (cc)	Pore pressure (kPag)	Flow Rate [Ml/min]	Interfacial tension (mN/m)	Pc (kPa)	Salinity (mg/L)	Method used	Viscosity ratio μ_{brine} / μ_{Co2}
Nisku 1	Dolomite	9.6	84	2049.9	3.2	3.81	11.4	56	3.54	17400	-	34.6	58	136800	Unsteady state	11.8

Table A. 3: Relative permeability data for Nisku (1) formation (Dolomite) (Bennion and Bachu, 2005, Bennion and Bachu, 2006a, Bachu and Bennion, 2008, Bennion and Bachu, 2008a, Survey, 2013)

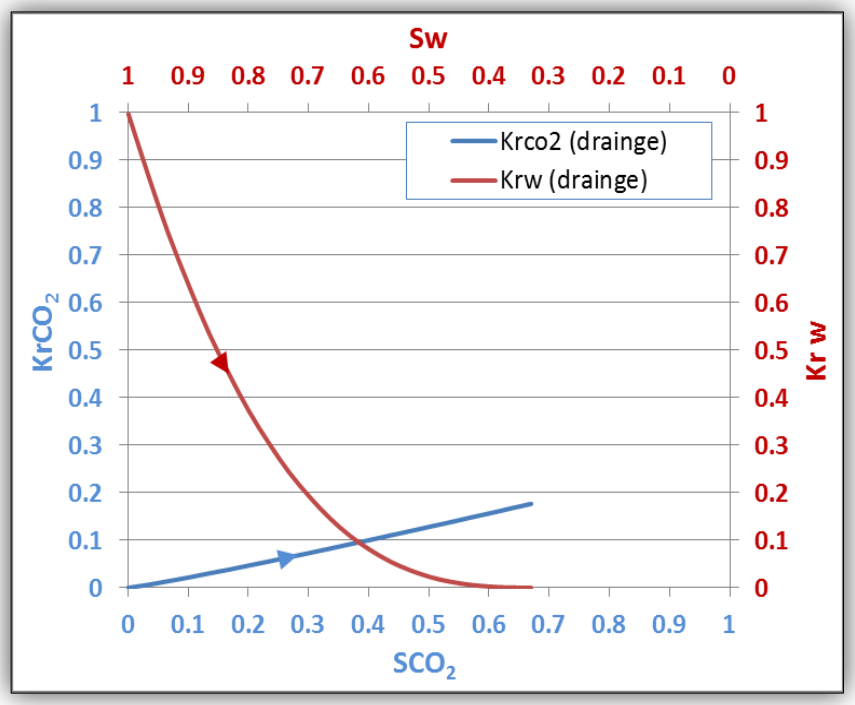

Figure A. 3: Relative permeability curves for Nisku (1) formation (Dolomite) (Bennion and Bachu, 2005)

Nisku (2) formation (Dolomite)

Drainage			
CO_2 Saturation Fraction	Krg	Water Saturation Fraction	Krw
0.0000	0.0000	1.0000	1.0000
0.0250	0.0000	0.9750	0.8698
0.0510	0.0001	0.9490	0.7509
0.0760	0.0002	0.9240	0.6429
0.1020	0.0003	0.8980	0.5454
0.1270	0.0004	0.8730	0.4578
0.1520	0.0007	0.8480	0.3798
0.1780	0.0011	0.8220	0.3108
0.2030	0.0019	0.7970	0.2504
0.2290	0.0029	0.7710	0.1981
0.2540	0.0046	0.7460	0.1533
0.2790	0.0069	0.7210	0.1157
0.3050	0.0100	0.6950	0.0845
0.3300	0.0143	0.6700	0.0594
0.3560	0.0198	0.6440	0.0396
0.3810	0.0270	0.6190	0.0247
0.4060	0.0362	0.5940	0.0141
0.4320	0.0476	0.5680	0.0070
0.4570	0.0618	0.5430	0.0028
0.5080	0.0999	0.4920	0.0000

Imbibition			
Water Saturation Fraction	Krw	CO_2 Saturation Fraction	Krg
0.4920	0.0000	0.5080	0.0999
0.5070	0.0011	0.4930	0.0800
0.5210	0.0042	0.4790	0.0633
0.5360	0.0096	0.4640	0.0495
0.5500	0.0176	0.4500	0.0381
0.5650	0.0281	0.4350	0.0289
0.5790	0.0414	0.4210	0.0215
0.5940	0.0575	0.4060	0.0157
0.6080	0.0765	0.3920	0.0112
0.6230	0.0985	0.3770	0.0078
0.6370	0.1234	0.3630	0.0053
0.6520	0.1515	0.3480	0.0035
0.6660	0.1827	0.3340	0.0022
0.6810	0.2171	0.3190	0.0014
0.6950	0.2546	0.3050	0.0008
0.7100	0.2955	0.2900	0.0005
0.7240	0.3396	0.2760	0.0003
0.7390	0.3871	0.2610	0.0002
0.7530	0.4380	0.2470	0.0001
0.7820	0.5500	0.2180	0.0000

Formation Name	Lithology	Avg Porosity %	Ka (mD)	Depth (m)	Core length (cm)	Core diameter (cm)	Flow area (cm^2)	Temp (°C)	pore volume injected (cc)	Pore pressure (kPag)	Flow Rate [Ml/min]	Interfacial tension (mN/m)	Pc (kPa)	Salinity (mg/L)	Method used	Viscosity ratio μ_{brine} / μ_{Co2}
Nisku 2	Dolomite	10.4	21	1953	-	-	-	56	-	17400	-	34.6	3.5	136800	Unsteady state	11.8

Table A. 4: Relative permeability data for Nisku (2) formation (Dolomite) (Bennion and Bachu, 2006a, Survey, 2013, Bachu and Bennion, 2008, Bennion and Bachu, 2008a)

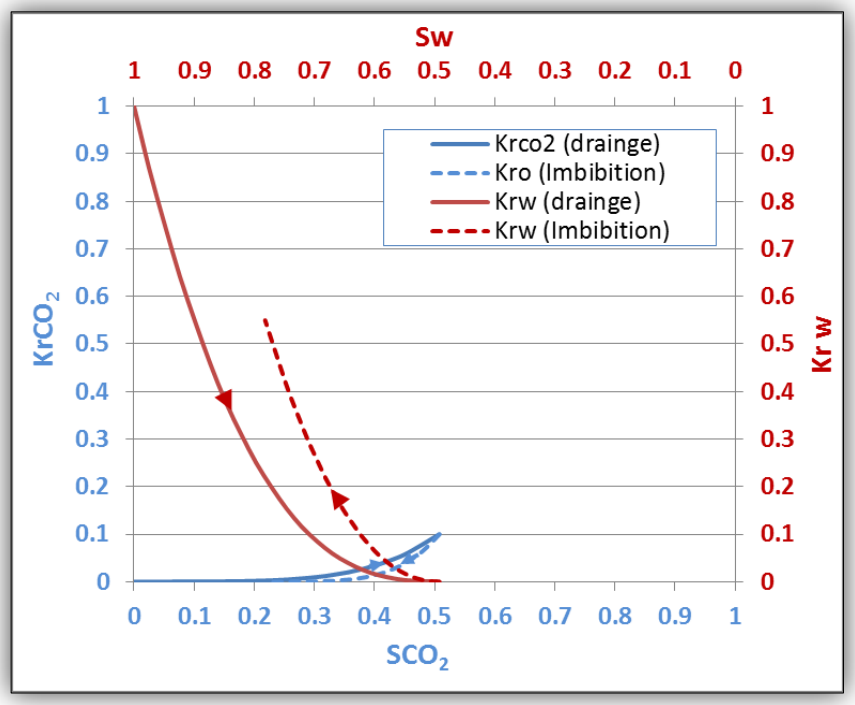

Figure A. 4: Relative permeability curves for Nisku (2) formation (Dolomite) (Survey, 2013)

Nisku (3) formation (Dolomite)

S_{gr} =	0.207	Drainge	Imbibition
S_{wir} =	0.397	ng = 2.93	ng = 2.56
Krg (wir) =	0.1078	nw = 2.27	nw = 1.01
Krw (gr) =	0.3821		

Drainage

CO_2 Saturation Fraction	Krg	Water Saturation Fraction	Krw
0.0000	0.0000	1.0000	1.0000
0.0350	0.0000	0.9650	0.8731
0.0700	0.0002	0.9300	0.7557
0.1050	0.0006	0.8950	0.6477
0.1400	0.0015	0.8600	0.5490
0.1750	0.0029	0.8250	0.4593
0.2100	0.0049	0.7900	0.3784
0.2450	0.0077	0.7550	0.3062
0.2800	0.0114	0.7200	0.2424
0.3150	0.0161	0.6850	0.1869
0.3500	0.0219	0.6500	0.1392
0.3850	0.0290	0.6150	0.0993
0.4200	0.0374	0.5800	0.0667
0.4550	0.0472	0.5450	0.0412
0.4900	0.0587	0.5100	0.0223
0.5250	0.0718	0.4750	0.0096
0.6030	0.1078	0.3970	0.0000

Imbibition

Water Saturation Fraction	Krw	CO_2 Saturation Fraction	Krg
0.3970	0.0000	0.6030	0.1078
0.4200	0.0216	0.5800	0.0925
0.4430	0.0434	0.5570	0.0786
0.4660	0.0654	0.5340	0.0660
0.4890	0.0875	0.5110	0.0548
0.5120	0.1096	0.4880	0.0448
0.5350	0.1318	0.4650	0.0360
0.5580	0.1540	0.4420	0.0283
0.5810	0.1762	0.4190	0.0218
0.6040	0.1984	0.3960	0.0162
0.6270	0.2207	0.3730	0.0116
0.6500	0.2430	0.3500	0.0079
0.6730	0.2654	0.3270	0.0051
0.6960	0.2877	0.3040	0.0029
0.7190	0.3101	0.2810	0.0015
0.7420	0.3324	0.2580	0.0006
0.7930	0.3821	0.2070	0.0000

Formation Name	Lithology	Avg Porosity %	Ka (mD)	Depth (m)	Core length (cm)	Core diameter (cm)	Flow area (cm^2)	Temp (°C)	pore volume injected (cc)	Pore pressure (kPag)	Flow Rate [Ml/min]	Interfacial tension (mN/m)	Pc (kPa)	Salinity (mg/L)	Method used	Viscosity ratio μ_{brine} / μ_{Co2}
Nisku 3	Dolomite	10.9	74.4	1179.5	-	-	-	56	-	17400	-	34.6	28.2	136800	Unsteady state	

Table A. 5: Relative permeability data for Nisku (3) formation (Dolomite) (Bennion and Bachu, 2010, Bennion and Bachu, 2006a, Bachu and Bennion, 2008, Bennion and Bachu, 2008a, Sciences, 2013, Survey, 2013, Mathias et al., 2013)

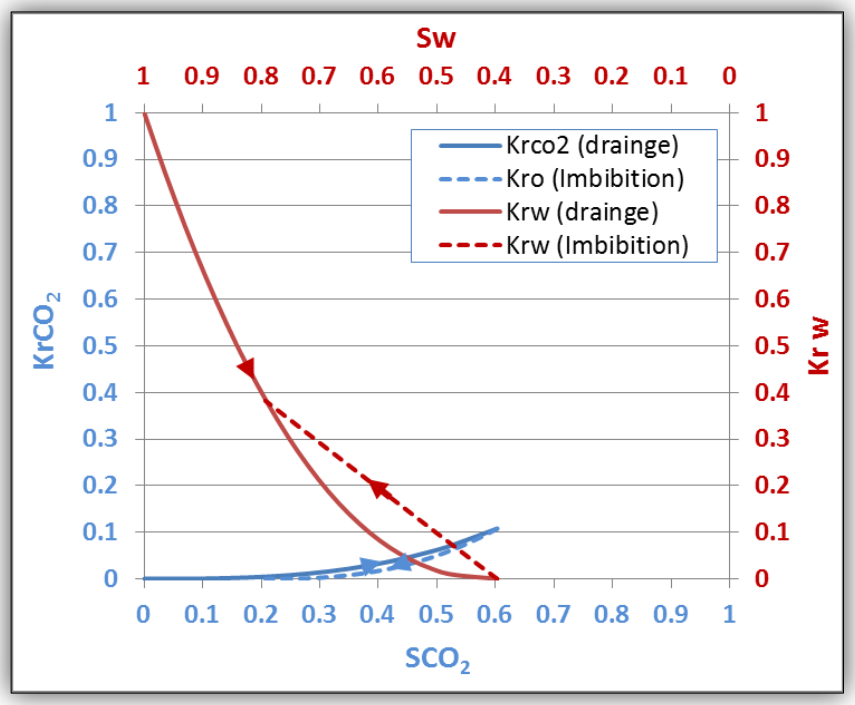

Figure A. 5: Relative permeability curves for Nisku (3) formation (Dolomite), (Bennion and Bachu, 2010)

Grosmont formation (Dolomite)

		Drainge		Imbibition	
S_{gr} =	0.356				
S_{wir} =	0.520	ng =	5.19	ng =	2.76
Krg (wir) =	0.1101	nw =	1.73	nw =	2.25
Krw (gr) =	0.0249				

Drainage

CO_2 Saturation Fraction	Krg	Water Saturation Fraction	Krw
0.0000	0.0000	1.0000	1.0000
0.0280	0.0000	0.9720	0.9012
0.0560	0.0000	0.9440	0.8069
0.0840	0.0000	0.9160	0.7169
0.1120	0.0001	0.8880	0.6315
0.1400	0.0002	0.8600	0.5507
0.1680	0.0005	0.8320	0.4746
0.1960	0.0011	0.8040	0.4034
0.2240	0.0021	0.7760	0.3371
0.2520	0.0039	0.7480	0.2759
0.2800	0.0067	0.7200	0.2199
0.3080	0.0110	0.6920	0.1694
0.3360	0.0173	0.6640	0.1246
0.3640	0.0262	0.6360	0.0857
0.3920	0.0385	0.6080	0.0531
0.4200	0.0551	0.5800	0.0274
0.4800	0.1101	0.5200	0.0000

Imbibition

Water Saturation Fraction	Krw	CO_2 Saturation Fraction	Krg
0.5200	0.0000	0.4800	0.1101
0.5267	0.0000	0.4730	0.0938
0.5336	0.0002	0.4660	0.0791
0.5405	0.0004	0.4590	0.0660
0.5474	0.0008	0.4520	0.0543
0.5543	0.0014	0.4450	0.0441
0.5612	0.0021	0.4380	0.0352
0.5681	0.0030	0.4310	0.0275
0.5750	0.0040	0.4240	0.0210
0.5819	0.0052	0.4170	0.0155
0.5888	0.0066	0.4100	0.0111
0.5957	0.0082	0.4030	0.0076
0.6026	0.0100	0.3960	0.0048
0.6095	0.0120	0.3890	0.0029
0.6164	0.0141	0.3820	0.0015
0.6233	0.0165	0.3750	0.0006
0.6440	0.0249	0.3560	0.0000

Formation Name	Lithology	Avg Porosity %	Ka (mD)	Depth (m)	Core length (cm)	Core diameter (cm)	Flow area (cm^2)	Temp (°C)	pore volume injected (cc)	Pore pressure (kPag)	Flow Rate [Ml/min]	Interfacial tension (mN/m)	Pc (kPa)	Salinity (mg/L)	Method used	Viscosity ratio μ_{brine} / μ_{Co2}
Grosmont	Dolomite	11.8	153.9	502.4	-	-	-	41	-	11900	-	34.2	14.5	144300	Unsteady state	

Table A. 6: Relative permeability data for Grosmont formation (Dolomite) (Bennion and Bachu, 2010, Bennion and Bachu, 2006a, Bachu and Bennion, 2008, Bennion and Bachu, 2008a, Sciences, 2013, Survey, 2013, Mathias et al., 2013)

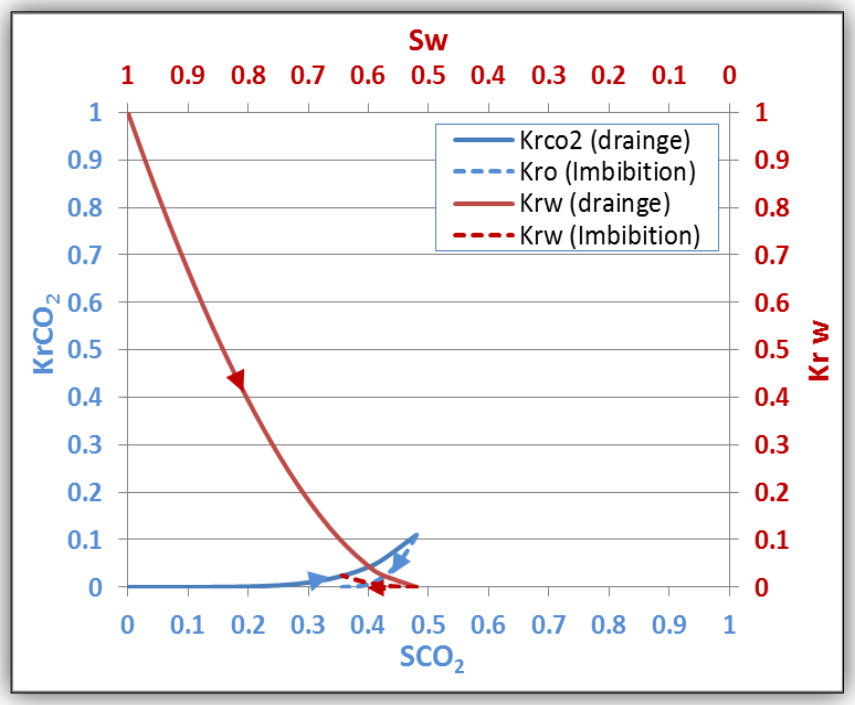

Figure A. 6: Relative permeability curves for Grosmont formation (Dolomite), (Bennion and Bachu, 2010)

Morinville Leduc formation (Dolomite)

		Drainge		Imbibition	
S_{gr} =	0.131				
S_{wir} =	0.530	ng =	3.67	ng =	1.57
Krg (wir) =	0.0746	nw =	1.82	nw =	2.53
Krw (gr) =	0.7888				

Drainage			
CO_2 Saturation Fraction	Krg	Water Saturation Fraction	Krw
0.0000	0.0000	1.0000	1.0000
0.0270	0.0000	0.9730	0.8979
0.0540	0.0000	0.9460	0.8008
0.0810	0.0001	0.9190	0.7087
0.1080	0.0003	0.8920	0.6218
0.1350	0.0008	0.8650	0.5400
0.1620	0.0015	0.8380	0.4634
0.1890	0.0026	0.8110	0.3921
0.2160	0.0043	0.7840	0.3263
0.2430	0.0066	0.7570	0.2659
0.2700	0.0098	0.7300	0.2112
0.2970	0.0138	0.7030	0.1622
0.3240	0.0190	0.6760	0.1191
0.3510	0.0256	0.6490	0.0821
0.3780	0.0335	0.6220	0.0514
0.4050	0.0432	0.5950	0.0273
0.4320	0.0547	0.5680	0.0103
0.4590	0.0684	0.5410	0.0011
0.4700	0.0746	0.5300	0.0000

Imbibition			
Water Saturation Fraction	Krw	CO_2 Saturation Fraction	Krg
0.5300	0.0000	0.4700	0.0746
0.5490	0.0005	0.4510	0.0681
0.5680	0.0031	0.4320	0.0619
0.5870	0.0087	0.4130	0.0559
0.6060	0.0179	0.3940	0.0501
0.6250	0.0316	0.3750	0.0445
0.6440	0.0501	0.3560	0.0392
0.6630	0.0739	0.3370	0.0341
0.6820	0.1037	0.3180	0.0293
0.7010	0.1397	0.2990	0.0248
0.7200	0.1823	0.2800	0.0205
0.7390	0.2320	0.2610	0.0166
0.7580	0.2892	0.2420	0.0129
0.7770	0.3541	0.2230	0.0096
0.7960	0.4271	0.2040	0.0067
0.8150	0.5085	0.1850	0.0042
0.8340	0.5987	0.1660	0.0021
0.8530	0.6980	0.1470	0.0006
0.8690	0.7888	0.1310	0.0000

Formation Name	Lithology	Avg Porosity %	Ka (mD)	Depth (m)	Core length (cm)	Core diameter (cm)	Flow area (cm^2)	Temp (°C)	pore volume injected (cc)	Pore pressure (kPag)	Flow Rate [Ml/min]	Interfacial tension (mN/m)	Pc (kPa)	Salinity (mg/L)	Method used	Viscosity ratio μ_{brine} / μ_{Co2}
Morinville Leduc	Dolomite	11.6	371.9	1185.1	-	-	-	40	-	11400	-	33.1	14.5	103701	Unsteady state	

Table A. 7: Relative permeability data for Morinville formation (Dolomite) (Bennion and Bachu, 2010, Bennion and Bachu, 2006a, Bachu and Bennion, 2008, Bennion and Bachu, 2008a, Sciences, 2013, Survey, 2013, Mathias et al., 2013)

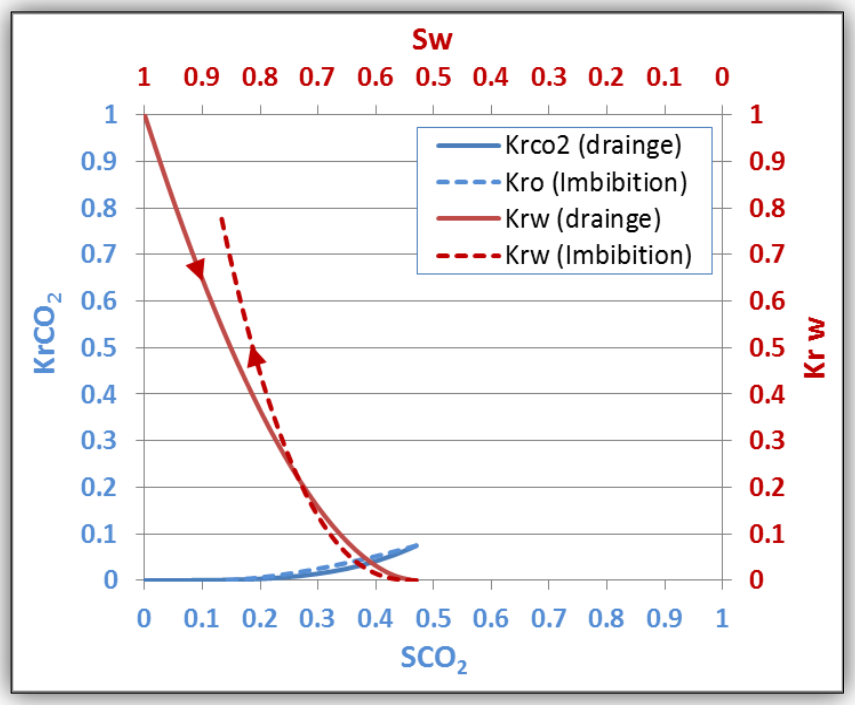

Figure A. 7: Relative permeability curves for Morinville formation (Dolomite) (Bennion and Bachu, 2010)

Slave point formation (Dolomite)

		Drainge		Imbibition	
S_{gr} =	0.256				
S_{wir} =	0.546	ng =	1.16	ng =	4.28
Krg (wir) =	0.5037	nw =	1.56	nw =	5.68
Krw(gr) =	0.0802				

Drainage			
CO_2 Saturation Fraction	Krg	Water Saturation Fraction	Krw
0.0000	0.0000	1.0000	1.0000
0.0260	0.0183	0.9740	0.9121
0.0520	0.0408	0.9480	0.8272
0.0780	0.0653	0.9220	0.7452
0.1040	0.0911	0.8960	0.6664
0.1300	0.1181	0.8700	0.5908
0.1560	0.1459	0.8440	0.5185
0.1820	0.1744	0.8180	0.4497
0.2080	0.2037	0.7920	0.3845
0.2340	0.2335	0.7660	0.3230
0.2600	0.2638	0.7400	0.2654
0.2860	0.2947	0.7140	0.2121
0.3120	0.3260	0.6880	0.1631
0.3380	0.3577	0.6620	0.1190
0.3640	0.3898	0.6360	0.0801
0.4540	0.5037	0.5460	0.0000

Imbibition			
Water Saturation Fraction	Krw	CO_2 Saturation Fraction	Krg
0.5460	0.0000	0.4540	0.5037
0.5570	0.0000	0.4430	0.3944
0.5680	0.0000	0.4320	0.3043
0.5790	0.0000	0.4210	0.2308
0.5900	0.0000	0.4100	0.1718
0.6010	0.0001	0.3990	0.1251
0.6120	0.0002	0.3880	0.0888
0.6230	0.0004	0.3770	0.0612
0.6340	0.0008	0.3660	0.0407
0.6450	0.0016	0.3550	0.0259
0.6560	0.0028	0.3440	0.0157
0.6670	0.0049	0.3330	0.0088
0.6780	0.0080	0.3220	0.0046
0.6890	0.0126	0.3110	0.0021
0.7000	0.0192	0.3000	0.0008
0.7440	0.0802	0.2560	0.0000

Formation Name	Lithology	Avg Porosity %	Ka (mD)	Depth (m)	Core length (cm)	Core diameter (cm)	Flow area (cm^2)	Temp (°C)	pore volume injected (cc)	Pore pressure (kPag)	Flow Rate [Ml/min]	Interfacial tension (mN/m)	Pc (kPa)	Salinity (mg/L)	Method used	Viscosity ratio μ_{brine} / μ_{Co2}
Slave point	Dolomite	9.9	0.217	1373.9	-	-	-	43	-	18800	-	29.5	802	129145	Unsteady state	

Table A. 8: Relative permeability data for Slave point formation (Dolomite) (Bennion and Bachu, 2010, Bennion and Bachu, 2006a, Bachu and Bennion, 2008, Bennion and Bachu, 2008a, Sciences, 2013, Survey, 2013, Mathias et al., 2013)

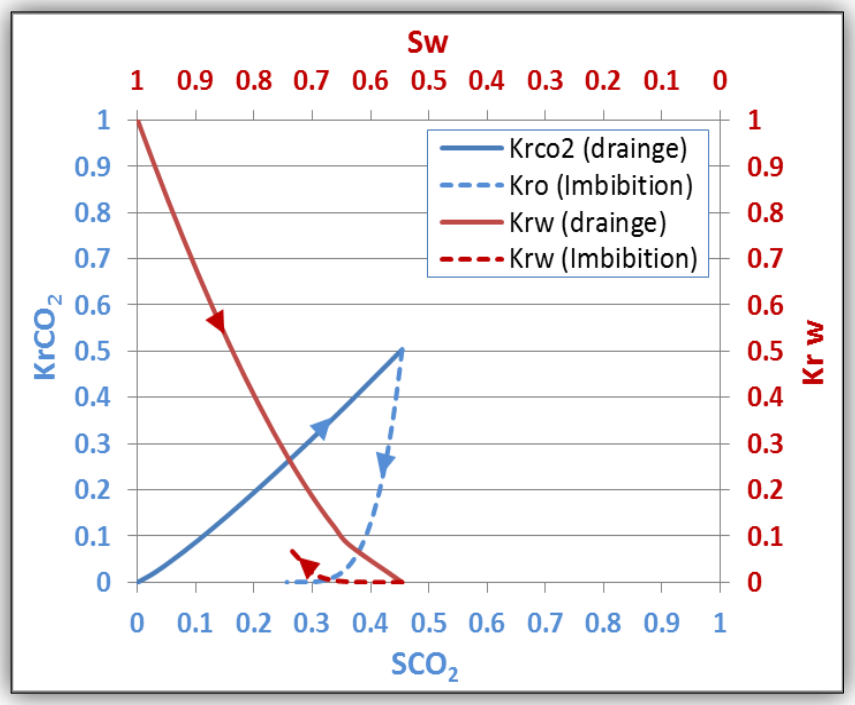

Figure A. 8: Relative permeability curves for Slave point formation (Dolomite) (Bennion and Bachu, 2010)

Winnipegosis formation (Dolomite)

S_{gr} =	0.4149	Drainge		Imbibition	
S_{wir} =	0.2108	ng =	4.5	ng =	1.55
Krg (w ir) =	0.6117	nw =	2.4	nw =	1.65
Krw (gr) =	0.1346				

Drainage

CO_2 Saturation Fraction	Krg	Water Saturation Fraction	Krw
0.0000	0.0000	1.0000	1.0000
0.0460	0.0000	0.9540	0.8658
0.0920	0.0000	0.9080	0.7427
0.1380	0.0002	0.8620	0.6305
0.1840	0.0009	0.8160	0.5288
0.2300	0.0024	0.7700	0.4374
0.2760	0.0054	0.7240	0.3560
0.3220	0.0108	0.6780	0.2842
0.3680	0.0197	0.6320	0.2216
0.4140	0.0336	0.5860	0.1679
0.4600	0.0539	0.5400	0.1226
0.5060	0.0828	0.4940	0.0855
0.5520	0.1224	0.4480	0.0559
0.5980	0.1755	0.4020	0.0333
0.6440	0.2450	0.3560	0.0172
0.6900	0.3342	0.3100	0.0069
0.7360	0.4468	0.2640	0.0015
0.7892	0.6117	0.2108	0.0000

Imbibition

Water Saturation Fraction	Krw	CO_2 Saturation Fraction	Krg
0.2108	0.0000	0.7892	0.6117
0.2328	0.0013	0.7672	0.5569
0.2548	0.0039	0.7452	0.5039
0.2768	0.0077	0.7232	0.4529
0.2988	0.0123	0.7012	0.4038
0.3208	0.0178	0.6792	0.3567
0.3428	0.0241	0.6572	0.3117
0.3648	0.0311	0.6352	0.2690
0.3868	0.0388	0.6132	0.2285
0.4088	0.0471	0.5912	0.1904
0.4308	0.0560	0.5692	0.1549
0.4528	0.0655	0.5472	0.1220
0.4748	0.0757	0.5252	0.0921
0.4968	0.0863	0.5032	0.0652
0.5188	0.0976	0.4812	0.0418
0.5408	0.1093	0.4592	0.0224
0.5628	0.1216	0.4372	0.0077
0.5851	0.1346	0.4149	0.0000

Formation Name	Lithology	Avg Porosity %	Ka (mD)	Depth (m)	Core length (cm)	Core diameter (cm)	Flow area (cm^2)	Temp (°C)	pore volume injected (cc)	Pore pressure (kPag)	Flow Rate [Ml/min]	Interfacial tension (mN/m)	Pc (kPa)	Salinity (mg/L)	Method used	Viscosity ratio μ_{brine} / μ_{Co2}
Winnipegosis	Dolomite	14.8	3.09	1140	-	-	-	36	-	8730	-	45.3	55	320847	Unsteady state	

Table A. 9: Relative permeability data for Winnipegosis formation (Dolomite) (Bennion and Bachu, 2010, Bennion and Bachu, 2006a, Bachu and Bennion, 2008, Bennion and Bachu, 2008a, Sciences, 2013, Survey, 2013, Mathias et al., 2013)

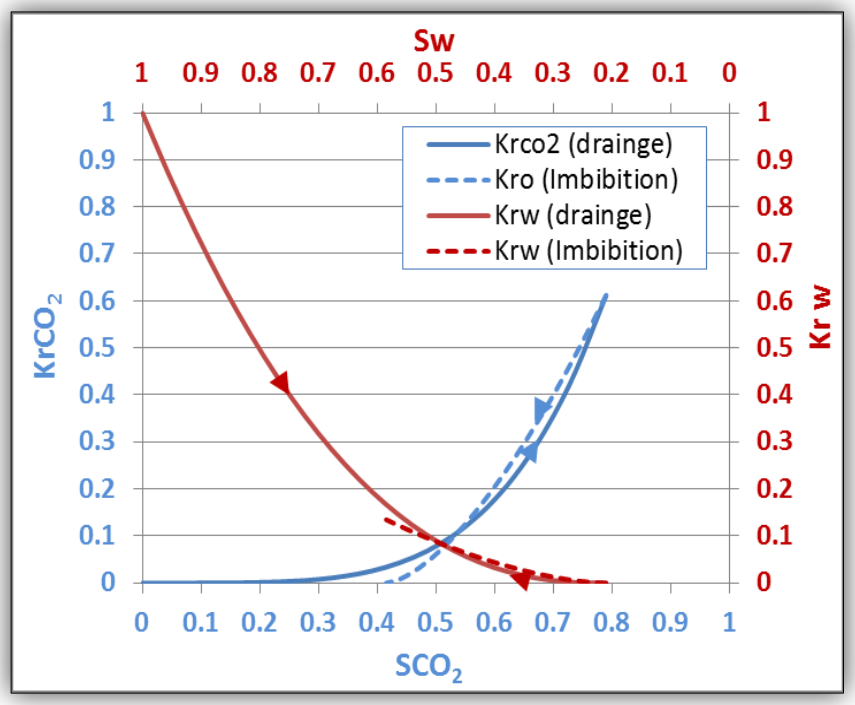

Figure A. 9: Relative permeability curves for Winnipegosis formation (Dolomite) (Bennion and Bachu, 2010)

A.1.2) Limestone

Wabamun (2) formation (Limestone)

Drainage			
CO_2 Saturation Fraction	Krg	Water Saturation Fraction	Krw
0.0000	0.0000	1.0000	1.0000
0.0220	0.0004	0.9780	0.9303
0.0430	0.0016	0.9570	0.8621
0.0650	0.0037	0.9350	0.7955
0.0860	0.0066	0.9140	0.7304
0.1080	0.0104	0.8920	0.6670
0.1290	0.0152	0.8710	0.6053
0.1510	0.0210	0.8490	0.5453
0.1720	0.0277	0.8280	0.4872
0.1940	0.0354	0.8060	0.4311
0.2160	0.0441	0.7840	0.3770
0.2370	0.0538	0.7630	0.3251
0.2590	0.0645	0.7410	0.2754
0.2800	0.0763	0.7200	0.2283
0.3020	0.0891	0.6980	0.1838
0.3230	0.1029	0.6770	0.1423
0.3450	0.1179	0.6550	0.1040
0.3660	0.1339	0.6340	0.0694
0.3880	0.1509	0.6120	0.0393
0.4090	0.1691	0.5910	0.0149
0.4310	0.1883	0.5690	0.0000

Imbibition			
Water Saturation Fraction	Krw	CO_2 Saturation Fraction	Krg

Formation Name	Lithology	Avg Porosity %	Ka (mD)	Depth (m)	Core length (cm)	Core diameter (cm)	Flow area (cm^2)	Temp (°C)	pore volume injected (cc)	Pore pressure (kPag)	Flow Rate [Ml/min]	Interfacial tension (mN/m)	Pc (kPa)	Salinity (mg/L)	Method used	Viscosity ratio μ_{brine} / μ_{Co2}
Wabamun (2) formation	Limestone	14.8	66.98	1603	11.91	3.81	11.4	41	20.09	11920	-	29.5	57.2	144304	Unsteady state	

Table A. 10: Relative permeability data for Wabamun (2) formation (Limestone) (Sciences, 2013, Bennion and Bachu, 2005, Bennion and Bachu, 2006a, Bachu and Bennion, 2008, Bennion and Bachu, 2008a, Bennion and Bachu, 2010, Survey, 2013, Mathias et al., 2013)

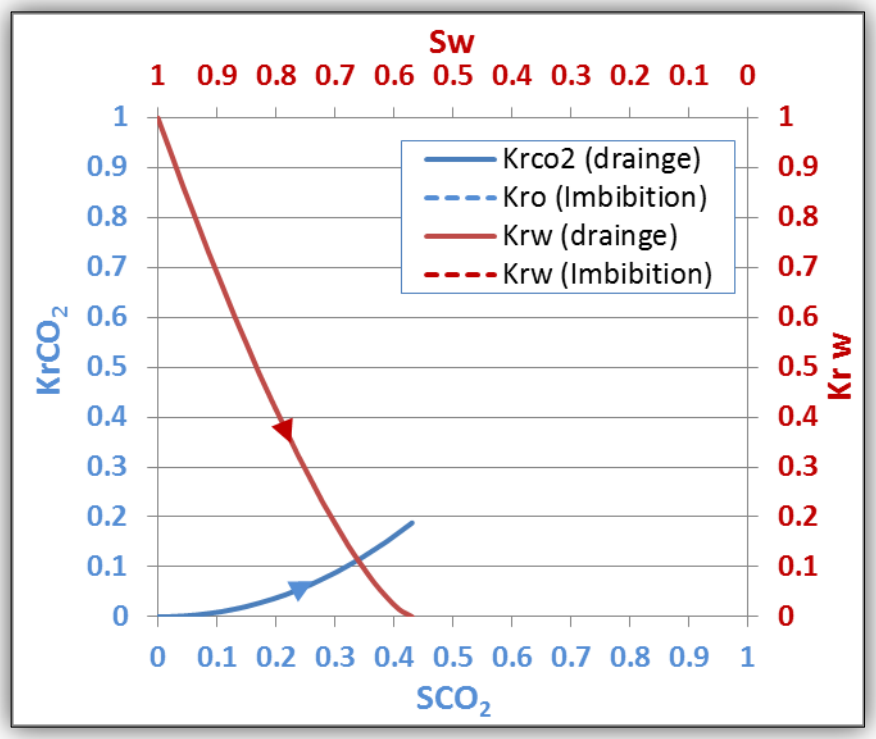

Figure A. 10: Relative permeability curves for Wabamun (2) formation (Limestone) (Sciences, 2013)

Wabamun (3) formation (Limestone)

		Drainge		Imbibition	
Sgr =	0.045	ng =	5.78	ng =	1.72
Swirr =	0.8520	nw =	2.76	nw =	6.25
Krg @ swirr =	0.1015				
Krw @ sgr =	0.9165				

Drainage

CO_2 Saturation Fraction	Krg	Water Saturation Fraction	Krw
0.0000	0.0000	1.0000	1.0000
0.0080	0.0000	0.9920	0.8578
0.0160	0.0000	0.9840	0.7292
0.0240	0.0000	0.9760	0.6137
0.0320	0.0000	0.9680	0.5105
0.0400	0.0001	0.9600	0.4191
0.0480	0.0002	0.9520	0.3389
0.0560	0.0004	0.9440	0.2692
0.0640	0.0008	0.9360	0.2095
0.0720	0.0016	0.9280	0.1589
0.0800	0.0029	0.9200	0.1169
0.0880	0.0050	0.9120	0.0828
0.0960	0.0083	0.9040	0.0558
0.1040	0.0132	0.8960	0.0352
0.1120	0.0203	0.8880	0.0202
0.1200	0.0302	0.8800	0.0101
0.1480	0.1015	0.8520	0.0000

Imbibition

Water Saturation Fraction	Krw	CO_2 Saturation Fraction	Krg
0.8520	0.0000	0.1480	0.1015
0.8530	0.0000	0.1420	0.0915
0.8590	0.0000	0.1360	0.0820
0.8650	0.0000	0.1300	0.0729
0.8710	0.0000	0.1240	0.0643
0.8770	0.0001	0.1180	0.0561
0.8830	0.0005	0.1120	0.0484
0.8890	0.0015	0.1060	0.0412
0.8950	0.0039	0.1000	0.0345
0.9010	0.0088	0.0940	0.0283
0.9070	0.0182	0.0880	0.0226
0.9130	0.0347	0.0820	0.0174
0.9190	0.0624	0.0760	0.0129
0.9250	0.1066	0.0700	0.0089
0.9310	0.1746	0.0640	0.0055
0.9370	0.2759	0.0580	0.0029
0.9550	0.9165	0.0450	0.0000

Formation Name	Lithology	Avg Porosity %	Ka (mD)	Depth (m)	Core length (cm)	Core diameter (cm)	Flow area (cm^2)	Temp (°C)	pore volume injected (cc)	Pore pressure (kPag)	Flow Rate [Ml/min]	Interfacial tension (mN/m)	Pc (kPa)	Salinity (mg/L)	Method used	Viscosity ratio μ_{brine} / μ_{Co2}
Wabamun (3) formation	Limestone	15.4	54.3	661				41		11900		29.5	35	144300		15.41

Table A. 11: Relative permeability data for Wabamun (3) formation (Limestone) (Bennion and Bachu, 2010, Bennion and Bachu, 2005, Bennion and Bachu, 2006a, Bachu and Bennion, 2008, Bennion and Bachu, 2008a, Sciences, 2013, Survey, 2013, Akbarabadi and Piri, 2013, Mathias et al., 2013)

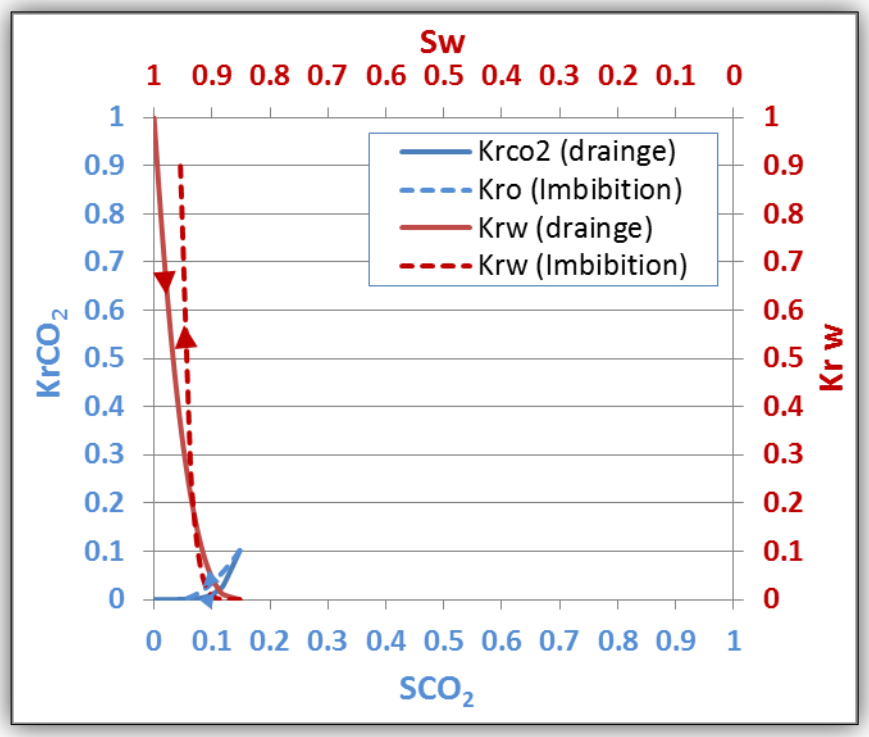

Figure A. 11: Relative permeability curves for Wabamun (3) formation (Limestone) (Bennion and Bachu, 2010)

Wabamun (4) formation (Limestone)

Drainage			
CO_2 Saturation Fraction	Krg	Water Saturation Fraction	Krw
0.0000	0.0000	1.0000	1.0000
0.0160	0.0011	0.9840	0.9258
0.0320	0.0029	0.9680	0.8535
0.0480	0.0053	0.9520	0.7832
0.0640	0.0080	0.9360	0.7150
0.0800	0.0112	0.9200	0.6489
0.0950	0.0146	0.9050	0.5850
0.1110	0.0183	0.8890	0.5234
0.1270	0.0223	0.8730	0.4641
0.1430	0.0265	0.8570	0.4072
0.1590	0.0310	0.8410	0.3529
0.1750	0.0356	0.8250	0.3013
0.1910	0.0405	0.8090	0.2525
0.2070	0.0456	0.7930	0.2067
0.2230	0.0508	0.7770	0.1640
0.2380	0.0563	0.7620	0.1248
0.2540	0.0619	0.7460	0.0893
0.2700	0.0677	0.7300	0.0581
0.2860	0.0736	0.7140	0.0317
0.3020	0.0797	0.6980	0.0113
0.3180	0.0860	0.6820	0.0000

Imbibition			
Water Saturation Fraction	Krw	CO_2 Saturation Fraction	Krg

Formation Name	Lithology	Avg Porosity %	Ka (mD)	Depth (m)	Core length (cm)	Core diameter (cm)	Flow area (cm^2)	Temp (°C)	pore volume injected (cc)	Pore pressure (kPag)	Flow Rate [Ml/min]	Interfacial tension (mN/m)	Pc (kPa)	Salinity (mg/L)	Method used	Viscosity ratio μ_{brine} / μ_{Co2}
Wabamun (4) formation	Limestone	14.8	174	1603	11.91	3.81	11.4	20	20.09	3445	-	49.24			Unsteady state	75

Table A. 12: Relative permeability data for Wabamun (3) formation (Limestone) (Sciences, 2013, Bennion and Bachu, 2005, Bennion and Bachu, 2006a, Bachu and Bennion, 2008, Bennion and Bachu, 2008a, Bennion and Bachu, 2010, Survey, 2013)

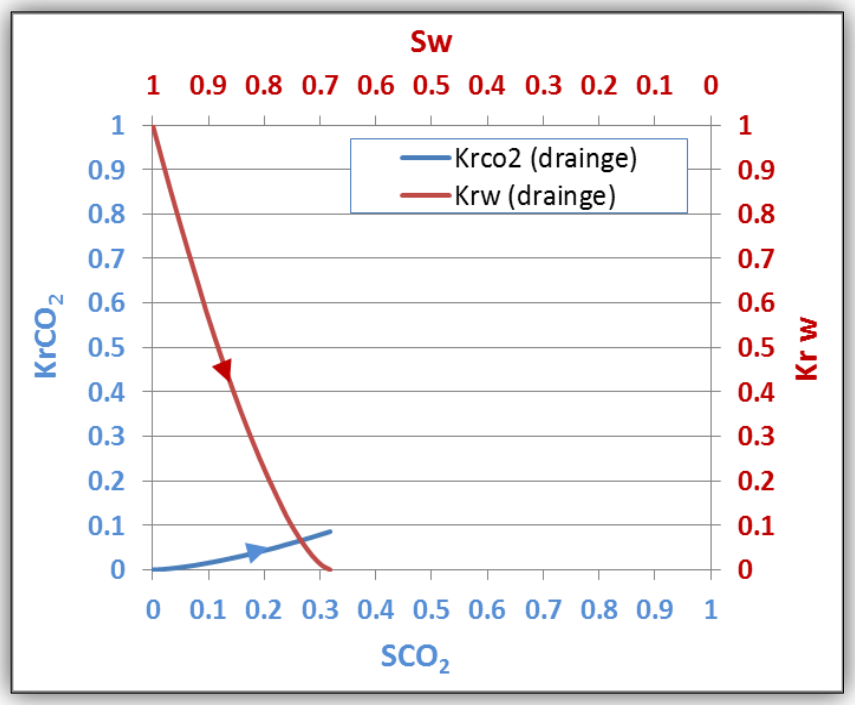

Figure A. 12: Relative permeability curves for Wabamun (3) formation (Limestone) (Sciences, 2013)

A.2) **Siliclastics**

A.2.1) Sandstone

Viking (1) formation (Sandstone)

Drainage			
CO_2 Saturation Fraction	Krg	Water Saturation Fraction	Krw
0.044	0.0007	0.956	0.7156
0.066	0.0018	0.934	0.5970
0.088	0.0037	0.912	0.4927
0.111	0.0067	0.889	0.4018
0.133	0.0110	0.867	0.3232
0.155	0.0168	0.845	0.2559
0.177	0.0244	0.823	0.1990
0.199	0.0339	0.801	0.1516
0.221	0.0457	0.779	0.1127
0.243	0.0599	0.757	0.0814
0.265	0.0767	0.735	0.0567
0.287	0.0964	0.713	0.0379
0.309	0.1191	0.691	0.0240
0.331	0.1451	0.669	0.0142
0.354	0.1747	0.646	0.0077
0.376	0.2079	0.624	0.0038
0.398	0.2451	0.602	0.0016
0.42	0.2863	0.58	0.0006
0.442	0.3319	0.558	0.0000

Imbibition			
Water Saturation Fraction	Krw	CO_2 Saturation Fraction	Krg

Formation Name	Lithology	Avg Porosity %	Ka (mD)	Depth (m)	Core length (cm)	Core diameter (cm)	Flow area (cm^2)	Temp (°C)	pore volume injected (cc)	Pore pressure (kPag)	Flow Rate [Ml/min]	Interfacial tension (mN/m)	Pc (kPa)	Salinity (mg/L)	Method used	Viscosity ratio μ_{brine} / μ_{Co2}
Viking (1)	Sandstone	12.5	5.78	1240	5.51	3.81	11.4	35	7.85	8610		32.1	28.8	28286	Unsteady state	13.98

Table A. 13: Relative permeability data for Viking (1) formation (Sandstone) (Bennion and Bachu, 2005, Bennion and Bachu, 2006a, Bennion and Bachu, 2008a, Bachu and Bennion, 2008, Sciences, 2013, Survey, 2013)

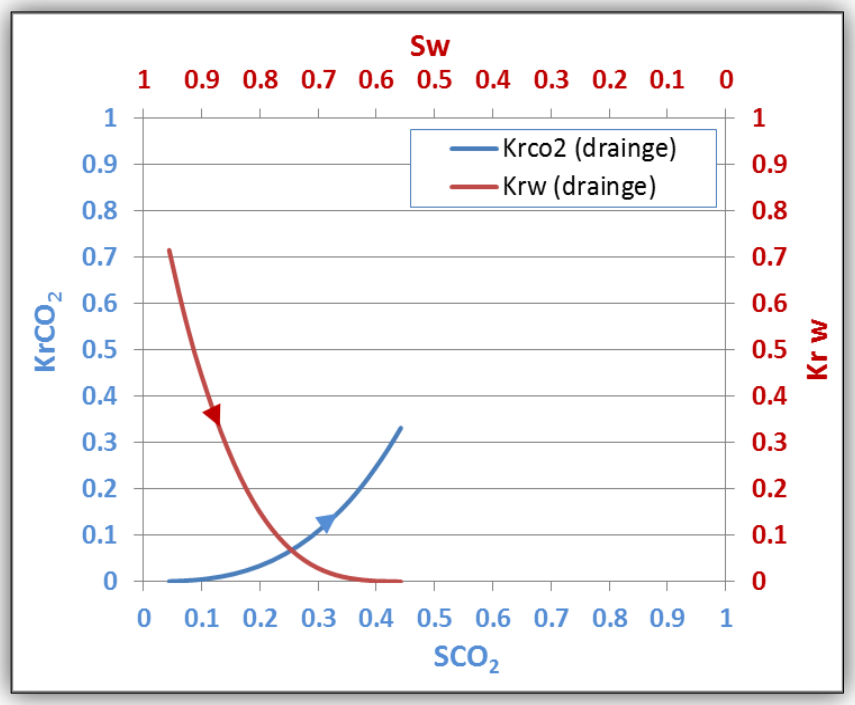

Figure A. 13: Relative permeability curves for Viking (1) formation (Sandstone) (Bennion and Bachu, 2005)

Viking (2) formation (Sandstone)

Drainage			
CO_2 Saturation Fraction	Krg	Water Saturation Fraction	Krw
0.0000	0.0000	1.0000	1.0000
0.0290	0.0002	0.9710	0.9150
0.0580	0.0006	0.9420	0.8332
0.0870	0.0015	0.9130	0.7546
0.1150	0.0031	0.8850	0.6794
0.1440	0.0055	0.8560	0.6076
0.1730	0.0090	0.8270	0.5392
0.2020	0.0138	0.7980	0.4743
0.2310	0.0199	0.7690	0.4130
0.2600	0.0276	0.7400	0.3553
0.2890	0.0370	0.7110	0.3014
0.3170	0.0484	0.6830	0.2512
0.3460	0.0619	0.6540	0.2050
0.3750	0.0776	0.6250	0.1628
0.4040	0.0957	0.5960	0.1248
0.4330	0.1163	0.5670	0.0912
0.4620	0.1398	0.5380	0.0622
0.4900	0.1660	0.5100	0.0380
0.5190	0.1954	0.4810	0.0190
0.5480	0.2279	0.4520	0.0059
0.5770	0.2638	0.4230	0.0000

Imbibition			
Water Saturation Fraction	Krw	CO_2 Saturation Fraction	Krg
0.4230	0.0000	0.5770	0.2638
0.4370	0.0010	0.5630	0.2152
0.4510	0.0036	0.5490	0.1737
0.4650	0.0079	0.5350	0.1386
0.4790	0.0141	0.5210	0.1091
0.4930	0.0220	0.5070	0.0846
0.5070	0.0317	0.4930	0.0645
0.5210	0.0432	0.4790	0.0483
0.5350	0.0566	0.4650	0.0354
0.5490	0.0719	0.4510	0.0253
0.5630	0.0890	0.4370	0.0176
0.5770	0.1080	0.4230	0.0119
0.5910	0.1288	0.4090	0.0077
0.6050	0.1516	0.3950	0.0048
0.6190	0.1763	0.3810	0.0029
0.6330	0.2029	0.3670	0.0017
0.6470	0.2314	0.3530	0.0009
0.6610	0.2618	0.3390	0.0005
0.6750	0.2941	0.3250	0.0003
0.6890	0.3284	0.3110	0.0001
0.7030	0.3646	0.2970	0.0000

Formation Name	Lithology	Avg Porosity %	Ka (mD)	Depth (m)	Core length (cm)	Core diameter (cm)	Flow area (cm^2)	Temp (°C)	pore volume injected (cc)	Pore pressure (kPag)	Flow Rate [Ml/min]	Interfacial tension (mN/m)	Pc (kPa)	Salinity (mg/L)	Method used	Viscosity ratio μ_{brine} / μ_{Co2}
Viking (2)	Sandstone	19.8	21.72	1342				35		8610		32.1	3.5	28300	Unsteady state	13.98

Table A. 14: Relative permeability data for Viking (2) formation (Sandstone) (Bennion and Bachu, 2006b, Survey, 2013, Bennion and Bachu, 2008a, Bachu and Bennion, 2008)

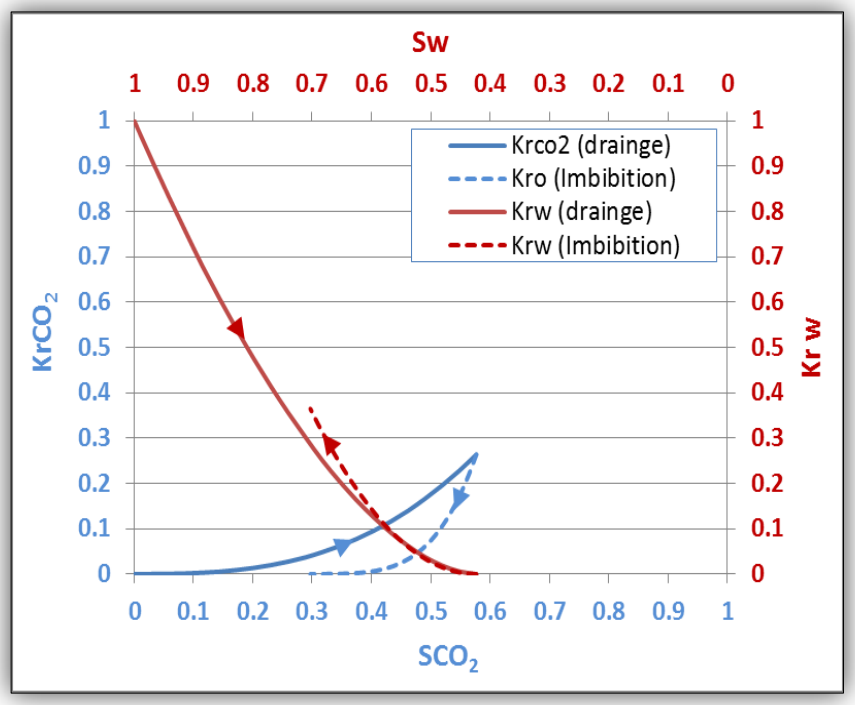

Figure A. 14: Relative permeability curves for Viking (2) formation (Sandstone) (Bennion and Bachu, 2006b)

Cardium 1 formation (Sandstone)

Drainage			
CO_2 Saturation Fraction	Krg	Water Saturation Fraction	Krw
0.0000	0.0000	1.0000	1.0000
0.0400	0.0103	0.9600	0.9145
0.0800	0.0255	0.9200	0.8323
0.1210	0.0434	0.8790	0.7534
0.1610	0.0633	0.8390	0.6779
0.2010	0.0849	0.7990	0.6059
0.2410	0.1079	0.7590	0.5373
0.2810	0.1322	0.7190	0.4723
0.3210	0.1576	0.6790	0.4109
0.3610	0.1840	0.6390	0.3532
0.4020	0.2114	0.5980	0.2993
0.4420	0.2397	0.5580	0.2492
0.4820	0.2687	0.5180	0.2032
0.5220	0.2986	0.4780	0.1612
0.5620	0.3292	0.4380	0.1234
0.6020	0.3605	0.3980	0.0900
0.6420	0.3925	0.3580	0.0612
0.6830	0.4251	0.3170	0.0373
0.7230	0.4583	0.2770	0.0186
0.7630	0.4921	0.2370	0.0057
0.8030	0.5265	0.1970	0.0000

Imbibition			
Water Saturation Fraction	Krw	CO_2 Saturation Fraction	Krg
0.1970	0.0000	0.8030	0.5265
0.2320	0.0290	0.7680	0.4964
0.2670	0.0644	0.7330	0.4665
0.3020	0.1025	0.6980	0.4369
0.3370	0.1426	0.6630	0.4075
0.3720	0.1843	0.6280	0.3784
0.4070	0.2272	0.5930	0.3495
0.4420	0.2711	0.5580	0.3210
0.4770	0.3161	0.5230	0.2928
0.5120	0.3619	0.4880	0.2650
0.5470	0.4084	0.4530	0.2375
0.5820	0.4556	0.4180	0.2104
0.6180	0.5035	0.3820	0.1838
0.6530	0.5520	0.3470	0.1577
0.6880	0.6010	0.3120	0.1321
0.7230	0.6506	0.2770	0.1072
0.7580	0.7006	0.2420	0.0829
0.7930	0.7512	0.2070	0.0596
0.8280	0.8021	0.1720	0.0374
0.8630	0.8535	0.1370	0.0169
0.8980	0.9053	0.1020	0.0000

Formation Name	Lithology	Avg Porosity %	Ka (mD)	Depth (m)	Core length (cm)	Core diameter (cm)	Flow area (cm^2)	Temp (°C)	pore volume injected (cc)	Pore pressure (kPag)	Flow Rate [Ml/min]	Interfacial tension (mN/m)	Pc (kPa)	Salinity (mg/L)	Method used	Viscosity ratio μ_{brine} / μ_{Co2}
Cardium (1)	Sandstone	15.3	31.11	1626.3	3.73	3.77	11.16	43	6.37	20000		19.8	31.8	27089	Unsteady state	8.68

Table A. 15: Relative permeability data for Cardium (1) formation (Sandstone) (Bennion and Bachu, 2006c, Bennion and Bachu, 2008a, Bachu and Bennion, 2008, Sciences, 2013)

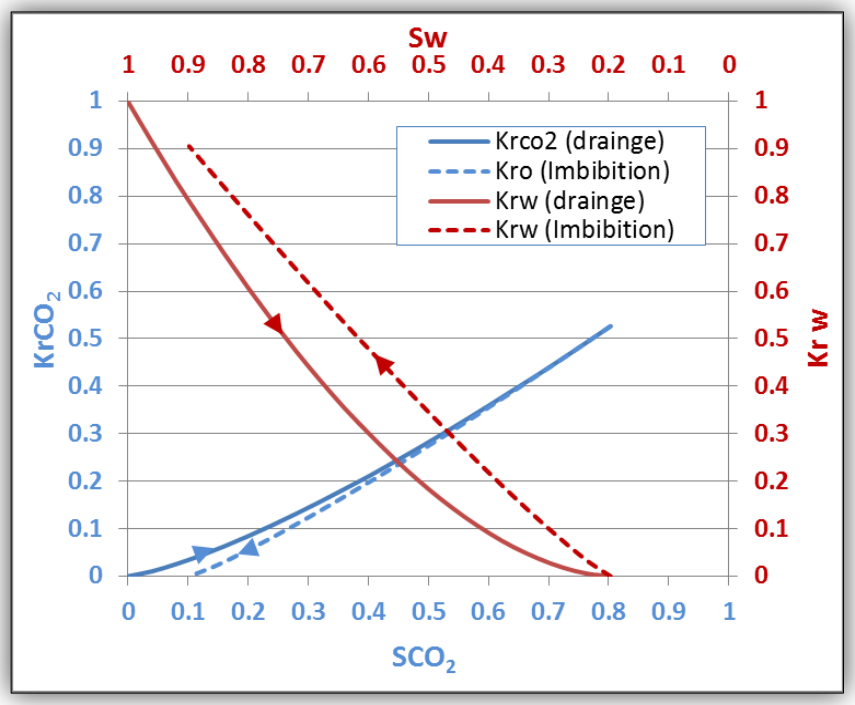

Figure A. 15: Relative permeability curves for Cardium (1) formation (Sandstone) (Bennion and Bachu, 2006c)

Cardium 2 formation (Sanstone)

Drainage			
CO_2 Saturation Fraction	Krg	Water Saturation Fraction	Krw
0.0000	0.0000	1.0000	1.0000
0.0370	0.0030	0.9630	0.8893
0.0730	0.0095	0.9270	0.7859
0.1090	0.0186	0.8910	0.6897
0.1460	0.0302	0.8540	0.6006
0.1820	0.0439	0.8180	0.5183
0.2190	0.0596	0.7810	0.4428
0.2550	0.0773	0.7450	0.3740
0.2920	0.0969	0.7080	0.3117
0.3280	0.1182	0.6720	0.2558
0.3650	0.1412	0.6350	0.2060
0.4010	0.1658	0.5990	0.1622
0.4370	0.1921	0.5630	0.1243
0.4740	0.2199	0.5260	0.0920
0.5100	0.2493	0.4900	0.0651
0.5470	0.2801	0.4530	0.0433
0.5830	0.3124	0.4170	0.0264
0.6200	0.3462	0.3800	0.0141
0.6560	0.3813	0.3440	0.0060
0.6930	0.4179	0.3070	0.0015
0.7290	0.4558	0.2710	0.0000

Imbibition			
Water Saturation Fraction	Krw	CO_2 Saturation Fraction	Krg
0.2710	0.0000	0.7290	0.4558
0.3020	0.0206	0.6980	0.4232
0.3330	0.0488	0.6670	0.3914
0.3640	0.0808	0.6360	0.3604
0.3950	0.1157	0.6050	0.3301
0.4260	0.1528	0.5740	0.3008
0.4580	0.1917	0.5420	0.2722
0.4890	0.2324	0.5110	0.2446
0.5200	0.2745	0.4800	0.2179
0.5510	0.3179	0.4490	0.1921
0.5820	0.3625	0.4180	0.1674
0.6130	0.4083	0.3870	0.1438
0.6440	0.4551	0.3560	0.1213
0.6750	0.5028	0.3250	0.1001
0.7060	0.5515	0.2940	0.0801
0.7370	0.6011	0.2630	0.0616
0.7690	0.6515	0.2310	0.0447
0.8000	0.7027	0.2000	0.0295
0.8310	0.7546	0.1690	0.0165
0.8620	0.8073	0.1380	0.0061
0.8930	0.8606	0.1070	0.0000

Formation Name	Lithology	Avg Porosity %	Ka (mD)	Depth (m)	Core length (cm)	Core diameter (cm)	Flow area (cm^2)	Temp (°C)	pore volume injected (cc)	Pore pressure (kPag)	Flow Rate [Ml/min]	Interfacial tension (mN/m)	Pc (kPa)	Salinity (mg/L)	Method used	Viscosity ratio μ_{brine} / μ_{Co2}
Cardium (2)	**Sandstone**	**16.1**	**21.17**	**1626.3**	**3.73**	**3.77**	**11.16**	**43**	**6.37**	**20000**		**32.2**	**44.3**	**27089**	**Unsteady state**	**18.57**

Table A. 16: Relative permeability data for Cardium (2) formation (Sandstone) (Bennion and Bachu, 2006c, Bennion and Bachu, 2008a, Bachu and Bennion, 2008, Survey, 2013)

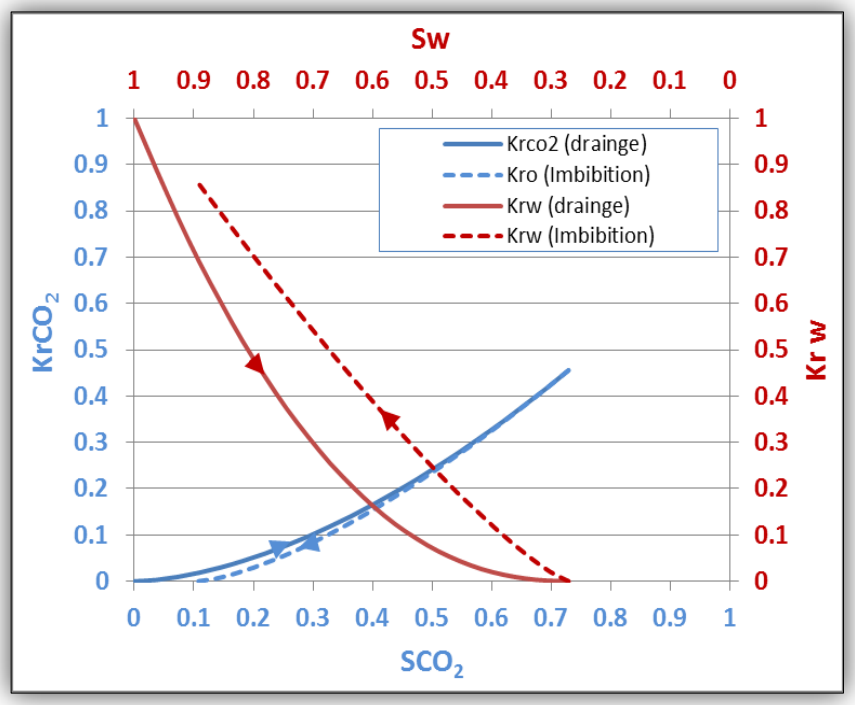

Figure A. 16: Relative permeability curves for Cardium (2) formation (Sandstone) (Bennion and Bachu, 2006c)

Cardium 3 formation (Sandstone)

Drainage			
CO_2 Saturation Fraction	Krg	Water Saturation Fraction	Krw
0.0000	0.0000	1.0000	1.0000
0.0310	0.0002	0.9690	0.8715
0.0620	0.0008	0.9380	0.7539
0.0930	0.0019	0.9070	0.6468
0.1240	0.0038	0.8760	0.5499
0.1550	0.0068	0.8450	0.4628
0.1860	0.0110	0.8140	0.3849
0.2170	0.0166	0.7830	0.3159
0.2480	0.0239	0.7520	0.2552
0.2800	0.0329	0.7200	0.2025
0.3110	0.0438	0.6890	0.1573
0.3420	0.0569	0.6580	0.1191
0.3730	0.0723	0.6270	0.0874
0.4040	0.0902	0.5960	0.0616
0.4350	0.1107	0.5650	0.0413
0.4660	0.1340	0.5340	0.0259
0.4970	0.1602	0.5030	0.0148
0.5280	0.1896	0.4720	0.0074
0.5590	0.2222	0.4410	0.0030
0.5900	0.2582	0.4100	0.0008
0.6210	0.2978	0.3790	0.0000

Imbibition			
Water Saturation Fraction	Krw	CO_2 Saturation Fraction	Krg
0.3790	0.0000	0.6210	0.2978
0.3990	0.0002	0.6010	0.2715
0.4190	0.0005	0.5810	0.2463
0.4380	0.0009	0.5620	0.2222
0.4580	0.0016	0.5420	0.1993
0.4780	0.0028	0.5220	0.1774
0.4980	0.0049	0.5020	0.1567
0.5180	0.0082	0.4820	0.1371
0.5380	0.0130	0.4620	0.1188
0.5570	0.0198	0.4430	0.1016
0.5770	0.0291	0.4230	0.0856
0.5970	0.0414	0.4030	0.0708
0.6170	0.0574	0.3830	0.0573
0.6370	0.0777	0.3630	0.0451
0.6560	0.1029	0.3440	0.0343
0.6760	0.1339	0.3240	0.0247
0.6960	0.1715	0.3040	0.0166
0.7160	0.2164	0.2840	0.0100
0.7360	0.2695	0.2640	0.0049
0.7560	0.3319	0.2440	0.0015
0.7750	0.4045	0.2250	0.0000

Formation Name	Lithology	Avg Porosity %	Ka (mD)	Depth (m)	Core length (cm)	Core diameter (cm)	Flow area (cm^2)	Temp (°C)	pore volume injected (cc)	Pore pressure (kPag)	Flow Rate [Ml/min]	Interfacial tension (mN/m)	Pc (kPa)	Salinity (mg/L)	Method used	Viscosity ratio μ_{brine} / μ_{Co2}
Cardium (3)	sandstone	15.3		1626.3	3.73	3.77	11.16	43	6.37	1378		56.2		27089	Unsteady state	46.36

Table A. 17: Relative permeability data for Cardium (3) formation (Sandstone) (Bennion and Bachu, 2006c, Sciences, 2013)

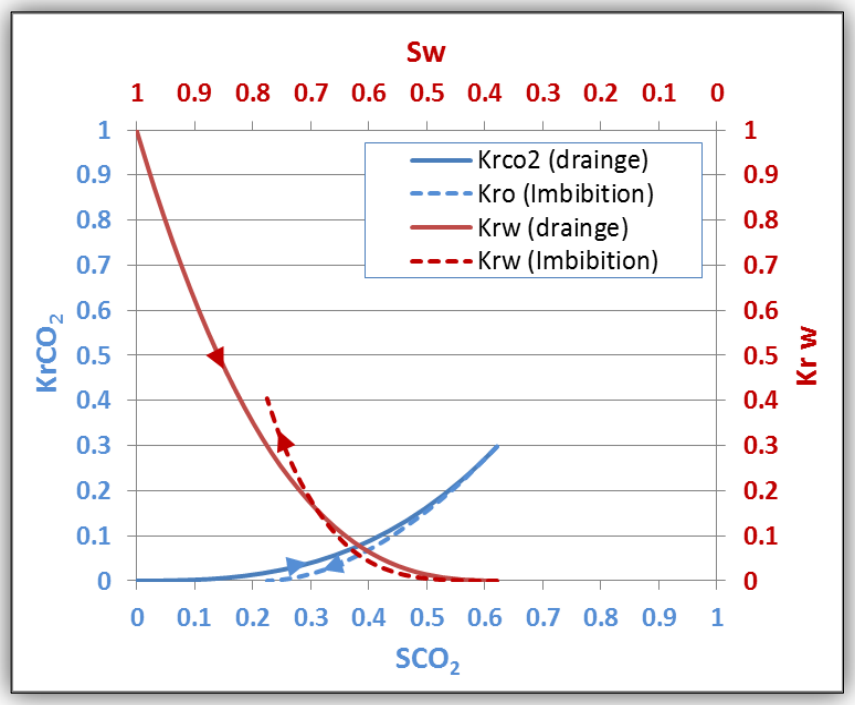

Figure A. 17: Relative permeability curves for Cardium (3) formation (Sandstone) (Bennion and Bachu, 2006c)

Basel Cambrian formation (Sandstone)

Drainage			
CO_2 Saturation Fraction	Krg	Water Saturation Fraction	Krw
0.0000	0.0000	1.0000	1.0000
0.0350	0.0003	0.9650	0.9105
0.0710	0.0005	0.9290	0.8248
0.1060	0.0008	0.8940	0.7430
0.1410	0.0012	0.8590	0.6650
0.1770	0.0019	0.8230	0.5911
0.2120	0.0029	0.7880	0.5211
0.2470	0.0047	0.7530	0.4552
0.2820	0.0076	0.7180	0.3933
0.3180	0.0123	0.6820	0.3356
0.3530	0.0194	0.6470	0.2821
0.3880	0.0299	0.6120	0.2328
0.4240	0.0449	0.5760	0.1879
0.4590	0.0657	0.5410	0.1474
0.4940	0.0940	0.5060	0.1114
0.5290	0.1315	0.4710	0.0800
0.5650	0.1805	0.4350	0.0535
0.6000	0.2433	0.4000	0.0318
0.6350	0.3228	0.3650	0.0154
0.6710	0.4221	0.3290	0.0045
0.7060	0.5446	0.2940	0.0000

Imbibition			
Water Saturation Fraction	Krw	CO_2 Saturation Fraction	Krg

Formation Name	Lithology	Avg Porosity %	Ka (mD)	Depth (m)	Core length (cm)	Core diameter (cm)	Flow area (cm^2)	Temp (°C)	pore volume injected (cc)	Pore pressure (kPag)	Flow Rate [Ml/min]	Interfacial tension (mN/m)	Pc (kPa)	Salinity (mg/L)	Method used	Viscosity ratio μ_{brine} / μ_{Co2}
Basal Cambrian	sandstone	11.7	0.55	2734	9.23	3.81	11.4	75	12.32	27000	-	27	31.9	248000	Unsteady state	11.82

Table A. 18: Relative permeability data for Basel Cambrian formation (Sandstone) (Bennion and Bachu, 2005, Sciences, 2013, Survey, 2013, Bennion and Bachu, 2006a, Bennion and Bachu, 2008a, Bachu and Bennion, 2008)

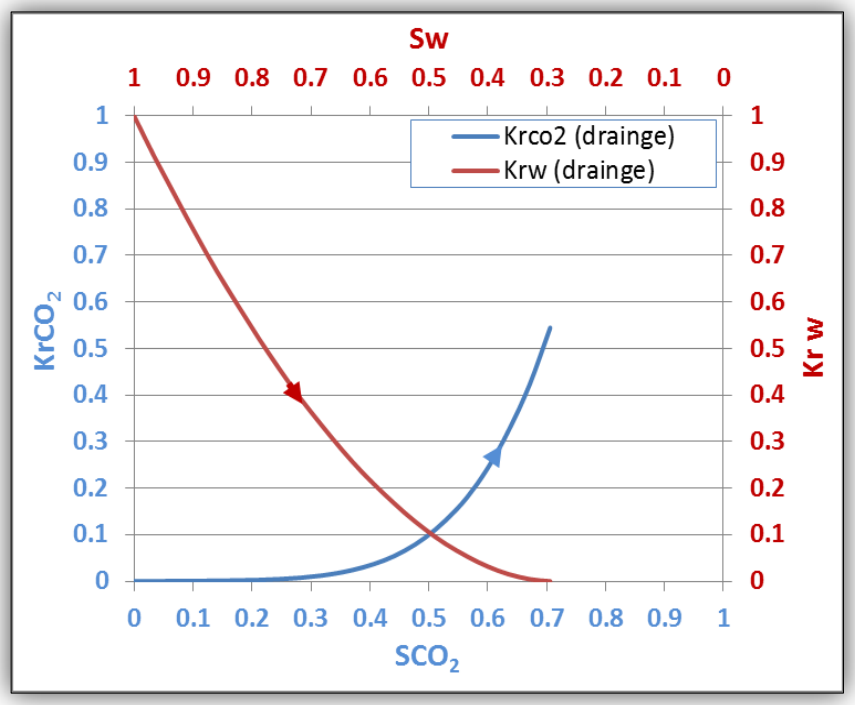

Figure A. 18: Relative permeability curves for Basel Cambrian formation (Sandstone) (Bennion and Bachu, 2005)

Ellerlie formation (Sandstone)

Drainage			
CO_2 Saturation Fraction	Krg	Water Saturation Fraction	Krw
0.0340	0.0008	0.9660	0.8052
0.0510	0.0018	0.9490	0.7159
0.0680	0.0034	0.9320	0.6320
0.0850	0.0055	0.9150	0.5535
0.1020	0.0082	0.8980	0.4804
0.1190	0.0115	0.8810	0.4127
0.1360	0.0153	0.8640	0.3502
0.1530	0.0199	0.8470	0.2930
0.1700	0.0250	0.8300	0.2411
0.1880	0.0309	0.8120	0.1943
0.2050	0.0374	0.7950	0.1528
0.2220	0.0446	0.7780	0.1164
0.2390	0.0525	0.7610	0.0851
0.2560	0.0612	0.7440	0.0588
0.2730	0.0706	0.7270	0.0375
0.2900	0.0807	0.7100	0.0211
0.3070	0.0916	0.6930	0.0095
0.3240	0.1032	0.6760	0.0025
0.3410	0.1156	0.6590	0.0000

Imbibition			
Water Saturation Fraction	Krw	CO_2 Saturation Fraction	Krg

Formation Name	Lithology	Avg Porosity %	Ka (mD)	Depth (m)	Core length (cm)	Core diameter (cm)	Flow area (cm^2)	Temp (°C)	pore volume injected (cc)	Pore pressure (kPag)	Flow Rate [Ml/min]	Interfacial tension (mN/m)	Pc (kPa)	Salinity (mg/L)	Method used	Viscosity ratio μ_{brine} / μ_{Co2}
Ellerslie	Sandstone	12.6	2.2	1355	19.76	3.83	11.52	40	28.77	10850	-	32.5	56.3	97217	Unsteady state	14.52

Table A. 19: Relative permeability data for Basel Cambrian formation (Sandstone) (Bennion and Bachu, 2005, Survey, 2013, Sciences, 2013, Bennion and Bachu, 2006a, Bennion and Bachu, 2008a, Bachu and Bennion, 2008)

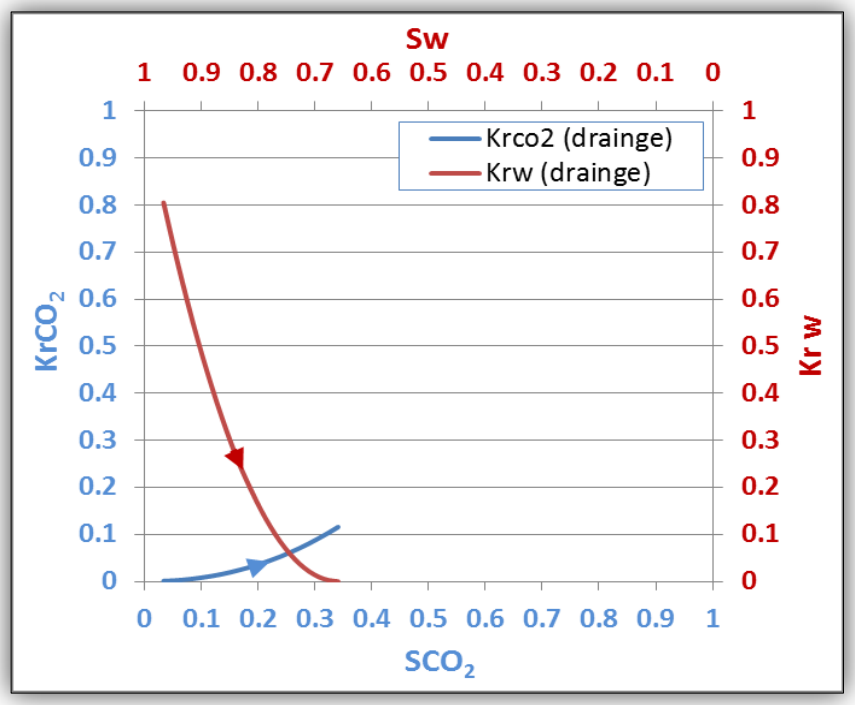

Figure A. 19: Relative permeability curves for Basel Cambrian formation (Sandstone) (Bennion and Bachu, 2005)

Berea (Sample1) (Sandstone)

Drainage			
CO_2 Saturation Fraction	Krg	Water Saturation Fraction	Krw
0.000	0.000	1.000	1.000
0.060	0.019	0.946	0.445
0.152	0.015	0.867	0.234
0.205	0.023	0.790	0.172
0.273	0.031	0.773	0.154
0.342	0.042	0.731	0.090
0.430	0.063	0.620	0.000

Imbibition			
Water Saturation Fraction	Krw	CO_2 Saturation Fraction	Krg

Formation Name	Lithology	Avg Porosity %	Ka (mD)	Depth (m)	Core length (cm)	Core diameter (cm)	Flow area (cm^2)	Temp (°C)	pore volume injected (cc)	Pore pressure (kPag)	Flow Rate [Ml/min]	Interfacial tension (mN/m)	Pc (kPa)	Salinity (mg/L)	Method used	Viscosity ratio μ_{brine} / μ_{Co2}
Berea (sample1)	sandstone	20.3	430	-	15.24	5.08	40.53	50	62.7	12400	1.2	30	-	5028	steady state	-

Table A. 20: Relative permeability data for Berea (sample 1) (Sandstone) (Perrin and Benson, 2010, Sciences, 2013, Akbarabadi and Piri, 2013, Mathias et al., 2013)

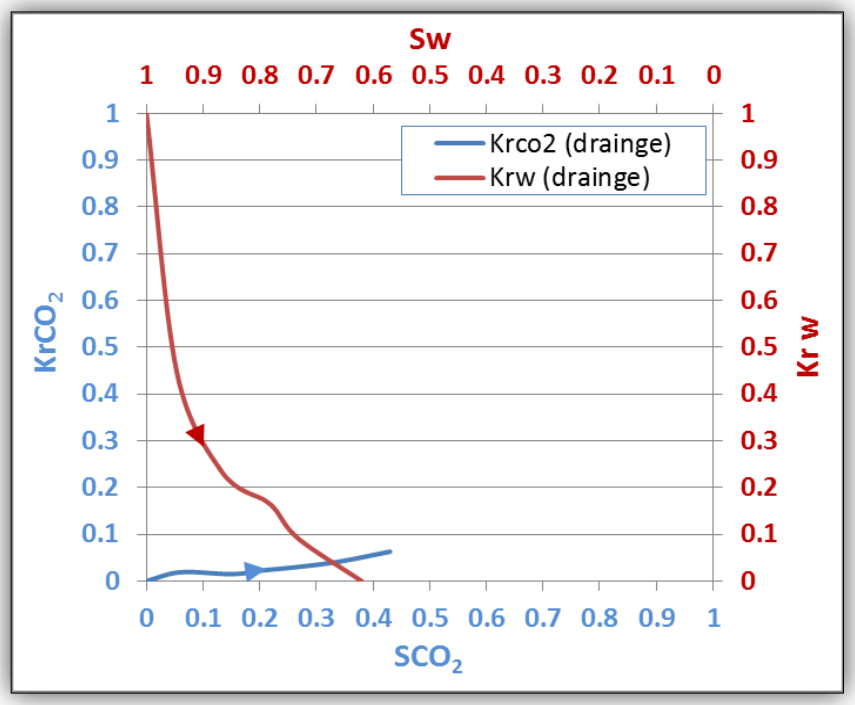

Figure A. 20: Relative permeability curves for Berea (sample 1) (Sandstone) (Perrin and Benson, 2010, Sciences, 2013)

Berea (Sample 2) (Sandstone)

Drainage			
CO_2 Saturation Fraction	Krg	Water Saturation Fraction	Krw
0.000	0.000	1.000	1.000
0.060	0.023	0.940	0.528
0.152	0.023	0.848	0.341
0.205	0.035	0.795	0.266
0.273	0.037	0.727	0.186
0.342	0.057	0.658	0.096
0.430	0.098	0.570	0.000

Imbibition			
Water Saturation Fraction	Krw	CO_2 Saturation Fraction	Krg

Formation Name	Lithology	Avg Porosity %	Ka (mD)	Depth (m)	Core length (cm)	Core diameter (cm)	Flow area (cm^2)	Temp (°C)	pore volume injected (cc)	Pore pressure (kPag)	Flow Rate [Ml/min]	Interfacial tension (mN/m)	Pc (kPa)	Salinity (mg/L)	Method used	Viscosity ratio μ_{brine} / μ_{Co2}
Berea (sample2)	sandstone	20.3	430	-	15.24	5.08	40.53	50	62.7	12400	2.6	-	-	5028	steady state	-

Table A. 21: Relative permeability data for Berea (sample 2) (Sandstone) (Perrin and Benson, 2010, Sciences, 2013)

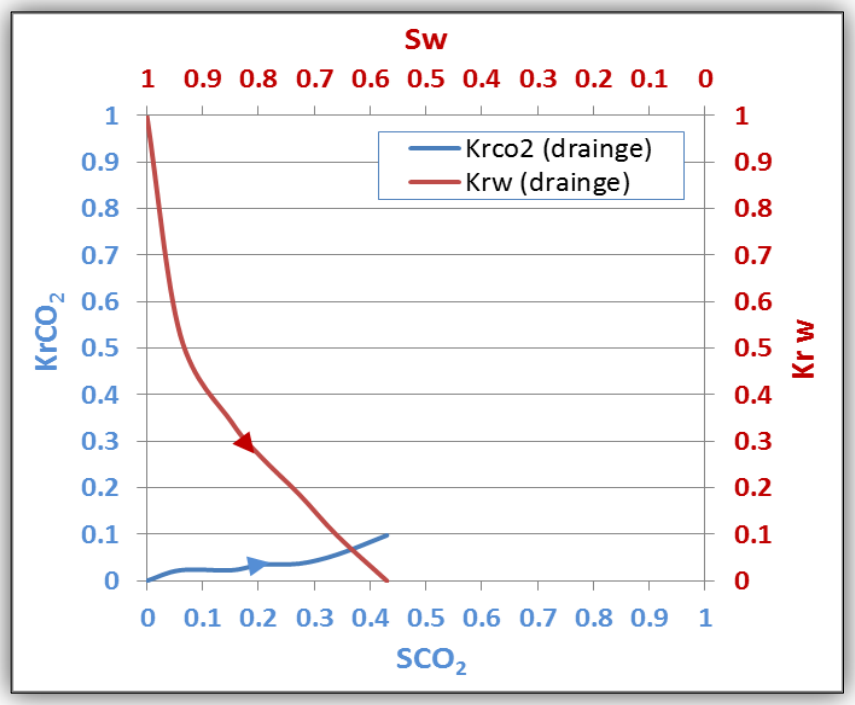

Figure A. 21: Relative permeability curves for Berea (sample 2) (Sandstone) (Perrin and Benson, 2010, Sciences, 2013)

Berea (Sample 3) (Sandstone)

Drainage			
CO_2 Saturation Fraction	Krg	Water Saturation Fraction	Krw
0	0	1	1
0.003	0.005	0.997	0.484
0.005	0.006	0.995	0.42
0.012	0.011	0.988	0.404
0.014	0.012	0.986	0.312
0.031	0.021	0.969	0.266
0.072	0.025	0.928	0.155
0.164	0.037	0.836	0.114
0.23	0.056	0.77	0.093
0.276	0.062	0.724	0.051
0.324	0.09	0.676	0.037
0.356	0.104	0.644	0.022
0.379	0.128	0.621	0.02
0.423	0.141	0.577	0.007
0.447	0.167	0.553	0.007
0.485	0.187	0.515	0

Imbibition			
Water Saturation Fraction	Krw	CO_2 Saturation Fraction	Krg
0.522	0.008	0.478	0.185
0.536	0.009	0.464	0.181
0.553	0.017	0.447	0.167
0.588	0.028	0.412	0.136
0.604	0.027	0.396	0.099
0.613	0.032	0.387	0.096
0.618	0.033	0.382	0.079
0.633	0.046	0.367	0.056
0.635	0.048	0.365	0.043
0.636	0.059	0.364	0.036
0.636	0.057	0.364	0.023
0.639	0.055	0.361	0.011
0.64	0.06	0.36	0.006
0.641	0.065	0.359	0.004
0.642	0.067	0.358	0.002
0.644	0.089	0.356	0

Formation Name	Lithology	Avg Porosity %	Ka (mD)	Depth (m)	Core length (cm)	Core diameter (cm)	Flow area (cm^2)	Temp (°C)	pore volume injected (cc)	Pore pressure (kPag)	Flow Rate [Ml/min]	Interfacial tension (mN/m)	Pc (kPa)	Salinity (mg/L)	Method used	Viscosity ratio μ_{brine} / μ_{Co2}
Berea (sample 3)	**sandstone**							**55**		**11000**					**steady state**	

Table A. 22: Relative permeability data for Berea (sample 3) (Sandstone) (Akbarabadi and Piri, 2013)

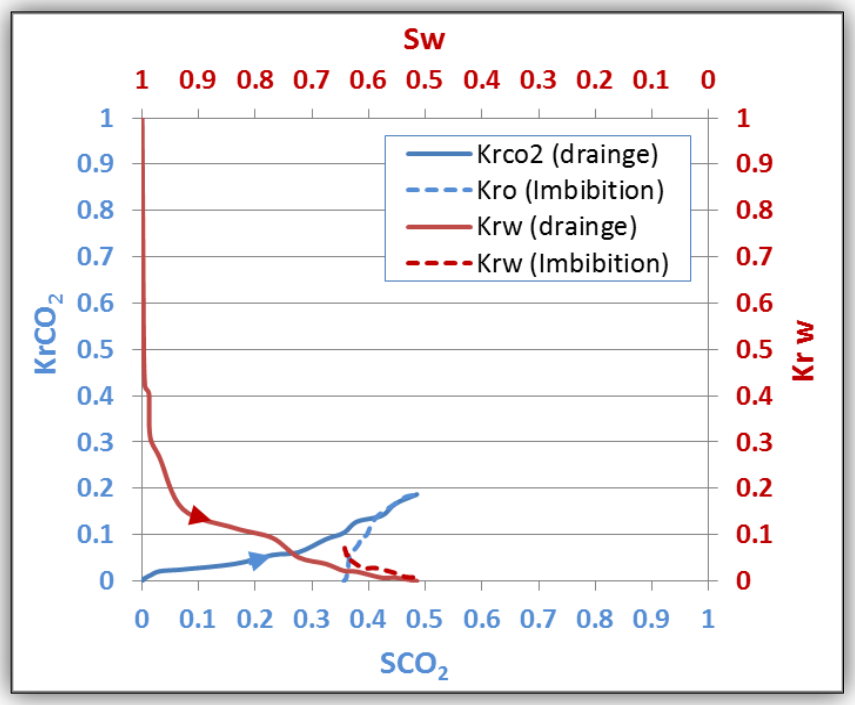

Figure A. 22: Relative permeability curves for Berea (sample 3) (Sandstone) (Akbarabadi and Piri, 2013)

Berea (Sample 4) (Sandstone)

S_{gr} =	0	Drainge	Imbibition
S_{wir} =	**0.4438**	ng = 3.2	ng =
Krg (wir) =	**0.3948**	nw = 2.6	nw =
Krw (gr) =	0		

Drainage			
CO_2 Saturation Fraction	Krg	Water Saturation Fraction	Krw
0.0000	0.0000	1.0000	1.0000
0.0237	0.0000	0.9763	0.8930
0.0474	0.0001	0.9526	0.7933
0.0711	0.0005	0.9289	0.7007
0.0948	0.0014	0.9052	0.6152
0.1185	0.0028	0.8815	0.5364
0.1422	0.0050	0.8578	0.4641
0.1659	0.0082	0.8341	0.3981
0.1896	0.0126	0.8104	0.3383
0.2133	0.0184	0.7867	0.2843
0.2370	0.0258	0.7630	0.2360
0.2607	0.0349	0.7393	0.1931
0.2844	0.0462	0.7156	0.1554
0.3081	0.0596	0.6919	0.1226
0.3318	0.0756	0.6682	0.0944
0.5562	**0.3948**	**0.4438**	0.0000

Imbibition			
Water Saturation Fraction	Krw	CO_2 Saturation Fraction	Krg

Formation Name	Lithology	Avg Porosity %	Ka (mD)	Depth (m)	Core length (cm)	Core diameter (cm)	Flow area (cm^2)	Temp (°C)	pore volume injected (cc)	Pore pressure (kPag)	Flow Rate [Ml/min]	Interfacial tension (mN/m)	Pc (kPa)	Salinity (mg/L)	Method used	Viscosity ratio μ_{brine} / μ_{Co2}
Berea (sample4)	**sandstone**	**22.1**	**914**		**10**			**50**		**9000**		**32**			**steady state**	

Table A. 23: Relative permeability data for Berea (sample 4) (Sandstone) (Krevor et al., 2012, Akbarabadi and Piri, 2013, Mathias et al., 2013)

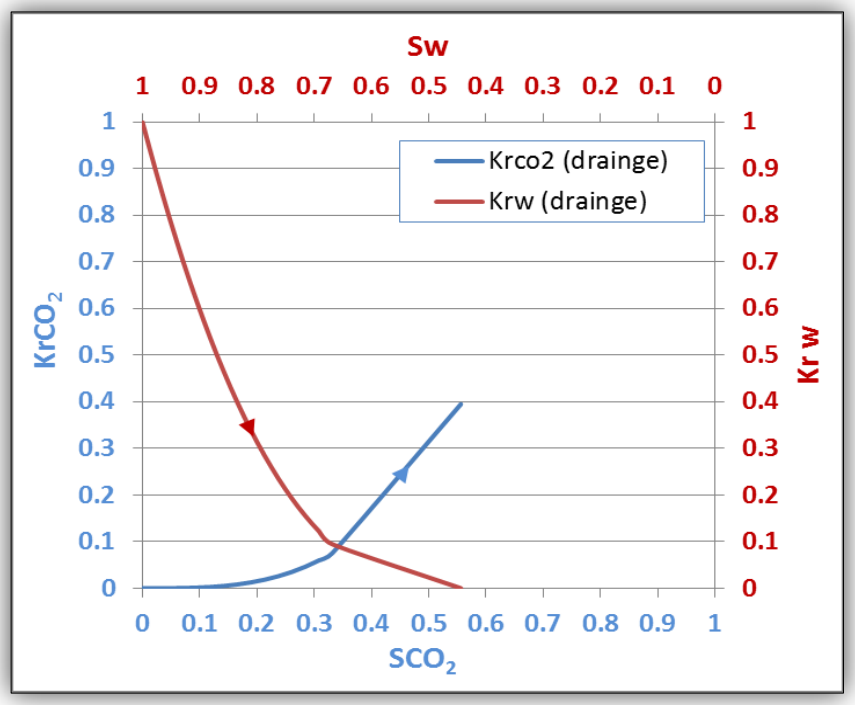

Figure A. 23: Relative permeability curves for Berea (sample 4) (Sandstone) (Krevor et al., 2012, Mathias et al., 2013)

Otway sandstone rock

Drainage			
CO_2 Saturation Fraction	Krg	Water Saturation Fraction	Krw
0.000	0.0000	1.0000	1.0000
0.050	0.0020	0.8610	0.5140
0.200	0.0090	0.8230	0.3790
0.300	0.0140	0.8030	0.3250
0.500	0.0250	0.7650	0.2460
0.600	0.0340	0.7320	0.2220
0.700	0.0440	0.7220	0.1860
0.800	0.0550	0.6500	0.1360
0.850	0.0860	0.5860	0.1490
0.950	0.1570	0.5490	0.0810
1.000	0.6080	0.4440	0.0000

Imbibition			
Water Saturation Fraction	Krw	CO_2 Saturation Fraction	Krg

Formation Name	Lithology	Avg Porosity %	Ka (mD)	Depth (m)	Core length (cm)	Core diameter (cm)	Flow area (cm^2)	Temp (°C)	pore volume injected (cc)	Pore pressure (kPag)	Flow Rate [Ml/min]	Interfacial tension (mN/m)	Pc (kPa)	Salinity (mg/L)	Method used	Viscosity ratio μ_{brine} / μ_{Co2}
otway	sandstone	18.2	45	-	8.3	5.08		63		12400	2	30		3202	steady state	-

Table A. 24: Relative permeability data for Otway sandstone rock (Perrin and Benson, 2010, Akbarabadi and Piri, 2013, Mathias et al., 2013)

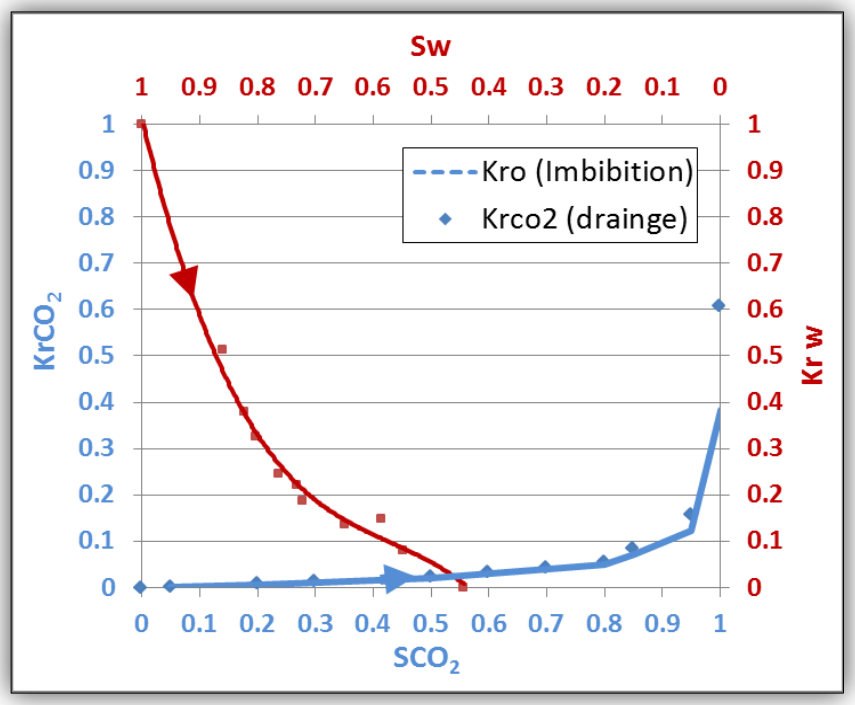

Figure A. 24: Relative permeability curves for Otway sandstone rock (Perrin and Benson, 2010)

Paaratte (Sandstone)

		Drainge		Imbibition	
S_{gr} =	0				
S_{wir} =	**0.3894**	ng =	4.6	ng =	
Krg (wir) =	**0.3284**	nw =	3	nw =	
Krw (gr) =	0				

Drainage			
CO_2 Saturation Fraction	Krg	Water Saturation Fraction	Krw
0.0000	0.0000	1.0000	1.0000
0.0359	0.0000	0.9641	0.8338
0.0718	0.0000	0.9282	0.6871
0.1077	0.0001	0.8923	0.5587
0.1436	0.0004	0.8564	0.4474
0.1795	0.0012	0.8205	0.3519
0.2154	0.0027	0.7846	0.2711
0.2513	0.0055	0.7487	0.2038
0.2872	0.0102	0.7128	0.1486
0.3231	0.0176	0.6769	0.1044
0.3590	0.0285	0.6410	0.0700
0.3949	0.0442	0.6051	0.0441
0.4308	0.0660	0.5692	0.0255
0.4667	0.0954	0.5333	0.0131
0.5026	0.1341	0.4974	0.0055
0.5385	0.1842	0.4615	0.0016
0.6106	**0.3284**	**0.3894**	0.0000

Imbibition			
Water Saturation Fraction	Krw	CO_2 Saturation Fraction	Krg

Formation Name	Lithology	Avg Porosity %	Ka (mD)	Depth (m)	Core length (cm)	Core diameter (cm)	Flow area (cm^2)	Temp (°C)	pore volume injected (cc)	Pore pressure (kPag)	Flow Rate [Ml/min]	Interfacial tension (mN/m)	Pc (kPa)	Salinity (mg/L)	Method used	Viscosity ratio μ_{brine} / μ_{Co2}
Paaratte	**sandstone**	**28.3**	**1156**		**9.5**			**50**		**9000**		**32**			**steady state**	

Table A. 25: Relative permeability data for Paaratte sandstone rock (Krevor et al., 2012, Akbarabadi and Piri, 2013, Mathias et al., 2013)

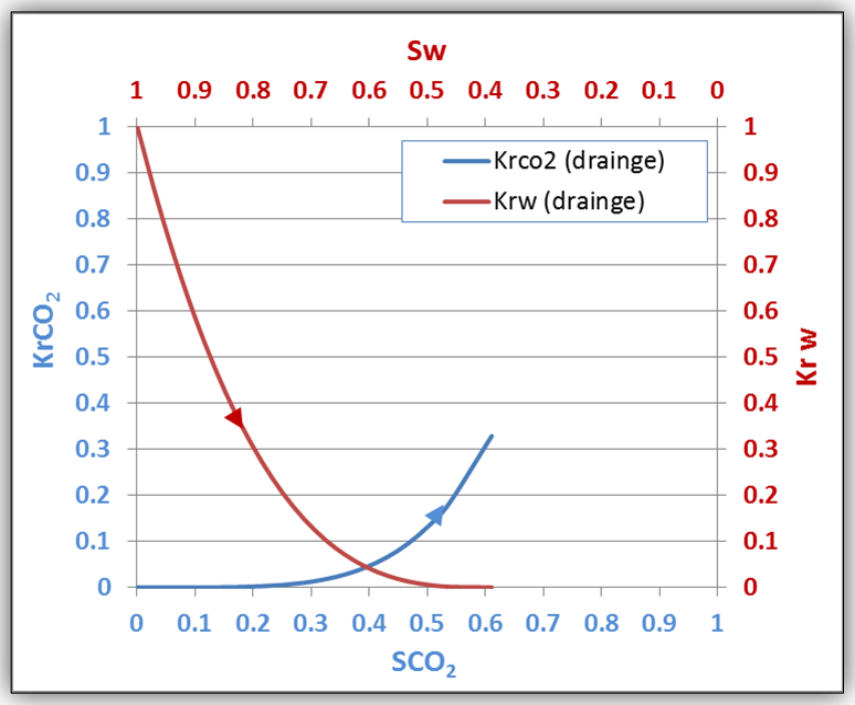

Figure A. 25: Relative permeability curves for Paaratte sandstone rock (Krevor et al., 2012, Mathias et al., 2013)

Mt. Simon (Sandstone)

S_{gr} =	0	Drainge		Imbibition	
S_{wir} =	0.4371	ng =	6	ng =	
Krg (wir) =	0.4929	nw =	1.6	nw =	
Krw(gr) =	0				

Drainage

CO_2 Saturation Fraction	Krg	Water Saturation Fraction	Krw
0.0000	0.0000	1.0000	1.0000
0.0330	0.0000	0.9670	0.9079
0.0660	0.0000	0.9340	0.8191
0.0990	0.0000	0.9010	0.7338
0.1320	0.0001	0.8680	0.6521
0.1650	0.0003	0.8350	0.5740
0.1980	0.0009	0.8020	0.4998
0.2310	0.0024	0.7690	0.4295
0.2640	0.0052	0.7360	0.3632
0.2970	0.0106	0.7030	0.3012
0.3300	0.0200	0.6700	0.2437
0.3630	0.0354	0.6370	0.1908
0.3960	0.0598	0.6040	0.1430
0.4290	0.0966	0.5710	0.1005
0.4620	0.1507	0.5380	0.0639
0.4950	0.2279	0.5050	0.0339
0.5629	0.4929	0.4371	0.0000

Imbibition

Water Saturation Fraction	Krw	CO_2 Saturation Fraction	Krg

Formation Name	Lithology	Avg Porosity %	Ka (mD)	Depth (m)	Core length (cm)	Core diameter (cm)	Flow area (cm^2)	Temp (°C)	pore volume injected (cc)	Pore pressure (kPag)	Flow Rate [Ml/min]	Interfacial tension (mN/m)	Pc (kPa)	Salinity (mg/L)	Method used	Viscosity ratio μ_{brine} / μ_{Co2}
Mt Simon	sandstone	24.4	7.5		9.6			50		9000		32			steady state	

Table A. 26: Relative permeability data for Mt. Simon sandstone rock (Krevor et al., 2012, Akbarabadi and Piri, 2013, Mathias et al., 2013)

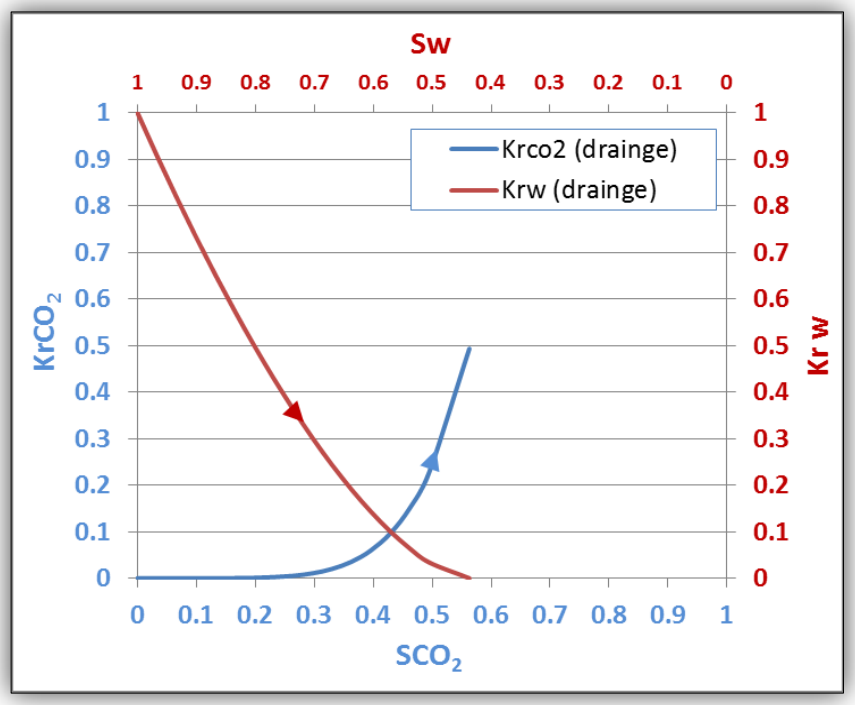

Figure A. 26: Relative permeability curves for Mt. Simon sandstone rock (Krevor et al., 2012, Mathias et al., 2013)

Tuscaloosa (Sandstone)

		Drainge		Imbibition	
S_{gr} =	0				
S_{wir} =	**0.7030**	ng =	4.7	ng =	
Krg (wir) =	**0.0767**	nw =	3.2	nw =	
Krw (gr) =	0				

Drainage

CO_2 Saturation Fraction	Krg	Water Saturation Fraction	Krw
0.0000	0.0000	1.0000	1.0000
0.0170	0.0000	0.9830	0.8281
0.0340	0.0000	0.9660	0.6777
0.0510	0.0000	0.9490	0.5472
0.0680	0.0001	0.9320	0.4352
0.0850	0.0002	0.9150	0.3400
0.1020	0.0005	0.8980	0.2602
0.1190	0.0010	0.8810	0.1943
0.1360	0.0020	0.8640	0.1409
0.1530	0.0034	0.8470	0.0986
0.1700	0.0056	0.8300	0.0660
0.1870	0.0087	0.8130	0.0417
0.2040	0.0131	0.7960	0.0243
0.2210	0.0191	0.7790	0.0128
0.2380	0.0271	0.7620	0.0057
0.2970	**0.0767**	**0.7030**	0.0000

Imbibition

Water Saturation Fraction	Krw	CO_2 Saturation Fraction	Krg

Formation Name	Lithology	Avg Porosity %	Ka (mD)	Depth (m)	Core length (cm)	Core diameter (cm)	Flow area (cm^2)	Temp (°C)	pore volume injected (cc)	Pore pressure (kPag)	Flow Rate [Ml/min]	Interfacial tension (mN/m)	Pc (kPa)	Salinity (mg/L)	Method used	Viscosity ratio μ_{brine} / μ_{Co2}
Tuscaloosa	**sandstone**	**23.6**	**220**		**10.8**			**50**		**9000**		**32**			**steady state**	

Table A. 27: Relative permeability data for Tuscaloosa sandstone rock (Krevor et al., 2012, Akbarabadi and Piri, 2013, Mathias et al., 2013)

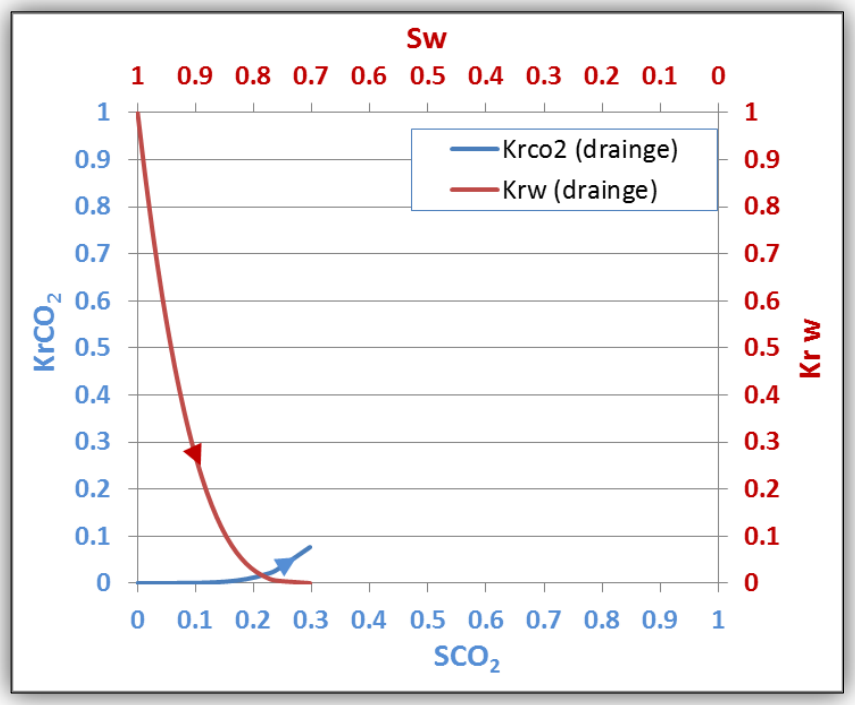

Figure A. 27: Relative permeability curves for Tuscaloosa sandstone rock (Krevor et al., 2012, Mathias et al., 2013)

B) Pore-network extraction

B.1) **Introduction**

Two basic matters are considered when applying pore-network extraction, which are:

i. Pore definition

The pore space is usually defined depending on pore geometry, i.e. pore bodies and pore throats (connections). Jiang et al. (2007) stated that from the topological point of view, there were two types of pores, either junctions (with more than two junctions) which corresponded to pore bodies and conjunctions equivalent to pore throats; finally, the junctions were re-identified as Nodes and non-junctions as Bonds, and the next step was to measure their geometrical characteristics such as volumes, radii (cross-section area), shape and coordination number.

ii. Algorithm Efficiency

To make the extracted pore-network a very accurate representative for the internal structure of the rock, the extraction must be made from a 3D image[9] with high-resolution. These types of images need quite efficient algorithms to extract the pore network and save the computational time. The Algorithm applied must preserve the geometrical and topological properties of the original pore space (Jiang et al., 2007).

B.2) **An overview of existing network extraction methods**

According to Jiang et al. (2007), most existing algorithms could be classified into four types:

B.2.1) Medial Axis Transformations (MAT)

The medial axis of the pore space was used by Lindquist et al. (1996) in order to define the centres of the pore and throat bodies. Delerue et al. (1999) adopted a ball-growing algorithm for extracting the skeleton of the pore network. Generally, and as Jiang et al. (2007) mentioned, the idea is to calculate the distance map of the object in an image, to find local maxima, and to reconnect the maxima. The resulting skeleton based on MAT is centred in the local pore space by construction, depending on the local maxima threshold.

[9] Many ways could be used to get a 3D image, but the computer-tomography scan (CT-Scan) is the best.

The disadvantage of this method is not being always topology-preserving, as it depends on the path reconstruction and might produce redundant points on the skeleton.

B.2.2) Thinning algorithms methods

This method can be imagined as peeling off the boundary of the foreground of an image in a layer by layer manner (removing the foreground points as efficiently as possible without changing the topology of the original image). Kong and Rosenfeld (1989) described thinning algorithms as procedures for iteratively deleting points with some additional geometrical or topological constrained conditions, until no more such points can be deleted.

The concept of "simple point" (to be deleted from the foreground) was introduced by Center and Morgenthaler (1981) cited in Jiang et al. (2007). Saito (1995), cited in Jiang et al. (2007), suggested that the deletion of simple points (from the foreground) was done sequentially, whereas Lohou and Bertrand (2004), and Lohou and Bertrand (2005) considered the deletion to be in parallel. Jonker (2000) introduced simple points deletion to be with morphological operations.

The main advantage of Thinning algorithms is being a topology-preservative method, which could be summarized in Jiang et al. (2007):

- There is no change of connectivity of objects (pores) during the whole thinning process.
- The resultant skeleton is thin (there is no redundant points in the sense of topology preservation.
- The skeleton is not necessarily centred.

B.2.3) Hybrid algorithms

These methods include the advantages of the previous ones. The "DOHT" method (Distance Ordered Homotopic Thinning) is one of the most famous under this group. It iteratively deletes simple points in the increasing distance map order [Morgenthaler, 1981].

B.2.4) UDOHT method (Upgraded Distance Ordered Homotopic Thinning)

A disadvantage was noted when applying the ordinary "DOHT" algorithm, as the resulting skeleton is still not truly in the central region (Figure B. 1 a). This problem is due to the fact that the location of the skeleton depends on the scanning order inside the region of the same distance values. Jiang et al. (2007) developed the algorithm to a new one with symmetry deletion and independent of the scanning order (Figure B. 1 b)

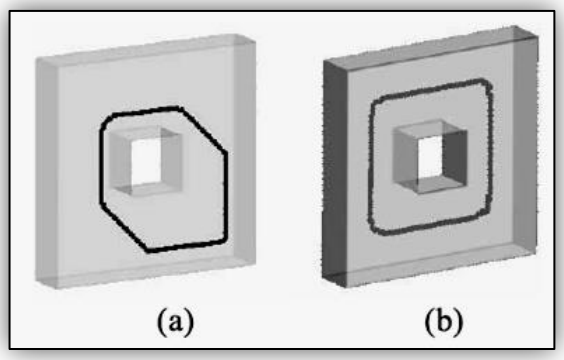

Figure B. 1: Medialness of skeletons in three dimensions (Jiang et al., 2007)

B.3) **Pore network extraction considerations**

Both geometrical and topological (GT) properties must be taken under high degree of consideration when extracting the pore network. To achieve this end, the algorithm must focus on the following:

B.3.1) Topology Preservation (Homotopy)

The extracted skeleton of the pore space must be topologically identical to that existing in the original image, which means all the components, cavities and tunnels of the skeleton should be kept the same as in the original image.

B.3.2) Single Voxel Width (Thinness)

Thinning algorithm can extract a skeleton of single voxel width. The importance of the single-voxel-width skeleton is the ability to be used to locate the centres and orientations of flow paths (Jiang et al., 2007).

B.3.3) Medial Location ("Medialness")

The skeleton must be in the centre of the pore space. This is essential for calculating cross-sectional areas normal to the central flow path and to determining radii of cross sections. Most algorithms applied do not guarantee this issue as the skeleton voxel locating depends on the arbitrary scanning order in which points are being deleted. Jiang et al. (2007) solved this problem by introducing an upgraded DOHT algorithm (Figure B. 1b).

B.3.4) Integration of Geometry

According to Jiang et al. (2007), the pore cross section must always be perpendicular to its medial line (skeleton). Jiang et al. (2007) added that the resulting skeleton is called a pure topological network if all simple points (in thinning algorithms) are all to be deleted; practically some simple points (called endpoints) should not be deleted to show up some extra geometrical features.

B.4) **Steps of pore-network extraction**

Jiang et al. (2007) stated that five steps were used to extract the pore-network as follows:

1. Calculation of the three-dimensional Euclidean distance map
2. Clustering of Voxels
3. Extraction of the network of the pore space (also called skeletonization and calculation of medial axis)
4. Partitioning of the pore space
5. Computation of shape factors

B.5) **An upgraded algorithm method (as example) to extract pore network**

Jiang et al. (2007) introduced an upgraded algorithm to extract pore network. Here are some positive characteristics of their upgraded algorithm:

B.5.1) Fast Thinning to Extract the Medial Axis

The advantages and fast feature in this algorithm could be summarized in the following:

i. It is a compound algorithm consisting of novel thinning technique and an improved version of the Euclidean distance transformation (EDT), and used to extract the medial axis of foreground voxels (i.e., pore voxels). This upgraded algorithm gives an advantage of checking the foreground voxels in ascending distance order as mentioned in Lohou and Bertrand (2005). This advantage is very important to determine if the foreground voxels can be removed or not. Another advantage of their thinning upgraded algorithm is that it works on the concept of detecting and deleting as many points as possible, rather than just one point, before invoking a clustering procedure that previously applied in (Hoshen and Kopelman, 1976).

ii. As followed in Bertrand and Malandain (1994) and in this upgraded algorithm, the topological numbers are defined as the number of particular 6-connected background components and the number of 26-connected (adjacent) foreground components in the neighbourhood. If both numbers are equal to one, the point is called "simple" and it could be deleted without changing the topology of the 3D image.

iii. Gau and Yung Kong (2003) extended the concept of a simple point to a simple set; to find a simple set, Jiang et al. (2007) introduced the concept of a foreground pure 6-component (which is a component of single width aligned along one of the grid coordinates) to be used as candidate for the checking in their upgraded algorithm, and they added "in the envelope of this pure 6-component, two particular types of adjacency are defined (for foreground and background components) analogous to the adjacencies in the neighbourhood of a single point, and we proved Theorem 1 stating that if the pure 6-component has exactly one foreground and one background adjacent component, then the 6-component is simple; consequently, in the thinning algorithm the entire simple pure 6-component can be deleted at once. Notice that the theorem only provides

a sufficient condition for the "simplicity" of a pure 6-component; in other words, if it does not have exactly one foreground and one background adjacent component, then the pure 6-component needs to be checked point by point. In our numerical experiments, we find that clustering voxels in the neighbourhood of a single point are almost as time-consuming as clustering voxels in the envelope of a set (about 2.45 voxels per set for our samples); therefore, the total number of invoking clustering procedure is reduced in the whole thinning process, greatly improving the efficiency of the thinning method".

iv. According to Jiang et al. (2007), as the detection strategy is within envelopes of a pure 6-component, simple set detection could be carried out in parallel at alternating rows or columns of the image; subsequently, the foreground points are checked only once.

v. Centring the skeleton is a crucial issue in pore-network extracting. Most ordinary algorithms have a defect in this matter. Palágyi and Kuba (1997) and Palágyi and Kuba (1998) tried to find the solution by introducing scanning in 6 or 12 directions. Jiang et al. (2007) in this upgraded algorithm could guarantee in only 2 directions (forward and backward), medialness through scanning. They achieved central-aligned skeleton by using the Euclidean distance map to control the main order of scanning (voxels of small distances are checked first then voxels of equal distance in a given layer of the distance map). This will mean that all removable points are to be kept until the end of the two scans, which leads to the fact that each point in the layer of the same distance has an equal probability of being detected and subsequently removed.

B.5.2) Extension of Euclidean Distance Transformation

i. As the Euclidean is an accurate distance metric (because of its rotational constancy), it should be used to optimize the centring "medialness" of the GT network and to measuring the inscribed radii of the skeleton voxel, in this matter, Jiang et al. (2007) used the squared (integer) value of the Euclidean to save the computing time.

ii. Jiang et al. (2007) mentioned that in their algorithm and during the two scans (forward and backward), for each foreground point, the index of its nearest background voxel is being recorded. This is subsequently propagated to nearby

voxels within its 3 x 3 x 3 neighbourhood. Shih and Wu (2004) mentioned that by using the distance to each neighbour and the distances of its neighbours to their nearest background voxels, the new value (distance of the current point corresponding to the minimum of these distances for all neighbours) is determined. Jiang et al. (2007) kept this advantage as mentioned in Shih and Wu (2004).

B.5.3) Geometry Preservation

Apart from preserving the topological information, there are other crucial flow-properties information (called endpoints) which must not be missed. This information includes the following:

i. Boundary Points

It is known that most of the thinning algorithms remove the points from the inlet and outlet parts of 3D image. Jiang et al. (2007) solved the problem by introducing a region constraint principle in order to keep one voxel in a local maximum Squared Euclidean Distance region at the relevant boundaries, even if this voxel is a simple point.

ii. Branch points

In some flow calculations, involving a diffusion process as an example, the medial lines of dead-end pores (Figure B. 2) must be kept in the resulting GT network. To achieve this, Jiang et al. (2007) calculated in 3D a map of the geodesic distance from the pure topological medial line (black line in Figure B. 2). A branch of the medial axis is kept in dead end regions (grey in Figure B. 2) that have a geodesic distance larger than the threshold (Jiang et al., 2007), and a voxel in this region (a branch point) is retained if it has only one 26-neighbor.

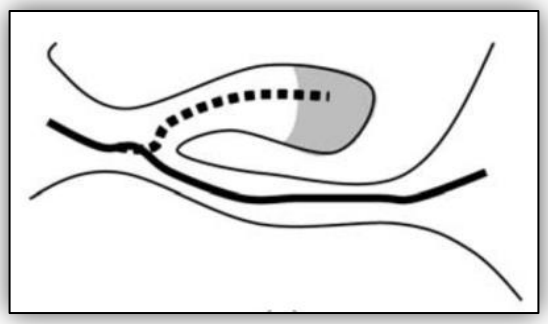

Figure B. 2: Dead-end pores (Jiang et al., 2007)

iii. Anchor points process

According to Jiang et al. (2007), the large 3-D images are known as being very difficult to be processed therefore; they must be divided into sub images. The boundary link points (Anchor points) located on the boundaries of these sub images must be kept to preserve a specific property and to integrate the various sub skeletons into a global skeleton.

B.5.4) Implementation of the GT Network Extraction

Jiang et al. (2007), in their upgraded algorithm method, introduced a sequence of extraction which depends on that the pure topological skeleton extraction (extracting the topologically representative and centred Skeleton without geometry preservation) is firstly applied, then the geometry preservation is considered secondly. The extraction without geometry preservation includes the following:

1. Computation of the Squared Euclidean

   According to Jiang et al. (2007), the Squared Euclidean Distance Map (SEDM), obtained from application of the Signed Squared Euclidean Distance Transformation (SSEDT) of I (a gray-scale image denoted by Map $_{(I)}$) is calculated as described in paragraph (B.5.2), in which the value Map (p) of a foreground voxel p is the shortest Squared Euclidean Distance from this voxel to the background of I, while the value of all background voxels is zero. During the thinning operation, Map (I) is updated when points are deleted, i.e. removed from the foreground. Two queues of voxels, denoted by Q_1 and Q_2, are used in our algorithm. All candidate voxels are stored in Q_1. These voxels comprise the (layer of) foreground voxels with current minimum Squared Euclidean Distance. In Q_2 all voxels are stored that are marked for deletion during an iteration. Such points p get the value Map(p)= ∞.

2. Initialization

   At the start of the thinning process, Q_1 contains all voxels of current minimum Squared Euclidean Distance (usually 1) in Map (I), and Q_2 is empty (Jiang et al., 2007).

3. Thinning Iteration Steps

The thinning consists of five steps as mentioned in Jiang et al. (2007). Examples of extracted GT networks without end-points (i.e. without geometry preservation) are shown in Figure B. 3a and Figure B. 3b for a sandstone sample.

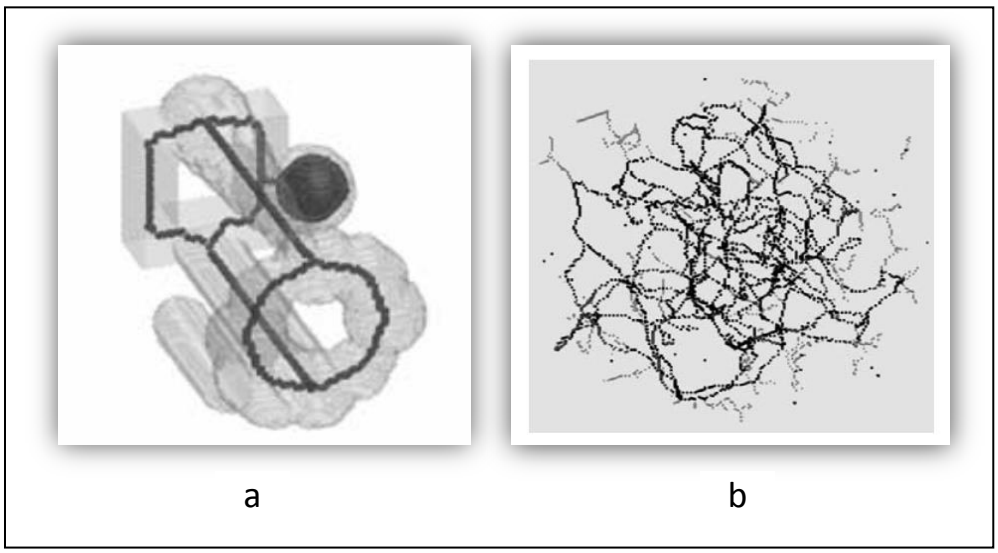

Figure B. 3: a) Two-dimensional example of a skeleton with a branch (dashed curve), where the gray area indicates a Geodesic distance to the pure topological medial axis (black curve), larger than a given threshold. b) Pure topological skeleton in black and GT network with boundary links and some branches in gray (Jiang et al., 2007).

4. Extraction with Geometry Preservation

A GT network with geometry preservation (i.e., with endpoints) is necessary, in addition to the algorithm for extraction of the general skeleton discussed above, so the geometrical properties must be included in the GT network also.

5. Removing Isolated Pores and Cavities (Preprocessing)

Any parts of the rock which do not contribute to fluid flow (like isolated pores and cavities) are removed in the construction of the pore network model to make fluid flow predictions logical.

6. Computing SEDM Near Boundaries

To keep boundary points on the inlet/outlet for calculation of the distance map, they suppose that all voxels beyond the boundaries are pore voxels.

7. Retaining Endpoints

In step 4 above, marked voxels are checked to determine whether they occur on a boundary. If a marked voxel occurs on a boundary without any other 26-adjacent voxels of larger or equal distance value, then it is retained as a boundary point.

C) Physical properties and behaviour of Carbon dioxide CO_2

C.1) Nekouzad (2007) stated CO_2 could exist in solid, liquid and gas phases.

C.2) **Table C. 1** summarizes some physical properties of CO_2 at the conditions (1.01MPa, 0º C).

Molecular weight	44 g/mol
Specific gravity with respect to air	1.529
Density	1.95 kg/m^3
Viscosity	0.0137 MPa/s
Critical pressure, Pc	7.38 MPa (1070 Psi)
Critical temperature, Tc	30.76 ^{o}C 87.76 ^{o} F
Critical volume, Vc	94 cm^3/mol

Table C. 1: Physical properties and behaviour of Carbon dioxide CO_2

The density of CO_2 is about 50 percent greater than that to air at atmospheric conditions.

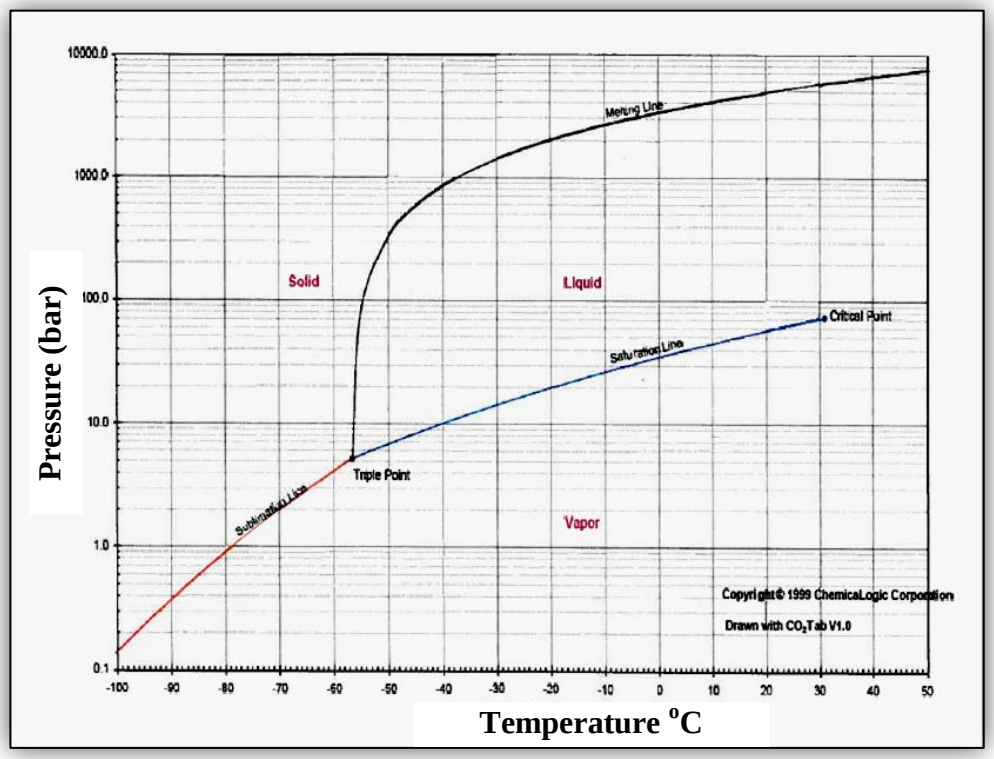

Figure C. 1: Phase behaviour diagram for Carbon dioxide CO_2 (Nekouzad, 2007)

C.3) The viscosity of CO_2 depends strongly on temperature and pressure as appears in Figure C. 2.

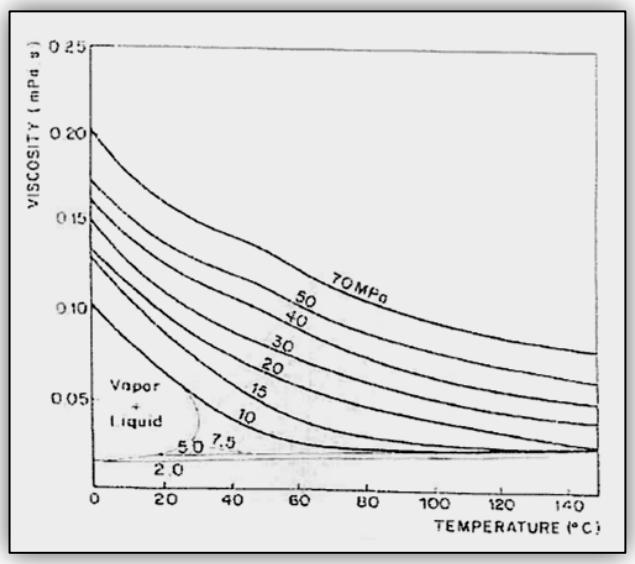

Figure C. 2: CO_2 viscosity as a function of pressure and temperature (Nekouzad, 2007)

C.4) The solubility of CO_2 in oil depends strongly on temperature and pressure in addition to the composition of the oil (Figure C. 3).

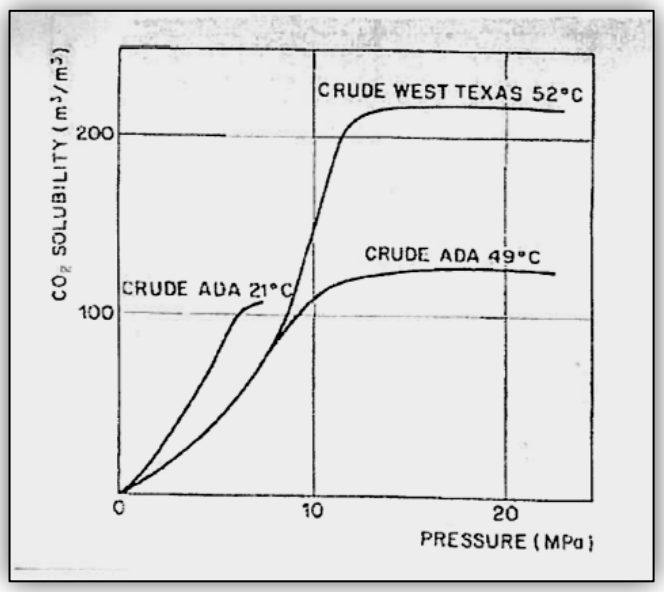

Figure C. 3: CO_2 solubility in oil (Nekouzad, 2007)

References

ABE, A. A. 2005. *Relative Permeability and Wettability Implications of Dilute Surfactants at Reservoir Conditions.* Idaho State University, Idaho, USA.

ABU-KHAMSIN, S. A. 2004. Basic Properties of Reservoir Rocks. 96-99.

AHMED, T. 2011. Resrvoir engineering handbook.

AKBARABADI, M. & PIRI, M. 2013. Relative permeability hysteresis and capillary trapping characteristics of supercritical CO2/brine systems: An experimental study at reservoir conditions. *Advances in Water Resources,* 52**,** 190-206.

ASAR, H. & HANDY, L. L. 1988. Influence of Interfacial Tension on Gas/Oil Relative Permeability in a Gas-Condensate System. *SPE Reservoir Engineering,* 3**,** 257-264.

BACHU, S. & BENNION, B. 2008. Effects of in-situ conditions on relative permeability characteristics of CO2-brine systems. *Environmental Geology,* 54**,** 1707-1722.

BENNION, B. & BACHU, S. 2005. Relative Permeability Characteristics for Supercritical CO2 Displacing Water in a Variety of Potential Sequestration Zones in the Western Canada Sedimentary Basin. *SPE Annual Technical Conference and Exhibition.* Dallas, Texas: Society of Petroleum Engineers.

BENNION, B. & BACHU, S. 2008a. Drainage and Imbibition Relative Permeability Relationships for Supercritical CO2/Brine and H2S/Brine Systems in Intergranular Sandstone, Carbonate, Shale, and Anhydrite Rocks. *SPE Reservoir Evaluation & Engineering,* 11**,** 487-496.

BENNION, D. B. & BACHU, S. 2006a. The Impact of Interfacial Tension and Pore Size Distribution/Capillary Pressure Character on CO2 Relative Permeability at Reservoir Conditions in CO2-Brine Systems. *SPE/DOE Symposium on Improved Oil Recovery.* Tulsa, Oklahoma, USA: Society of Petroleum Engineers.

BENNION, D. B. & BACHU, S. 2006b. Supercritical CO2 and H2S—Brine Drainage and Imbibition Relative Permeability Relationships for Intergranular Sandstone and Carbonate Formations. *SPE Europec/EAGE Annual Conference and Exhibition.* Vienna, Austria: Society of Petroleum Engineers.

BENNION, D. B. & BACHU, S. 2006c. Dependence on Temperature, Pressure, and Salinity of the IFT and Relative Permeability Displacement Characteristics of CO2 Injected in Deep Saline Aquifers. *SPE Annual Technical Conference and Exhibition.* San Antonio, Texas, USA: Society of Petroleum Engineers.

BENNION, D. B. & BACHU, S. 2010. Drainage and Imbibition CO2/Brine Relative Permeability Curves at Reservoir Conditions for High-Permeability Carbonate Rocks. *SPE Annual Technical Conference and Exhibition.* Florence, Italy: Society of Petroleum Engineers.

BERG, S., OEDAI, S. & OTT, H. 2013. Displacement and mass transfer between saturated and unsaturated CO2–brine systems in sandstone. *International Journal of Greenhouse Gas Control,* 12**,** 478-492.

BERTRAND, G. & MALANDAIN, G. 1994. A new characterization of three-dimensional simple points. *Pattern Recognition Letters,* 15**,** 169-175.

CENTER, U. O. M. A. C. P. C. S. & MORGENTHALER, D. 1981. *Three-dimensional simple points: serial erosion, parallel thinning, and skeletonization* [Online]. Available: http://scholar.google.co.uk/scholar?hl=en&q=Three-dimensional+simple+points%3A+Serial+ero-+sion%2C+parallel+thinning+and+skeletonization&btnG=&as_sdt=1%2C5&as_sdtp=.

DELERUE, J., PERRIER, E., YU, Z. & VELDE, B. 1999. New algorithms in 3D image analysis and their application to the measurement of a spatialized pore size distribution in soils. *Physics and Chemistry of the Earth, Part A: Solid Earth and Geodesy,* 24**,** 639-644.

DRIA, D. E., POPE, G. A. & SEPEHRNOORI, K. 1993. Three-Phase Gas/Oil/Brine Relative Permeabilities Measured Under CO2 Flooding Conditions. *SPE Reservoir Engineering,* 8**,** 143-150.

GAU, C.-J. & YUNG KONG, T. 2003. Minimal non-simple sets in 4D binary images. *Graphical Models,* 65**,** 112-130.

GHANBARI, S., AL-ZAABI, Y., PICKUP, G. E., MACKAY, E., GOZALPOUR, F. & TODD, A. C. 2006. Simulation of CO2 Storage In Saline Aquifers. *Chemical Engineering Research and Design,* 84**,** 764-775.

H., A. & HANDY, L. 1988. Influence of interfacial tension on Gas/oil relative permeability in a gas - condensate system.

HONARPOUR, M. M., KOEDERITZ, F. & HERBERT, A. 1986. *Relative permeability of petroleum reservoirs*.

HOSHEN, J. & KOPELMAN, R. 1976. Percolation and cluster distribution. I. Cluster multiple labeling technique and critical concentration algorithm. *Physical Review B,* 14**,** 3438.

JIANG, Z., WU, K., COUPLES, G., VAN DIJKE, M. I. J., SORBIE, K. S. & MA, J. 2007. Efficient extraction of networks from three-dimensional porous media. *Water Resources Research,* 43**,** W12S03.

JONKER, P. P. Morphological operations on 3D and 4D images: From shape primitive detection to skeletonization. Discrete Geometry for Computer Imagery, 2000. Springer, 371-391.

KONG, T. Y. & ROSENFELD, A. 1989. Digital topology: Introduction and survey. *Computer Vision, Graphics, and Image Processing,* 48**,** 357-393.

KREVOR, S. C. M., PINI, R., LI, B. & BENSON, S. M. 2011. Capillary heterogeneity trapping of CO2 in a sandstone rock at reservoir conditions. *Geophysical Research Letters,* 38**,** L15401.

KREVOR, S. C. M., PINI, R., ZUO, L. & BENSON, S. M. 2012. Relative permeability and trapping of CO2 and water in sandstone rocks at reservoir conditions. *Water Resources Research,* 48**,** W02532.

LEVINE, J. 2011. Relative Permeability Experiments of Carbon Dioxide Displacing Brine and Their Implications for Carbon Sequestration.

LINDQUIST, W. B., LEE, S. M., COKER, D. A., JONES, K. W. & SPANNE, P. 1996. Medial axis analysis of void structure in three-dimensional tomographic images of porous media. *Journal of Geophysical Research: Solid Earth (1978–2012),* 101**,** 8297-8310.

LOHOU, C. & BERTRAND, G. 2004. A 3D 12-subiteration thinning algorithm based on< i> P</i>-simple points. *Discrete applied mathematics,* 139**,** 171-195.

LOHOU, C. & BERTRAND, G. 2005. A 3D 6-subiteration curve thinning algorithm based on< i> P</i>-simple points. *Discrete applied mathematics,* 151**,** 198-228.

MATHIAS, S. A., GLUYAS, J. G., GONZÁLEZ MARTÍNEZ DE MIGUEL, G. J., BRYANT, S. L. & WILSON, D. 2013. On relative permeability data uncertainty and CO2 injectivity estimation for brine aquifers. *International Journal of Greenhouse Gas Control,* 12**,** 200-212.

MCCARDELL, W. A Review of the Physical Basis for the Use of the J-Function. Eighth Oil Recovery Conference, Texas Petroleum Research Committee, 1955.

NEKOUZAD, M. 2007. *Study of effects of thickneses , viscosity and depth in Co2 injection in heavy oil reservoirs. .* Heriot - Watt university.

OKABE, H., TSUCHIYA, Y., MIHAMA-KU, H. & SHINJYUKU-KU, O. Experimental investigation of residual CO 2 saturation distribution in carbonate rock. International symposium of the society of core analysts, Abu Dhabi, UAE, 2008.

PALÁGYI, K. & KUBA, A. A parallel 12-subiteration 3d thinning algorithm to extract medial lines. Computer Analysis of Images and Patterns, 1997. Springer, 400-407.

PALÁGYI, K. & KUBA, A. 1998. A 3D 6-subiteration thinning algorithm for extracting medial lines. *Pattern Recognition Letters,* 19**,** 613-627.

PENTLAND, C. H., EL-MAGHRABY, R., IGLAUER, S. & BLUNT, M. J. 2011. Measurements of the capillary trapping of super-critical carbon dioxide in Berea sandstone. *Geophysical Research Letters,* 38**,** L06401.

PERRIN, J.-C. & BENSON, S. 2010. An Experimental Study on the Influence of Sub-Core Scale Heterogeneities on CO2 Distribution in Reservoir Rocks. *Transport in Porous Media,* 82**,** 93-109.

PISTONE, S. 2011. *The significance of co2 solubility in deep subsurface environments.,* Stanford University.

SAITO, T. A sequential thinning algorithm for three dimensional digital pictures using the Euclidean distance transformation. Proc. 9th SCIA (Scandinavian Conf. on Image Analysis, 1995. 507-516.

SCIENCES, S. O. E. 2013. *Relative Permeability Explorer* [Online]. Stanfod university. Available: https://pangea.stanford.edu/research/bensonlab/relperm/index.html.

SHI, J.-Q., XUE, Z. & DURUCAN, S. 2009. History matching of CO2 core flooding CT scan saturation profiles with porosity dependent capillary pressure. *Energy Procedia,* 1**,** 3205-3211.

SHIH, F. Y. & WU, Y.-T. 2004. Fast Euclidean distance transformation in two scans using a 3× 3 neighborhood. *Computer Vision and Image Understanding,* 93**,** 195-205.

SUEKANE, T., NOBUSO, T., HIRAI, S. & KIYOTA, M. 2008. Geological storage of carbon dioxide by residual gas and solubility trapping. *International Journal of Greenhouse Gas Control,* 2**,** 58-64.

SURVEY, A. G. 2013. *Relative Permeability Data for Supercritical CO2 Displacing Water* [Online]. Alberta Geological Survey. Available: http://www.ags.gov.ab.ca/co2_h2s/wabamun/relative_permeability.html.

VAN GENUCHTEN, M. T. 1980. A Closed-form Equation for Predicting the Hydraulic Conductivity of Unsaturated Soils1. *Soil Sci. Soc. Am. J.,* 44**,** 892-898.

YUQI1, D., BOLAJI, O. B. & DACUN, L. 2004. Literature Review on Methods toObtain Relative Permeability Data.

ZUO, L., KREVOR, S., FALTA, R. & BENSON, S. 2012. An Experimental Study of CO2 Exsolution and Relative Permeability Measurements During CO2 Saturated Water Depressurization. *Transport in Porous Media,* 91**,** 459-478.